2020

# Understanding the role of dMob4 in postembryonic Neural Stem Cell mitotic reactivation

Gonzaga, Eleanor

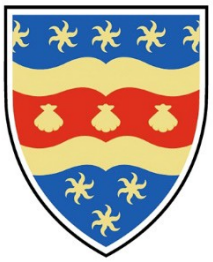

UNIVERSITY OF PLYMOUTH

# Understanding the role of dMob4 in postembryonic Neural Stem Cell mitotic reactivation

by

ELEANOR GONZAGA

A thesis submitted to the University of Plymouth in partial fulfilment
for the degree of

DOCTOR OF PHILOSOPHY

Peninsula Medical School

July 2020

## AUTHOR'S DECLARATION

At no time during the registration for the degree of Doctor of Philosophy has the author been registered for any other University award without prior agreement of the Doctoral College Quality Sub-Committee.

Work submitted for this research degree at the University of Plymouth has not formed part of any other degree either at the University of Plymouth or at another establishment.

Publications:

Gil-Ranedo, J, Gonzaga, E, Jaworek, KJ, Berger, C, Bossing, T and Barros, CS.(2019). STRIPAK Members Orchestrate Hippo and Insulin Receptor Signalling to Promote Neural Stem Cell Reactivation. Cell Rep 27, 2921-2933 e2925 10.1016/j.celrep.2019.05.023.

I have contributed with data to figures 2, 3, 4, 5, 6 and supplementary figures 2 and 3.

Presentations at conferences:

BSDB/BSCB/Genetics Society Joint meeting, Warwick, April 2017: Poster

Poster Title: dMob4 is required for mitotic reactivation of *Drosophila* neural stem cells.

Annual presentation for the University of Plymouth seminar series (2014-2016): oral., ARSC Cornwall (2014-2016): oral and poster presentation.

Word count of main body of thesis: 31923

Signed….. EGonzaga

Date…….16.07.2020

*For Nan*

## ACKNOWLEDGMENTS

First and foremost, I must express enormous gratitude to my director of studies and overall mentor, Dr Claudia Barros. Thank you for welcoming me into your lab and for this incredible opportunity. Your work ethic is genuinely inspirational, and it has been a privilege to work with you and learn by your example. I am so grateful for the years of guidance, patience and support throughout this PhD journey. I would also like to extend my gratitude to my incredibly knowledgeable supervisory team, Dr Torsten Bossing and Dr Iain Robinson, for your continued advice and support throughout my studies and after.

The PhD journey may occasionally resemble an assault course, and I am incredibly grateful for my lab team/comrades. From celebrating the completion of an experiment, statistically significant results, or merely a successful egg-lay, we would celebrate together. Therefore, special thanks to Karolina, Jon, Owen and Laura for your camaraderie, roaring laughter, and our epic international food extravaganzas! I hope we can recreate these wonderful memories. I must also express gratitude to Mark, Simon and Juliet; a few JBB out-of-hours heroes! Furthermore, over the years, our lab welcomed many talented students, and it was a pleasure working with all of you. I still have your post-it note (#YKWYA).

Similar to the stem cells I studied, I relied on a supportive microenvironment, or ‘niche’. Thank you LaC, ShRD, MoN, ToB, MaD, SiT, EmW, ChC, NaB, KaP, NaG, JoL, ChR, ChO, SoB, KaE, GeG, LiK, KaD, PaD, LaD, MaH, and JeD for your endless support, unique wisdom, and for your continued understanding for my absences over the years.

Lastly, thank you to my family; for continually encouraging me to I pursue my dreams and forever teaching me that laughter is the best medicine, and a smile is your best attire. Officer RMD, thank you for adapting your life around my ‘*Drosphalias’*, encouraging me to take rest, and also motivating me when I needed it the most. Jenna and Harriet, thank you for always being one phone call away and providing hilarious family updates while I was away. Mum and dad, I can only dream of having half of your strength and resilience; I am extremely happy we can celebrate this together. Eva, always remember that you can do anything you set your mind to. Just believe and achieve!

## ABSTRACT

UNDERSTANDING THE ROLE OF DMOB4 IN POSTEMBRYONIC NEURAL STEM CELL MITOTIC REACTIVATION

Eleanor Gonzaga

Brain homeostasis supports cognition and neural plasticity, the brains' ability to adapt to its environment throughout life. These processes rely on replenishment from stem cells in the brain, termed Neural Stem Cells (NSCs). In the adult brain, most NSCs exist in a quiescent state and must activate to generate new neural progeny. Understanding how NSCs balance quiescence and activation is crucial for the development of brain repair therapies. *Drosophila* NSCs, termed neuroblasts (NBs), are a model to study reactivation from quiescence. The Hippo and Insulin pathways were reported to promote NB quiescence and reactivation, respectively. However, the underlying mechanisms are not fully understood. This thesis describes my investigation of Monopolar spindle-one-binder 4 (Mob4), a member of the highly conserved Striatin-Interacting Phosphatase and Kinases (STRIPAK) complex, identified by our laboratory in a transcriptome analysis comparing quiescent and reactivating NBs. I show that Mob4 is upregulated in reactivating NBs, and its loss prevents NB reactivation. Mob4 overexpression accelerates reactivation, which can be mimicked by human MOB4 expression, suggesting a conserved function. I provide evidence that Mob4 acts primarily cell-autonomously in pNBs and demonstrate that inactivation or activation of Hippo and Insulin signalling, respectively, in mob4 pNBs can restore reactivation. Finally, I show that Mob4 cooperates with another STRIPAK member, Cka, to promote pNB reactivation, whereas PP2A phosphatase with its regulatory subunit Widerborst maintains NB quiescence. My results, together with data from our group, lead to a model whereby Mob4 and other STRIPAK members assist the coordination of Insulin and Hippo pathways to promote NB reactivation. Given the evolutionary conservation of the molecules investigated, my findings may also be relevant to mammalian NSCs and other stem cells.

## CONTENTS

## LIST OF FIGURES

## LIST OF TABLES

## LIST OF ABBREVIATIONS

| | |
|---|---|
| A.A | Amino Acid |
| ALH | After Larval Hatching |
| ana | anachronism |
| aNSC | Adult Neural Stem Cell |
| Antp | Antennapedia |
| APKC | Atypical Protein Kinase C |
| ASCL1 | Achaete-Scute Homolog 1 |
| Ase | Asense |
| Ban | Bantam |
| Baz | Bazooka |
| BBB | Blood-Brain Barrier |
| b-HLH | Basic Helix-Loop-Helix |
| BMP | Bone Morphogenetic Protein |
| Bp | Base Pair |
| Brat | Brain Tumour |
| Brdu | Bromodeoxyuridine |
| BV | Blood Vessels |
| Cas | Castor |
| CB | Central Brain |
| CCM3 | Cerebral Cavernous Malformations 3 |
| CD8-GFP | Membrane-Bound Green Fluorescent Protein |
| ChIP | Chromatin immunoprecipitation |
| Chro | Chromator |
| Cka | Connector Of Kinase To AP-1 |
| CLK | CLOCK |
| CNS | Central Nervous System |
| CNTR | Control |
| Co-IP | Co-immunoprecipitation |
| CRL4 | Cullin4-RING |
| CSF | Cerebral Spinal Fluid |
| Cul4 | Cullin4 |
| CYC | CYCLE |
| DCX+ | Double Cortin Positive |
| DDB1 | Damaged DNA-Binding Protein 1 |
| DG | Dentate Gyrus |
| DILP | *Drosophila* Insulin-Like Peptides |
| Dll1 | Delta-Like 1 |
| DNA | Deoxyribonucleic acid |
| Dpn | Deadpan |
| East | Enhanced Adult Sensory Threshold |
| ECL | Enhanced chemiluminescence |
| Edu | 5-Ethynyl-2'-Deoxyuridine |
| ERK | Extracellular Signal-Regulated Kinases |
| Eve | Even-skipped |
| EZ | Ependymal Zone |

| | |
|---|---|
| FACS | Fluorescence-Activated Cell Sorting |
| FB | Fat Body |
| FDS | Fat Body-Derived Signal |
| FGFR1OP2 | Fibroblast Growth Factor Oncogene Partner 2 |
| FMRP | Fragile X Protein |
| Foxo | Forkhead Box O3 |
| FUCCI | Fluorescent Ubiquitination-Based Cell Cycle Indicator |
| GABA | Gamma-Aminobutyric Acid |
| GCK | Germinal Centre Kinase |
| GCL | Granule Cell Layer |
| GCL | Granule Cell Layer |
| GFAP | Glial Fibrillary Acidic Protein |
| GFP | Green Fluorescent Protein |
| GMC | Ganglion Mother Cell |
| GO | Gene Ontology |
| Grh | Grainyhead |
| H | Hour |
| Hb | Hunchback |
| Hes1 | Enhancer Of Split 1 |
| Hpo | Hippo |
| HRP | Horse Radish Peroxidase |
| Hsp83/ Hsp90 | Heat Shock Protein 83 |
| IGF | Insulin-Like Growth Factor |
| ILP | Insulin-Like Peptides |
| INP | Intermediate Neural Progenitor |
| InR | Insulin-Like Receptor |
| Insc | Inscuteable |
| IPC | Intermediate Progenitor Cell |
| JNK | C-Jun N-Terminal Kinases |
| Kr | Kruppel |
| Mahj | Mahjong |
| MAPK | Mitogen-Activated Protein Kinase |
| mbNB | Mushroom Body Nbs |
| Mfge8 | Milk Fat Globule-Epidermal Growth Factor |
| ML | Molecular Layer |
| Mob4 | Monopolar Spindle-One-Binder 4 |
| mRNA | Messenger RNA |
| Msn | Misshapen |
| Mst1/2 | Mammalian Hippo Kinase |
| Mts | Microtubule Star |
| Mud | Mushroom Body Defect |
| N.R | Nutrition Restrictino |
| NB | Neuroblasts |
| NDR | Nuclear Dbf2-Related |
| NEP | Neuroepithelial Progenitors |
| NFIX | Nuclear Factor One Family Member |
| NRP | Non-Radial-Precursors |

| | |
|---|---|
| NS | Non-Significant |
| NSC | Neural Stem Cells |
| NT-3 | Neurotrophin-3 |
| OB | Olfactory Bulb |
| OL | Optic Lobe |
| P-AKT | Phosphorylated-AKT |
| PBS | Phosphate Buffered Saline |
| PCNA | Proliferating Cell Nuclear Antigen |
| PCR | Polymerase Chain Reaction |
| Pdm | Pou Domain 2 |
| PH3 | Phospho-Histone H3 |
| PH-GFP | Pleckstrin Homology Domain-GFP Fusion Protein |
| PH-Like | Pleckstrin Homology-Like |
| PI3K | Phosphatidylinositol 3-Kinase |
| Pins | Partner Of Inscuteable |
| pNB | Postembryonic Neuroblasts |
| Pnt | Pointed P1 |
| Pon | Partner Of Numb |
| PP2A | Protein Phosphatase 2A |
| PRC2 | Complex Polycomb Repressor Complex 2 |
| Pros | Prospero |
| Pros1 | Protein S |
| qaNSC | Quiescent Adult Neural Stem Cells |
| Repo | Reversed Polarity |
| REST | Repressor Element 1-Silencing Transcription |
| RGL | Radial Glial Cell |
| RGL | Radial Glia-Like |
| RHEB | Ras Homologue Enriched In Brain |
| RMS | Rostral Migratory Stream |
| RNA | Ribonucleic Acid |
| ROC | RING Of Cullin |
| RT-QPCR | Real-Time Quantitative Polymerase Chain Reaction |
| Sav | Salvador |
| SDS | Sodium dodecyl sulphate |
| SEM | Standard Error of the Mean |
| SG2NA | S/G2 Nuclear Autoantigen |
| SGZ | Subgranular Zone |
| SIKE1 | Suppressor Of IKBKE 1 |
| SIRT1 | Sirtuin 1 |
| Slif | Slimfast |
| SLMAP | Sarcolemmal Membrane-Associated Protein |
| Sox-2 | Sex Determining Region Y-Box 2 |
| Strip1/2 | STRN-Interacting Protein 1/2 |
| STRIPAK | Striatin-Interacting Phosphatase And Kinases |
| STRN | Striatin |
| SVZ | Subventricular Zone |
| TACs | Transient Amplifying Cells |

| | |
|---|---|
| Tara | Taranis |
| TBS | Tris Buffered Saline |
| TBST | Tris buffered saline containing Tween-20 |
| Tcs1/2 | Tuberous Sclerosis Complex 1 And 2 |
| TEMED | Tetramethylethylenediamine |
| TLX | Orphan-Nuclear Receptor |
| TOR | Target Of Rapamycin |
| Trol | Terribly Reduced Optic Lobes |
| Tws | Twins |
| UAS | Upstream Activation Sequence |
| VCAM1 | Vascular Cell Adhesion Molecule-1 |
| VEGF | Vascular Endothelial Growth Factor |
| VNC | Ventral Nerve Cord |
| VS | Ventricular Space |
| Wdb | Widerborst |
| *wdb*-DN | Dominant Negative widerborst |
| Wrd | Well Rounded |
| WT | Wild-Type |
| Wts | Warts |
| Yki | Yorkie |

# CHAPTER 1

# INTRODUCTION

## 1.1. Neural stem cells, the progenitors of the central nervous system

Stem cells are multipotent, self-renewing cells capable of making differentiated progeny, providing a homeostatic function to the tissue in which they reside (Li and Clevers, 2010; Cheung and Rando, 2013). Neural Stem Cells (NSCs) are the progenitor cells of the central nervous system (CNS), defined by their ability to self-renew and generate further committed progeny, such as neurons and glia (astrocytes and oligodendrocytes). It is the NSCs which are responsible for generating the enormous cell number and diversity of neural tissue which animals rely on for CNS functions including learn- ing, memory formation and plasticity (Blau *et al.,* 2001; Sahay *et al.,* 2011; Spalding *et al.,* 2013; Eichenbaum, 2004). Thus, it is imperative that the correct type and number of these cells are generated at the correct time points (Cheung and Rando, 2013). Understanding the mechanisms controlling NSCs which are affected by various physiological and environmental factors could be the leading avenue for the development of new therapies against a variety of brain disorders.

The process by which NSCs generate new neural cells is called neurogenesis (Altman,1962). NSCs exist during embryonic development and adulthood. Embryonic NSCs are multipotent and generate multiple subtypes of neural cells. The earliest NSCs are called neuroepithelial progenitors (NEPs) and, in vertebrates, these reside in the neural tube, which arises from the neuroectoderm during embryogenesis. NEPs give rise to NSCs in a spatially and temporally controlled manner (Temple, 2001; Alvarez-Buylla *et al.,* 2009). NEPs initially undergo symmetric division to expand the NSC pool, but later switch to asymmetric divisions to self-renew and give rise to a post-mitotic neuron or an intermediate progenitor cell (IPC) (Temple, 2001; Mori *et al.,* 2005; Kriegstein and Alvarez-Buylla, 2009; Anthony *et al.,* 2004). During this time, the embryonic NSCs acquire astrocyte-like properties and are termed radial glial cells (RGCs), based on their radial processes and morphological resemblance to astrocytes (Mori *et al.,* 2005). IPCs, located in the subventricular zone (SVZ), eventually generate a pair of post-mitotic neurons via symmetrical division (Noctor *et al.,* 2004). The

neurons generated migrate vast distances in the developing cortex using RGCs as contacts or scaffolds (Kriegstein and Alvarez-Buylla, 2009). RGCs and IPCs become a significant source of neural cells; RGCs expand the cortex tangentially, and IPCs fill the cortical layers radially to create the functional CNS. The CNS generated during embryogenesis was thought to be complete and therefore last an adult mammalians' lifetime, incapable of generating new neural tissue for regeneration or repair (Ramón y Cajal, 1909). However, this was overturned by a growing body of evidence showing multipotent NSCs within distinct niches of the adult mammalian CNS (Reynolds and Weiss, 1992; Richards *et al.,* 1992; Gage and Fisher, 1995; Eriksson *et al.,* 1998; Gould *et al.,* 1999a; Gould *et al.,* 1999b; Fuentealba *et al*., 2012; Fuentealba *et al.,* 2015).

## 1.2. Adult NSCs and neurogenesis in mammals

Adult neurogenesis is the formation, maturation and integration of new neurons into the existing circuitry. It was previously believed that the mammalian brain lacked adult neurogenesis and was, therefore, incapable of regeneration or repair (Ramón y Cajal, 1909). However, in the 1960s, Joseph Altman discovered the first evidence of adult neurogenesis - the source of adult-born olfactory neurons, in adult rat and guinea pig brains using 3H-thymidine autoradiography (Altman, 1962; Altman, 1963; Altman, 1969). In the 1990s, adult neurogenesis was demonstrated *in-vitro* using mammalian NSCs (Reynolds and Weiss, 1992) and in the adult rat brain (Gage and Fisher, 1995). The excitement was propagated by evidence of adult neurogenesis obtained in the human brain using bromodeoxyuridine (BrdU) and specific neuronal markers such as NeuN (Eriksson *et al.,* 1998). One year later, Elizabeth Gould showed that neurogenesis contributes to the adult macaque neocortex (Gould *et al.,* 1999). Due to the growing body of evidence, neurogenesis in humans is now generally acknowledged (Abdissa, 2020).

Unlike embryonic NSCs, which are the highly proliferative, adult NSCs (aNSCs) have been shown in mammalian models to be mostly quiescent and restricted to only a few neurogenic regions. Most notably are the subgranular zone (SGZ) of the hippocampal dentate gyrus (DG), and the subventricular zone (SVZ) lining the lateral ventricles (**Figure 1.A**). Both regions contain an environment or 'niche' which provides a tightly

controlled microenvironment to regulate the residing aNSCs. Two non-canonical sites of adult neurogenesis have also been reported in the striatum and the hypothalamus (**Figure 1.A**).

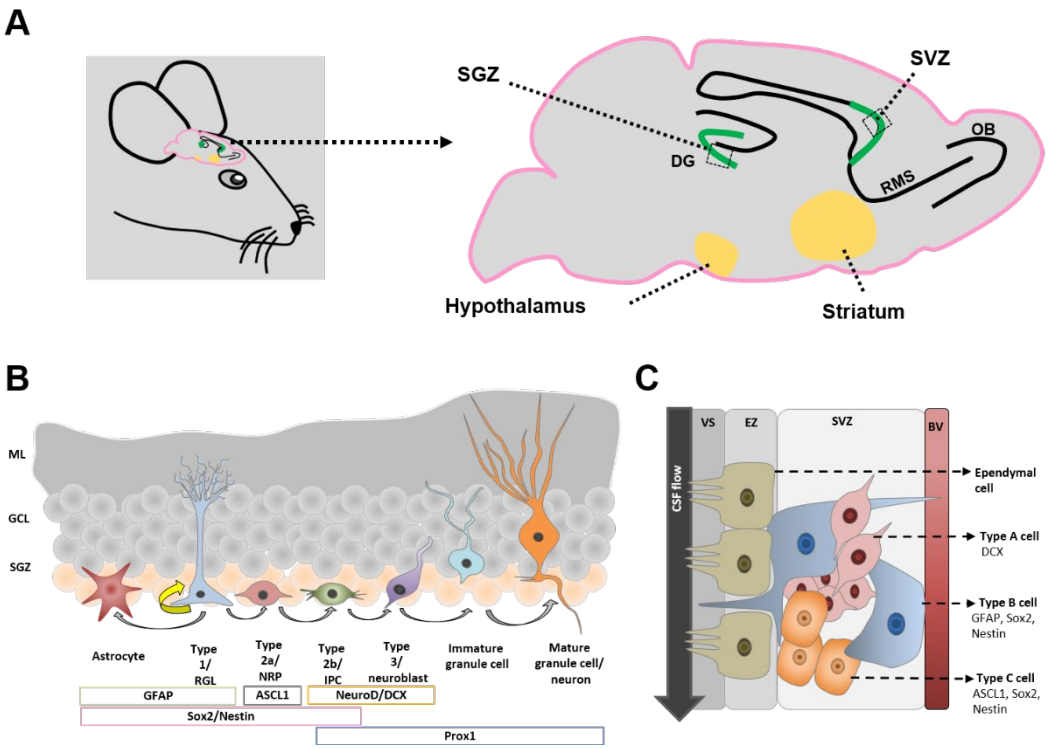


**Figure 1.1. Mammalian neurogenic regions and NSC lineages.** A. A schematic representation of a mouse brain with the neurogenic regions outlined. Neurogenesis in the subgranular zone (SGZ) of the hippocampus produces mature granule neurons for the dentate gyrus (DG). Neurogenesis in the subventricular zone (SVZ) produces neuroblasts which migrate through the rostral migratory stream (RMS) to the olfactory bulb (OB). The SGZ and the SVZ are known as classical neurogenesis regions. Two non-canonical sites of neurogenesis are the hypothalamus and the Striatum. **B.** The SGZ NSC lineages and **C.** the SVZ NSC lineages and common markers used to distinguish them. Molecular layer (ML); Granule cell layer (GCL); Radial glial cell (RGL); Glial fibrillary acidic protein (GFAP); Achaete-scute homolog 1 (ASCL1); Sex determining region y-box 2 (Sox-2); Neuronal Differentiation (NeuroD); Doublecortin (DCX); Prospero homeobox 1 (Prox1); Intermediate progenitor cell (IPC); Cerebral spinal fluid (CSF); Ependymal Zone (EZ); blood vessels (BV).

### 1.2.1. aNSCs in the hippocampus

In mammalian adult brain models such as in mice and rats, aNSCs in the SGZ of the hippocampus generate mature granule cells of the DG (**Figure 1.1. A**), an area critical for learning and memory (Song *et al.,* 2012a). The DG of the hippocampus has three distinct layers; the molecular layer, the granule layer and the SGZ (**Figure 1.1. B**).

Three types of aNSCs exist in the dentate gyrus: self-renewing 'Type 1 NSCs'; 'Type 2' amplification cells; and migratory 'Type 3 cells/neuroblasts' which give rise to granule cells/neurons. In the DG, aNSCs follow a characterised, multistep lineage development and are identifiable by a subset of temporally expressed markers (summarised in **Figure 1.1. B**). 'Type 1'/Radial glia-like (RGL) NSCs resemble RGCs of the embryonic brain and reside at the border of the granulate layer. These cells usually exist in a quiescent (G0) state and rarely divide, favouring asymmetric division if they are activated (Kemperman, 2011). They extend an elongated radial process through the granule cell layer (GCL) to the molecular layer (ML) and have a cilium in contact with blood vessels and cerebrospinal fluid (Kemperman, 2004). Two populations of Type 1 NSCs exist in the hippocampus. Both populations express Sex determining region y-box 2 (Sox-2), but one is a quiescent RGL population expressing Nestin and Glial fibrillary acidic protein (GFAP); and another population, of non-radial glia-like cells, are more proliferative (active) and lack radial-glia-like markers (Suh *et al.,* 2007). RGL NSCs give rise to two 'Type 2' intermediate progenitor cell (IPC) subgroups: Type 2a/non-radial- precursors (NRPs) express Achaete-scute homolog 1 (ASCL1); Type 2b/intermediate progenitor cells (IPCs) do not express ASCL1 and are further committed. After a limited round of division, Type 2b IPCs exit the cell cycle and terminally differentiate into astrocytes and neurons (Ming and Song, 2011; Bonaguidi *et al*., 2011). Both Type 2 populations are relatively active, have limited divisions, demonstrate short processes and differentially express migration and neuronal markers (Kempermann *et al.,* 2004; Encinas *et al.,* 2011). Type 3 cells/neuroblasts tangentially migrate through the SGZ, lack previous lineage markers (Nestin, Sox2, GFAP) and express Neuronal Differentiation 1 (NeuroD) and Prospero Homeobox 1 (Prox1) to give rise to immature granule cells/neurons. The immature granule cells/neurons migrate radially into the GCL, mature and differentiate into dentate granular cells/neurons. After 7-8 weeks, they integrate into the hippocampal circuitry (Göritz and Frisén, 2012; Jessberger and Kempermann, 2003) and contribute to hippocampus-associated learning/memory (Kempermann *et al.,* 2015). It has been estimated that the young rat hippocampus produces approximately 9000 new cells every day (Cameron and McKay, 2001), with ~30% of these cells (~800) thought to survive past four weeks and develop dendritic and axonal structures required for proper functioning (Snyder and Cameron *et al.,* 2009; Sailor *et al*., 2017; Sun and Song *et al.,* 2013). Defects in hippocampal neurogenesis are linked to brain-related

disorders, for example, depression, impaired spatial learning and memory, pattern separation and mood regulation (Clelland *et al.,* 2009; Hill *et al.,* 2015; Lee *et al*., 2013; Anacker, 2014; Anacker and Hen, 2017; Apple *et al.,* 2017; Oppenheim, 2019).

### 1.2.2. aNSCs in the subventricular zone

The subventricular zone (SVZ) is located next to the lateral ventricles and is the largest germinal region in the adult brain (Obernier and Alvarez-Buylla, 2019; Lim and Alvarez-Buylla, 1999; Doetsch *et al.,* 1999). The SVZ is a thin layer of proliferating cells located along the ependymal cell layer/zone (EZ), which separates the ventricular space (VS) from the SVZ (**Figure 1.1. C**); at the edge of the striatum (**Figure 1.1. C**). SVZ aNSCs arise from striatal radial glia and function to continually give rise to oligodendrocytes, astrocytes and olfactory bulb (OB, in rodents) or striatal interneurons (in humans) (Lim and Alvarez-Buylla, 2016; Obernier and Alvarez-Buylla, 2019; Ming and Song, 2016). Overall, the SVZ contains four cell types: Type B/RGL cells (NSCs); Type C/transient amplifying cells (TACs); Type A cells/neuroblasts, and multiciliated ependymal cells, which produce and circulate cerebral spinal fluid (CSF), essential for the niche (**Figure 1.1. C**).

Type B/RGL NSCs have a radial/astrocyte-like morphology, extend an apical process with a primary cilium through the EZ and into the VS, and a basal process which terminates on the blood vessels (BVs) (Mirzadeh *et al.,* 2008). Type B/RGL NSCs of the SVZ express stem cells markers such as GFAP, Nestin and Sox2 (Liu *et al.,* 2006; Zhang and Jiao, 2015). Type B/RGL NSCs are not described as quiescent but do divide slowly to produce highly proliferative type C/TACs (Doetsch *et al.,* 1999; Zhang and Jiao, 2015), also known as the progenitors of the SVZ. The Type C/TACs lack GFAP expression but do express Nestin, Sox2 and ASCL1 (Kempermann, 2011; Zhang and Jiao, 2015). After multiple rounds of divisions, TACs become Double cortin positive (DCX+) type A cells/neuroblasts. These neuroblasts form a chain and migrate radially along the rostral migratory stream (RMS) to the olfactory bulb (OB), and differentiate into dopamine and GABA-producing interneurons that integrate into the OB circuitry (Ming and Song, 2011; Zhu *et al.,* 2018). The OB receives an estimated 30,000 new neuroblasts every day (Lois and Alvarez, 1994), with ~40% of these cells (12,000) surviving past four weeks and effectively integrating into the

circuitry (Mouret *et al.,* 2008). SVZ neurogenesis is linked to olfactory function and learning (Lledo *et al.,* 2006; Bragado *et al.,* 2019), and decreased SVZ neurogenesis causes impaired odour discrimination (Valley *et al.,* 2009; Sahay *et al.,* 2011). SVZ proliferation and differentiation are altered in response to stroke/ ischemia, whereby SVS aNSCs and neuroblasts are redirected to the injury site and can directly or indirectly generate the appropriate neural cells towards attempt repair (Arvidsson *et al.,* 2002; Zhang *et al.,* 2004; Zhang *et al.,* 2008b; Faiz *et al.,* 2015). Reduced SVZ neurogenesis is linked to neurodegenerative diseases in rodents (Curtis *et al.,* 2007b; Rodríguez and Verkhratsky, 2011; Winner and Winkler, 2015; Scopa *et al.,* 2019; Sung *et al.,* 2020).

### 1.2.3. Non-canonical adult NSC niches: striatum and hypothalamus

The striatum is located in the subcortical basal ganglia of the forebrain and is a significant input area for the basal ganglia and critical to the reward system (**Figure 1.1. A**). Local astrocytes in the mouse striatum can produce new neurons in response to stroke (Magnusson *et al.,* 2014). Striatal adult neurogenesis has been observed in adult humans (Bergmann *et al.,* 2012; Ernst *et al.,* 2014; Wang, C. *et al.,* 2014; Wang *et al.,* 2011), where it continually gives rise to interneurons (Ernst *et al.,* 2014); and neuroblasts in the SVZ are observed to migrate to the striatum in humans (Ernst *et al.,* 2014). The striatum is associated with motor function, cognitive flexibility, cognitive function and, more recently, schizophrenia pathology (Simpson *et al.,* 2010; Ernst and Frisén, 2015). Impaired striatal neurogenesis is observed in patients with Parkinson's disease (Ernst *et al.,* 2014); the striatal cell death found is thought to induce SVZ growth to aid migration via the caudate nucleus (Curtis *et al.,* 2007a). However, as decreased neuronal production has been observed in Parkinson's disease patients, it suggests that the increased neuronal migration is insufficient to replenish the lost neurons (Ernst *et al.,* 2014). Also, the striatum is associated with Huntington's disease, whereby striatal adult-born neurons are selectively depleted (Ernst *et al.,* 2014). Although there are currently fewer studies on striatal neurogenesis compared to other neurogenic regions, there is growing evidence for its importance.

Most recently, adult neurogenesis has also been observed in the hypothalamus, a small area and the organisms' homeostatic regulator (**Figure 1.1. A**). It was first shown

that cells from the hypothalamic VZ could generate neurospheres *in-vitro* (Weiss *et al.,* 1996). Later it was reported that the tanycytes (hypothalamic RGCs) function as neural precursors (Robins *et al.,* 2013; Xu *et al.,* 2005; Haan *et al.,* 2013; Lee *et al.,* 2012). Tanycytes resemble embryonic neural progenitors and are exposed to CSF (Bolborea and Dale, 2013; Rodríguez *et al.,* 2005). They extend one or two apical cilia into the VZ and a long basal process into the parenchyma or pial surface, depending on location. Much like the NSCs in the SVZ and SGZ, tanycytes are reportedly influenced by diet and also regulate weight gain (Niwa *et al.,* 2016; Lee *et al*., 2014; Whalley, 2012); hypothalamic adult neurogenesis helps regulate body weight and energy balance by replacing degenerated neurons (Pierce and Xu, 2010; McNay *et al.,* 2012). Overall levels of hypothalamic adult-born neurons are low compared to the other neurogenic niches (Lee and Blackshaw, 2014), which adds difficulty in exploring the functional significance of hypothalamus neurogenesis.

It is becoming clear that adult neurogenesis in areas of the mammalian brain, canonical and non-canonical, offer advantages; and its deregulation is associated with cognitive disadvantages. How exactly adult neurogenesis is achieved, the pathways and regulators involved, and therapeutic advantages are significant questions in stem cell biology.

### 1.3. Quiescence and activation of aNSCs

Mammalian aNSCs interconvert between actively proliferating and temporary quiescent states. The transition is regulated by a variety of extrinsic and intrinsic cues, which we are only beginning to understand (Basak *et al.,* 2012; Basak *et al.,* 2014; Basak *et al.,* 2018; Costa *et al.,* 2011; Giachino *et al.,* 2014; Ziebell *et al.,* 2018; Velthoven and Rando, 2019; Morales and Mira, 2019; Mohammad *et al*., 2019). Below, I describe some of the key literature contributing to our current knowledge of aNSC quiescence and activation.

#### 1.3.1 aNSCs are actively maintained in cellular quiescence but can reactivate in response to appropriate signals

Quiescence is a highly conserved, reversible cell cycle arrested state. Most of our knowledge on cell quiescence comes from *Saccharomyces cerevisiae, Schizo-saccharomyces pombe,* and *Escherichia coli* (Werner-Washburne *et al.,* 1993; Lillie

and Pringle, 1980). Stem cell quiescence is conserved in mammals across various tissues such as skin, gut and brain and all share commonalities: decreased transcription of cell-cycle progression genes increased expression of genes involved in suppressing apoptosis, differentiation and senescence, a decreased cell size, stress resistance, condensed chromosomes and elevated autophagy (Cho *et al.,* 2019; Velthoven and Rando, 2019). The quiescent state was first observed *in-vitro* in 1951 and later observed in unicellular and multicellular organisms (Dubrovsky, 2003; Velthoven and Rando, 2019; Howard and Pelc, 1986). In mammals, during G1, before committing to mitosis, somatic cells may withdraw from replication and enter quiescence (Pardee, 1974). Quiescent aNSCs (qaNSCs) only rarely divide, making them challenging to label using lineage-tracing methods labelling dividing cells only. Quiescence allows increased longevity, tolerance to metabolic stress, and ultimately acts to preserve the stem cell pool, maintaining tissue homeostasis. Previously, quiescent NSCs were thought to exhibit little activity; however, it is now regarded as an actively 'restrained' state. These 'poised' quiescent somatic cells are ready for activation in response to appropriate stimuli to regenerate tissue. Cell-extrinsic stimuli such as nutrition, exercise, stress, and cell-intrinsic epigenetic, transcriptional and post-transcriptional mechanisms regulate quiescence (Cheung and Rando, 2013).

The heterogeneity and dynamics of aNSCs populations have made qaNSCs challenging to study. Quiescence was previously assumed based on low RNA levels, poor label-retaining ability and lack of proliferation markers such as Proliferating cell nuclear antigen (PCNA), Ki67 and phospho-histone H3 (PH3). The last decade has provided technology to study qaNSCs such as *in-vivo* imaging, clonal lineage tracing, fluorescence-activated cell sorting (FACS), whereby subpopulations of aNSCs can be purified and subjected to a microarray, and single-cell RNA sequencing (Ming and Song, 2014; Bonaguidi *et al.,* 2011; Shin *et al.,* 2015; Marcy, G. and Raineteau, 2019). The advancement has allowed a single-cell transcriptomic analysis of qaNSCs and activated aNSCs cells at population and cell level. Multiple studies show that aNSCs (RGLs) are actively maintained in quiescence (Codega *et al.,* 2014; Llorens-Bobadilla *et al.,* 2015; Dulken *et al.,* 2017; Velthoven and Rando, 2019). Mammalian qaNSCs can be identified by specific markers such as GFAP, Sox2, and Nestin. They appear smaller in size with a more radial morphology and favour glycolytic and lipid metabolism compared to active NSCs (Alvarez-Buylla *et al.,* 2001; Llorens-Bobadilla

*et al.,* 2015; Shin *et al.,* 2015; Renault *et al.,* 2009). Interestingly, most aNSCs exist primarily in a quiescent state (Codega *et al.,* 2014; Llorens-Bobadilla *et al.,* 2015).

aNSC quiescence is described to enhance stress resistance, defends against deleterious gene mutations and exhaustion to secure the NSC pool (Urbán and Guillemot, 2014); it is therefore tightly regulated by extracellular and intracellular signals. The neurogenic niche communicates the needs of the organism to the qaNSCs, including via the vasculature and CSF, which are in contact with the NSC basal and apical processes, respectively. Extracellular receptor activation can lead to the activation of intrinsic factors such as signal transduction pathways, transcription pathways, metabolism and epigenetic modifications. These extrinsic/intrinsic mechanisms crosstalk and feedback on each other to modulate aNSC cellular activity within the neurogenic niche (Otsuki and Brand, 2017; Faigle and Song, 2013; Ming and Song, 2015; Tian *et al.,* 2018; Chaker *et al.,* 2016; Cavallucci *et al.,* 2016). Many studies describe the effects of molecules and signalling pathway that enhance neurogenesis and NSC proliferation in general., Below, I provide examples of molecules and pathways implicated in aNSC quiescence, specifically.

Notch signalling regulates tissue homeostasis and cell-fate determination throughout development. Direct cell-cell contact is required as the transmembrane Notch receptor is activated by binding to its neighbouring cell via Delta or Jagged ligands (Ables *et al.,* 2011). Notch regulates aNSCs by stimulating cell-cycle exit and decreasing the neural progenitor pool (Hitoshi *et al.,* 2002; Imayoshi *et al.,* 2010; Ehm *et al.,* 2010). Notch signalling has also been shown to maintain aNSCs in quiescence by repressing genes associated with the cell cycle and inhibiting differentiation (Ottone *et al.,* 2014; Engler *et al.,* 2018) and via the Delta-like 1 (Dll1) ligand as a homeostatic feedback mechanism (Kawaguchi *et al.,* 2013). Recently, a downstream target of the Notch pathway, *Id4*, was shown to maintain quiescence of hippocampal NSCs (Zhang *et al.,* 2019). Cell-cell contact is required for signalling pathways such as Notch, and cell adhesion molecules that help position NSCs, such as vascular cell adhesion molecule-1 (VCAM1) and the laminin receptor α6β1-integrin; support NSC quiescence (Kokovay *et al.,* 2012; Shen *et al.,* 2008).

Bone morphogenetic protein (BMPs) growth factors/BMP signalling has been shown

to regulate mammalian neurogenesis (Wang, R. *et al.,* 2014; Lim *et al.,* 2000; Bonaguidi *et al.,* 2008; Mira *et al.,* 2010; Ming and Song, 2015; Mira *et al.,* 2016; Joppé *et al.,* 2015; Morell *et al.,* 2015). BMP restricts proliferation; BMP inactivation was shown to promote aNSC proliferation but later caused decreased proliferation and production of new neurons (Mira *et al.,* 2016). However, this study partially contradicts other studies (Bonaguidi *et al.,* 2008; Gobeske *et al.,* 2009; Bond *et al*., 2012) which did not find any subsequent loss in NSC proliferation or new neuron production. Bonaguidi *et al.* showed that overexpressing the BMP antagonist, Noggin, gave rise to increased numbers of proliferative GFAP+ NSCs *in-vitro*, and in the mouse SGZ (Bonaguidi *et al.,* 2008). Interestingly, Noggin is secreted by ependymal cells and aids NSC activation (Lim *et al.,* 2000). Also, the anti-proliferative effects of BMP signalling are dominant over the pro-proliferative signalling molecule, EGF, *in-vitro* and *in-vivo* (Joppé *et al.,* 2015). Further studies are therefore needed to elucidate the function of BMP signalling on aNSCs.

Several transcription factors promote aNSC quiescence, for example, the Nuclear factor one (NFI) family member NFIX is expressed during aNSC quiescence, and activation, but is upregulated in quiescent aNSCs compared to activated aNSCs; NFIX directly activates quiescence-promoting genes, and loss of NFIX leads to a loss of aNSC quiescence (Martynoga *et al.,* 2013).

The Repressor Element 1-Silencing Transcription factor (REST) regulates unique aspects of neural development embryonically and postembryonically (Ballas *et al*., 2005; Mukherjee *et al*., 2016; Gao *et al*., 2011; Gao *et al.,* 2012). REST has been shown to bind and control the expression of different gene targets in a developmental and cell-context dependent fashion (Ballas *et al*., 2005; Mukherjee *et al*., 2016; Gao *et al*., 2011). REST is highly expressed in embryonic pluripotent stem cells (ES cells), and its expression decreases via post-translational degradation as these cells develop into NSCs. REST is completely transcriptionally repressed in mature neurons (Ballas *et al*., 2005). In the transition from pluripotent ES to NSCs, the expression of REST is thought to be just enough to maintain neuronal gene chromatin inactive, whereas as progenitors neural cells differentiate into neurons, REST together with its co-repressors dissociate from their DNA target binding sites, allowing activation of neuronal genes (Ballas *et al*., 2005). Postembryonically, REST is required to

maintain aNSC quiescence, and to prevent neurogenesis over time (Mukherjee *et al*., 2016; Gao *et al*., 2011). Mukherjee *et al.* found that conditional deletion of REST in adult mouse hippocampal quiescent aNSCs results in their premature mitotic activation. Furthermore, its deletion from adult neural progenitors (transient amplifying cells, TAPs) led to increased TAP proliferation as well as increased numbers of resulting immature and mature neurons. The authors concluded that REST deletion from TAPs activated the neuronal differentiation program (Mukherjee *et al*., 2016). The same laboratory team used genome-wide chromatin immunoprecipitation sequencing (ChIP-seq) and RNA-sequencing profiling to identify REST binding sites and targets, and found, not surprisingly, that many were neuronal genes (Mukherjee *et al*., 2016).

Furthermore, the transcription factor Forkhead Box O3 (FoxO) promotes aNSC quiescence; loss of FoxO leads to an initial rise in aNSC proliferation but an overall depletion of the stem cell pool (Paik *et al.,* 2009; Renault *et al.,* 2009; Santo and Paik, 2018). FoxO is inhibited by AKT, the downstream component of the conserved Insulin signalling/Insulin-like growth factor (IGF) pathway (Tzivion *et al*., 2011). Also, within this pathway, upstream of AKT is the phosphatase and tensin homolog (Pten) which is also required for NSC quiescence (Bonaguidi *et al.,* 2011). The tumour suppressor, Pten, maintains NSC quiescence by suppressing self-renewal and regulating the G0-G1 transition cell cycle entry; Pten depletion causes NSC activation from quiescence and depletion of the NSC pool (Bonaguidi *et al.,* 2011). In addition to Pten, other cell cycle regulators include the cyclin-dependant kinase inhibitors p27 and p57 which are expressed in non-dividing aNSCs and inhibit the cell cycle from maintaining the NSC pool; depletion of which leads to loss of NSC quiescence and increased neurogenesis (Andreu *et al.,* 2015; Furutachi *et al.,* 2013).

Some neurotransmitters are also known to promote aNSC quiescence. Gamma-aminobutyric acid (GABA) and its precursor glutamate create a negative feedback mechanism (Liu *et al.,* 2005) and promote quiescence by preventing aNSC-cycle progression (Fernando *et al.,* 2011); decreasing GABA signalling causes aNSCs to exit quiescence (Song *et al.,* 2012b). Pineda and colleagues found that using a GABA antagonist caused activation of quiescent NSCs (Pineda *et al.,* 2013). Vascular-derived growth factors also maintain NSC quiescence. The endothelial-

derived neurotrophin- 3 (NT-3) mediates quiescence; NT-3 mutant mice showed higher aNSCs proliferation and increased number of neural cells (Delgado *et al.,* 2014). Recently, Zhou *et al.* showed that Milk fat globule-epidermal growth factor (Mfge8), otherwise known as lactadherin, promotes quiescence via mTOR signalling and its deletion causes NSC depletion and decreases neurogenesis (Zhou *et al.,* 2018).

Lastly, the secreted glycoprotein Protein S (Pros1) maintains quiescence by mediating Notch expression and activity; loss of Pros1 in aNSCs leads to increased proliferation (Zelentsova-Levytskyi *et al.,* 2017). Interestingly, in *Pros1* knockout mice, the increase in aNSC proliferation leads to an enriched aNSC pool and does not lead to aNSC pool depletion up to one year of age (Zelentsova-Levytskyi *et al.,* 2016).

The mechanisms governing aNSC quiescence are still being elucidated. **Figure 1.2** summarises some of the known involved factors and molecular mechanisms mentioned above. Variable states (or levels) of quiescence have also been identified, suggesting there is a 'gradient' of quiescence from 'dormant' to 'primed' (Llorens-Bobadilla *et al.,* 2015). This has also been observed in other adult stem cell systems (Rodgers *et al.,* 2014; Malam *et al.,* 2014; Zismanov *et al.,* 2016). aNSCs may also differ in their ability to return to quiescence after initially activating (Urbán *et al.,* 2016). In this study, a 'resting' population and a 'dormant' population of qNSCs was described (Urbán *et al.,* 2016). The majority of the stem cells are 'dormant' and thought to have never divided, whereas the resting population are fewer in number and have previously activated but returned to quiescence; the latter pool is essential for adult neurogenesis (Urbán *et al.,* 2016).

There is increasing evidence of heterogenic populations of quiescent aNSCs. Contrary to the long-held belief that quiescent stem cells are arrested in the $G_0$ phase of the cell cycle, emerging evidence suggests NSCs can be arrested in $G_2$ and that the latter are more readily reactivated than NSCs in $G_0$ (Otsuki and Brand, 2018). Deregulation of quiescence or activation from quiescence can lead to impaired homeostasis. How precisely the NSCs are maintained in quiescence, as well as how they can be

activated are essential questions in stem cell biology with implications for therapeutic strategies, which remain to be fully elucidated.

### 1.3.2. Mitotic activation of quiescent aNSCs

aNSCs exit from quiescence and entry into an active proliferative state requires tight coordination between the extracellular signals from the neurogenic niche and intrinsic factors. For example, one of the vascular endothelial growth factor (VEGF) receptors are expressed by aNSCs; VEGF receptor activation causes activation from quiescence (Han *et al.,* 2015). Significant evidence shows a variety of external stimuli can modulate mammalian adult neurogenesis, and specifically the activation of aNSCs. For example, aNSCs were shown to become activated upon brain injury (Wang *et al.,* 2016; Chang *et al.,* 2016; Llorens-Bobadilla *et al.,* 2015), ischemia (Nakatomi *et al.,* 2002; Nemirovich-Danchenko and Khodanovich *et al.,* 2019), and medial temporal lobe epileptic seizures (Parent *et al.,* 1997). Although a great deal of literature exists surrounding the regulation of mammalian NSC proliferation and other stages of neurogenesis (Recently reviewed by Obernier and Alvarez-Buylla, 2019; Morales and Mira, 2019; Petrik and Encinas, 2019), there is less understanding about the process of NSC activation from quiescence specifically. The few factors that have been identified to regulate this process are described below.

One of the identified aNSC activators is the basic helix-loop-helix (bHLH) transcription factor, Achaete-scute-like 1 (ASCL1), also known as Mash1. ASCL1 is a mammalian proneural gene (Guillemot and Hassan, 2017; Guillemot, 2007) which has been associated with NSC activation in multiple studies (Llorens-Bobadilla *et al.,* 2015; Dulken *et al.,* 2017; Basak *et al.,* 2018). ASCL1 is required throughout mouse embryogenesis to promote neuronal fate and progenitor proliferation (Castro *et al.,* 2011; Bertrand *et al.,* 2002), and has been observed in the developing human neocortex suggesting a conserved function (Hansen *et al.,* 2010). Postembryonically, ASCL1 is famously required for NSC activation from quiescence and neurogenesis but is also expressed in quiescent NSCs, although at low levels (Anderson *et al.,* 2014). ASCL1 loss blocks quiescent NSC activation, the production of new neurons and causes a depletion of the stem cell pool (Anderson *et al.,* 2014). ASCL1 can also promote NSC cell-cycling by activating pro-proliferative genes such as Cyclin D1 (Castro *et al.,* 2011; Urbán *et al.,* 2016).

ASCL1 is regulated by Notch signalling; Notch inactivation causes ASCL1 upregulation (Anderson *et al.,* 2014). Hairy and enhancer of split 1 (Hes1), a transcriptional repressor and downstream target of the Notch pathway, inhibits ASCL1 in embryonic NSCs (Shimojo *et al.,* 2008; Imayoshi *et al.,* 2013) and adult mammalian NSCs (Sueda *et al.,* 2019). Sueda and colleagues showed that Hes1 expression oscillates in both quiescent and activated NSCs; however, more so during quiescence to subsequently periodically suppress ASCL1 expression (Sueda *et al.,* 2019). Hes1 levels were higher in quiescent NSCs compared to active NSCs. High Hes1 expression maintained adult NSC quiescence and oscillating ASCL1 expression controlled NSC activation, whereas continued ASCL1 expression controlled differentiation (Sueda *et al.,* 2019). Inactivating Hes1 lead to more ASCL1 expression and subsequent NSC activation from quiescence but also decreased overall neurogenesis (Sueda *et al.,* 2019).

ASCL1 is also controlled via post-translational modification by the ubiquitin ligase Huwe1 that stimulates ASCL1 degradation, causing more NSC activation from quiescence (Urbán *et al.,* 2016). Inactivating Huwe1 increases ASCL1 stability and causes the overproliferation of NSCs, which are unable to return to quiescence (Urbán *et al.,* 2016). In embryonic NSCs, both AKT (Oishi *et al.,* 2009) and cyclin-dependant kinases (Ali *et al.,* 2014) promote or inhibit ASCL1 function, respectively. Given the role of Insulin signalling in promoting adult neurogenesis, it would be interesting to investigate its activity upon ASCL1 and NSCs activation.

Another intrinsic regulator of NSC activation is the Orphan-Nuclear receptor (TLX), also known as Nr2e1 and Tailless, belongs to a family of intracellular transcription factors involved in embryonic patterning (Monaghan *et al.,* 1995). TLX is part of a superfamily of nuclear hormone receptors which recruit corepressors to cause transcriptional repression of target genes (Niu *et al.,* 2011; Wang and Xiong, 2016; Wang *et al.,* 2013). Although TLX is expressed during embryonic development, after initially declining, TLX expression later increases to peak within the adult mouse brain (Monaghan *et al.,* 1995). Postembryonically, TLX is expressed highly in the stem cells of neurogenic niches and maintains adult NSCs self-renewal capacity and its overexpression or deletion results in enhanced neurogenesis or reduced NSC

proliferation, respectively (Murai *et al.,* 2014; Shi *et al.,* 2004; Li *et al.,* 2012; Sobhan *et al.,* 2017; Zhang *et al.,* 2008a). TLX represses transcription of some of its target genes, for example, Pten and p21 (Niu *et al.,* 2011; Sun *et al.,* 2007), alternatively, it activates proneural gene transcription of ASCL1 (Elmi *et al.,* 2010). TLX has been shown to regulate the Wnt signalling pathway (Qu *et al.,* 2010) and be regulated by MicroRNA's such as microRNA-9 (Zhao *et al.,* 2009; Sun *et al.,* 2011). MicroRNA's are highly conserved short strands of non-coding RNA, which interfere with mRNAs via complementary base pairing that can lead to mRNA destabilisation (Fabian *et al.,* 2010). TLX was previously shown to be upregulated in activated NSCs, and NSCs in *tlx* mutant mice have cell-cycle entry and proliferation defects (Obernier *et al.,* 2011). Most recently, TLX was shown to negatively regulate transcription of the Notch effector, Hes1, in the mouse brain (Luque-Molina *et al.,* 2019). Elevated Hes1 levels and Notch signalling in *tlx* mutants lead to disrupted quiescence and the downregulation of ASCL1/Mash1 (Luque-Molina *et al.,* 2019).

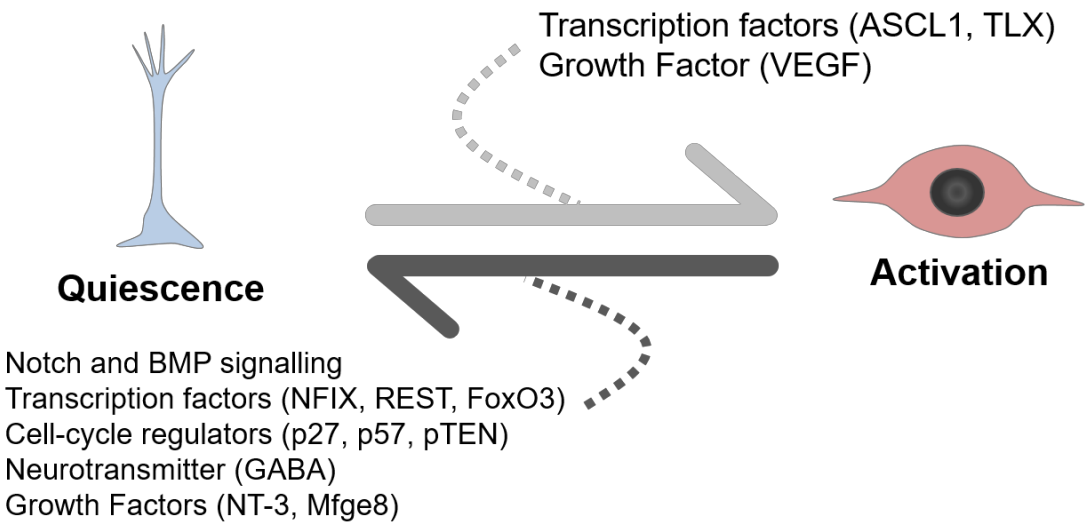


**Figure 1.2: Summary of factors known to regulate mammalian adult NSCs transit between quiescence and activation states.** Notch signalling maintains quiescence by repressing genes associated with the cell cycle and inhibiting differentiation (Sueda *et al.,* 2019; Ottone *et al.,* 2014; Engler *et al.,* 2018; Kawaguchi *et al.,* 2013; Zhang *et al.,* 2019). Vascular cell adhesion molecule-1 (VCAM1) and the laminin receptor α6β1-integrin help position aNSCs and support quiescence (Kokovay *et al.,* 2012; Shen *et al.,* 2008). Bone morphogenetic protein (BMP) is thought to support quiescence, as Noggin, a BMP inhibitor secreted by ependymal cells, aids NSC activation (Lim *et al.,* 2000; Martynoga *et al.,* 2013). Nuclear factor one (NFI) family member (NFIX) stimulates quiescence-promoting genes (Martynoga *et al.,* 2013). The transcription factor repressor element 1-silencing transcription (REST) inhibits proneural genes to support quiescence (Ballas *et al*., 2005; Mukherjee *et al*., 2016; Gao *et al*., 2011). The Forkhead Box O3 (FoxO); however, the mechanisms are not fully understood transcription factors (Paik *et al*., 2009; Renault *et al*., 2009; Santo and Paik, 2018). The phosphatase and tensin homolog (Pten) promotes quiescence by inhibiting self-renewal and the G0-G1 transition (Bonaguidi *et al.,* 2011). The neurotransmitter Gamma-aminobutyric acid (GABA) prevent NSC cell-cycle progression (Song *et al.,* 2012; Pineda *et al.,* 2013). Cell-cycle regulators such as the cyclin-dependant kinase inhibitors p27 and p57 (Andreu *et al.,* 2015; Furutachi *et al.,* 2013) and growth factors received from the niche such as the endothelial-derived neurotrophin- 3 (NT-3) (Delgado *et al.,* 2014), and the Milk fat globule-epidermal growth factor (Mfge8) (Zhou *et al.,* 2018) and promote NSC quiescence. Molecules regulating the activation of quiescent adult NSCs is far less known, the Vascular endothelial growth factor (VEGF) receptors (VEGF3) expressed on NSCs cause activation upon receptor activation (Han *et al.,* 2016). The basic helix-loop-helix (bHLH) transcription factor, Achaete-scute-like 1 (ASCL1) promotes activation from quiescence by promoting pro cell-cycle and proliferation genes and is regulated by Notch signalling and post-translationally by the ubiquitin ligase Huwe1 (Anderson *et al.,* 2014; Castro *et al.,* 2011; Urbán *et al.,* 2016; Llorens-Bobadilla *et al.,* 2015; Dulken *et al.,* 2017; Basak *et al.,* 2018). The Orphan-Nuclear receptor (TLX) promotes activation of quiescent NSCs by promoting ASCL1, NSC self-renewal, and repressing quiescence-promoting genes such as pTen and p21 (Luque-Molina *et al.,* 2019; Obernier *et al.,* 2011; Yu *et al.,* 1994; Monaghan *et al.,* 1995; Wang *et al.,* 2006; Zhang *et al.,* 2006; Sun *et al.,* 2007; Yokoyama *et al.,* 2008).

### 1.4. *Drosophila melanogaster*, a model organism in neurobiology

The fruit fly *Drosophila melanogaster* is a model organism that has been extensively used in neurobiology studies, including postembryonic neurogenesis (Ramon-Cañellas *et al.,* 2019; Doe, 2017; Harding and White, 2017; Sullivan, 2019). The benefits of *Drosophila* as a model include a short life cycle of approximately 11 days at 25°C, cost-effectiveness compared to other models such as mice, highly fecund and, most importantly, *Drosophila* shares over 70% disease gene sequences with humans (Reiter *et al.,* 2001).

Moreover, there is a vast genetic toolkit available for easier gene manipulation, and, significantly for my work, one can study NSCs at a single-cell resolution in vivo (Schnorrenberg *et al.,* 2016; Jeibmann and Paulus, 2009; Pandey and Nichols, 2011). One of the key gene manipulation techniques used with *Drosophila* is the UAS-GAL4 system, a genetic tool allowing targeted gene expression (Brand and Perrimon 1993; Elliott and Brand, 2008). Since its establishment, the UAS/GAL4 system has been widely used, modified and expanded to allow for more specific temporal and spatial control of targeted gene expression. For example, it can be used for a variety of loss and gain of function assays, employed simultaneously with other independent expression systems such as LexA/LexAop allowing additional manipulation, and depending on the system's reporters, it can inform on a variety of parameters including visualisation of cells and their organelles, cell activity status and behaviour (Caygill and Brand, 2016).

In its simplest form, the UAS/GAL4 system is based on a driver and a responder fly line. A transgenic fly line will contain a desired promoter gene region fused to the yeast transcriptional activator GAL4 - the 'driver line'. The latter must be crossed with a transgenic fly line containing a gene region of interest fused to an Upstream Activation Sequence (UAS), to which the GAL4 protein specifically binds, and is known as the 'responder line'. GAL4 only activates transcription when bound to its UAS promoter sequence. For example, an NSC-GAL4 'driver line' will only drive the expression of transgenes under the control of an Upstream Activation Sequence (UAS) promoter, such as UAS-Green Fluorescent Protein (GFP). Thus, when the transgenic driver and responder flies are crossed, their progeny will express the gene sequence of interest

(GFP) in the tissue pattern directed by the desired promoter (NSCs). In my studies, I took advantage of *Drosophila* as a model and extensively used the UAS/GAL4 system in the assays performed.

### 1.1.1. *Drosophila* embryonic NBs generate the functional larval CNS

NSCs in *Drosophila* are termed neuroblasts (NBs), the progenitors to the CNS neurons and glia. *Drosophila* NBs divide asymmetrically to self-renew and generate further committed progeny. Like mammalian neurogenesis, *Drosophila* neurogenesis is controlled by intrinsic programs and extrinsic stimuli (Doe, 2017; Harding and White, 2017). Yet, the *Drosophila* CNS offers a simpler model system to investigate conserved mechanisms. Neurogenesis in *Drosophila* occurs embryonically producing the larval CNS and ~ 10% of the adult fly CNS, and postembryonically producing the majority of the adult fly CNS (Prokop and Technau, 1991; Truman and Bate, 1988; Doe, 2017; Harding and White, 2017). The two neurogenic waves are separated by a period of cellular quiescence (**Figure 1.3.A**) (White and Kankel, 1978; Truman and Bate, 1988; Maurange *et al.,* 2008).

Depending on their location, NBs are referred to as being thoracic, abdominal, central brain (CB) and optic lobe (OL). During embryogenesis, *Drosophila* NBs delaminate from the neuroectodermal cells (Bossing *et al.,* 1996; Egger *et al.,* 2007). OL NBsare generated only postembryonically (Doe, 2017; Harding and White, 2017). Delamination and NB identity are specified by Notch-mediated lateral inhibition, members of the Sox family (*SoxN* and *Dicheate*) and the Snail family (*wornio*, *escargot* and *snail*) and subsequent expression of proneural genes (Ashraf, 2001; Harding and White, 2017). Neural diversity is achieved by spatial patterning and temporal patterning (Miyares and Lee, 2019; Doe, 2017; Harding and White, 2017). Spatial determination along the anterior-posterior axis is established by Hox genes: *abdominal*-A and *ultrabithorax* are differentially expressed between NBs to generate diverse neurons or glia (Prokop and Technau, 1994). The temporal transcription factors Hunchback (Hb), Kruppel (Kr), Pou domain 2 (Pdm), Castor (Cas), and Grainyhead (Grh) are sequentially expressed in NBs and their progeny to give rise to distinct cell types (Kambadur *et al.,* 1998; Doe, 2017; Harding and White, 2017).

The CNS is generated by around 1200 NBs found in the embryo (Bossing *et al.,* 1996; Schmidt *et al.,* 1997; Urbach *et al.,* 2003; Wheeler *et al.,* 2009; Birkholz *et al.,* 2015). To expand the embryonic CNS, each newly born embryonic NB begin limited rounds of asymmetric divisions, self-renewing and generating a smaller terminally differentiating ganglion mother cell (GMC). The NBs shrink with each division. Type 0 NBs do not produce a GMC (see below section **1.4.2.**) and are an exception (Karcavich and Doe, 2005; Ulvklo *et al.,* 2012; Baumgardt *et al.,* 2014). The GMCs produce neurons required by the larval CNS. Each NB generates a stereotyped family of neural progeny to the CNS (Bossing *et al.,* 1996). The post-mitotic neurons generated display a three-layered structure whereby Hb is detected in the deepest layer and Cas in the superficial layer, reminiscent of the developing mammalian cortex (Grieg *et al.,* 2013). Grh is the last factor expressed and persists into larval NBs, stimulating cell cycle progression and cell survival (Cenci and Gould, 2005). The NBs were reported to exit the cell cycle at around stage 16 of embryogenesis (**Figure 1.3.B**) either by programmed cell death (Maurange and Gould, 2005; Ulvklo *et al.,* 2012) or by entering cellular quiescence (Truman and Bate, 1988; Chell and Brand, 2010; Sousa-Nunes *et al.,* 2011). Recently, two types of NB quiescence, G2 and G0, were reported (Otsuki and Brand, 2018). Furthermore, at embryonic stage 17, thoracic NBs display both G2 and G0 quiescence, whereas abdominal NBs enter G0 quiescence or apoptose (Harding and White, 2019).

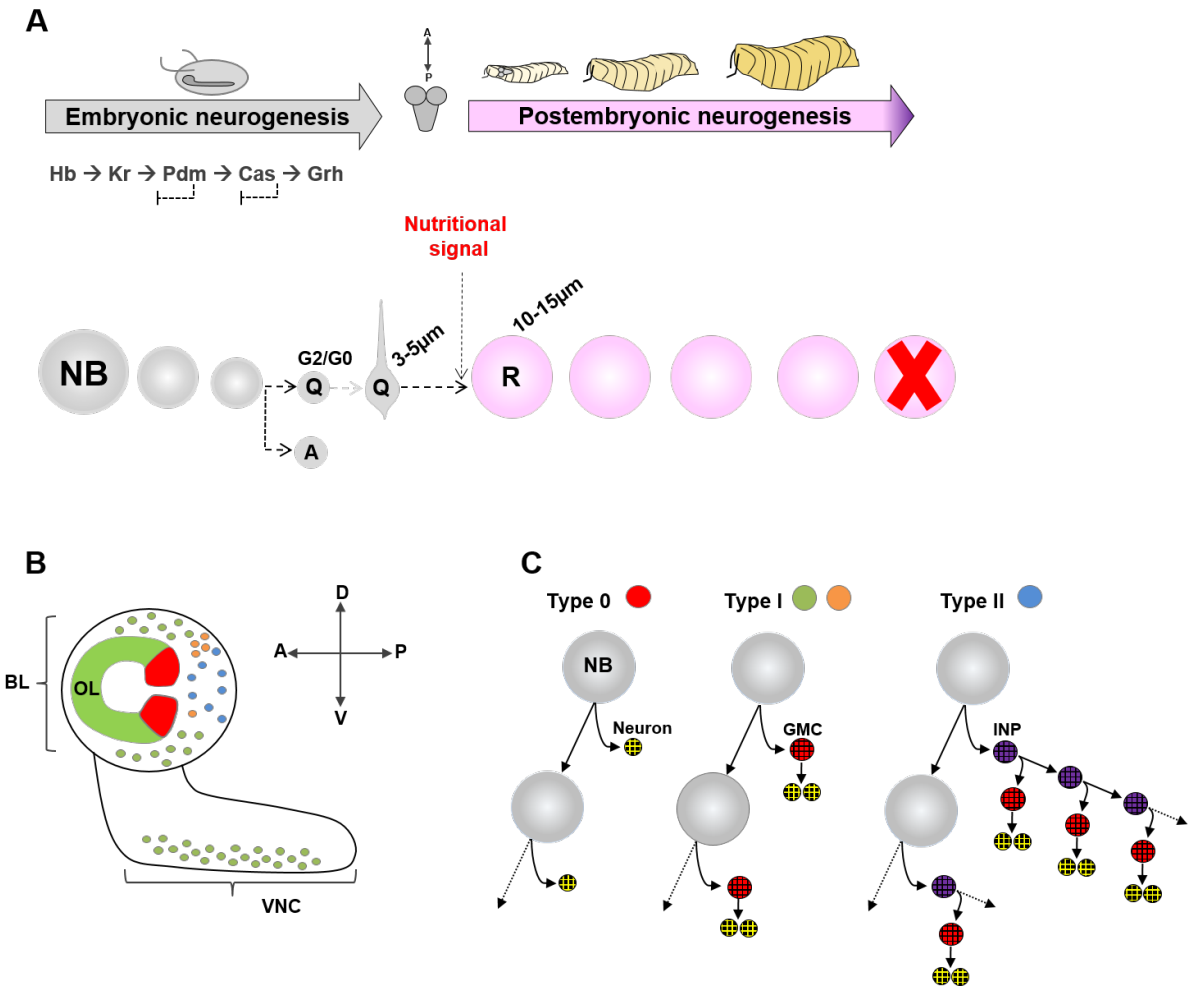


**Figure 1.3. *Drosophila* neurogenesis and proliferation patterns of NBs.** A. *Drosophila* neurogenesis occurs embryonically to generate the larval CNS, and postembryonically throughout the larval stages. Embryonic neuroblast (NB) size decreases at each division throughout embryonic neurogenesis, and a temporal transcriptional program determines if embryonic NBs enter apoptosis (Figure 1.3. A, 'A') or enter quiescence (Figure 1.3. A, 'Q'); except for the mushroom body NBs (B, orange). A nutritional stimulus stimulates quiescent NBs to enlarge and re-enter the cell cycle to proliferate and generate the adult fly CNS. **B.** *Drosophila* larval brain depicting the postembryonic NBs (pNB) populations and their locations. **C.** The proliferation patterns of postembryonic NBs (pNBs) and their lineages. Most pNBs follow the Type I pattern of division, present in the brain lobes (BL), ventral nerve cord (VNC) and Optic lobes (OL). A small population follow the Type II pattern of division and are only located in the central brain region. Type 0 is utilised by NBs in the outer proliferative centre of the OL. Hunchback (Hb), Kruppel (Kr), Pou domain 2 (Pdm), Castor (Cas), Grainyhead (Grh); Quiescent (Q); Apoptosis (A); Reactivated (R); Ganglion Mother Cell (GMC); Intermediate Neural Progenitor (INP). Schemes of larval brain depicted by arrows: A, anterior; P, posterior; D, dorsal; V, ventral., (Adapted from Hakes and Brand, 2019; Doe, 2017; Harding and White, 2017).

### 1.4.2. Proliferation patterns and lineages of *Drosophila* NBs

Three types of *Drosophila* NBs are identifiable based on their mode of division: Type 0, Type I and Type II (**Figure 1.3.C**). Type I NBs are prominent within the embryo, however, unlike embryonic NBs, type I postembryonic NBs (pNBs) maintain their original size after divisions. Embryonic NBs have been shown to switch from Type I divisions to Type 0 divisions (Doe, 2008; Baumgardt *et al.,* 2009; Baumgardt *et al.,* 2014; Karcavich and Doe, 2005; Monedero Cobeta *et al.,* 2017. Type 0 NB division produces a smaller terminally differentiating cell to generate a single neuron. Type 0 divisions occur during embryogenesis and postembryonically in the optic lobes (Baumgardt *et al.,* 2014; Bertet *et al.,* 2014; Mora *et al.,* 2018). Interestingly, the optic lobe NBs switch from Type 0 to Type I divisions which, like VNC pNBs, is under the control of a distinct temporal transcriptional program (Bertet *et al.,* 2014).

The two main types of *Drosophila* pNBs are type I and type II. Both types I and II pNBs divide asymmetrically and unequally segregate cell fate determinants but differ in their lineage pattern development (Homem and Knoblich, 2012; Doe, 2017; Harding and White, 2017). Type I is the most common mode of division; Type I NBs generate a terminally differentiating GMC, giving rise to a pair of sibling neural cells (neurons or glia). Type I pNBs are the most abundant, found throughout the larval brain lobes (mammalian hemispheres equivalent) and VNC (mammalian spinal cord; **Figure 1.3.B, C**). A subset of NBs located in the BLs called the mushroom body NBs (mbNBs) also follow the Type I division pattern (**Figure 1.3.B, C**). Type I pNBs are frequently distinguished by the self-renewal markers Deadpan (Dpn) and Asense (Ase), as well as Inscuteable (Insc). Their GMCs express nuclear Prospero (Pros), a pro-neural homeobox protein, which inhibits cell cycle genes (Choksi *et al.,* 2006; Homem and Knoblich, 2012; Doe, 2017; Harding and White, 2017). The GMC progeny, a pair of neurons or glia, can be distinguished by the neuronal marker Elav or the glia marker Reverse polarity (Repo), respectively.

Type II pNBs generate an intermediate neural progenitor (INP) which, upon maturation, undergoes limited rounds of division to self-renew and generate a GMC, giving rise to a pair of sibling neural cells (Homem and Knoblich 2012; Harding and White, 2017). There are less Type II pNBs, around ~8 per BL compared to ~90 for

Type I pNBs. Type II NBs are restricted to the central brain (CB; **Figure 1.3.B, C**) and generate higher numbers of neural progeny due to the amplifying INPs. Type II pNBs in the CB originate from the embryo whereby they specifically acquire expression of the transcription factor, Pointed P1 (Pnt), mediated by EGF signalling (Walsh and Doe, 2017; Álvarez and Diaz-Benjumea, 2018). Pnt is absent in Type I pNBs and is therefore used to distinguish the Type II pNBs and their lineages. In addition, unlike the Type I pNBs, Type II pNBs do not express Ase but do express the transcription factor/ self-renewal marker Dpn. Newborn immature INPs are smaller and do not express the transcription factors Ase, Dpn or Pros until they have 'matured' after 4-6 hours; at which point the mature INP will re-express those markers in that sequence (Bayraktar *et al.,* 2010). In addition, mature INPs express the transcription factor, Earmuff, which the Type I and II pNBs do not (Weng *et al.,* 2010). The mature INPs divide asymmetrically to generate a terminally differentiating GMC. INPs have less proliferative potential than pNBs but serve as an amplification step, like mammalian TACs (Bello *et al.,* 2008; Boone & Doe, 2008; Bowman *et al.,* 2008).

### 1.4.3. Asymmetric division in *Drosophila* NBs

Asymmetric division produces two cells with distinct fates (recently reviewed by Loyer and Januschke, 2020). Asymmetric division in *Drosophila* NBs is controlled by cell-intrinsic cues and requires subcellular localisation and segregation of specific cell fate determinants. Precise spindle orientation along the apical-basal axis is required to separate the apical cortex, retained by the NB, from the basal cortex, transmitted to the progeny. The process is mediated by the apical Par, Insc, atypical protein kinase C (aPKC) complexes (Sousa-Nunes and Somers, 2013; Yu *et al.,* 2006). The apical-basal polarity is inherited during embryogenesis from the neuroectoderm; the apical Par complex (Par3/Bazooka, Par6 and aPKC) is retained by the NB (Petronczki and Knoblich, 2001; Wodarz *et al*., 2005; Wodarz *et al*., 2000; Wodarz *et al*., 1999; Bello *et al*., 2006; Betschinger *et al*., 2006; Ikeshima- Kataoka *et al*., 1997; Knoblich *et al*., 1995; Lee *et al*., 2006; Rhyu *et al*., 1994). The Par complex recruits the adaptor protein Insc, which subsequently recruits the Partner of inscuteable (Pins), Mushroom body defect (Mud), and the *Drosophila* Gαi to form a Pins/Mud/ Gαi complex. The apical complexes undergo a phosphorylation cascade to direct cell fate determinants Brain tumour (Brat), Numb and Pros to the basal cortex of the dividing NB via the scaffolding proteins Miranda and Partner of Numb (Pon). These cell fate determinants

segregate into the progeny (GMC), inhibit self-renewal and promote differentiation (Doe *et al.,* 1991; Rhyu *et al.,* 1994; Hirata *et al.,* 1995; Knoblich *et al.,* 1995; Bello *et al.,* 2006; Betschinger *et al.,* 2006; Lee *et al.,* 2006; Doe, 2017; Harding and White, 2017). Miranda sequesters and prevents Pros activity in the NB, however within the GMC Miranda is degraded, and Pros can enter the nucleus to stimulate differentiation (Ikeshima-Kataoka *et al.,* 1997; Hirata *et al.,* 1995). Interestingly, cell cycle gene repression has been observed by Prox1, the mammalian ortholog of Pros (Foskolou *et al.,* 2013; Dyer, 2003). Incorrect spindle orientation and failure in proper unequal segregation of cell fate determinants can lead to excess progeny with stem-cell characteristics and even tumour formation (Choksi *et al.,* 2006; Shen *et al.,* 1997; Bello *et al.,* 2006; Betschinger *et al.,* 2006; Kraut *et al.,* 1996; Wodarz *et al.,* 1999; Doe *et al.,* 1991; Wodarz *et al.,* 2000). Also, loss of Insc function leads to Type I progeny with INP-like characteristics (An *et al.,* 2017).

### 1.4.4. *Drosophila* NBs enter quiescence at the end of embryogenesis

At the end of embryogenesis, after the embryonic lineages are generated, NBs switch from Type I to Type 0 divisions and many *Drosophila* NBs enter cellular quiescence (Tsuji *et al.,* 2008; Lai and Doe, 2014; Baumgardt *et al.,* 2014; Karlsson *et al.,* 2010; Monedero Cobeta *et al.,* 2017). These quiescent NBs are poised to mitotically reactivate postembryonically ~24 hours during the first instar larval stage to produce the neurons and glia required by the adult fly CNS. The only exceptions are the four mbNBs and one lateral NB which do not enter quiescence and will continually proliferate throughout development (Ito and Hotta, 1992).

As previously mentioned, quiescence is historically described as a G0 arrested state. However, recently *Drosophila* NB quiescence was shown to contain a mix of G2 and G0 quiescent pNBs (Otsuki and Brand, 2018) using cell cycle markers and the Fluorescent Ubiquitination-based Cell Cycle Indicator (FUCCI) system, which is a set of fluorescent probes enabling visualisation of the cell cycle (Sakaue-Sawano *et al.,* 2008). Here, the authors demonstrate ~75% of pNBs express Dpn, cyclin A, cyclin B and are arrested in G2. The remaining ~25% of pNBs express Dpn only and are arrested in G0 (Otsuki and Brand, 2018). Furthermore, the pNBs in G2 are mitotically reactivated faster than their G0 counterparts. The pseudokinase, *tribbles*, known to inhibit cell cycle progression by degrading Cdc25/String, regulates G2 quiescence by

inhibiting the AKT pathway (Otsuki and Brand, 2018). Tribbles expression in NBs begins at embryonic stage 15 and continues to mark quiescence until nutritional cues stimulate NB reactivation; it is not expressed in the mbNBs that do not undergo quiescence (Otsuki and Brand, 2018). It is the first gene identified that distinguishes quiescent pNBs in *Drosophila* (Otsuki and Brand, 2018). Tribbles expression continues under starved conditions, and expressing constitutively active AKT, but not Pi3K, in *tribble* mutants could fully rescue the defects observed in *tribble* mutant pNBs (Otsuki and Brand, 2018). In addition, they showed that tribble activity is normally inhibited by AKT upon the nutritionally-dependant secretion of *Drosophila* Insulin-like peptides (dilps) from the niche glia (Otsuki and Brand, 2018).

NB entry into quiescence is determined by numerous factors, including the Hox genes Antennapedia (Antp) and Abdominal-A (Abd-A). At the end of embryogenesis, Antp and Abd-A determine NB cell cycle exit and whether the NB will enter quiescence or apoptosis (Bello *et al*., 2003; Tsuji *et al*., 2008; Arya *et al*., 2015; Khandelwal *et al*., 2017; Otsuki and Brand, 2018; Harding and White, 2019). Interestingly, the Polycomb Repressor Complex 2 (PRC2 complex) is known to suppress Hox gene expression, counteracting their known anti-proliferating action and regulation of programmed cell death in the early *Drosophila* larval brain (Curt *et al*., 2019; Yaghmaeian Salmani *et al*., 2018; Bahrampour *et al.,* 2019). PRC2 mutants display anterior expansion of Hox gene expression, resulting in reduced NB proliferation in the brain (Curt *et al*., 2019; Yaghmaeian Salmani *et al*., 2018). It would be interesting to examine if PRC2 may also be involved in Hox gene regulation of NB entry into quiescence.

The temporal transcription factor cascade (**Figure 1.3.A**) determines NB fate; although the majority of NBs enter programmed cell death, and a smaller subset of Cas+ NBs enter quiescence (Tsuji *et al*., 2008; Miyares and Lee, 2019; Doe, 2017; Harding and White, 2018). It was recently found that a small subset of NBs belonging to the G2-quiescence category are terminated through an unknown mechanism (Harding and White, 2018).

Downstream of the temporal transcription cascade, Nab and Squeeze (also transcription factors) were found to be required for entry into quiescence (Tsuji *et al.,* 2008). The homeodomain transcription factor Pros, usually associated with

neuronal differentiation was found to regulate NB quiescence and act as a 'binary switch' between NB and differentiated progeny (Choksi *et al.,* 2006; Lai and Doe, 2014). Lai and Doe showed that different Pros levels determine various NB fates (Lai and Doe, 2014). A transient pulse of low-level Pros in the NB nucleus induces quiescence, but how this is achieved or the regulation by upstream temporal transcription factors is unknown (Lai and Doe, 2014).

### 1.4.5. Maintenance of *Drosophila* NB quiescence

NB quiescence must be properly maintained to ensure the appropriate NB lineages are only generated at the correct developmental time. Maintenance of quiescence is regulated by a variety of factors, including intrinsic and extrinsic. Glia cells surrounding the pNBs secrete a glycoprotein, anachronism (Ana), to promote quiescence in pNBs and prevent premature cell-cycle re-entry (Ebens *et al.,* 1993). The *Drosophila* Perlecan, Terribly reduced optic lobes (Trol), promotes cell-cycle progression by either inhibiting *ana* activity or functioning downstream of *ana* (Datta 1995; Voigt *et al.,* 2002). Fragile X protein (FMRP), which codes for the inherited mental retardation Fragile X syndrome, is reported to function first in pNBs and then in glia to maintain pNB quiescence and is regulated by Insulin signalling (Callan *et al.,* 2010; Callan *et al.,* 2012; Callan *et al.,* 2011; Monyak *et al.,* 2016).

Maintenance of pNB quiescence is further regulated by Hippo signalling (Ding *et al.,* 2016; Poon *et al.,* 2016). Hippo signalling is a growth inhibition pathway and highly conserved in *Drosophila* and vertebrates (Harvey and Tapon, 2007; Halder and Johnson, 2011; Lee *et al.,* 2018). Active canonical Hippo signalling activates a phosphorylation cascade whereby the Hippo kinase activates the Warts kinase, which phosphorylates Yorkie (Yap/Taz in mammals) via a 14-3-3 binding site; sequestering the transcriptional co-activator Yorkie in the cytoplasm causes its deactivation (Oh and Irvine, 2008). Inactive Hippo signalling allows Yorkie translocation to the nucleus where it activates the transcriptional program, promoting growth and proliferation (Saucedo and Edgar, 2007). Ding *et al.,* found that the Hippo pathway maintains pNB quiescence; the core kinases, Hippo and Warts, are phosphorylated (activated) in quiescent pNBs (Ding *et al.,* 2016). Also, quiescent pNBs and non-quiescent pNBs (the MBNBs)

can be identified by cytoplasmic-Yorkie (inactive), and nuclear-Yorkie (active), respectively. Loss of Hippo/Warts or upstream regulators caused premature pNB enlargement and mitotic reactivation from quiescence (Ding *et al.,* 2016). This process is mediated by the upstream glial transmembrane proteins, Echinoid and Crumbs, which lead to inhibition of Yorkie activity but are downregulated by nutrition to enable mitotic reactivation (Ding *et al.,* 2016; Poon *et al.,* 2016). Premature loss of Crumbs or Echinoid in NBs or glia resulted in earlier reactivation shown by NB enlargement at 4h ALH (Ding *et al.,* 2016). The Hippo pathway was also shown to regulate larval brain size and cell cycle speeds (Poon *et al.,* 2016). Here, altering Hippo pathway components caused increased NB size, precocious NB proliferation, faster cell cycle speeds, and clone size; leading to larval brain overgrowth (Poon *et al.,* 2016).

In vertebrates, deactivation of YAP stimulates proliferation of stem cells (Tremblay and Camargo, 2012) and the Hippo pathway is implicated in stem cells within the liver (Zhou *et al.,* 2009); the skin (Schlegelmilch *et al.,* 2011; Zhang *et al.,* 2011); and the intestines (Barry *et al.,* 2013; Zhou *et al.,* 2011; Staley *et al.,* 2010).

### 1.4.6. *Drosophila* NBs mitotically reactivate to generate the adult fly CNS

The exit from NB quiescence, termed reactivation, requires the coordination of multiple signalling pathways, in which the pNB niche glia cells has been shown to be crucial. Anti-proliferative Hox genes regulating patterning and quiescence must be inactivated (Prokop *et al.,* 1998; Tsuji *et al.,* 2008; Harding and White, 2019; Curt *et al.,* 2019); which is controlled by brain transcription factors and the PRC2 complex (Curt *et al.,* 2019; Monedero Cobeta *et al.,* 2017; Yaghmaeian Salmani et al., 2018). Reactivation of pNBs occurs in a 'wave' along the anterior to posterior (AP) axis (Doe, 1992; Skeath and Carroll, 1992; Skeath, 1992, Skeath, 1999; Tsuji et al., 2008; Kemelman et al., 2012; Rosenberg et al., 2009), beginning in the BL NBs first, and propagating through the VNC; the abdominal NBs are the last to reactivate. Anterior propagation, governed by Hox genes, is a requirement for proper CNS development and appears to be conserved in mammals (Monedero Cobeta *et al.,* 2017; Philippidou and Dasen, 2013; Yaghmaeian Salmani *et al.,* 2018; Metzis *et al.,* 2018).

Upon reactivation, pNBs grossly enlarge, enter S-phase and begin proliferating to generate the adult CNS. This provides a unique opportunity to study pNB mitotic reactivation using a simpler model. Reactivated pNBs can be initially distinguished

from their quiescent counterparts by their larger size; an increase from ~4-5 μm (quiescent) up to ~10-15 μm (Chell and Brand, 2010). Most pNBs reactivate within 24 hours of larval hatching and reactivation is initiated by a nutritional stimulus following larval feeding (**Figure 1.4**). Larval feeding increases the amount of circulating amino acids which is sensed by the fat body (FB, the *Drosophila* liver equivalent, **Figure 1.4**). This hepatic/adipose-like tissue was found to release a FB-derived signal (FDS) which enables pNB reactivation (Britton and Edgar 1998). Larval CNSs cultured alone or co-cultured with a gut or CNS from fed larvae failed to reactivate the NBs. Only when quiescent larval CNSs were co-cultured with a FB, were the NBs able to reactivate (Britton and Edgar, 1998). Further work revealed that the FB senses nutrition via the cationic amino-acid transporter Slimfast (slif) (Colombani, Raisin *et al.,* 2003; Géminard *et al.,* 2009), which activates the Target of Rapamycin (TOR) signalling pathway (Sousa-Nunes *et al.,* 2011). Upon TOR activation, the FDS is released and sensed by glia cells surrounding the NBs. The glia cells release Insulin-like peptides (ILPs, totalling 7) to which the single NB Insulin-like Receptor (InR) responds, activating the phosphatidylinositol 3-kinase (PI3K) and TOR pathway within the NB. As a consequence, NBs characteristically enlarge and re-enter the cell cycle (Truman and Bate 1988; Chell and Brand 2010; Sousa-Nunes *et al.,* 2011).
Of the 7 ILPs, ILP6 was found to be the most influenced by nutrition and a potent activator of NBs' reactivation (Sousa-Nunes *et al.,* 2011). Global inactivation of Tor, inhibition of slif within the FB, or FB specific activation of TOR inhibitors Tuberous sclerosis complex 1 and 2 (Tcs1/2) reduced the number of NBs exiting quiescence. Furthermore, inhibition of PI3K signalling also inhibits neuroblast reactivation. Conversely, overexpression of the TOR pathway activator Ras homologue enriched in brain (RHEB) and of PI3K pathway activators specifically in the NBs caused premature pNB reactivation (Chell and Brand, 2010; Sousa-Nunes *et al.,* 2011).

More recently, the highly conserved heat shock protein 83 (Hsp83/ Hsp90 in mammals) and its co-chaperon Cdc37 were found to function upstream of the InR/PI3K/AKT cascade to promote pNB reactivation; Hsp83 was shown to directly bind to the InR (Huang and Wang, 2018) (**Figure 1.4**). Insulin signalling and insulin-like growth factors (IGF) are highly conserved between invertebrates and mammals, regulating metabolism and growth. In mammals, dietary restriction or a high-fat diet causes increased or decreased levels of Sirtuin 1 (SIRT1), respectively (Cohen *et al.,*

2004; Chen *et al.,* 2008; Spéder and Brand, 2011). SIRT1 correlates to the nutritional status of the animal and modulates systemic IGF-1 (Cohen *et al.,* 2004; Cohen *et al.,* 2009; Cohen *et al.,* 2010). Like *Drosophila* glia cells, mammalian astrocytes have also been shown to release local insulin/IGF-1 (Garcia-Estrada *et al.,* 1992; Shetty *et al.,* 2005), however, unlike in *Drosophila*, a direct link between these glia and NSC reactivation has not yet been shown.

As described in section **1.3.2**, nutritional dependant neurogenesis has also been observed in rodents (Lee *et al.,* 2000; Poulose *et al.,* 2017; Shohayeb *et al.,* 2018; Norman *et al.,* 2008; Stranahan *et al.,* 2008; Alvarez *et al.,* 2009), and associated to cognitive decline in human patients (Spinelli *et al.,* 2019; Kodl and Seaquist 2008). In the *Drosophila* larval CNS, Spéder and Brand (2014) discovered a cell-autonomous role of the gap junction proteins within the glia forming the Blood-Brain Barrier (BBB, **Figure 1.4**). They found that the nutrient dependant ILP secretions essential for pNB reactivation are coordinated by gap junction proteins (Innexin 1/2) across the BBB and conditions that reduce/block Ca2+ oscillations impair pNB reactivation (Spéder and Brand 2014). Similar mechanisms are also seen in vertebrates, whereby the pancreatic beta cells release insulin in response to Ca2+ (MacDonald and Rorsman 2006).

The glia niche performs additional functions for pNB reactivation. Cortex glia has been shown to progressively remodel their membranes around each NB and its lineage in response to local and systemic signals (Spéder and Brand, 2018). The cortex glia undergoes three developmental steps: membrane expansion, encasing, and extension, creating cortex glia ‘chambers’ around pNBs (Spéder and Brand, 2018). A nutritional signal first induces expansion of the glia membranes via Pi3K/Akt, and the reactivating NBs signal for the remodelling process; the new glia niche structure is critical for the new neurons to survive and inhibiting pNB reactivation disrupts chamber formation. In addition, knocking down BBB glia gap junctions, or Insulin signalling in the cortex glia or pNBs, or the spindle matrix complex component, *east*, in pNBs, all impairs the chamber formation (Spéder and Brand, 2018). Similarly, mammalian astrocytes, and the local neurogenic niche, support neurogenesis (Gengatharan *et al.,* 2016; Goldman and Chen, 2011; Tavazoie *et al.,* 2008; Ottone *et al.,* 2014).

The *Drosophila* Perlecan homolog, Terribly reduced optic lobes (Trol), functions non-cell-autonomously to promote pNB reactivation, by antagonising Ana activity in niche glia (Ebens *et al.,* 1993; Datta, 1995; Voigt *et al.,* 2002). Trol also performs structural and function roles in FGF-2 signalling and Hedgehog signalling to stimulate pNB reactivation at the G1-S-phase transition (Park *et al.,* 2003). Thought to function similar to the mammalian Perlecan, Trol is proposed to function in the *Drosophila* extracellular matrix, modulating extrinsic signalling factors such as Ana, to stimulate pNB reactivation (Voigt *et al.,* 2002) (**Figure 1.4**). Furthermore, Trol-dependant action is enhanced by a transacting signal produced by *even-skipped* (Eve); a regulator of embryonic neurogenesis (Park *et al.,* 2001; Akam, 1987).

Also downstream of nutritional signals and InR/PI3K/AKT signalling, the spindle matrix protein complex, comprised of Chromator (Chro), Megator, Skeletor and Enhanced adult sensory threshold (East), stimulate pNB reactivation (**Figure 1.4**). Chro is critical for Insulin signalling detection by pNBs and maintaining pNB proliferation (Li *et al.,* 2017). Grainyhead (Grh) prevents pNB nuclear Pros to maintain proliferation in the VNC (Maurange *et al.,* 2008). Interestingly, Chro was also found to repress *pros* expression and stimulate *grh* expression, which further represses *pros*, to promote pNB reactivation (Li *et al.,* 2017). Chro and East have been found to modulate gene expression via chromatin modification (Rhee *et al*., 2014). In pNBs, the spindle matrix complex prevents re-entry into cellular quiescence by targeting Grh and *pros* (Li *et al.,* 2017).

An additional level of cell-autonomous regulation exists via *taranis* (*tara*), the mammalian SERTAD orthologue. Tara promotes the E2F1 pathway in pNBs to promote pNB reactivation; *tara* is expressed in mitotically active type I pNBs and absent in quiescent pNBs (Manansala *et al.,* 2013). More recently, a conserved ubiquitin ligase complex was shown to be essential for pNB reactivation (Ly *et al.,* 2019). Knocking down the complex components with mutations or by RNAi in pNBs impaired reactivation (Ly *et al.,* 2019). Here, the conserved ubiquitin ligase family, Cullin4-RING (CRL4) complex consisting of the adaptor damaged DNA-binding protein 1 (DDB1), the scaffold Cullin4 (Cul4), and the catalytic RING of Cullin (ROC), together with its substrate receptor Mahjong (Mahj; $CRL4^{Mahj}$) form a protein complex with Warts, causing warts ubiquitination and inhibition in S2 cells (Ly *et al.,* 2019).

Simultaneously expressing Warts-RNAi could suppress the reactivation defects observed upon Mahj-RNAi in pNBs (Ly *et al.,* 2019). Interestingly, rat Cul4B loss in neural progenitors leads to G2/M phase cell cycle arrest, and mutations of the human Cul4B gene is often associated with mental impairments (Tarpey *et al.,* 2007; Zou *et al.,* 2007; Liu *et al*., 2012).

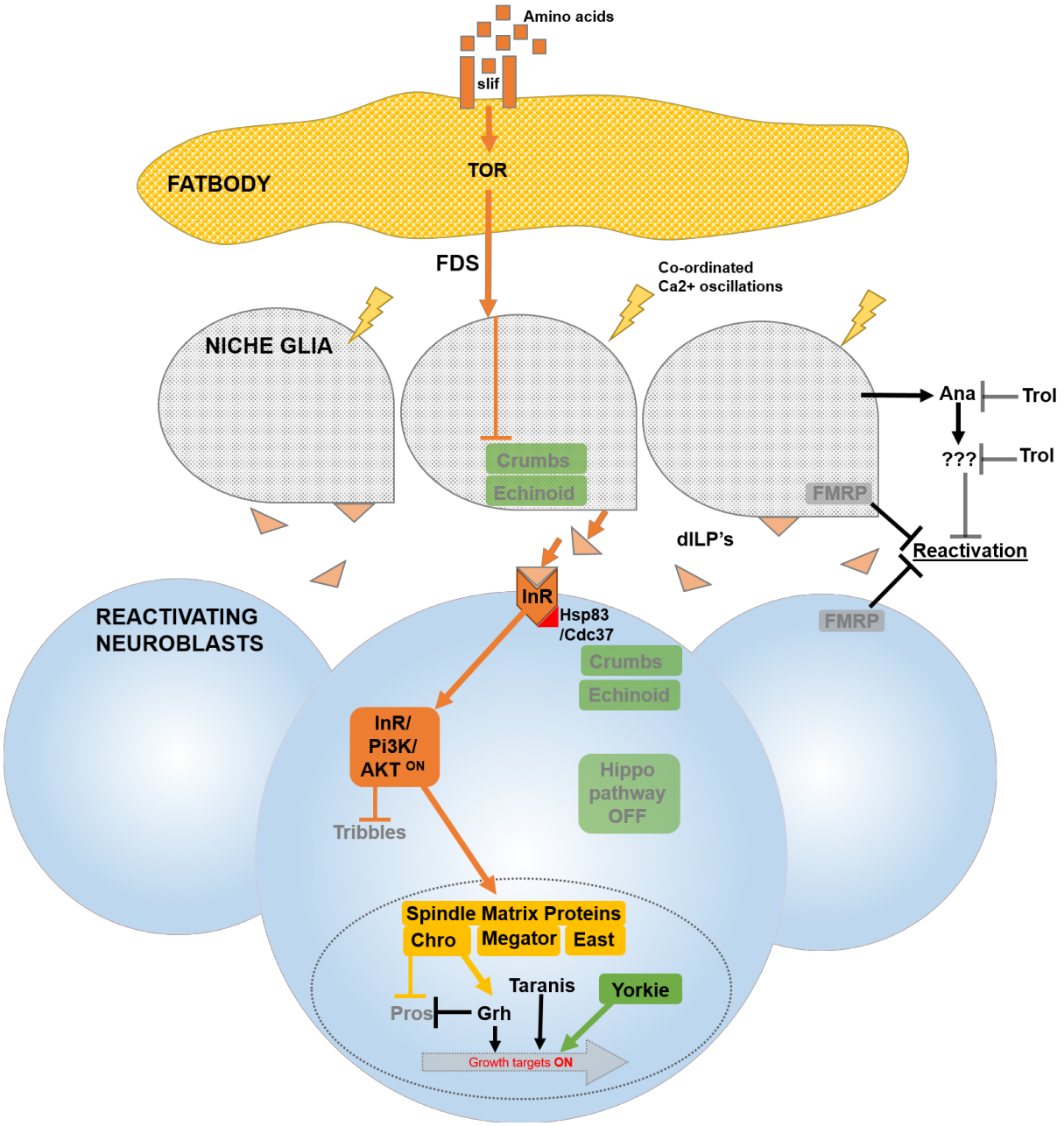
Amino acids
slif
FATBODY
TOR
FDS
Co-ordinated
Ca2+ oscillations
NICHE GLIA
Crumbs
Echinoid
Ana
Trol
???
Trol
FMRP
dILP's
Reactivation
InR
Hsp83
/Cdc37
REACTIVATING
NEUROBLASTS
FMRP
Crumbs
Echinoid
InR/
Pi3K/
AKT ON
Hippo
pathway
OFF
Tribbles
Spindle Matrix Proteins
Chro
Megator
East
Taranis
Yorkie
Pros
Grh
Growth targets ON

**Figure 1.4. A simplified summary of main regulators of *Drosophila* pNB reactivation.** *Drosophila* pNB reactivation is stimulated by larval feeding. Circulating amino acids are sensed by the Slimfast amino acid transporter (Slif) (Colombani *et al.,* 2003; Géminard *et al*., 2009), on the fat body (FB). This activates Target of Rapamycin (TOR) in the FB (Sousa-Nunes *et al*., 2011), stimulating the release of a fat body derived signal (FDS) (Britton and Edgar, 1998), which is sensed by the glia surrounding the NBs. The glia release Insulin-like peptides (ILPs). This release also requires coordinated Ca2+ oscillations across the gap junctions of the Blood-Brain Barrier (BBB) glia (Spéder and Brand 2014). Local ILP secretion is sensed by the NBs' InR, activating PI3K and TOR pathway within the NB (Chell and Brand 2010; Sousa-Nunes; Yee *et al.,* 2011). In contrast, the Hippo pathway functions to maintain NBs in quiescence, and therefore must be switched off for reactivation to occur (Ding *et al.,* 2016; Poon *et al.,* 2016). Phosphorylation and activation or Hippo and Warts leads to the inactivation of Yorkie, which is sequestered in the cytoplasm and degraded. Upstream regulators are the transmembrane proteins, Echinoid and Crumbs which stimulate the pathway until a nutritional stimulus inhibits their action. Inactivation of the Hippo pathway allows Yorkie to translocate to the nucleus and activate growth targets. Spindle matrix proteins Chromator (chro), Megator and Enhanced adult sensory threshold (East) (Li *et al.,* 2017; Song *et al.,* 2017), FMRP, Tribbles, and Ana (Ebens *et al.,* 1993; Datta, 1995; Voigt *et al.,* 2002) inhibit pNB reactivation whereas Heat shock protein 83 (Hsp83) (Huang and Wang, 2018), Taranis (Manansala *et al.,* 2013) and Trol (Ebens *et al.,* 1993; Datta, 1995; Voigt *et al.,* 2002) promote pNB reactivation.

### 1.4.7. *Drosophila* Mob4, a potential new player in NB reactivation

To enhance our knowledge of postembryonic neurogenesis and the process of pNB reactivation, a single-cell transcriptome microarray screen was performed in our laboratory comparing *Drosophila* quiescent versus reactivating pNBs (Gill-Renado *et al.,* 2019). The single cells were obtained directly from live transgenic *Drosophila* larval brains, in which pNBs were visualised by membrane-tagged Green Fluorescent Protein (GFP) driven by the *grainy-head* (*grh*) Gal4 driver (Ding *et al.,* 2016; Chell and Brand, 2010). pNBs were removed from the second and third thoracic segments of the VNCs to minimize potential differences from spatial positioning and avoiding retrieving a mix of type I and II NSCs, as the latter are not present in VNCs. The pNBs were identified by their size as quiescent pNBs are much smaller, measuring 4-5 µm (maximum cell diameter), than reactivating (enlarging) pNBs (Chell and Brand, 2010; Ding *et al.,* 2016). The pNBs were harvested at 17h after larval hatching (ALH) as, at this particular age, both quiescent and reactivating pNBs can be distinguished and simultaneously harvested. Only reactivating (enlarged) pNBs not in division and without any progeny were harvested. cDNA was obtained from each cell using an established single-cell transcriptome protocol (Liu and Bossing, 2016; Bossing *et al.,* 2012).

Expression of the NB markers *dpn* and *ase* was confirmed via real-time quantitative PCR (RT-qPCRs) in both quiescent and reactivating cell samples harvested, with levels being higher in the later, as expected. Single pNB samples were compared in pairs (quiescent versus reactivating; n=3 pairs) on whole-genome microarrays (FlyChip, Cambridge). The screen analysis revealed 145 transcripts up-regulated and 51 transcripts down-regulated ($p<0.05$) in reactivating compared to quiescent NBs. 90% of identified targets have human orthologues, and most (66%) show high orthology conservation levels. The data was independently validated for a subset of candidates, and differential expression for all targets tested (18 in total) was confirmed (Gil-Ranedo *et al.,* 2019).

Among the candidates identified as potential novel regulators of postembryonic pNB reactivation were genes encoding for several members of the highly conserved Striatin Interacting Phosphatase and Kinases complex (STRIPAK) protein complex (Shi *et al.,* 2016; Ribeiro *et al.,* 2010; Zheng *et al.,* 2017): MOB kinase activator 4, also known as Monopolar spindle-one binder (Mob4), the only *Drosophila* Striatin Connector of kinase to AP-1(Cka*)* and Microtubule Star (Mts), which is the catalytic subunit of Protein Phosphatase 2A (PP2A). *mob4 and cka* were found upregulated, whereas *mts* was downregulated. Interestingly the STRIPAK complex, through its PP2A phosphatase, has been shown to be is an inhibitor of the Hippo pathway (Goudreault *et al.,* 2009; Ribeiro *et al.,* 2010), a known regulator of pNB quiescence (Ding *et al.,* 2016; Poon *et al.,* 2016). Yet, no member of STRIPAK had been reported to be involved in the process of pNB reactivation.

The above mentioned data and literature, the availability of cellular and genetic tools (e.g. transgenic *Drosophila* lines and antibodies) and preliminary observations in our laboratory (Dr C. Barros) suggesting that the STRIPAK member Mob4 may be involved in pNB reactivation, formed the basis for my PhD project focused primarily on investigating this candidate gene and its mode of action.

In addition, to be a STRIPAK member, Mob4 belongs to the Mob family of non-catalytic, kinase interacting proteins highly conserved from yeast to humans (Luca and Winey 1998; Lai *et al.,* 2005; Mrkobrada *et al.,* 2006; Wei *et al.,* 2007). The two founding members of the Mob protein family, first identified in *Saccharomyces*

*cerevisiae* (Mob1 and Mob2), are involved in regulation and activation of Nuclear dbf2-related (NDR) kinases, which are cell cycle regulators (Komarnitsky *et al.,* 1998; Luca and Winey 1998; Lee *et al.,* 2001; Mah *et al.,* 2001; Wei *et al.,* 2007; Lai *et al.*, 2005; Mrkobrada *et al.,* 2006). Mob4, however, is the most divergent member of its family (Schulte *et al.,* 2010). On the other hand, RNA interference knocking down Mob4 in *Drosophila* embryonic cells (Schneider 2 cells, S2) showed a role in mitotic spindle assembly, specifically in fibre spindle focusing, and phenotypes similar to centrosomal protein mutants were reported (Trammell *et al.,* 2008). Furthermore, *in-vivo* analysis of *Drosophila mob4* null mutants showed abnormal synaptic development with a supernumerary bouton phenotype, disrupted axonal transport, disorganised microtubules and larval lethality (Schulte *et al.,* 2010). Interestingly, the lethality observed was rescued by ubiquitous expression of the human orthologue of Mob4, MOB4 (also called Phocein), which is over 80% identical at the amino acid level, highlighting also functional evolutionary conservation among the molecules (Schulte *et al.,* 2010) (see also Discussion).

### 1.5. Hypothesis and objectives of proposed PhD study

The hypothesis underlying my PhD project is that the candidate gene *mob4*, identified in a transcriptome screen performed in our laboratory as upregulated in reactivating compared to quiescent *Drosophila* postembryonic NSCs, is required for NSC mitotic reactivation. The overall aim is to characterize the expression and function of Mob4 towards identifying its potential mechanism of action regulating NSC mitotic reactivation.

### The specific objectives of my PhD project are:

1. Characterise Mob4 expression in quiescent and reactivated postembryonic NBs

2. Perform functional analysis of Mob4 in *Drosophila* pNBs during mitotic reactivation.

3. Identify a potential mechanism of Mob4 action on pNB reactivation.

# CHAPTER 2

# RESULTS

## 2.1 Mob4 is upregulated in reactivated versus quiescent pNBs

*mob4* transcript was found upregulated in reactivating versus quiescent pNBs in a single-cell transcriptome analysis performed in our laboratory, and the result was confirmed by RT-qPCR (see Introduction). Thus, my first step was to analyse Mob4 protein expression in the larval CNS, specifically in pNBs upon reactivation. The UAS-GAL4 system (Brand and Perrimon, 1993; Duffy, 2002) was used to visualise the larval pNBs. Membrane-bound GFP (*CD8-GFP*) was expressed using *grainyhead-GAL4* (*grh*-Gal4), specifically highlighting ~one-third of all pNBs in the larval CNS (Chell and Brand, 2010). *elav-Gal*$^{80}$ was simultaneously employed to repress any potential mild GFP expression in neurons driven by the *grh* promotor (Bray *et al.,* 1989), which are of similar size to quiescent pNBs. Larval brains (*grh-Gal4, UCD8-GFP; elav-Gal*$^{80}$) were dissected and immunostained first for Mob4 (red) and Green Fluorescent Protein (GFP, green) at 22h ALH. Consistent with previous observations of *mob4* mRNA and protein localisation in the *Drosophila* CNS (Schulte *et al.,* 2010), Mob4 was observed ubiquitously in the brain lobes (BLs, **Figure 2.1. A-A'**) and the ventral nerve cords (VNCs, **Figure 2.1. B-B'**), including within the cytoplasm of pNBs (white arrowheads) and their lineages (**Figure 2.1. A-B'**). Larval brains of the same genotype were immunostained with Mob4 (red, also shown separately in grey), GFP (green), and the NB marker Deadpan (Dpn, blue) to assess Mob4 protein levels in reactivated versus quiescent pNBs, at 18h ALH. Mob4 protein levels in reactivated versus quiescent pNBs were compared by measuring the Mob4 antibody signal intensity (average pixel intensity per cell area; see Methods). pNBs were determined to be quiescent (**Figure 2.10. E**) or reactivating (**Figure 2.10. F**) by their size, i.e. quiescent cells: 4-5 µm (maximum diameter), reactivating cells: enlarged (approximately 7 µm) (Chell and Brand, 2010; Ding *et al.,* 2016; Truman and Bate, 1988). The results show that Mob4 protein expression is significantly higher ($p$<0.01) in reactivating pNBs (**Figure 2.10. E, F**) compared to quiescent pNBs (**Figure 2.10.G**), in line with the microarray and RT- qPCR observations of our group.

Glia cells are vital transducers of the Insulin signal to reactivate pNBs (Chell and

Brand, 2010; Sousa-Nunes *et al.,* 2011). Since Mob4 is present ubiquitously in the brain, 24h ALH wild-type (WT) larvae were also immunostained for Mob4 (red, also shown in grey), Dpn (green) and Reversed polarity (Repo, a nuclear pan-glia marker, blue) antibodies to investigate expression in Glia. Mob4 seems to localise to the cytoplasm of glia (yellow arrowheads (**Figure 2.1. C-D'**) as inferred by absence from the nucleus, but its expression appears weaker compared to neighbouring pNBs (white arrows, **Figure 2.1.D'**).

In conclusion, the above assays show that Mob4 is abundant throughout the larval CNS and significantly upregulated in reactivating versus quiescent pNBs.

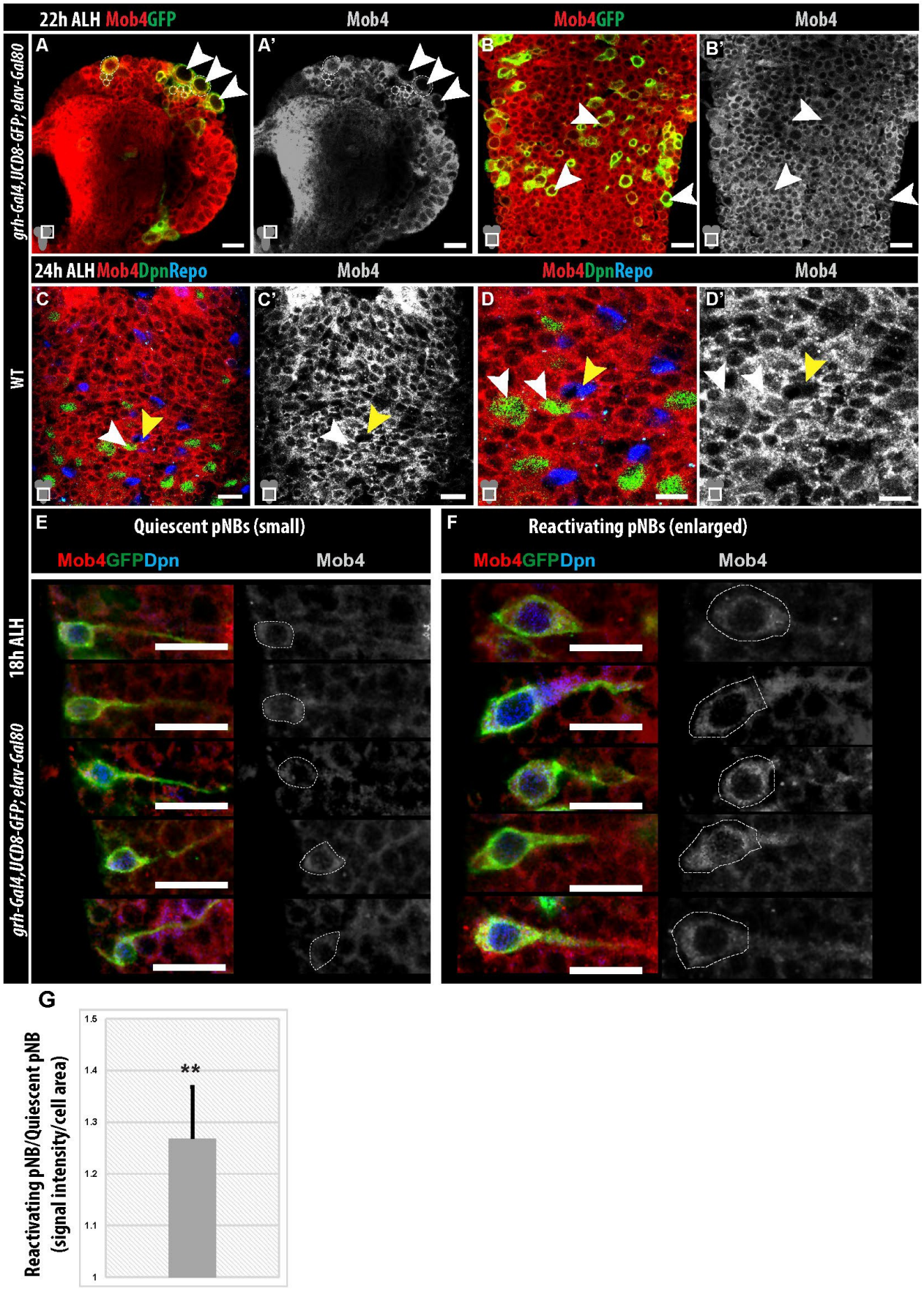
22h ALH Mob4GFP
Mob4
Mob4GFP
Mob4
A
A'
B
B'
grh-Gal4,UCD8-GFP; elav-Gal80
WT
24h ALH Mob4DpnRepo
Mob4
Mob4DpnRepo
Mob4
C
C'
D
D'
18h ALH
E
Quiescent pNBs (small)
Mob4GFPDpn
Mob4
F
Reactivating pNBs (enlarged)
Mob4GFPDpn
Mob4
grh-Gal4,UCD8-GFP; elav-Gal80
G
Reactivating pNB/Quiescent pNB
(signal intensity/cell area)
1.5
1.4
1.3
1.2
1.1
1
**

**Figure 2.1. Mob4 protein is upregulated upon pNB mitotic reactivation: (A, A'**) *grh-Gal4, UCD8-GFP; elav-Gal$^{80}$* larval brain lobe (BL) and **(B-B')** Ventral Nerve Cord (VNC) at 22 hours after larval hatching (ALH) immunostained for **Mob4** and **Green Fluorescent Protein (GFP).** Mob4 channel also shown in monochrome. **(C-D')** Wild-type (WT) VNCs were immunostained for **Mob4**, **Deadpan** (**Dpn**, NB marker) and **Repo** (glia nuclear marker) at 24h ALH. Mob4 channel also shown in monochrome. Mob4 is expressed ubiquitously throughout the BLs and VNCs and is found mainly in the cells' cytoplasm, including in pNBs (white arrows and dashed lines) and their progeny (dashed lines only) and glia (yellow arrowheads). **(E-F)** To quantify Mob4 expression levels in quiescent and reactivating pNBs, we used the same *Drosophila* line shown in A and immunostained brains with **Mob4**, **GFP** and **Dpn** antibodies at 18h ALH. Mob4 channel also shown in monochrome**. Mob4** signal intensity in small quiescent pNBs **(E)** is significantly less than in enlarged reactivating pNBs **(F). (G)** Mob4 protein quantification in reactivating pNBs (50 cells, 8 brains) normalized to quiescent pNBs (50 cells, 8 brains). Values are normalised average intensities +/- s.e.m. Wilcoxon rank-sum test ** $p$<0.01. All images are single focal planes, anterior up. Scale bar: 10 µm.

## 2.2 pNBs in *mob4* mutants fail to mitotically reactivate

Confident that Mob4 is upregulated in pNBs upon their reactivation, pNBs in *mob4* null mutants were next investigated. Previously in another lab, *mob4*$^{EY\Delta L3}$ null mutants (herein *mob4* mutants) were generated via a P transposable element excision screen (Schulte *et al.,* 2010). The P-element localised 33 base pairs upstream of the *mob4* start codon. In the *mob4*$^{EY\Delta L3}$ line, the excision resulted in a 357 base pair deletion including the sequence encoding the initiator methionine. Western blots on larval brain lysates made from these mutants show no Mob4 protein, which would be expected at ~25kDa weight (Schulte *et al.,* 2010). Homozygous *mob4*$^{\Delta L3}$ null mutants are larval lethal, but ~10% of larvae can survive to the third instar larval stage (Schulte *et al.,* 2010). To evaluate pNB reactivation in *mob4*$^{\Delta L3}$ mutants, pNBs' cell size (maximum diameter) and mitotic index were quantified and compared to Wild-type (WT) controls, using Dpn, phospho-HistoneH3 (Ph3) labelling mitosis and Discs-large marking cell membrane antibodies. At 1h ALH, there are no significant differences in pNB size or divisions (**Figure 2.11**). The proliferating NBs detected and scored correspond to the four mushroom body NBs (mbNBs, white asterisk) and one ventrolateral NB, which do not enter quiescence (**Figure 2.11. A, B**; Ito, K. & Hotta, 1992). These NBs remain proliferative from embryonic throughout larval stages development and are included in the proliferation scores. Overall at 1h ALH, the pNBs in *mob4*$^{\Delta L3}$ mutants are quiescent similar to those in WT controls.

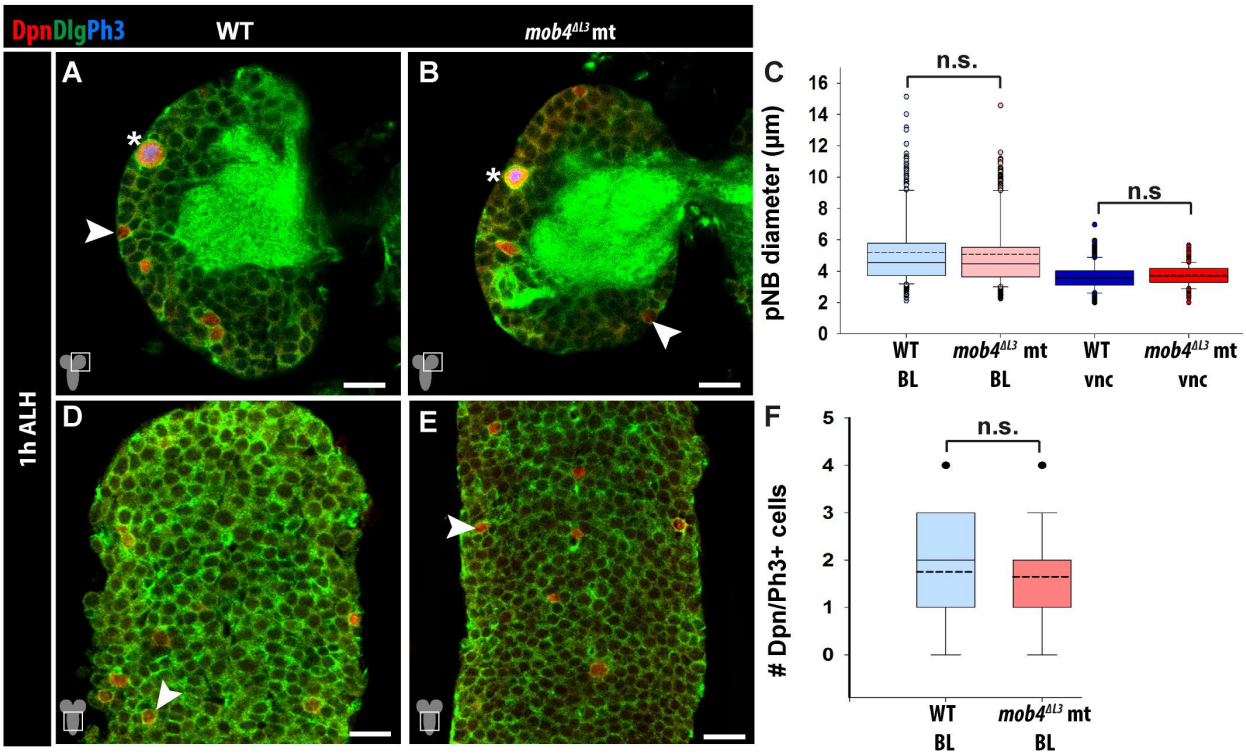


**Figure 2.2. pNBs are quiescent in both *mob4* mutants and controls immediately after larval hatching**: (**A, D)** Wild-type (WT, control) and **(B, E)** *mob4*$^{EY\Delta L3}$ (herein *mob4* $^{\Delta L3}$) mutant larval brain lobes (BLs) and ventral nerve cords (VNCs) at 1h after larval hatching (ALH), immunostained for **Deadpan (Dpn)**, **Discs large (Dlg)** and **Phospho-Histone-H3 (Ph3).** **(A-F)** All pNBs in mutants and controls (arrowheads) are quiescent (small size and not mitotic), except mushroom body pNBs (white asterisks). **(C)** Quantification of pNB diameters in BLs and VNCs shows that pNBs in *mob4*$^{\Delta L3}$ mutants are not statistically different compared to controls at 1h ALH (Control BL: median 4.5 µm, average 5.19 µm $n^{=359}$/10 BLs, 5 brains; mutant BL: median 4.5 µm, average 5 µm $n^{=441}$/10 BLs, 7 brains; Control VNC: median 3.6 µm, average 3.64 µm $n^{=321}$/7 VNCs; mutant VNC: median 3.7 µm, average 3.73 µm $n^{=171}$/5 VNCs). **(F)** Quantification of pNB divisions in BLs and VNCs in *mob4*$^{\Delta L3}$ mutants also shows no statistical differences compared to controls at 1h ALH (Control BL: median 2, average 1.75 Dpn/Ph3+ cells $n^{=24}$/24 BLs, 12 brains; mutant BL: median 2, average 1.65 Dpn/Ph3+ cells $n^{=20}$/20 BLs, 12 brains). There are no pNB divisions in the VNCs at this age. In this figure and throughout this thesis, the box and whisker plots show the data outliers (symbols above/below the boxplot); the minimum value (excluding outliers, lower whisker); the lower 25% quartile (box start); the average (dashed line); the median (solid line); upper 25% quartile (box end); the maximum value (excluding outliers, upper whisker). *p*=Wilcoxon rank-sum test. n.s non-significant *p*>0.05. All images are single focal planes, anterior up. Scale bar: 10 µm.

By 4h ALH, *mob4*$^{\Delta L3}$ mutant pNB diameters in BLs and VNCs are smaller compared to WT controls (**Figure 2.3. C**). There were no differences in pNB divisions, and the proliferating cells observed correspond to the mbNBs, and ventrolateral NB described earlier (**Figure 2.3. F**).

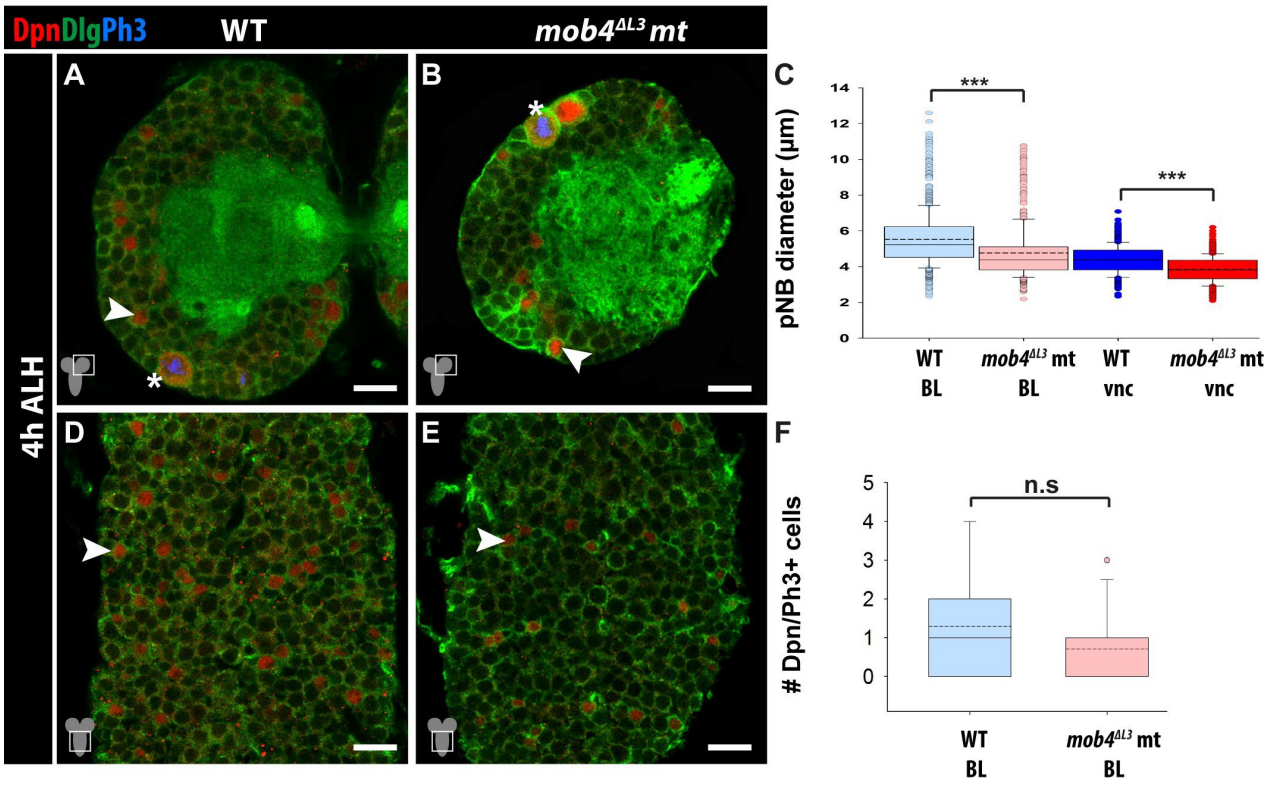


**Figure 2.3. pNBs in *mob4* mutants do not begin to enlarge in contrast to control pNBs**: **(A, D)** Wild-type (WT, control) and **(B, E)** *mob4*$^{\Delta L3}$ mutant larval brain lobes (BLs) and ventral nerve cords (VNCs) at 4h after larval hatching (ALH), immunostained for **Deadpan (Dpn)**, **Discs large (Dlg)** and **Phospho-Histone-H3 (Ph3)**. **(C)** Quantification of pNB diameters in BLs and VNCs shows that pNBs in *mob4*$^{\Delta L3}$ mutants are statistically smaller compared to controls at 4h ALH (Control BL: median 5.3 µm, average 5.5 µm $n^{=1121}$/14 BLs, 7 brains; *mob4*$^{\Delta L3}$ mutant BL: median 4.4 µm, average 4.8 µm $n^{=552}$/10 BLs, 5 brains; Control VNC: median 4.4 µm, average 4.4 µm $n^{=700}$/6 VNCs; *mob4*$^{\Delta L3}$ mutant VNC: median 3.8 µm, average 3.8 µm $n^{=331}$/5 VNCs). (F) Quantification of pNB divisions in BLs and VNCs in *mob4*$^{\Delta L3}$ mutants show no statistical difference compared to controls at 4h ALH (Control: median 1, average 1.3 Dpn/Ph3+ cells $n^{=24}$ 12 brains; mutant: median 0 , average 0.7 Dpn/Ph3+ cells $n^{=24}$ 12 brains). The only pNBs dividing at this stage are mushroom body pNBs (mbNBs, white asterisks). There are no pNB divisions in the VNCs at this age. *p*=Wilcoxon rank-sum test. *** $p<0.001$. n.s $p>0.05$. Arrowheads indicate pNBs. All images are single focal planes, anterior up. Scale bar: 10 µm.

At 24h ALH, the end of the first instar larval stage, the majority of pNBs have exited quiescence (Truman and Bate, 1988; Chell and Brand, 2010). As expected, the pNBs in the WT controls incorporate 5-ethynyl-2'-deoxyuridine (EdU) indicating entry into S-phase (DNA synthesis) of the cell cycle (**Figure 2.4. A, D**). However, pNBs in *mob4*$^{\Delta L3}$ mutants do not incorporate EdU, except the mbNBs (**Figure 2.4. B, E**). The *mob4*$^{\Delta L3}$ mutant BLs and VNCs are also dramatically smaller compared to the WT controls (**Figure 2.5. A, D** versus **Figure 2.5. B, E)**.

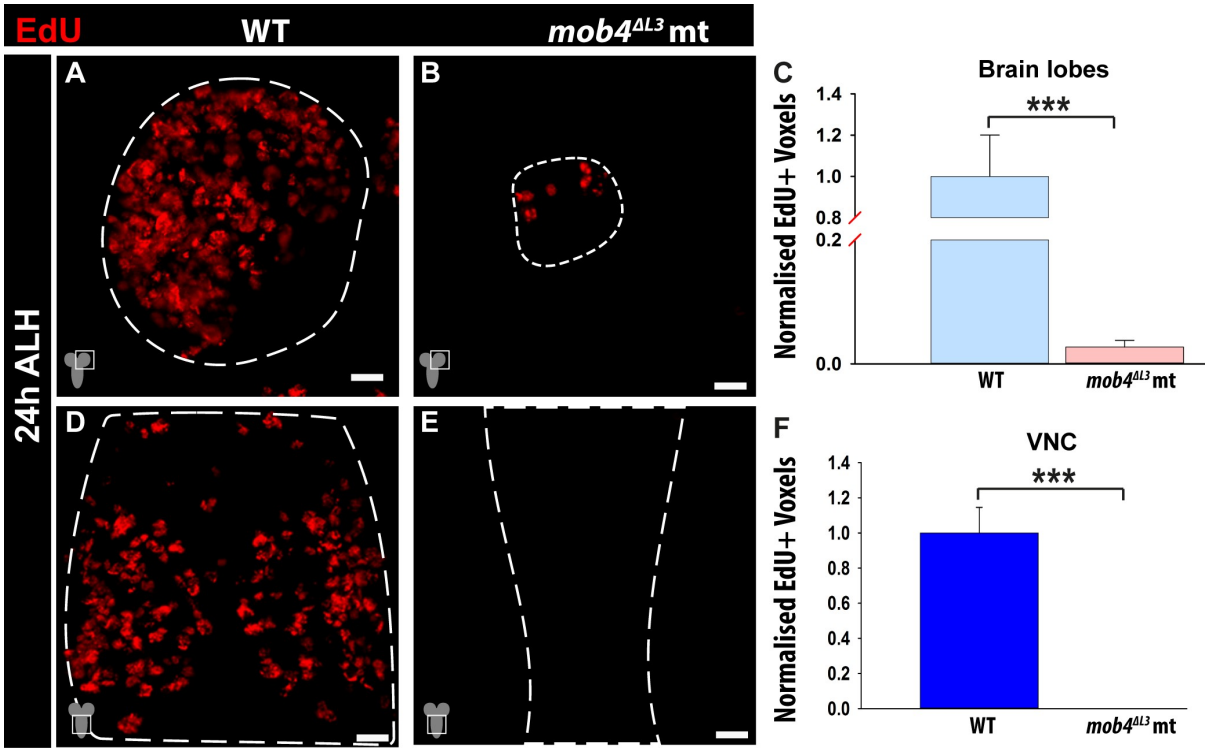


**Figure 2.4. *mob4* pNBs do not enter S-phase**: (**A, D)** Wild-type (WT, control) and **(B, E)** *mob4*$^{\Delta L3}$ mutant larval brain lobes (BLs) and ventral nerve cords (VNCs) at 24h after larval hatching (ALH), labelled with **5-ethynyl-2'-deoxyuridine (EdU)**. **(C)** Normalised EdU voxel quantification in either BLs or VNCs shows that pNBs in *mob4*$^{\Delta L3}$ mutants do not incorporate EdU in contrast to controls, indicating no entry into S-phase of the cell cycle, with the exception of mushroom body NBs (Control BL: average 1±0.2 $n^{=8}$/8 brains; *mob4*$^{\Delta L3}$ mutant BL: average 0.03±0.01 $n^{=8}$/8 brains; Control VNC: average 1±0.15 $n^{=7}$/7 brains; *mob4*$^{\Delta L3}$ mutant BL: average 0 $n^{=8}$/8 brains). Normalised average scores +/- s.e.m. are shown. *p*=Wilcoxon rank-sum test. *** *p*<0.001. White dashed lines mark BLs and VNCs. All images are Z-stack projections. Anterior up. Scale bar: 10 µm.

In addition to failing to enter S-phase, pNB size (white arrows) and mitotic index (yellow arrows) are dramatically smaller in the *mob4*$^{\Delta L3}$ mutants compared to WT controls at 24h ALH (**Figure 2.5.C, F**). At 48h ALH, pNBs in the *mob4*$^{\Delta L3}$ mutants are still unable to re-enter division (**Figure 2.5.G-I**). Interestingly, a tiny increase in the average size of pNBs in *mob4*$^{\Delta L3}$ mutants is observed at 4h ALH (**Figure 2.3.C**), and 24h ALH (**Figure 2.5.C**) compared to 1h ALH (**Figure 2.3C**), suggesting that the mutant pNBs attempt to enlarge but are unable to succeed (see Discussion).

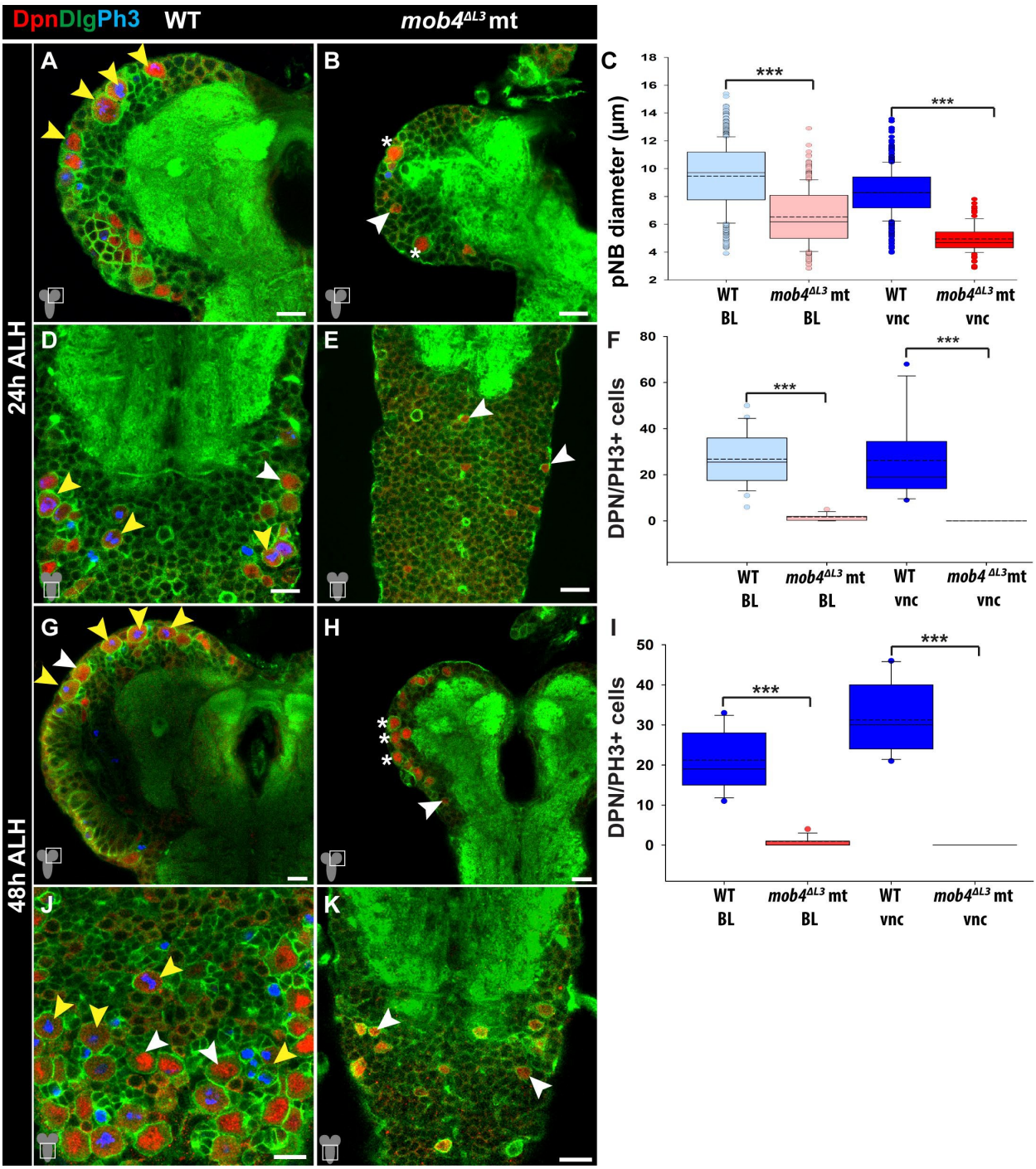
DpnDlgPh3 WT
mob4ΔL3 mt
24h ALH
48h ALH
A
B
C
D
E
F
G
H
I
J
K
pNB diameter (µm)
DPN/PH3+ cells
DPN/PH3+ cells
***
WT BL
mob4ΔL3 mt BL
WT vnc
mob4ΔL3 mt vnc

**Figure 2.5. *mob4* mutant pNBs fail to mitotically reactivate**: **(A, D, G, J)** Wild-type (WT, control) and **(B, E, H, K)** *mob4*$^{\Delta L3}$ mutant larval brain lobes (BLs) and ventral nerve cords (VNCs) immunostained for **Deadpan (Dpn)**, **Discs large (Dlg)** and **Phospho-Histone-H3 (Ph3)** at 24h ALH (A, B, D, E) and 48h ALH (G, H, J, K). **(C)** Quantification of pNB diameters in BLs and VNCs shows that pNBs in *mob4*$^{\Delta L3}$ mutants are smaller compared to controls at 24h After Larval Hatching (ALH) (Control BL: median 9.7 µm, average 9.5 µm n$^{=799}$/10 BLs, 7 brains; *mob4*$^{\Delta L3}$ mutant BL: median 6.2 µm, average 6.5 µm n$^{=}$ $^{395}$/18 BLs, 9 brains; Control VNC: median 8.3 µm, average 8.3 µm n$^{=584}$/5 VNCs; *mob4*$^{\Delta L3}$ mutant VNC: median 4.7 µm, average 4.9 µm n$^{=88}$/8 VNCs). **(F)** Quantification of pNB divisions in BLs and VNCs in *mob4*$^{\Delta L3}$ mutants shows no dividing pNBs compared to controls at 24h ALH, except mbNBs (Control BLs: median 25.5, average 26.8 Dpn/Ph3+ cells n$^{=24}$ 12 brains; *mob4*$^{\Delta L3}$ mutant BLs: median 2, average 1.7 Dpn/Ph3+ cells n$^{=}$ $^{24}$ 12 brains; Control VNCs: median 19, average 26.3 Dpn/Ph3+ cells n$^{=12}$/12 VNCs; *mob4*$^{\Delta L3}$ mutant VNCs: median 0, average 0 Dpn/Ph3+ cells n$^{=12}$/12 VNCs). **(G-I)** At 48h ALH, pNBs in *mob4* mutants remain not reactivated with no pNB divisions seen in BLs (except mbNBs ) or VNCs, in contrast to the controls (I; Control BLs: median 19, average 21.2 Dpn/Ph3+ cells n$^{=11}$/11 brains; *mob4*$^{\Delta L3}$ mutant BLs: median 1, average 1 Dpn/Ph3+ cells n$^{=}$ $^{11}$/11 brains; Control VNCs: median 30, average 31.3 Dpn/Ph3+ cells n$^{=11}$/11 VNCs; *mob4*$^{\Delta L3}$ mutant VNCs: median 0, average 0 Dpn/Ph3+ cells n$^{=11}$/11 VNCs). *p*=Wilcoxon rank-sum test. *** *p*<0.001. White arrowheads indicate pNBs; yellow arrowheads indicate Ph3+ pNBs**.** White asterisks label Ph3+ mbNBs. All images are single focal planes, anterior up. Scale bar: 10 µm.

Upon reactivation, type I pNBs divide asymmetrically to self-renew and generate GMCs which express the cell fate determinant *prospero* (*pros*) in their nuclei (reviewed in Jan and Jan, 1998). WT and *mob4*$^{\Delta L3}$ mutant CNSs were immunostained for Grainyhead (Grh, labelling NBs and GMCs, red), Pros (green) and Ph3 (blue) at 24h ALH. As expected, in WT, most of the pNBs in VNCs (type I) are reactivated and have generated GMCs (yellow arrows, **Figure 2.6. A**); contrasting with *mob4*$^{\Delta L3}$ mutant pNBs (white arrows, **Figure 2.6. B**). Together, the above results demonstrate that pNBs in *mob4*$^{\Delta L3}$ mutants fail to mitotically reactivate and generate progeny.

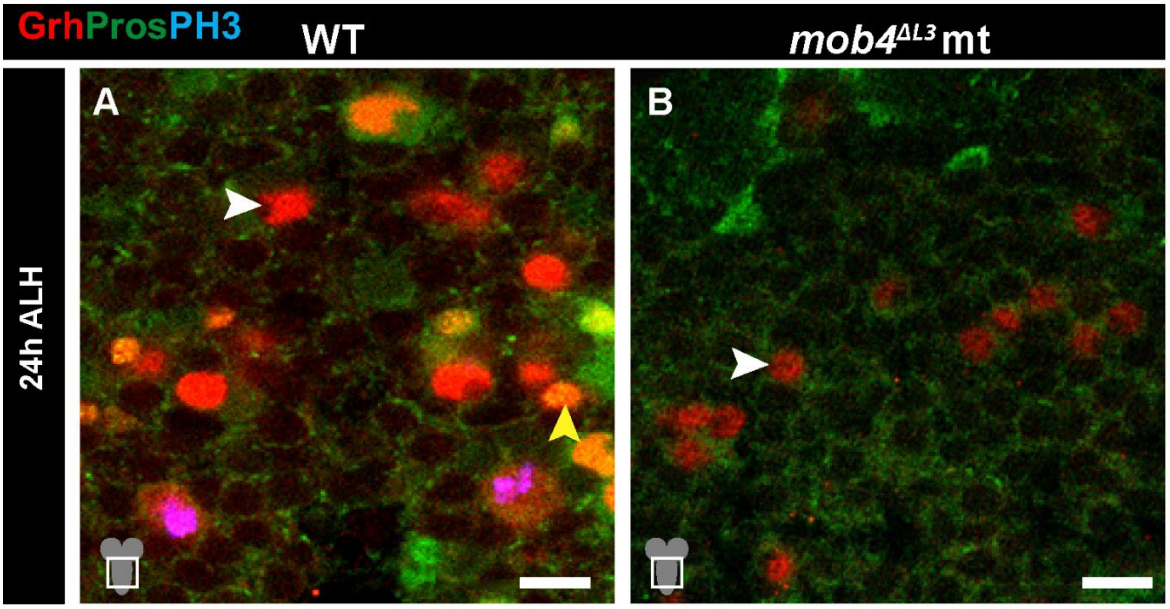


**Figure 2.6. *mob4* pNBs fail to generate neural progeny:** **(A)** Wild-type (WT, control) and **(B)** *mob4*$^{\Delta L3}$ mutant ventral nerve cords (VNCs) at 24h after larval hatching (ALH), labelled with **Grainyhead (Grh)**, **Prospero (Pros)** and **Phospho-Histone-H3 (Ph3)** antibodies. **(A)** WT pNBs (Grh+, no nuclear Pros) have mitotically reactivated to generate Ganglion Mother Cells (GMCs, Grh/nuclear Pros+). (**B**) *mob4* mutant pNBs remain small, do not divide (no Ph3 signal) and no GMCs can be observed. White arrowheads indicate pNBs. Yellow arrowhead labels a GMC. All images are single focal planes, anterior up. Scale bar: 10 µm.

## 2.3 Mob4 functions cell-autonomously in pNB reactivation

Since Mob4 expression in the CNS is not restricted to pNBs, an investigation was carried out to discern if Mob4 acts in a cell-autonomous way in pNBs. The *mob4*$^{\Delta L3}$ mutant strain was recombined with an *inscuteable*-Gal4 (*insc*-Gal4) line (see Materials and methods). This fly line allowed for any UAS constructs to be expressed in pNBs in a *mob4*$^{\Delta L3}$ mutant background. To validate the efficacy of this fly line, Mob4 antibody (red) was applied to 18h ALH *mob4*$^{\Delta L3}$ mutants with ectopic Mob4 expression in the pNBs (*mob4*$^{\Delta L3}$, *insc*-Gal4; UAS-*mob4;* herein *mob4*$^{\Delta L3}$, NB>*mob4;* **Figure 2.7. C, F**), control brains (*insc-Gal4* herein CNTRL, **Figure 2.7. A, D**) and *mob4* mutants recombined with insc-GAL4 (*mob4*$^{\Delta L3}$, *insc*-Gal4) (**Figure 2.7. B, E**). The brains were also immunostained for Dpn (green) and Dlg (blue). As anticipated, Mob4 protein is ubiquitous in control (CNTRL) brains including pNBs (white arrows, **Figure 2.7. A, D**) and is absent in the *mob4*$^{\Delta L3}$, *insc*-Gal4 mutant brains (white arrows, **Figure 2.7. B, E**). However, upon *mob4* ectopic expression in *mob4*$^{\Delta L3}$ mutant pNBs, Mob4 protein (red) can be readily seen in pNBs and their progeny (white arrows, **Figure 2.7. C, F**).

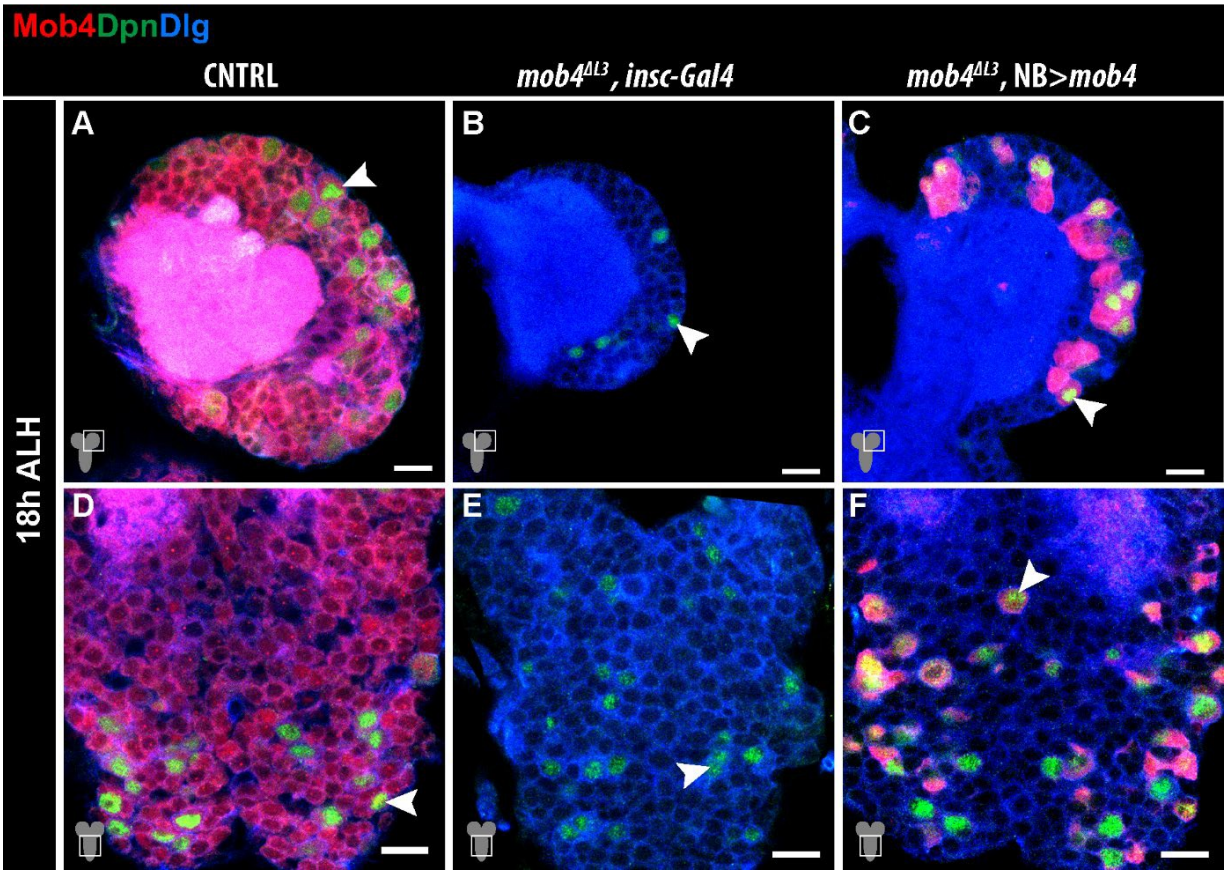


**Figure 2.7. Validation of *Drosophila* line allowing targeted Mob4 ectopic expression in *mob4* mutant pNBs:** Brain lobes **(A-C)** and ventral nerve cords **(D-F)** immunostained for **Mob4**, **Deadpan (Dpn)** and **Discs large (Dlg) at 18h ALH**. **(A, D) Mob4** is expressed throughout the larval brain lobes and ventral nerve cords of *Insc-Gal4* brains (control, CNTRL) and is absent in *mob4*$^{\Delta L3}$ mutants recombined with *Insc-Gal4 (mob4* $^{\Delta L3}$*, insc-Gal4)* **(B, E)**. However, **Mob4** protein is expressed in the pNBs and their progeny of these mutants when *mob4* is ectopically driven by *insc-Gal4*. White arrowheads indicate pNBs. All images are single focal planes, anterior up. Scale bar: 10 µm.

Once validated, the *mob4*$^{\Delta L3}$, NB>*mob4* flies were used for Mob4 rescue experiments (**Figure 2.8.**). First, it was determined if reintroducing Mob4 in pNBs of *mob4* mutants would rescue the observed pNB reactivation defects. Three fly strains were used for this experiment: *insc-Gal4* controls (CNTRLS, **Figure 2.8. A, D**); *mob4*$^{\Delta L3}$*,insc*-Gal4 mutants (**Figure 2.8. B, E**) and *mob4*$^{\Delta L3}$*,insc*-Gal4*;* UAS-*mob4* (*mob4*$^{\Delta L3}$,NB>*mob4* Rescue, **Figure 2.8. C, F**). The brains were immunostained for Dpn (red), Dlg (green) and Ph3 (blue) to quantify pNB size and mitotic index. Predictably, at 18h ALH, many CNTRL pNBs are enlarged (white arrows, **Figure 2.8. A, D**) and proliferate (yellow arrows, **Figure 2.8. A, D**) and the *mob4*$^{\Delta L3}$ mutant pNBs remain quiescent (white arrows, **Figure 2.8. B, E**). Remarkably, ectopic expression of Mob4 in pNBs of

*mob4*$^{\Delta L3}$ mutants can rescue pNB enlargement and re-entry into mitosis (yellow arrows, **Figure G, H**) to control values. The *mob4*$^{\Delta L3}$ mutant larval brains were small, whereas the pNB>*mob4* rescue larval brains were more akin to the controls. These results demonstrate that re-introduction of Mob4 in pNBs is sufficient to rescue pNB reactivation defects in *mob4* mutant brains.

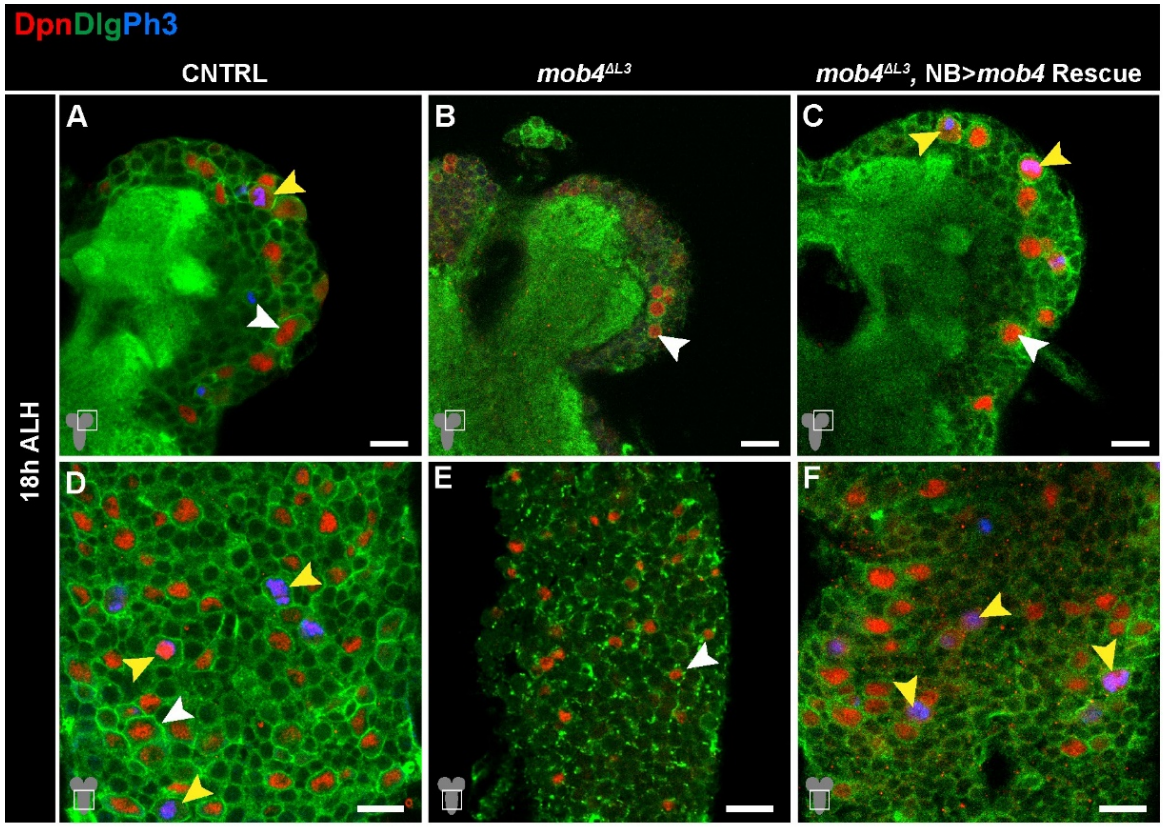


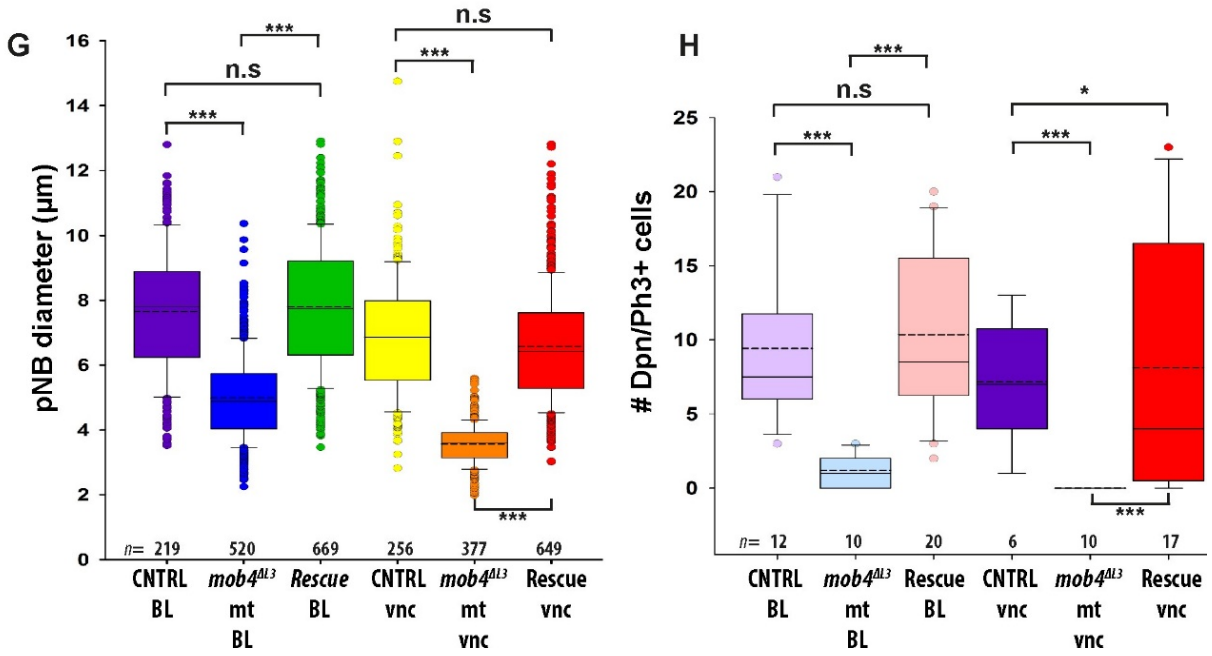

**Figure 2.8. Ectopic expression of Mob4 in pNBs of *mob4* mutants rescues mitotic reactivation.** **(A, D)** *Insc*-Gal4 (Control, CNTRL), **(B, E)** *mob4$^{\Delta L3}$*, *insc-Gal4* (*mob4* mt) and **(C, F)** *dmob4$^{\Delta L3}$, insc*-Gal4*;* UAS-*mob4* (*mob4$^{\Delta L3}$*, NB>*mob4* Rescue) brain lobes (BLs) and ventral nerve cords (VNCs) immunostained for **Deadpan (Dpn)**, **Discs large (Dlg)** and **Phospho-Histone-H3 (Ph3)**, at 18h ALH. pNBs of *mob4$^{\Delta L3}$* mutants have impaired enlargement and cannot re-enter division compared to controls. However, these defects can be rescued by ectopically expressing Mob4 in pNBs using the NB Gal4 driver *inscuteable-Gal4* (*insc-Gal4*). **(G)** Quantification of pNB sizes (BL pNB size – Control: median 7.8 µm, average 7.7 µm n$^{=219}$/3 BLs, 3 brains; *mob4* mutant: median 4.9 µm, average 5 µm n$^{=520}$/7 BLs, 7 brains; *mob4$^{\Delta L3}$*, NB>*mob4* Rescue: median 7.8 µm, average 7.8 µm n$^{=669}$/10 BLs, 5 brains. VNC pNB size – Control: median 6.9 µm, average 6.9 µm n$^{=256}$/3 VNCs; *mob4* mutant: median 3.6 µm, average 3.6 µm n$^{=377}$/4 VNCs; *mob4$^{\Delta L3}$*, NB>*mob4* Rescue: median 6.4 µm, average 6.6 µm n$^{=649}$/7 VNCs). **(H)** Quantification of pNB divisions (BL pNB divisions – Control: median 7.5, average 9.4 Dpn/Ph3+ cells n$^{=12}$/12 brains; *mob4* mutant: median 1, average 1.2 Dpn/Ph3+ cells n$^{=10}$/10 brains; *mob4$^{\Delta L3}$*,NB>*mob4* Rescue: median 8.5, average 10.4 Dpn/Ph3+ cells n$^{=10}$/10 brains. VNC pNB divisions Control: median 7, average 7.2 Dpn/Ph3+ cells n$^{=6}$/6 VNCs; *mob4* mutant: median 0, average 0 Dpn/Ph3+ cells n$^{=10}$/10 VNCs; *mob4$^{\Delta L3}$*, NB>*mob4* Rescue: median 4, average 8.1 Dpn/Ph3+ cells n$^{=10}$/10 VNCs). *p*=Wilcoxon rank-sum test. n.s. *p*>0.05, * *p*<0.05, *** *p*<0.001. White arrowheads indicate pNBs; yellow arrowheads indicate Ph3+ pNBs**.** All images are single focal planes, anterior up. Scale bar: 10 µm.

Second, since the glial niche performs vital roles in pNB quiescence and reactivation (Chell and Brand, 2010; Sousa-Nunes *et al.,* 2011; Ding *et al.,* 2016), the next step was to perform rescue experiments by expressing Mob4 in the glia of *mob4*$^{\Delta L3}$ mutant brains. The *mob4*$^{\Delta L3}$ mutant allele was combined with *repo-Gal4* to allow ectopic Mob4 expression in CNS glia in a *mob4*$^{\Delta L3}$ mutant background (*mob4*$^{\Delta L3}$ mt, Glia>*mob4* rescue). At 18h ALH, the overall brain size of the *mob4* mutants expressing Mob4 in glia is comparable to the *mob4*$^{\Delta L3}$ mutants; both are much smaller than the controls **Figure A-H**). The pNBs in *mob4*$^{\Delta L3}$ mutant brains (white arrows, **Figure 2.9. D, E**) and in the *mob4*$^{\Delta L3}$ mutants expressing Mob4 in glia (white arrows, **Figure 2.9. G, H**) are markedly smaller compared to the controls (white arrows, **Figure 2.9. A, B**). Quantifications confirmed that forcing Mob4 expression in the glia of *mob4*$^{\Delta L3}$ mutants cannot rescue pNB size (**Figure 2.9. C, F**) or mitotic activity defects (**Figure 2.9. I, L**) to the control values. However, a minimal yet significant increase is observed in both size and divisions when comparing brain lobe or VNC pNB sizes, as well as brain lobe pNB divisions, in the *mob4*$^{\Delta L3}$ mt, Glia>*mob4* expressing brains with *mob4*$^{\Delta L3}$ mutants (**Figure 2.9. C, F, I, L**). Overexpressing *mob4* in glia in a WT background using *repo-Gal4; UAS-mob4* (Glia>*mob4*) caused a tiny but significant VNC pNB size increase

compared to the controls, at 18h ALH (**Figure 2.9. F**; see Discussion). However, analysis of the size of brain lobe pNBs (**Figure 2.9. C**), or pNB divisions in either brain lobes or VNCs show no significant differences (**Figure 2.9. I, L**) compared to controls.

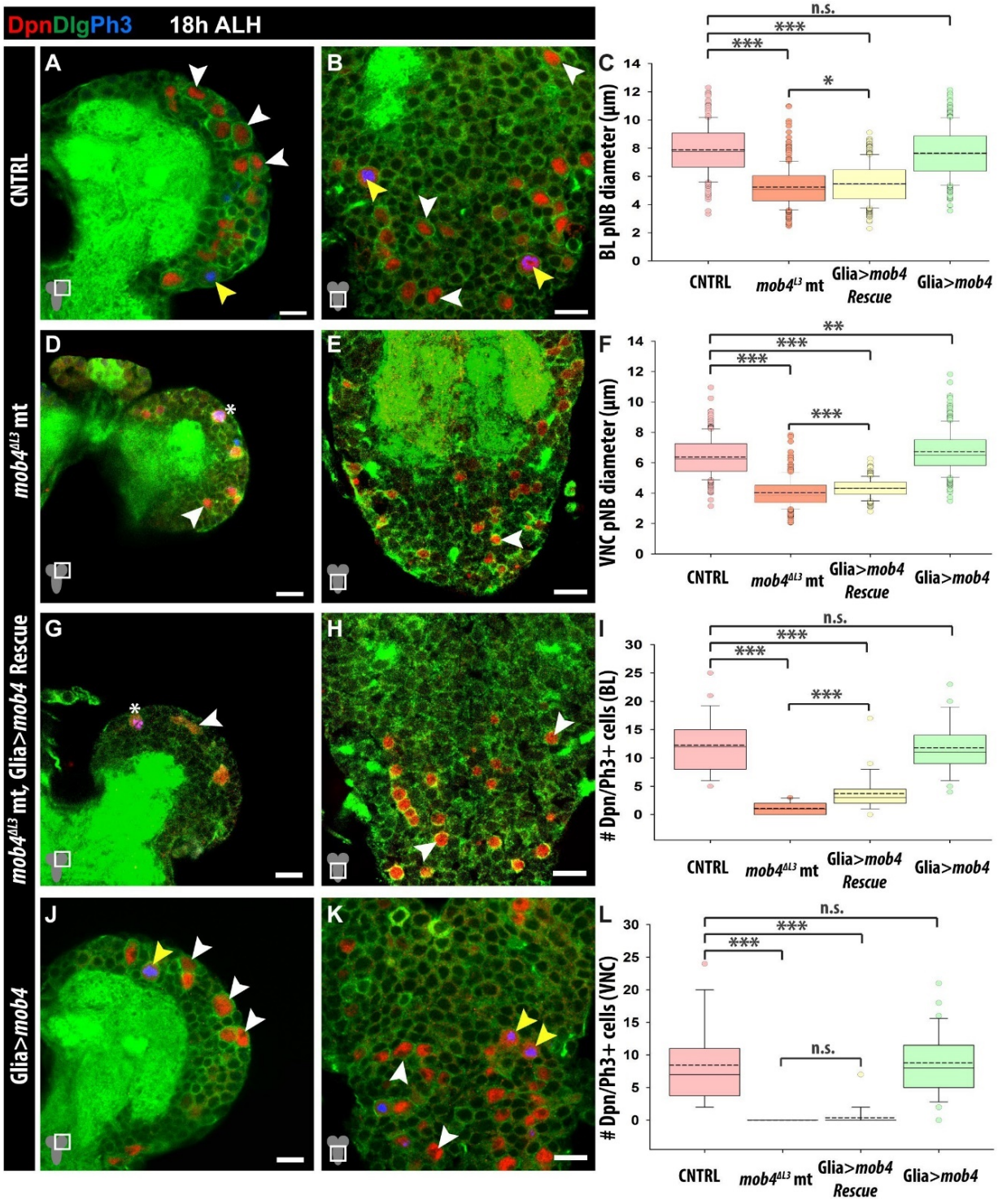

**Figure 2.9. Mob4 ectopic expression in glia is unable to rescue pNB reactivation in *mob4* mutants and its overexpression in control brains causes a minor premature enlargement only in VNC pNBs : (A, B)** *repo*-Gal4 (control, CNTRL), **(D, E)** $mob4^{\Delta L3}$ mutant ($mob4^{\Delta L3}$ *mt*), **(G, H)** $mob4^{\Delta L3}$*;* *repo*-Gal4; UAS-*mob4* ($mob4^{\Delta L3}$ mt*,* Glia>*mob4* Rescue)*,* **(J, K)** *repo*-Gal4; UAS-*mob4* (*Glia* > *mob4*). Larval brain lobes (BLs) and ventral nerve cords (VNCs) are immunostained for **Deadpan (Dpn)**, **Discs large (Dlg)** and **Phospho-Histone-H3 (Ph3)**, at 18 h After Larval Hatching (ALH)**. (C, F)** Quantification of pNB diameters in BLs **(C)** and VNCs (**F**) shows that driving *mob4* in glia of $mob4^{\Delta L3}$ mutants does not rescue the pNB enlargement defects to control values. However, there is a small increase in pNB size when compared to *mob4* mutant values. Also, *mob4* overexpression in glia in control background does not affect the size of pNBs in BLs but leads to a small increase in VNC pNBs. **(C)** pNB size quantifications in BLs (Control: median 7.8 µm, average 7.9 µm $n^{188}$/3 BLs, 2 brains; $mob4^{\Delta L3}$mt: median 5.1 µm, average 5.2 µm $n^{=307}$ /5 BLs, 4 brains; $mob4^{\Delta L3}$ mt, Glia> *mob4* Rescue: median 5.4 µm, average 5.5 µm $n^{= 310}$/4 BLs, 3 brains; Glia> *mob4*: median 7.6 µm, average 7.7 µm $n^{= 278}$/4 BLs, 2 brains). **(F)** pNB size quantifications in VNCs (Control: median 6.3 µm, average 6.4 µm $n^{=278}$/3 VNCs; $mob4^{\Delta L3}$mt: median 3.9 µm, average 4 µm $n^{=206}$/4 VNCs; $mob4^{\Delta L3}$ mt, Glia> *mob4* Rescue: median 2.8 µm, average 4.3 µm $n^{=253}$/5 VNCs; Glia> *mob4***:** median 6.5 µm, average 6.7 µm $n^{=233}$/3 VNCs). **(I, L)** Quantification of pNB divisions (Dpn/Ph3+ cells) in BLs **(I)** and VNCs **(L)** shows that ectopic expression of *mob4* in glia of *mob4* mutants cannot rescue the mitotic defects to control values. However, there is a small increase in dividing pNBs in the BLs when compared to *mob4* mutant values. *mob4* overexpression in glia in control background does not affect pNB divisions compared to controls. **(I)** BL pNB division quantifications (Control: median 12, average 12.3 Dpn/Ph3+ cells $n^{=28}$ 28 BLs, 14 brains; $mob4^{\Delta L3}$ mt: median 1, average 1.2 Dpn/Ph3+ cells $n^{=34}$ 17 brains; $mob4^{\Delta L3}$ mt, Glia> *mob4*: median 3, average 3.7 Dpn/Ph3+ cells $n^{=57}$ 26 brains; Glia> *mob4*: median 11, average 11.8 Dpn/Ph3+ cells $n^{=66}$ 66 BLs, 33 brains). **(L)** VNC pNB division quantifications (Control: median 7, average 8.4 Dpn/Ph3+ cells $n^{=14}$/14 VNCs; $mob4^{\Delta L3}$ mt: median 0, average 0.4 Dpn/Ph3+ cells $n^{=17}$/17 VNCs; $mob4^{\Delta L3}$ mt, Glia> *mob4*: median 0, average 0.4 Dpn/Ph3+ cells $n^{=29}$/29 VNCs; Glia> *mob4***:** median 8, average 8.8 Dpn/Ph3+ cells $n^{=33}$/33 VNCs). *p*=Wilcoxon rank-sum test. n.s (non-significant) $p>0.05$ * $p<0.05$, ***$p<0.001$. White arrowheads indicate pNBs; yellow arrowheads indicate Ph3+ pNBs. The white asterisk indicates mbNBs. All images are single focal planes, anterior up. Scale bar: 10 µm.

Finally, RNA interference was used to knockdown *mob4* expression, specifically in pNBs using *insc-Gal4* (**Figure 2.10.**). Membrane-tagged GFP was simultaneously expressed (UAS-CD8-GFP, *UCD8-GFP*). Larval brains with *mob4* knock-down in the pNBs (UAS-*dicer*; *insc*-Gal4*, UCD8-GFP*; UAS-*mob4*-RNAi) were dissected and immunostained for Dpn (red), GFP (green) and Ph3 (blue), and compared to the controls (UAS-*dicer*; *insc*-Gal4*,UCD8-GFP*, CNTRL), at 18h ALH. *mob4*-RNAi specifically in pNBs RNAi (NB>*mob4*-RNAi, **Figure 2.10. B, E**) leads to a small but significant reduction in pNB enlargement (**Figure 2.10. C**) compared to the controls

(**Figure 2.10. A, D)**. NB>*mob4*-RNAi pNBs also showed significantly reduced mitotic reactivation compared to the controls (yellow arrows, **Figure 2.10. F**). Together, the above results indicate that Mob4 acts primarily cell-autonomously in pNBs promoting reactivation.

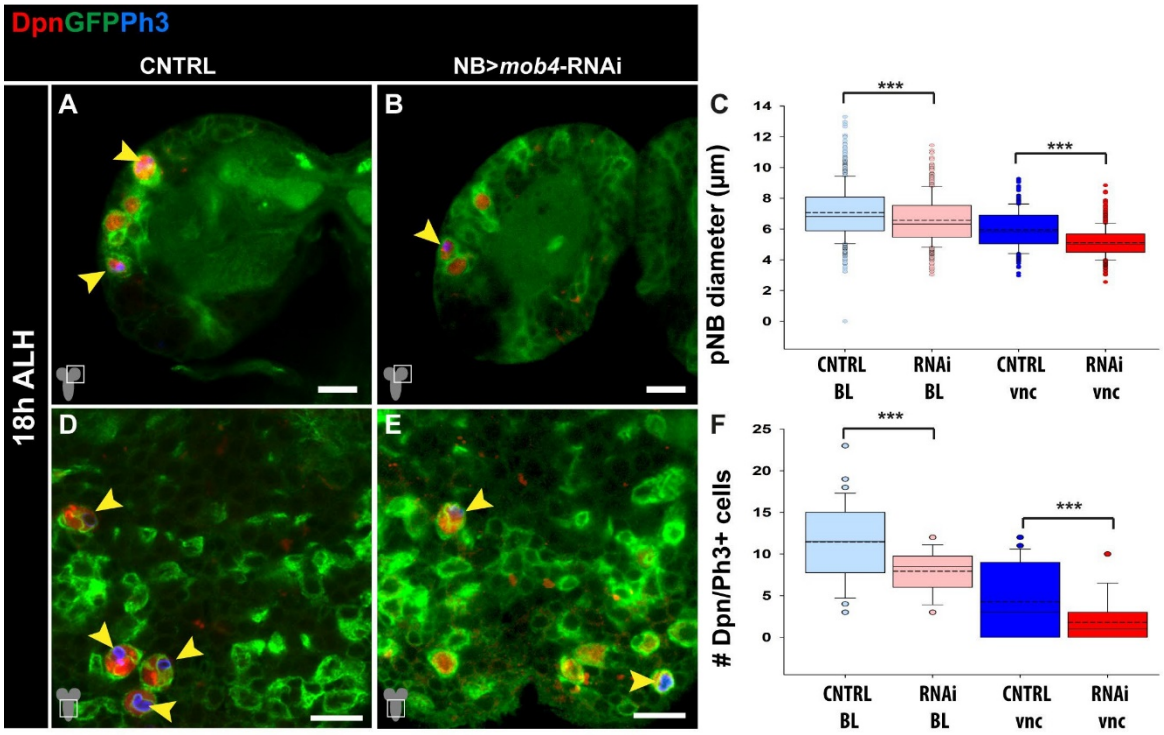


**Figure 2.10. Mob4 inhibition via RNAi delays pNBs mitotic reactivation:** (**A, D)** UAS-*dicer*; *insc*-Gal4, *UCD8-GFP* (control, CNTRL) and **(B, E)** UAS-*dicer*; *insc*-Gal4, *UCD8-GFP*; UAS-*mob4*-RNAi (NB>*mob4*-RNAi) brain lobes (BLs) and ventral nerve cords (VNCs) immunostained for **Deadpan (Dpn)**, **green fluorescent protein (GFP)** and **Phospho-Histone-H3 (Ph3),** at 18h After Larval Hatching (ALH). **(C)** Quantification of pNB diameters in BLs and VNCs shows that pNBs with *mob4*-RNAi are smaller compared to controls (Control BL: median 6.8 µm, average 7 µm $n^{=684}$/9 BLs, 9 brains; *mob4*-RNAi BL: median 6.3 µm, average 6.6 µm $n^{= 614}$/8 BLs, 8 brains; Control VNC: median 5.8 µm, average 6 µm $n^{=441}$/5 VNCs; *mob4*-RNAi VNC: median 5 µm, average 5.1 µm $n^{=686}$/5 VNCs). **(F)** pNB divisions in BLs and VNCs in pNBs with *mob4*-RNAi are also statistically less compared to controls (Control BL: median 11.5, average 11.4 Dpn/Ph3+ cells $n^{=46}$ 23 brains; *mob4*-RNAi BL: median 8.5, average 7.9 Dpn/Ph3+ cells $n^{= 28}$ 14 brains; Control VNC: median 3, average 4.3 Dpn/Ph3+ cells $n^{=23}$/23 VNCs; *mob4*-RNAi VNC: median 1, average 1.8 Dpn/Ph3+ cells $n^{=14}$/14 VNCs). *p*=Wilcoxon rank-sum test. *** $p<0.001$. Yellow arrowheads indicate Ph3+ pNBs**.** All images are single focal planes, anterior up. Scale bar: 10 µm.

## 2.4 Mob4 or human MOB4 (Phocein) overexpression leads to premature pNB reactivation

To strengthen the results indicating that Mob4 is required for pNB reactivation, the next step was to analyse the potential effects of Mob4 overexpression in pNBs. Mob4 was overexpressed using *insc-Gal4* during a period of when pNB are still mitotically quiescent (6h ALH) and when pNB reactivation is ongoing (18h ALH). Larval brains with Mob4 overexpressing pNBs (*insc*-Gal4*, UCD8-GFP*; UAS-*mob4,* NB>*mob4*) were dissected and immunostained for Dpn (red), GFP (green) and Ph3 (blue), and compared to controls (*insc*-Gal4*, UCD8-GFP*, CNTRL) (**Figure 2.11**). At 6h ALH, pNBs are of small size and only the mbNBs/vNB are mitotically active (white asterisk, **Figure 2.11. A, B**). In contrast, pNBs in NB>*mob4* larval brains (white arrows, **Figure 2.11. B, E**) showed a significant increase in pNB size (**Figure 2.11. C**) compared to the controls (white arrows, **Figure 2.11. A, D**). However, there were no significant differences in pNB divisions between the two groups at this time point (**Figure 2.11. F**). At 18h ALH, overexpression of Mob4 (NB>*mob4*; **Figure 2.11. H, K**) did not cause a further increase in pNB diameters (**Figure 2.11. I**) compared to the controls (**Figure 2.11. G, J**), yet more pNBs in division were detected compared to the controls (yellow arrows, **Figure 2.11. L**). These experiments demonstrate that Mob4 overexpression leads to premature pNB reactivation.

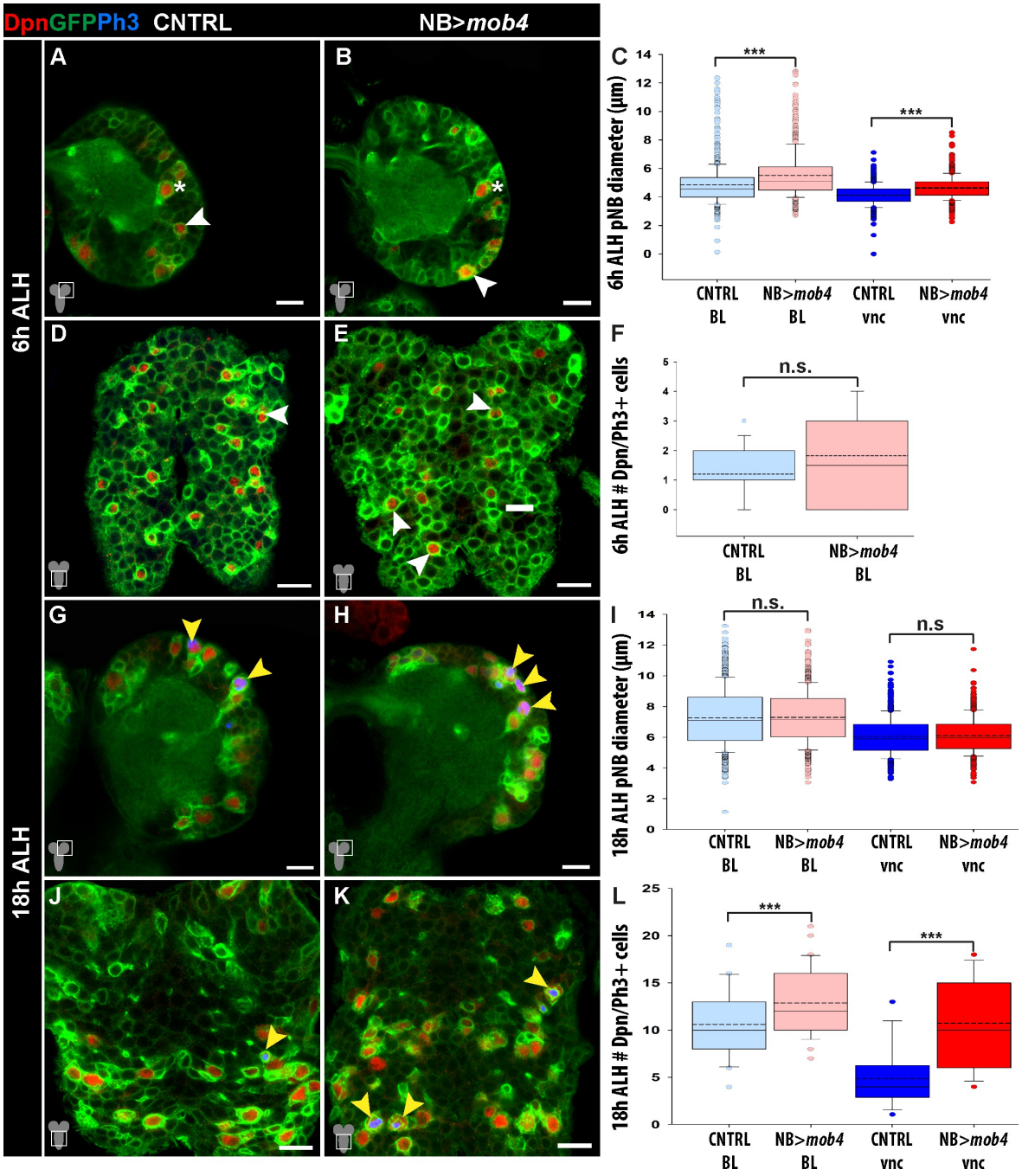
DpnGFPPh3 CNTRL
NB>mob4
6h ALH
18h ALH
A
B
C
D
E
F
G
H
I
J
K
L
6h ALH pNB diameter (µm)
6h ALH # Dpn/Ph3+ cells
18h ALH pNB diameter (µm)
18h ALH # Dpn/Ph3+ cells
***
n.s.
n.s
CNTRL BL
NB>mob4 BL
CNTRL vnc
NB>mob4 vnc

**Figure 2.11. pNBs overexpressing Mob4 show premature enlargement and entry into division**: (**A, D, G, J)** *insc-Gal4, UCD8-GFP* (control; CNTRL) and **(B, E, H, K)** *mob4* overexpression specifically in pNBs (*insc-Gal4, UCD8-GFP; UAS-mob4*) larval brain lobes (BLs) and ventral nerve cords (VNCs) immunostained for **Deadpan (Dpn)**, **green fluorescent protein (GFP)** and **Phospho-Histone-H3 (Ph3)** and at 6h and 18h after larval hatching (ALH)**. (C)** Quantification of pNB diameters in BLs and VNCs shows that pNBs with Mob4 overexpression (NB>*mob4*) enlarge prematurely compared to controls at 6h ALH (Control BL: median 4.6 µm, average 4.9 µm $n^{=664}$/10 BLs, 5 brains; NB>*mob4* BL: median 5.3 µm, average 5.6 µm $n^{=478}$/10 BLs, 5 brains; Control VNC: median 4.1 µm, average 4.1 µm $n^{=613}$/6 VNCs; NB>*mob4* VNC: median 4.6 µm, average 4.7 µm $n^{=657}$/6 VNCs). **(F)** pNB divisions in BLs show no statistical difference between *mob4* overexpression compared to controls at 6h ALH (Control BL: median 1, average 1.2 Dpn/Ph3+ cells $n^{=24}$ 12 brains; NB>*mob4* BL: median 1.5, average 1.8 Dpn/Ph3+ cells $n^{=22}$ 11 brains). pNB division corresponds to only mbNBs. No Dpn/Ph3+ cells were observed in the VNCs of either group at this age. **(I)** At 18h ALH, pNB diameters in BLs and VNCs show no statistical differences (Control BL: median 7.1 µm, average 7.3 µm $n^{=1052}$/14 BLs, 7 brains; NB>*mob4* BL: median 7.2 µm, average 7.3 µm $n^{=1004}$/14 BLs, 9 brains; Control VNC: median 5.9 µm, average 6.1 µm $n^{=657}$/6 VNCs; NB>*mob4* VNC: median 6 µm, average 6.1 µm $n^{=630}$/6 VNCs). **(L)** At 18h ALH overexpression of *mob4* in pNBs shows increased numbers of dividing pNBs compared to controls in both BLs and VNCs (Control BL: median 10, average 10.6 Dpn/Ph3+ cells $n^{=24}$ 12 brains; NB>*mob4* BL: median 12, averaged 12.9 Dpn/Ph3+ cells $n^{=20}$ 10 brains; Control VNC: median 4, average 4.9 Dpn/Ph3+ cells $n^{=10}$ 10 brains; NB>*mob4* VNC: median 10, average 10.7 Dpn/Ph3+ cells $n^{=15}$ 15 brains). *p*=Wilcoxon rank-sum test. *** $p<0.001$, $p>0.05$ ns (non-significant). White arrowheads indicate pNBs; yellow arrowheads indicate Ph3+ pNBs**.** Mushroom body pNBs (white asterisks). All images are single focal planes, anterior up. Scale bar: 10 µm.

Mob4 shares 80% amino acid homology with its human ortholog, MOB4 (also known as Phocein), and can rescue the lethality of *mob4* mutants (Schulte *et al.,* 2010). To assess whether Mob4 action in pNB reactivation may be evolutionary conserved, *phocein* was overexpressed in pNBs at 6h ALH and 18h ALH (**Figure 2.12.**). Larval brains with *phocein* overexpressing pNBs (*insc*-Gal4*, UCD8-GFP*; UAS-*phocein,* NB> *phocein*) were dissected and immunostained for Dpn (red), GFP (green) and Ph3 (blue), and compared to the controls (*insc*-Gal4*, UCD8-GFP*, CNTRL) (**Figure 2.12**). At 6h ALH the pNBs are small with only the mbNBs/vNB enlarged and mitotically active (white asterisk, **Figure 2.12. A, B**). pNBs in NB>*phocein* larval brains (white arrows, **Figure 2.12. B, E**) showed a significant increase in pNB size and a small increase in divisions (**Figure 2.12. C, F**) compared to the controls (**Figure 2.12. A, D**). At 18 h ALH, pNBs in NB>*phocein* brains (yellow arrows, **Figure 2.12. H, K**) also displayed significant increases in pNB diameters and divisions (yellow arrows, **Figure 2.12. L**)

compared to the controls (yellow arrows, **Figure 2.12. G, J**). The results indicate that Phocein overexpression causes precocious pNB reactivation, similar to mob4 overexpression, which suggests a conserved function.

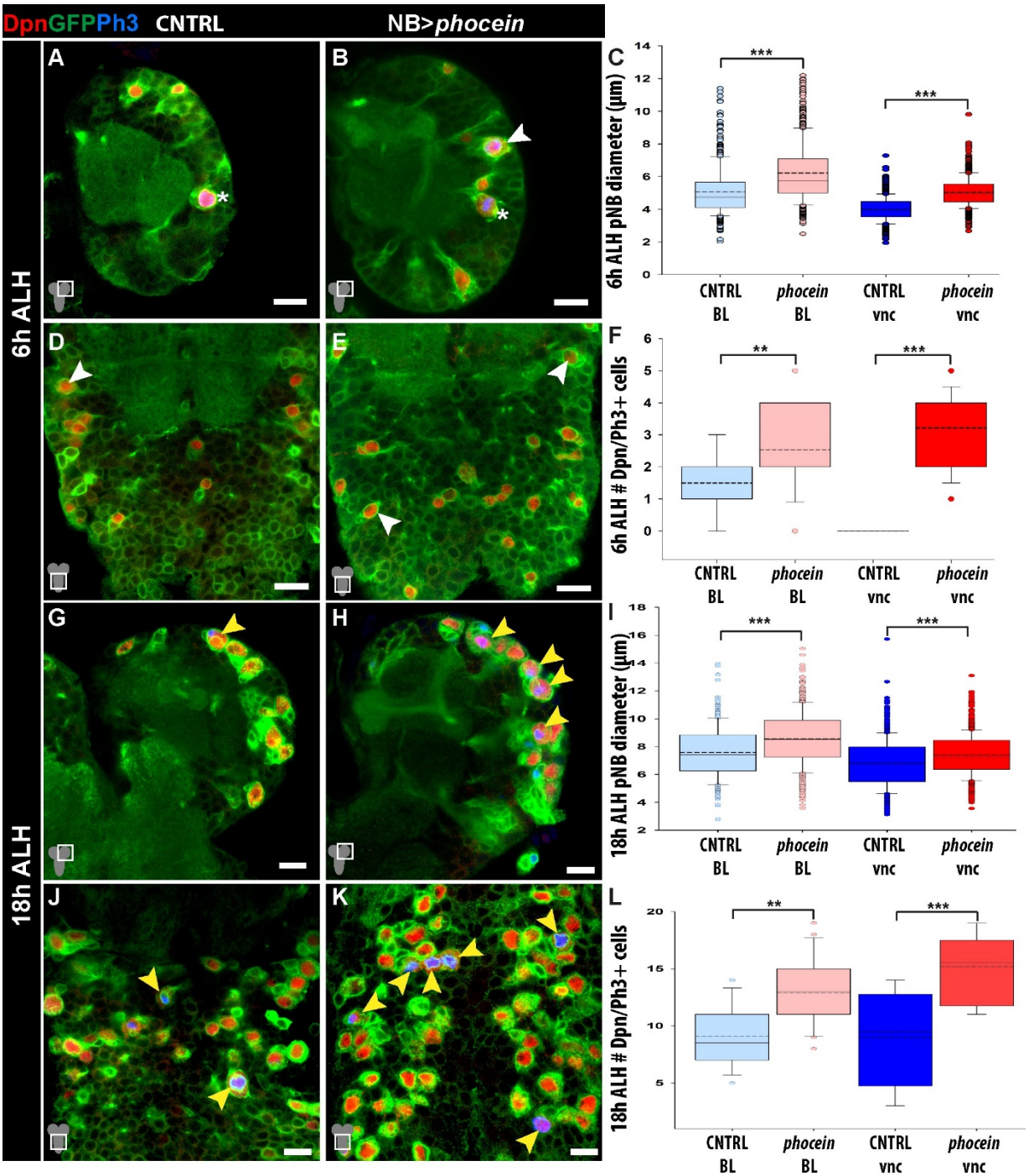

**Figure 2.12. Overexpressing the human ortholog of *mob4*, *phocein*, results in premature pNB reactivation:** (**A, D, G, J)** *Insc*-Gal4,*UCD8-GFP* (controls; CNTRL) and **(B, E, H, K)** Human MOB4 (Phocein) overexpression specifically in pNBs (*Insc*-Gal4,*UCD8-GFP*; UAS-*phocein,* NB>*phocein*) larval brain lobes (BLs) and ventral nerve cords (VNCs) immunostained for **Deadpan (Dpn)**, **green fluorescent protein (GFP)** and **Phospho-Histone-H3 (Ph3)** at 6h and 18h after larval hatching (ALH). **(C, F)** Quantification of pNB diameters in BLs and VNCs shows that pNBs with *phocein* overexpression enlarge and start dividing prematurely compared to controls at 6h ALH. **(C)** pNB diameters quantifications at 6h ALH (Control BL: median 4.7 µm, average 5.1 µm $n^{466}$/32 BLs, 16 brains; NB>*phocein* BL: median 5.7 µm, average 6.2 µm $n^{= 508}$/6 BLs, 3 brains; Control VNC: median 3.9 µm, average 4 µm $n^{=682}$/5 VNCs; NB>*phocein* VNC: median 5 µm, average 5 µm $n^{=654}$/5 VNCs). **(F)** pNB divisions at 6h ALH (Control BL: median 1, average 1.5 Dpn/Ph3+ cells $n^{=32}$ 16 brains; NB>*phocein* BL: median 2, average 2.5 Dpn/Ph3+ cells $n^{= 28}$ 14 brains; Control VNC: median 0, average 3.2 Dpn/Ph3+ cells $n^{=32}$ 12 VNCs; *phocein* VNC: median 2, average 2.5 Dpn/Ph3+ cells $n^{= 28}$ 14 VNCs). **(I, L)** At 18h ALH pNBs with *phocein* overexpression also enlarge and mitotically reactivate prematurely compared to controls. **(I)** pNB diameters quantifications (Control BL: median 7.4 µm, average 7.6 µm $n^{521}$/7 BLs, 5 brains; NB>*phocein* BL: median 8.5 µm, average 8.6 µm $n^{= 533}$/7 BLs, 5 brains; Control VNC: median 6.8 µm, average 6.8 µm $n^{=697}$/6 VNCs; NB>*phocein* VNC: median 7.3 µm, average 7.4 µm $n^{=710}$/6 VNC). **(L)** pNB divisions quantifications (Control BL: median 8.5, average 9.1 Dpn/Ph3+ cells $n^{=26}$/13 brains; NB>*phocein* BL: median 13, average 12.9 Dpn/Ph3+ cells $n^{= 40}$/20 brains; Control VNC: median 9.5, average 9 Dpn/Ph3+ cells $n^{=13}$/13 brains; NB>*phocein* VNC: median 15.5, average 15.2 Dpn/Ph3+ cells $n^{= 20}$/ 20 brains). *p*=Wilcoxon rank-sum test. ****p*<0.01 *****p*<0.001. White arrowheads indicate pNBs; yellow arrowheads indicate Ph3+ pNBs. Mushroom body pNBs (white asterisks). All images are single focal planes, anterior up. Scale bar: 10 µm.

Given that *mob4* overexpression in pNBs leads to premature reactivation, the next step was to determine if it also leads to overproliferation of pNBs later in development. Using the same fly strains for the *mob4* overexpression experiments, larval brains with *mob4* overexpressing pNBs (*insc*-Gal4*, UCD8-GFP*; UAS-*mob4,* NB>*mob4*) were dissected and immunostained for Dpn (red), GFP (green) and Ph3 (blue), and compared to the controls (*insc*-Gal4*, UCD8-GFP*, CNTRL) (**Figure 2.13**) at 48h and 94h ALH. pNBs in NB>*mob4* VNCs only (white arrows, **Figure 2.13. B, E**) showed a significant increase in pNB divisions (**Figure 2.13. C**) compared to the controls (white arrows, **Figure 2.13. A, D**) at 48h ALH, a time when pNB reactivation still occurs but is about to cease (White and Kankel, 1978; Truman and Bate, 1988; Maurange *et al.,* 2008). However, there were no significant differences in pNB divisions in NB>mob4 brain lobes or VNCs (white arrows, **Figure 2.13. H, K**) compared to the controls (white

arrows, **Figure 2.13. G, J**) at 94h ALH (**Figure 2.13. I**). Therefore, mob4 overexpression in the pNBs leads to early reactivation but does not cause overproliferation.

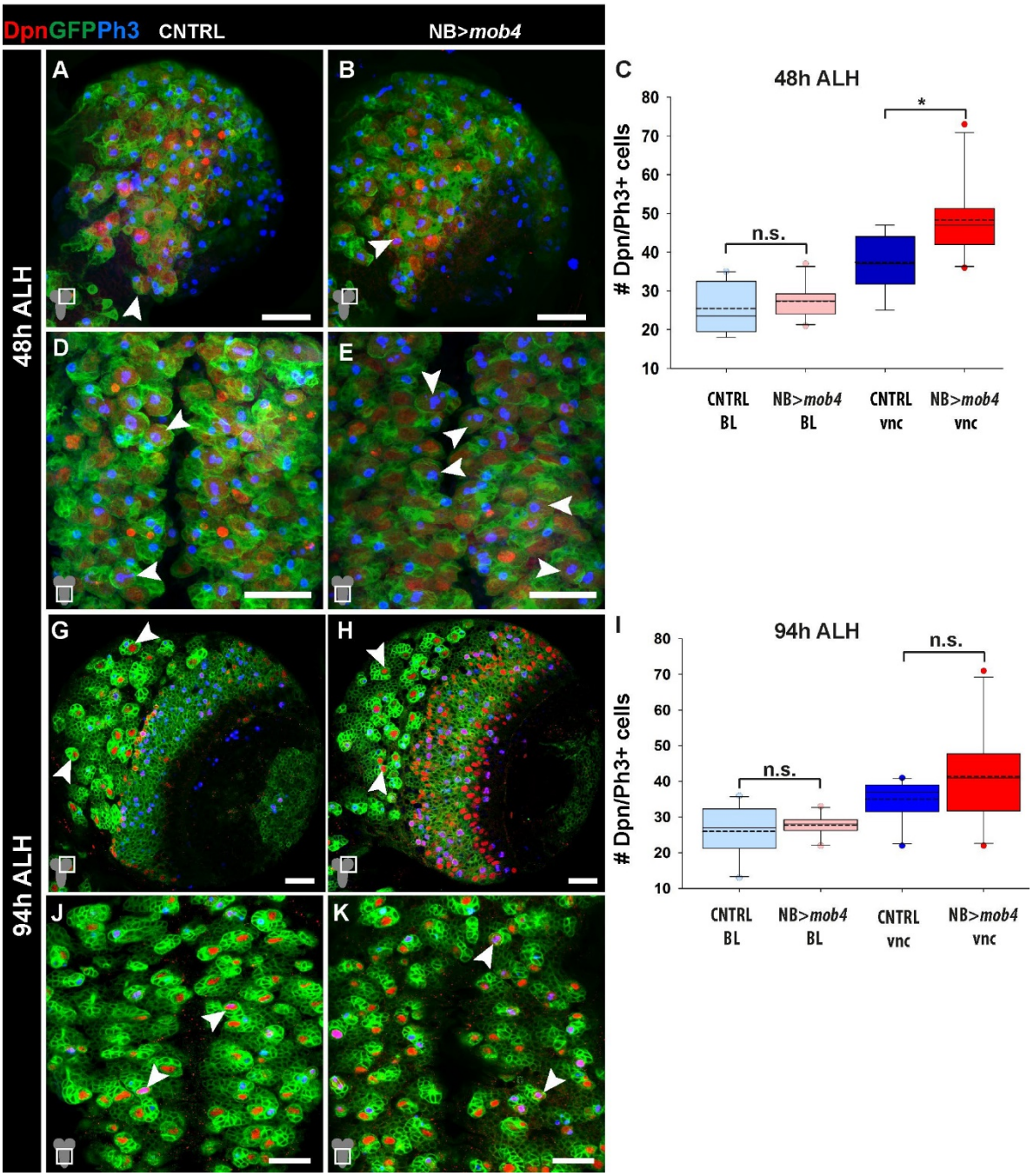

**Figure 2.13. Mob4 overexpression in pNBs does not cause overproliferation**: (**A, D, G, J)** *Insc*-Gal4,*UCD8-GFP* (control; CNTRL) and **(B, E, H, K)** Mob4 overexpression specifically in pNBs (*Insc*-Gal4,*UCD8-GFP*; UAS-*mob4,* NB>*mob4*) larval brain lobes (BLs) and ventral nerve cords (VNCs) immunostained for **Deadpan (Dpn)**, **green fluorescent protein (GFP)** and **Phospho-Histone-H3 (Ph3)** at 48 and 94h ALH. **(C)** At 48h ALH, pNB divisions in VNCs are higher in pNBs with mob4 over-expression (NB> *mob4*) compared to controls however there was not a difference in divisions in the BLs (Control BL: median 23.5, average 25.5 Dpn/Ph3+ cells $n^{=10}$ 9 brains; NB> *mob4* BL: median 27.5, average 27.4 Dpn/Ph3+ cells $n^{=10}$ 10 brains; Control VNC: median 31.5, average 33.4 Dpn/Ph3+ cells $n^{=8}$ 8 brains; NB> *mob4* VNC: median 49.5, average 52.1 Dpn/Ph3+ cells $n^{=10}$ 10 brains). **(I)** At 94h ALH pNB divisions in the BLs and VNCs are not statistically different from controls (Control BL: median 23.5, average 25.5 Dpn/Ph3+ cells $n^{=10}$ 10 brains; NB> *mob4* BL: median 27.5, average 27.4 Dpn/Ph3+ cells $n^{=10}$ 10 brains; Control VNC: median 37, average 37.4 Dpn/Ph3+ cells $n^{=10}$ 10 brains; NB> *mob4* VNC: median 47, average 48.3 Dpn/Ph3+ cells $n^{=10}$ 10 brains). *p*=Wilcoxon rank-sum test. *p*>0.05 n.s (non-significant), * *p*<0.05, ***p*<0.001. White arrowheads indicate pNBs. All images are single focal planes, anterior up. Scale bars: 25 μm.

## 2.5. Activation of the Insulin-like receptor (InR)/PI3K/Akt signalling cascade in pNBs of *mob4* mutants partially rescues reactivation defects

In the absence of nutrition, specifically circulating amino acids, CNS glia do not receive a yet to be defined systemic signal from the larval fat body, and consequently, do not release insulin-like peptides that activate the InR/TOR signalling cascade in pNBs promoting their reactivation. pNB reactivation can be restored by activation of the InR/TOR cascade within pNBs (Chell and Brand, 2010; Sousa-Nunes *et al.,* 2011). As *mob4* overexpression in pNBs was able to cause early reactivation, it was first determined if it could also induce pNB reactivation in the absence of the nutritional cue. *mob4* was overexpressed in pNBs under nutrition-restrictive conditions (sucrose-only diet) (**Figure 2.14**). Nutritionally deprived larval brains with Mob4 overexpressing pNBs (*insc*-Gal4*, UCD8-GFP*; UAS-*mob4,* NB>*mob4* N.R.) (**Figure 2.14. B, E**) or controls (*insc*-Gal4*,UCD8-GFP*, CNTRL N.R.) (**Figure 2.14. A, D**) were dissected and immunostained for Dpn (red), GFP (green) and Ph3 (blue) at 18h ALH. In the control larvae, pNBs fail to reactivate (**Figure 2.14. A, B**) and pNBs in NB>*mob4* N.R larval brains (white arrows, **Figure 2.14. B, E**) showed a minor significant increase in pNB size in the VNC only (**Figure 2.14. C**) at 18h ALH. Nevertheless, there were no significant differences in pNB divisions in either brain lobes or VNCs (**Figure 2.14. F**). Overall, *mob4* overexpression in the pNBs is not sufficient to induce pNB mitotic reactivation upon loss of the extrinsic nutrition cue.

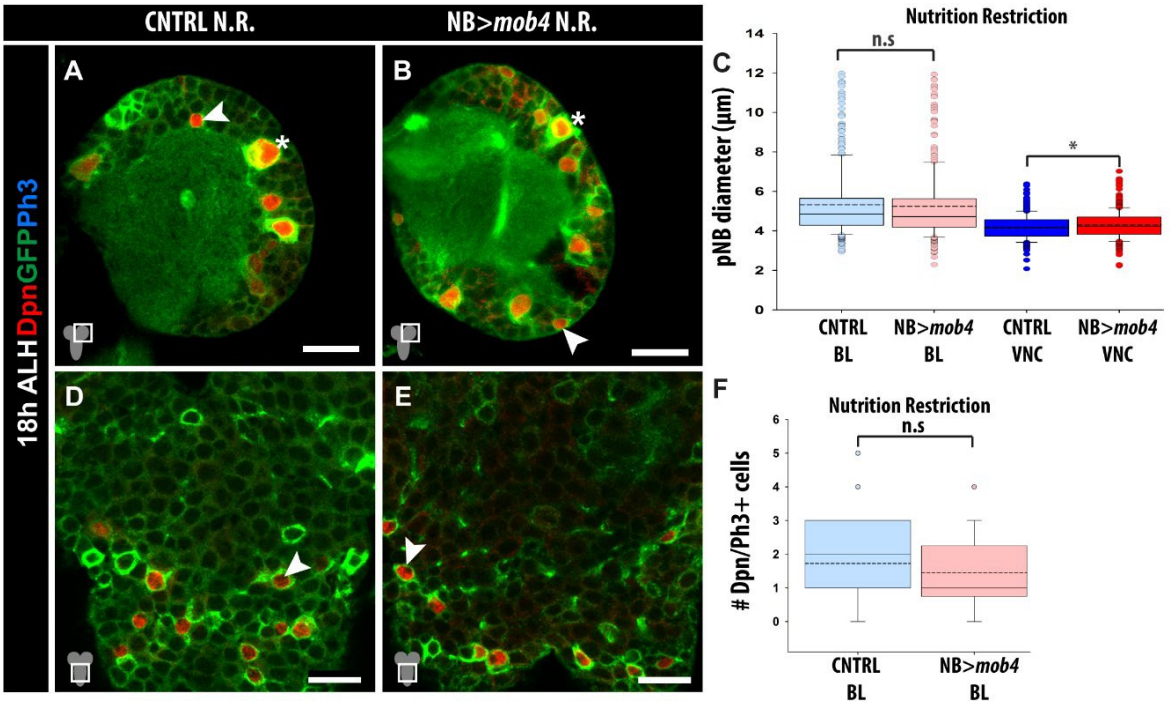


**Figure 2.14. Overexpression of *mob4* is not sufficient to induce pNB reactivation under nutrition-restriction conditions: (A, D)** *Insc-Gal4, UCD8-GFP* (control; CNTRL) and **(B, E)** *mob4* overexpression specifically in pNBs (*Insc-Gal4, UCD8-GFP; UAS-mob4*) upon nutrition restrictive conditions (sucrose-only diet). Larval brain lobes (BLs) and ventral nerve cords (VNCs) are immunostained for **Deadpan (Dpn)**, **green fluorescent protein (GFP)** and **Phospho-Histone-H3 (Ph3)** at 18 hours After Larval Hatching (ALH). Quantification of pNB diameters in BLs shows that *mob4* overexpression (pNB>*mob4*) is not sufficient to overcome reactivation defects observed under nutrition restriction, with exception of a minor increase in pNB sizes in VNCs. **(C)** pNB diameters quantification (Control BL: median 4.9 µm, average 5.3 µm $n^{398}$/6 BLs, 5 brains; pNB>*mob4* BL: median 4.7 µm, average 5.2 µm $n^{=376}$/5 BLs, 5 brains; Control VNC: median 4.2 µm, average 4.2 µm $n^{=325}$/5 VNCs; pNB>*mob4* VNC: median 4.2 µm, average 4.3 µm $n^{=440}$/5 VNCs). Under nutrition restriction, pNBs with *mob4* overexpression also did not significantly alter the number of dividing pNBS. **(F)** pNB divisions (Control BL: median 2, average 1.7 Dpn/Ph3+ cells $n^{=58}$ 29 brains; pNB>*mob4* BL: median 1, average 1.5 Dpn/Ph3+ cells $n^{=66}$ 33 brains). No Dpn/Ph3+ cells were detected in the VNCs at this age. *p*=Wilcoxon rank-sum test. **p<0.05, p>0.05* ns (non significant). White arrowheads indicate pNBs. Mushroom body pNBs (white asterisks) remain mitotically active. All images are single focal planes, anterior up. Scale bar: 10 µm.

Since active InR/PI3K/Akt signalling is essential for pNB reactivation, and pNBs in *mob4*$^{\Delta L3}$ mutants are unable to reactivate, it was investigated if activation of this cascade was impaired in *mob4* mutant brains. Using 24h ALH brain lysates from

control wild-type and mutants, I have analysed the levels of activated (phosphorylated) Akt, an essential component of the InR/PI3K/Akt cascade via western blot. Reduced levels of pAkt compared to total AKT were observed in *mob4*$^{\Delta L3}$ mutant brains compared to controls (**Figure 2.15. A, B**). This initial observation was then replicated in our laboratory by Dr Barros, confirming that *mob4*$^{\Delta L3}$ mutant brains have impaired insulin signalling as shown by reduced levels of p-Akt (Gil-Ranedo *et al.,* 2019). Next, I tested whether activating the InR/PI3K/Akt cascade in pNBs of *mob4* mutants could rescue reactivation defects. Stimulation of TOR signalling by RHEB overexpression activates the InR/PI3K/Akt cascade promoting NSC exit from quiescence (Sousa-Nunes *et al.,* 2011). *mob4*$^{\Delta L3}$ mutant larval brains with *rheb* overexpression in the pNBs (*mob4*$^{\Delta L3}$, *insc*-Gal4; *UAS-rheb, mob4*$^{\Delta L3}$*, NB>rheb*), *mob4*$^{\Delta L3}$ mutants (*mob4*$^{\Delta L3}$) and the *insc- Gal4* controls (CNTRL) were dissected and immunostained for Dpn (red), Dlg (green) and Ph3 (blue) at 18h ALH (**Figure 2.15. C-H**). As observed before, the *mob4*$^{\Delta L3}$ pNBs (white arrow) are unable to reactivate (**Figure 2.15. D, G**). *mob4*$^{\Delta L3}$, NB>*rheb* pNBs show significantly increased pNB enlargement (**Figure 2.15. E, H, I**) and pNB divisions (**Figure 2.15. J**) compared to the mutants. However, the pNB>*rheb* rescue did not reach levels observed in controls (white arrows, **Figure 2.15. C, F**), and although VNC pNB size increased, the number of divisions detected was not significantly different (**Figure 2.15. I-J**). Nevertheless, together these experiments reveal that activation of the InR/PI3K/Akt cascade can partially restore reactivation upon loss of Mob4 (see Discussion), and suggested that Mob4 may act in pNBs upstream or at the same level of Rheb.

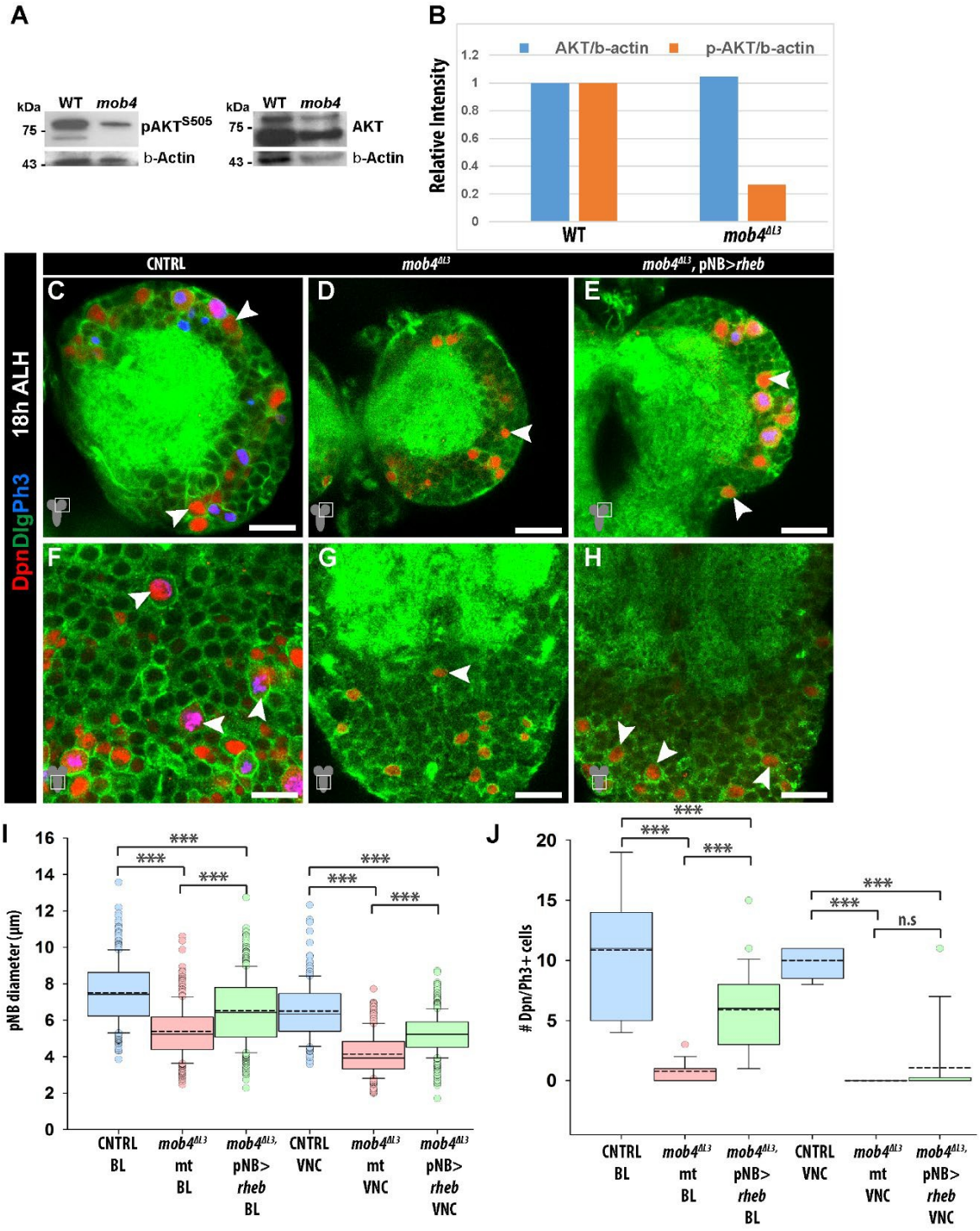
A
kDa
WT
mob4
75 -
pAKT S505
43 -
b-Actin
kDa
WT
mob4
75 -
AKT
43 -
b-Actin
B
AKT/b-actin
p-AKT/b-actin
Relative Intensity
1.2
1
0.8
0.6
0.4
0.2
0
WT
mob4ΔL3
CNTRL
mob4ΔL3
mob4ΔL3, pNB>rheb
18h ALH
DpnDlgPh3
C
D
E
F
G
H
I
pNB diameter (µm)
16
14
12
10
8
6
4
2
0
***
CNTRL BL
mob4ΔL3 mt BL
mob4ΔL3, pNB> rheb BL
CNTRL VNC
mob4ΔL3 mt VNC
mob4ΔL3 pNB> rheb VNC
J
# Dpn/Ph3+ cells
20
15
10
5
0
***
n.s
CNTRL BL
mob4ΔL3 mt BL
mob4ΔL3, pNB> rheb BL
CNTRL VNC
mob4ΔL3 mt VNC
mob4ΔL3, pNB> rheb VNC

**Figure 2.15. Expression of the InR/PI3K/Akt signalling cascade activator Rheb in pNBs of *mob4* mutants can rescue reactivation defects: (A, B)** Western-blot test on *mob4*$^{\Delta L3}$ mutant brain lysate shows a decrease in phosphorylated-AKT (p-AKT) indicating reduced insulin signalling, compared to WT control larval brain lysate. Levels of total AKT remain very similar. β-Actin served as a loading control. Lysates are from 24 ALH brains (**B**) Quantification of protein signals (n=1 independent assay using 67 WT brains and 90 *mob4* mutants). **(C-H)** pNBs in *mob4* mutants fail to enlarge and divide; however, this defect can be rescued by overexpressing *ras homolog enriched in brain* (*rheb*) in pNBs (*mob4*$^{\Delta L3}$, NB>*rheb*). **(C, F)** *Insc*-gal4 (control; CNTRL), **(D, G)** *mob4*$^{\Delta L3}$, *insc*-Gal4 mutants, **(E, H,)** *mob4*$^{\Delta L3}$, insc-gal4; UAS-*rheb* (*mob4*$^{\Delta L3}$, NB>*rheb*) immunostained for **Deadpan (Dpn)**, **Discs large (Dlg)** and **Phospho-Histone-H3 (Ph3)** at 18 hours After Larval Hatching (ALH). **(I)** Quantification of the diameters in the BLs and VNCs shows that pNBs in *mob4*$^{\Delta L3}$ mutants overexpressing *rheb* were significantly larger compared to the *mob4*$^{\Delta L3}$ mutants, however still smaller compared to controls (Control BL: median 7.4 μm, average 7.5 μm $n^{334}$/5 BLs, 4 brains; *mob4*$^{\Delta L3}$ mutants BL: median 5.2 μm, average 5.4 μm $n^{357}$/9 BLs, 9 brains; *mob4*$^{\Delta L3}$, NB> *rheb* BL: median 6.4 μm, average 6.5 μm $n^{= 466}$/5 BLs, 5 brains; Control VNC: median 6.4 μm, average 6.5 μm $n^{181}$/3 BLs, 3 brains; *mob4*$^{\Delta L3}$ mutants VNC: median 3.9 μm, average 4.1 μm $n^{251}$/4 BLs, 4 brains; *mob4*$^{\Delta L3}$, NB> *rheb* VNC: median 5.2 μm, average 5.2 μm $n^{= 454}$/5 BLs, 5 brains). **(J)** The mitotic index of the pNBs in *mob4*$^{\Delta L3}$ mutants expressing *rheb* was significantly higher in the BLs compared to that in *mob4*$^{\Delta L3}$ mutants, but the results were not statistically different in the VNCs. Dividing pNBs in *mob4*$^{\Delta L3}$ mutants expressing *rheb* were less compared to the controls (Control BL: median 11, average 10.9 Dpn/Ph3+ cells $n^{=7}$ 7 brains; *mob4*$^{\Delta L3}$ mutants BL: median 1, average 0.8 Dpn/Ph3+ cells $n^{=32}$ 16 brains; *mob4*$^{\Delta L3}$, NB> *rheb* BL: median 6, average 5.9 Dpn/Ph3+ cells $n^{=28}$ 14 brains; Control VNC: median 11, average 10 Dpn/Ph3+ cells $n^{=5}$ 5 brains; *mob4*$^{\Delta L3}$ mutants VNC: median 0, average 0 Dpn/Ph3+ cells $n^{=16}$ 16 brains; *mob4*$^{\Delta L3}$, NB> *rheb* VNC: median 0, average 1.1 Dpn/Ph3+ cells $n^{=14}$ 14 brains). *p*=Wilcoxon rank-sum test. *p>0.05* ns (non- significant), ***$p$<0.001. White arrowheads indicate pNBs. All images are single focal planes, anterior up. Scale bar: 10 μm.

## 2.6. Deactivating the Hippo pathway in pNBs of *mob4* mutants can rescue reactivation defects

The Hippo signalling is another highly conserved pathway and has recently been shown to maintain pNB quiescence (Ding *et al.,* 2016; Poon *et al.,* 2016). As detailed in the Introduction, the canonical Hippo pathway prevents pNB cell growth via a phosphorylation cascade of the core components Hippo (Hpo), Warts (Wts), and the transcriptional co-activator Yorkie (Yki). In quiescent pNBs, the Hippo pathway is active, and Yki is phosphorylated and inactivated in the cytoplasm. However, when the Hippo pathway is deactivated, Yki translocates to the nucleus to activate cell growth. Interestingly, Mob4 has been shown to interact physically and genetically with Hpo: in the *Drosophila* wing, Mob4 knockdown can rescue the overgrowth phenotype caused by Hpo knockdown (Ribeiro *et al.,* 2010). Also, the STRIPAK complex containing Protein Phosphatase 2 A (PP2A), to which Mob4 belongs to, has been shown to inhibit the Hippo pathway in both *Drosophila* and mammals (Liu *et al.,* 2016; Goudreault *et al.,* 2009; Couzens *et al.,* 2013; Shi *et al.,* 2016; Ribeiro *et al.,* 2010; Straßburger *et al.,* 2012; Tumaneng *et al.,* 2012). Since pNBs upon loss of Mob4 are unable to reactivate, it was postulated that Hippo signalling might remain switched-on in pNBs of *mob4* mutant brains. Indeed, this was confirmed in our laboratory by Drs Barros and Gil-Ranedo. I have examined if deactivating Hippo signalling in pNBs of *mob4* mutant brains could rescue mitotic reactivation. Hpo and Wts were knocked down via RNAi in pNBs of $mob4^{\Delta L3}$ mutants (**Figure 2.16.**). The RNAi strains used had been previously shown to induce pNB premature reactivation in control pNBs (Ding *et al.,* 2016). Larval brains of *Insc*-Gal4 (controls; CNTRL, **Figure 2.16. A-B**), $mob4^{\Delta L3}$*, insc-gal4* mutants (*mob* $^{\Delta L3}$ mt, **Figure 2.16. D-E**), $mob4^{\Delta L3}$*,insc-gal4; UAS-hippo-RNAi (*$mob4^{\Delta L3}$*,*NB>*hpo-RNAi,* **Figure 2.16. G-H**) and $mob4^{\Delta L3}$*,insc-gal4; UAS-warts-RNAi (*$mob4^{\Delta L3}$*, NB>wts-RNAi,* **Figure 2.16. J-K**) were immunostained for Dpn (red), Dlg (green) and Ph3 (blue) at 18h ALH. Quantifications showed a significant increase of pNB enlargement (white arrows, **Figure 2.16.**) and pNB divisions (yellow arrows, **Figure 2.16**) in $mob4^{\Delta L3}$*,* NB>*hpo-RNAi* and $mob4^{\Delta L3}$*, NB>wts-RNAi* pNBs compared to those in *mob4* mutants, although not to the control values (**Figure 2.16. C, F**). Therefore, deactivating the Hippo pathway within *mob4* mutant pNBs can rescue the pNB enlargement and division defects observed (see Discussion).

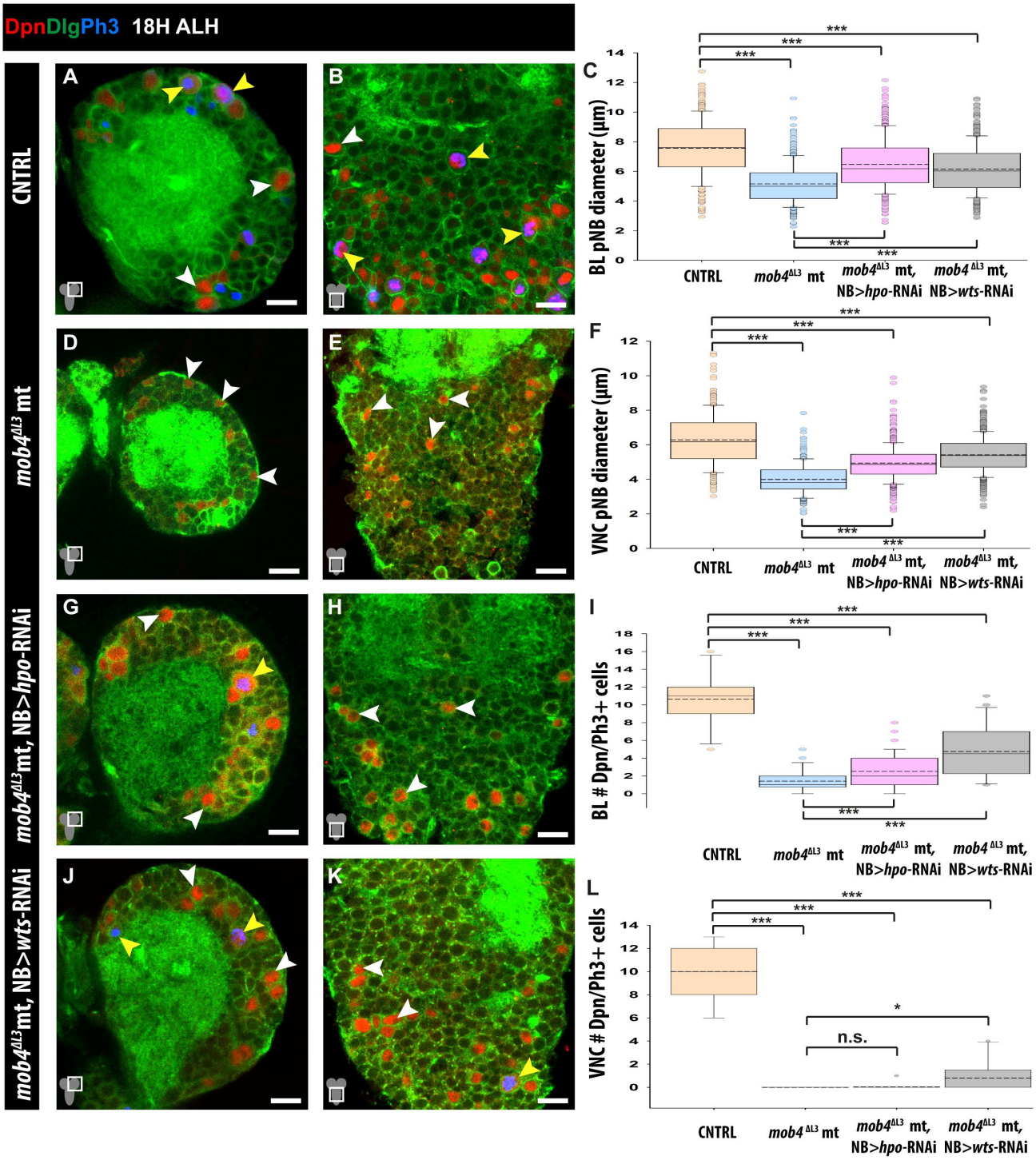
DpnDlgPh3 18H ALH
CNTRL
mob4ΔL3 mt
mob4ΔL3mt, NB>hpo-RNAi
mob4ΔL3mt, NB>wts-RNAi
A
B
C
D
E
F
G
H
I
J
K
L
BL pNB diameter (µm)
VNC pNB diameter (µm)
BL # Dpn/Ph3+ cells
VNC # Dpn/Ph3+ cells
CNTRL
mob4ΔL3 mt
mob4ΔL3 mt, NB>hpo-RNAi
mob4ΔL3 mt, NB>wts-RNAi
***
n.s.
*

**Figure 2.16. Deactivating the Hippo pathway in pNBs of *mob4* mutants can rescue reactivation defects: (A, B)** *Insc*-Gal4 (controls; CNTRL), **(D, E)** *mob4$^{\Delta L3}$, insc-gal4* mutants (*mob4 $^{\Delta L3}$* mt), **(G, H)** *mob4$^{\Delta L3}$,insc-gal4; UAS-hippo-RNAi (mob4$^{\Delta L3}$,* NB>*hpo-RNAi*), **(J, K)** *mob4$^{\Delta L3}$,insc-gal4; UAS-warts-RNAi (mob4$^{\Delta L3}$, NB>wts-RNAi*) larval brain lobes (BLs) and ventral nerve cords (VNCs) immunostained for **Deadpan (Dpn)**, **Discs large (Dlg)** and **Phospho-Histone-H3 (Ph3)**, at 18h After Larval Hatching (ALH). **(C, F)** Quantification of pNB diameters in BLs and VNCs shows that deactivating the Hippo pathway within *mob4* mutant pNBs can rescue pNB enlargement defects observed, yet not to control levels. **(C)** BL pNB diameters quantifications (Control BL: median 7.6 µm, average 7.6 µm $n^{289}$/3 BLs, 3 brains; *mob4$^{\Delta L3}$* BL: median 5 µm, average 5.1 µm $n^{= 380}$/9 BLs, 9 brains; *mob4$^{\Delta L3}$,* NB>*hpo*-RNAi BL: median 6.2 µm, average 6.5 µm $n^{531}$/ 8 BLs, 5 brains; *mob4$^{\Delta L3}$,* NB>*wts*-RNAi BL: median 6 µm, average 6.2 µm $n^{466}$/8 BLs, 5 brains). **(F)** VNC pNB diameters quantifications (Control VNC: median 6.2 µm, average 6.3 µm $n^{=4}$/4 VNCs; *mob4$^{\Delta L3}$* VNC: median 3.8 µm, average 4 µm $n^{=5}$/5 VNCs; *mob4$^{\Delta L3}$,* NB>*hpo*-RNAi VNC: median 4.9 µm, average 5 µm $n^{=5}$/5 VNCs; *mob4$^{\Delta L3}$,* NB>*wts*-RNAi VNC: median 5.4 µm, average 5.4 µm $n^{=5}$/5 VNCs). **(I, L)** Quantification of pNB mitosis in BLs and VNCs shows that deactivating the Hippo pathway in *mob4* mutant pNBs leads to an increased in pNB divisions, except for VNC pNBs upon knock-down of hippo. However, in all cases, the rescue is partial, not reaching levels seen in controls **(I)** BL pNB division quantifications (Control BL: median 11, average 10.6 Dpn/Ph3+ cells $n^{=11}$ 8 brains; *mob4$^{\Delta L3}$* BL: median 1, average 1.4 Dpn/Ph3+ cells $n^{=34}$ 17 brains; *mob4$^{\Delta L3}$,*NB>*hpo*-RNAi BL: median 2, average 2.5 Dpn/Ph3+ cells $n^{=60}$ 30 brains; *mob4$^{\Delta L3}$,* NB>*wts*-RNAi BL: median 4.5, average 4.8 Dpn/Ph3+ cells $n^{=20}$ 10 brains). **(L)** VNC pNB division quantifications (Control VNC: median 10, average 10 Dpn/Ph3+ cells $n^{=5}$ 5 VNCs; *mob4$^{\Delta L3}$* VNC: median 0, average 0 Dpn/Ph3+ cells $n^{=16}$ 16 VNCs; *mob4$^{\Delta L3}$,* NB>*hpo*-RNAi VNC: median 0, average 0 Dpn/Ph3+ cells $n^{=30}$ 30 VNCs; *mob4$^{\Delta L3}$,*NB>*wts*-RNAi VNC: median 0, average 1 Dpn/Ph3+ cell $n^{=10}$ 10 VNCs). *p*=Wilcoxon rank-sum test. n.s. (non-significant) *p*>0.05, * *p*<0.05, ***p*<0.001. White arrowheads indicate pNBs; yellow arrowheads indicate Ph3+ pNBs. All images are single focal planes, anterior up. Scale bar: 10 µm.

## 2.7. Mob4 and another STRIPAK component, Cka, cooperate to promote pNB reactivation

Connector of Kinase to AP-1 (Cka) is another candidate gene which was found to be upregulated in reactivating versus quiescent pNBs on the transcriptome analysis performed in the laboratory. Data acquired previously by the group revealed that, like Mob4, Cka promotes pNB reactivation (Gil-Ranedo *et al.,* 2019). As mentioned in the Introduction, Mob4 and Cka physically interact with each other and are core components of a STRIPAK protein complex that inhibits Hippo signalling (Ribeiro *et al.,* 2010). Thus, the next aim addressed whether Mob and Cka may cooperate to promote pNB reactivation. Larval brains simultaneously overexpressing Mob4 and Cka within pNBs (*Insc-Gal4, UCD8-GFP; UAS-cka, UAS-mob4*, NB>*cka+mob4*) and controls (*Insc-Gal4, UCD8-GFP*; CNTRL) were immunostained for Dpn (red), GFP (green) and Ph3 (blue) at 6h ALH and 18h ALH (**Figure 2.17**). At 6h ALH, control pNBs are not mitotically active except the mbNBs/vNB (white asterisk, **Figure 2.17. A-B**). NB>*cka+mob4* pNBs (white arrows, **Figure 2.17. B, E**) were significantly larger (**Figure 2.17. C**) compared to the controls (white arrows, **Figure 2.17. A, D**). However, there were no significant differences in pNB divisions (**Figure 2.17. F**) at this stage. At 18h ALH, NB>*cka+mob4* pNBs (**Figure 2.17. H, K**) were also significantly larger (**Figure 2.17. I**) and had more divisions (yellow arrows, **Figure 2.17. L**) compared to the controls (yellow arrows, **Figure 2.17. G, J**). The increase in pNB size and divisions is stronger when both Cka and Mob4 are overexpressed compared to the results observed upon overexpression of each alone (**Figure 2.11** Gil-Ranedo *et al.,* 2019). These experiments suggest that Mob4 and Cka may cooperate to promote pNB reactivation.

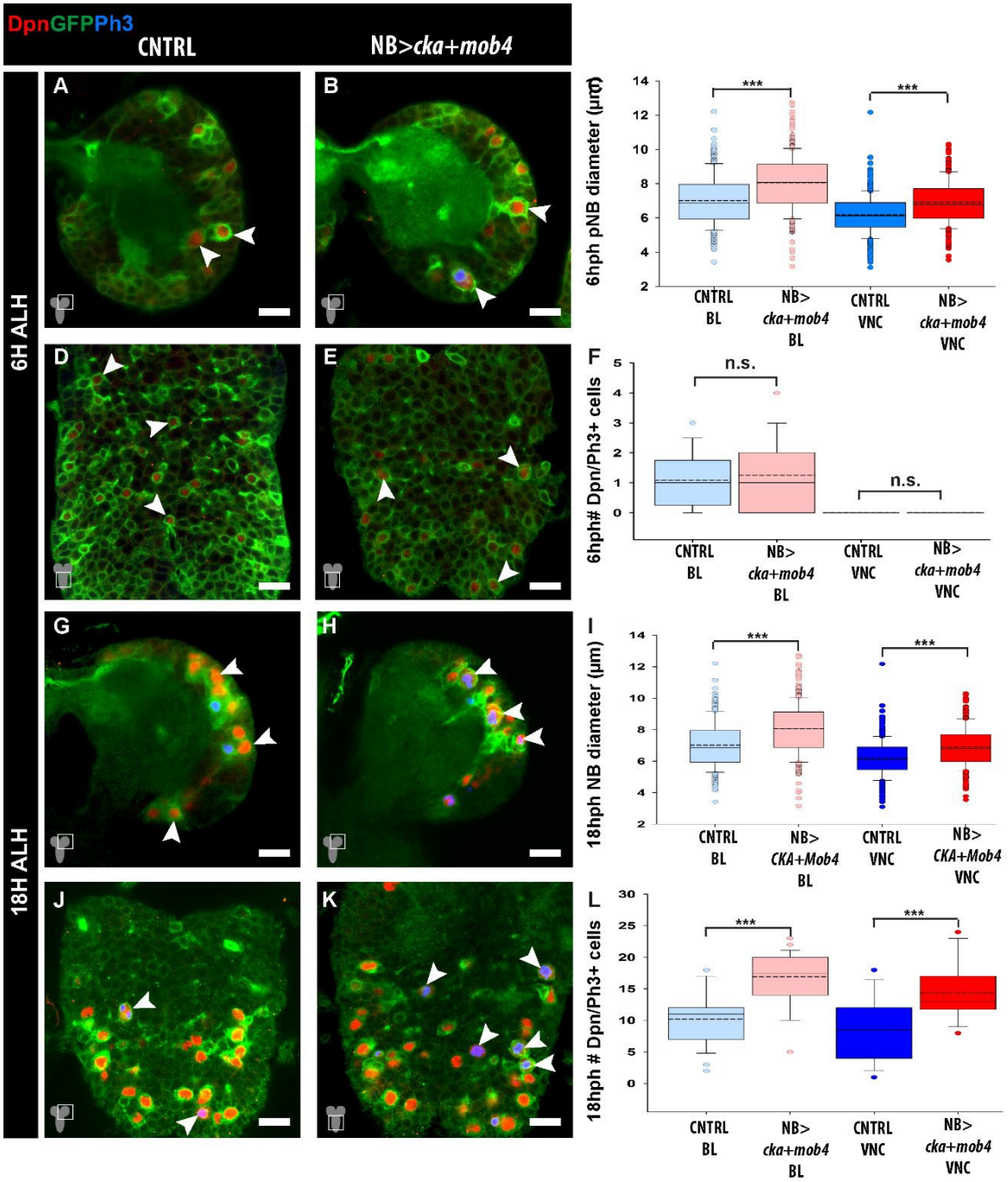
DpnGFPPh3
CNTRL
NB>cka+mob4
6H ALH
18H ALH
A
B
D
E
G
H
J
K
6hph pNB diameter (µm)
***
***
CNTRL BL
NB> cka+mob4 BL
CNTRL VNC
NB> cka+mob4 VNC
F
6hph# Dpn/Ph3+ cells
n.s.
n.s.
CNTRL BL
NB> cka+mob4 BL
CNTRL VNC
NB> cka+mob4 VNC
I
18hph NB diameter (µm)
***
***
CNTRL BL
NB> CKA+Mob4 BL
CNTRL VNC
NB> CKA+Mob4 VNC
L
18hph # Dpn/Ph3+ cells
***
***
CNTRL BL
NB> cka+mob4 BL
CNTRL VNC
NB> cka+mob4 VNC

**Figure 2.17. Simultaneously overexpressing Cka and Mob4 in pNBs causes stronger premature pNB reactivation than that previously seen with single Mob4 overexpression:** (**A, D, G, J)** *Insc-Gal4, UCD8-GFP* (controls; CNTRL) and *Insc-Gal4, UCD8-GFP; UAS-cka, UAS-mob4* (NB>*cka+mob4*) larval brain lobes (BLs) and ventral nerve cords (VNCs) immunostained for **Deadpan (Dpn)**, **green fluorescent protein (GFP)** and **Phospho-Histone-H3 (Ph3)** at 6h and 18h ALH. **(C, F, I, L)** Quantification of pNB diameters in BLs and VNCs shows that simultaneous *cka* and *mob4* overexpression specifically in pNBs causes earlier enlargement 6h and 18h ALH, and increased entry into mitosis at 18h ALH. **(C)** 6h ALH pNB diameters quantifications (Control BL: median 3.6 µm, average 3.9 µm $n^{306}$/3 BLs, 3 brains; NB>*cka+mob4* BL: median 4.3 µm, average 4.8 µm $n^{=374}$/3 BLs, 3 brains; Control VNC: median 3.4 µm, average 3.4 µm $n^{=393}$/3 VNCs; NB>*cka+mob4* VNC: median 4.0 µm, average 4.1 µm $n^{=387}$/3 VNCs). **(F)** 6h ALH pNB divisions (Control BL: median 1, average 1.1 Dpn/Ph3+ cells $n^{=24}$ 12 brains; NB>*cka+mob4* BL: median 1, average 1.3 Dpn/Ph3+ cells $n^{=32}$ 16 brains; Control VNC: median 0, average 0 Dpn/Ph3+ cells $n^{=12}$ 12 VNCs; NB>*cka+mob4* VNC: median 2, average 2.5 Dpn/Ph3+ cells $n^{=16}$ 16 VNCs). **(I)** 18h ALH pNB diameters quantifications (Control BL: median 6.9 µm, average 7.0 µm $n^{=339}$/4 BLs, 3 brains; NB>*cka+mob4* BL: median 8.1 µm, average 8.1 µm $n^{=400}$/4 BLs, 4 brains; Control VNC: median 6.1 µm, average 6.2 µm $n^{=323}$/3 VNCs; NB>*cka+mob4* VNC: median 6.8 µm, average 6.9 µm $n^{=391}$/4 VNCs). **(L)** 18h ALH pNB divisions (Control BL: median 11, average 10.2 Dpn/Ph3+ cells $n^{=28}$ 14 brains; NB>*cka+mob4* BL: median 17.5, average 16.9 Dpn/Ph3+ cells $n^{=28}$ 14 brains; Control VNC: median 8.5, average 8.6 Dpn/Ph3+ cells $n^{=14}$ 14 VNCs; NB>*cka+mob4* VNC: median 13.0, average 14.4 Dpn/Ph3+ cells $n^{=14}$ 14 VNCs). *p*=Wilcoxon rank-sum test. n.s (non-significant) $p>0.05$, ***$p<0.001$. Overall, effects with double *cka/mob4* overexpresion are stronger than those obtained by overexpressing just *mob4* (compare to Fig. 2.11). White arrowheads indicate pNBs; yellow arrowheads indicate Ph3+ pNBs. All images are single focal planes, anterior up. Scale bar: 10 µm.

## 2.8. PP2A inhibition promotes pNB reactivation

Together with Mob4 and Cka, the serine/threonine phosphatase PP2A forms part of a STRIPAK complex known to inhibit Hippo signalling (Couzens *et al.,* 2013; Ribeiro *et al.,* 2010). In *Drosophila*, the unique PP2A catalytic subunit is called Microtubule Star (Mts). STRIPAK components act as regulatory subunits of Mts, directing it to Hippo kinase, which leads to its de-phosphorylation and Hippo signalling inhibition. Since Mts was also detected in the transcriptome analysis comparing reactivating with quiescence pNBs performed in our group (Gil-Ranedo *et al.,* 2019), I next analysed pNB reactivation in *mts* trans-heterozygote mutants ($mts^{299}/mts^{XE-2258}$; Wang *et al.,* 2009). The reason for using trans-heterozygotes was that *mts* null mutants ($mts^{XE-2258}$) die embryonically but survive until pupae stages if combined with a copy of a

hypomorphic allele (*mts*$^{299}$; Wang *et al.,* 2009). WT control (CNTRL) and *mts*$^{299}$/*mts*$^{XE-2258}$ mutant larval brains were dissected and immunostained for Dpn (red), Dlg (green) and Ph3 (blue) at 18h ALH. *mts*$^{299}$/*mts*$^{XE-2258}$ pNBs (white arrows, **Figure 2.18. B, E**) were significantly larger (**Figure 2.18. C**) than the controls (white arrows, **Figure 2.18. A, D**) at 18h ALH. However, there were no significant differences in the number of pNB divisions in the BLs (**Figure 2.18. A-B**) or the VNCs (yellow arrows, **Figure 2.18. D-E**).

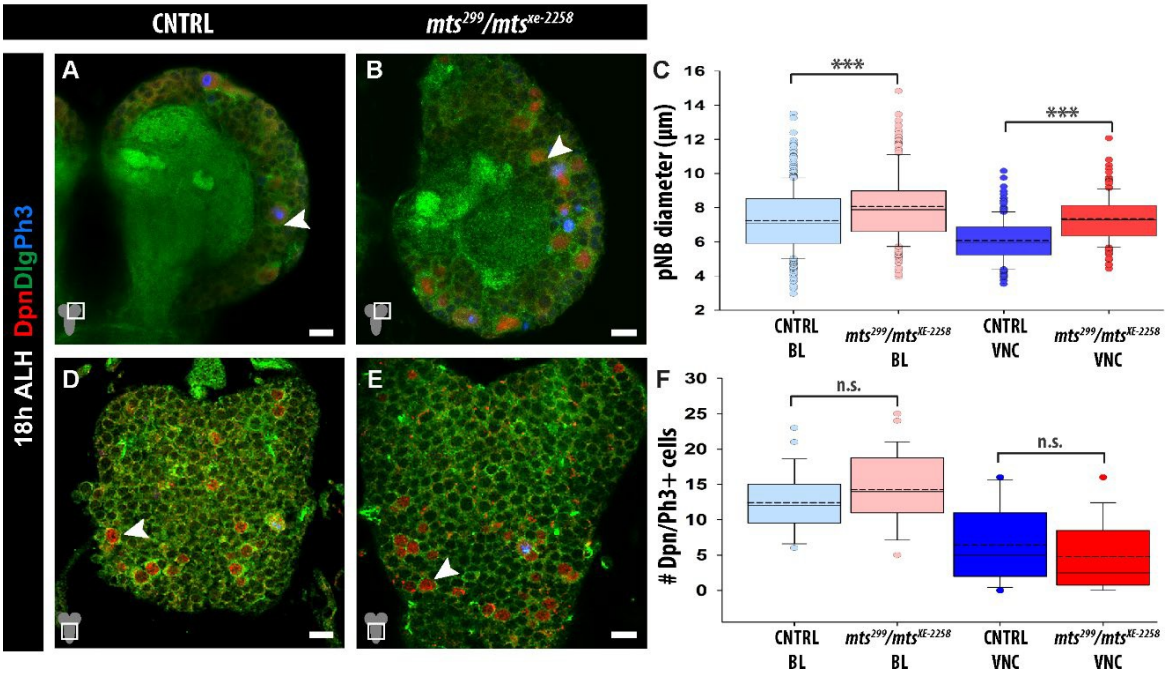


**Figure 2.18. *mts* mutants display premature pNB enlargement: (A, D)** Wild-type (control; CNTRL) and **(B, E)** *mts* mutant (*mts*$^{299/XE2258}$ ) larval brain lobes (BLs) and ventral nerve cords (VNCs) immunostained for **Deadpan (Dpn)**, **Discs large (Dlg)** and **Phospho-Histone-H3 (Ph3)** at 18h After Larval Hatching (ALH). Quantification of pNB diameters and divisions (Dpn/Ph3+) in BLs and VNCs shows that pNBs in mutants enlarge earlier, but no difference is seen in division numbers compared to controls. **(C)** pNB diameters quantification (Control BL: median 7.1 µm, average 7.2 µm n$^{362}$/3 BLs, 3 brains *mts*$^{299/XE2258}$ *mt* BL : median 7.9 µm, average 8.1 µm n$^{= 235}$/4 BLs, 4 brains; Control VNC: median 6 µm, average 6.1 µm n$^{=203}$/2 VNCs; *mts*$^{299/xe2258}$ *mt* VNC: median 7.3 µm, average 7.3 µm n$^{=189}$/2 VNCs). **(F)** pNB division quantification (Control BL: median 12, average 12.4 Dpn/Ph3+ cells n$^{=26}$ 13 brains; *mts*$^{299/XE2258}$ *mt* BL: median 14, average 14.2 Dpn/Ph3+ cells n$^{= 36}$ 18 brains; Control VNC: median 5, average 6.4 Dpn/Ph3+ cells n$^{=13}$ 13 VNCs; *mts*$^{299/xe2258}$ *mt* VNC: median 2.5, average 4.8 Dpn/Ph3+ cells n$^{= 18}$ 18 VNCs). Wilcoxon rank-sum test. n.s (non-significant) $p>0.05$, ***$p<0.001$. White arrowheads indicate pNBs. All images are single focal planes, anterior up. Scale bar: 10 µm.

Next, to explore PP2A/Mts function specifically in pNBs, a Dominant-Negative Mts *Drosophila* UAS line (*UAS-mts*-DN) was used (Hannus *et al*., 2002) together with the Inscuteable-Gal4 driver. The expression of Mts-DN results in a truncated Mts form lacking its phosphatase domain, which binds to the endogenous Mts protein and impairs its function (Hannus *et al*., 2002). Larval brains expressing *mts* dominant-negative (*mts*-DN) form specifically in pNBs (*Insc-Gal4, UCD8-GFP; UAS-mts*-DN; NB>*mts*-DN) and controls (*Insc-Gal4, UCD8-GFP*; CNTRL) were dissected and immunostained for Dpn (red), GFP (green) and Ph3 (blue) at 18h ALH (**Figure 2.19. A, C, D, F**). A significant increase in pNB size and divisions was observed compared to the controls (**Figure 2.19. G, H**). The results strengthen those obtained using the trans-heterozygote *mts* mutants and together indicate that knocking-down PP2A/Mts leads to premature exit from quiescence. The findings were surprising as they contrast with the effect of inhibiting Mob4 (**Figures 2.2-2.6, 2.10**) or Cka in pNBs (Gill-Renedo *et al.,* 2019), and suggested that PP2A/Mts contributes to maintaining pNBs in quiescence independently from a separate potential role in pNBs as part of STRIPAK (see Discussion).

PP2A is a pleiotropic phosphatase; in addition to a role within STRIPAK, multiple functions have been assigned to it. This variety is provided mainly by the association of the catalytic subunit Mts to possible variable regulatory subunits, which direct PP2A/Mts to different targets (Andreazza *et al.,* 2015; Vereshchagina *et al.,* 2008; Rodgers *et al.,* 2011; Padmanabhan *et al.,* 2009). To date, the *Drosophila* PP2A regulatory subunits better studied are Well rounded (Wrd), Twins and Widerborst (Wdb; Shi, 2009). Of significance, PP2A-Wdb has been shown to negatively regulate insulin signalling by dephosphorylation of Akt in both *Drosophila* and mammals (Fischer *et al.,* 2015; Fischer *et al.,* 2016). However, it had not been implicated in pNB quiescence/ reactivation processes. Thus, I next functionally tested Wdb using a *Drosophila* UAS strain expressing a truncated form of Wdb acting as Dominant Negative (*wdb-DN*; Hannus *et al.,* 2002). Knocking down Wdb (**Figure 2.19. B, E**) in pNBs leads to a significant increase in the pNB size (**Figure 2.19. G**) compared to the controls (**Figure 2.18. A, D**), at 18h ALH. In the BLs, Wdb knockdown in pNBs also lead to significantly more pNB divisions compared to the controls (**Figure 2.19. A, B, H**). Overall, knocking down PP2A subunits Mts or Wdb causes earlier pNB reactivation, suggesting that PP2A/Mts with its regulatory subunit Wbd acts to maintain

pNB quiescence (see Discussion).

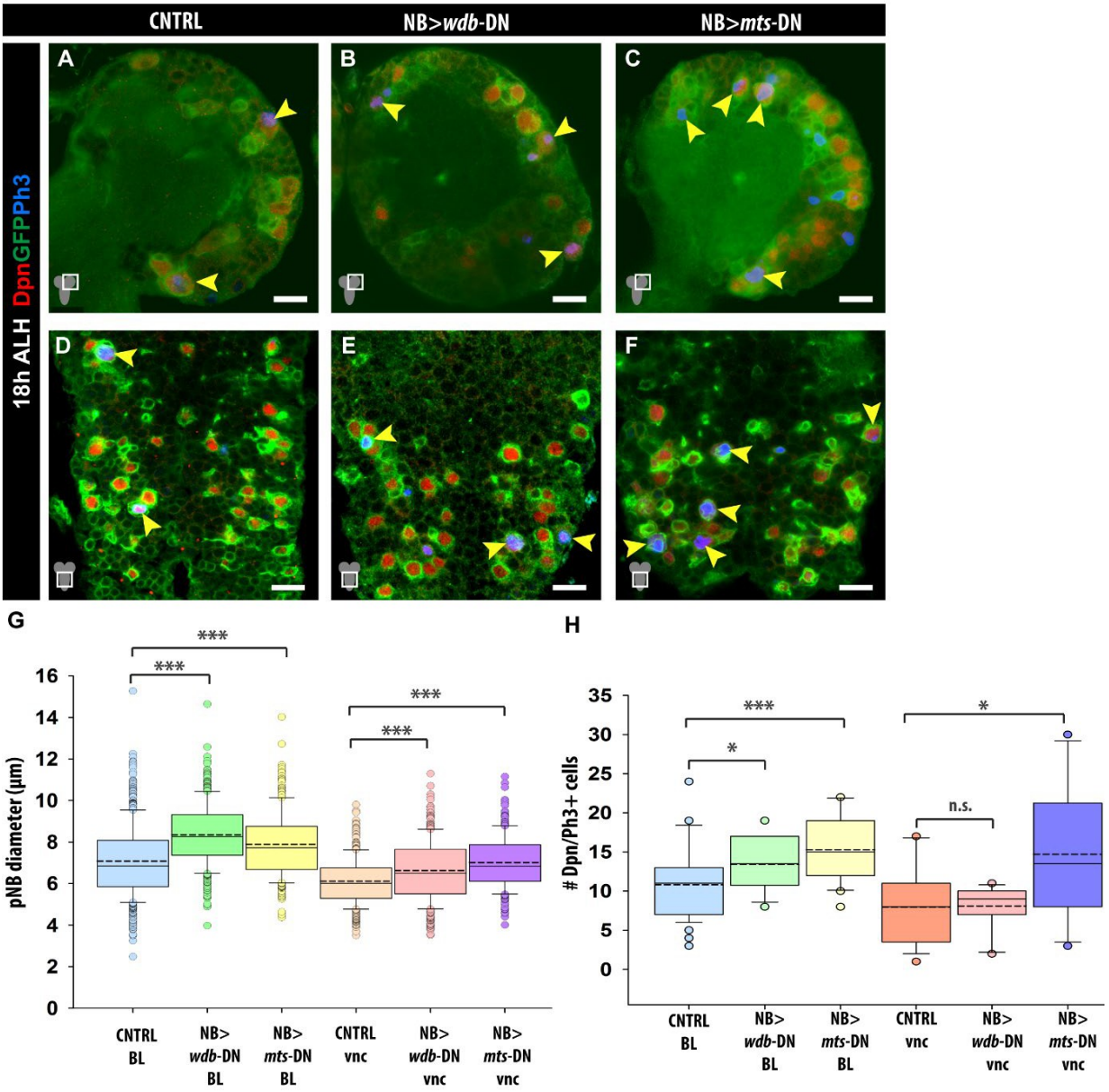

**Figure 2.19. Inhibition of the PP2A subunits Microtubule Star (Mts) or Widerborst (Wdb) cause premature pNB reactivation:** Larval brain lobes (BLs) and ventral nerve cords (VNCs) of **(A, D)** *Insc-Gal4, UCD8-GFP* (control, CNTRL), **(B, E)** expressing a Wdb Dominant Negative form specifically in pNBs (*Insc-Gal4, UCD8-GFP; UAS-wdb-DN*; NB>*wdb*-DN) or **(C, F)** expressing an Mts Dominant Negative form specifically in pNBs (*Insc-Gal4, UCD8-GFP; UAS-mts*-DN; NB>*mts*-DN), immunostained for **Deadpan (Dpn)**, **green fluorescent protein (GFP)** and **Phospho-Histone-H3 (Ph3)** at 18h After Larval Hatching (ALH). **(G)** Quantification of pNB diameters in BLs and VNCs shows that knocking down Wdb or Wdb in pNBs causes earlier pNB enlargement compared to controls. pNB enlargement quantifications (Control BL: median 6.8 µm, average 7.1 µm $n^{541}$/8 BLs, 5 brains; NB>*wdb*-DN BL: median 8.3 µm, average 8.3 µm $n^{= 313}$/5 BLs, 3 brains; NB>*mts*-DN BL: median 7.7 µm, average 7.9 µm $n^{= 263}$/5 BLs, 3 brains; Control VNC: median 6.0 µm, average 6.1 µm $n^{=362}$/4 VNCs; NB>*wdb*-DN VNC: median 6.5 µm, average 6.6 µm $n^{=318}$/3 VNCs; NB>*mts*-DN VNC: median 6.8 µm, average 7 µm $n^{=258}$/3 VNCs). **(H)** Quantification of pNB divisions shows that knocking down Wdb in pNBs leads to increased pNB divisions in BLs but not a statistically significant difference in VNCs, while knockdown of Mts causes an increase in pNBs of both BLs and VNCs compared to controls. pNB divisions (Control BL: median 11, average 10.8 Dpn/Ph3+ cells $n^{=42}$ 21 brains; NB>*wdb*-DN BL: median 13.5, average 13.4 Dpn/Ph3+ cells $n^{= 22}$ 11 brains; NB>*mts*-DN BL: median 15, average 15.3 Dpn/Ph3+ cells $n^{=20}$ 10 brains; Control VNC: median 8, average 8 Dpn/Ph3+ cells $n^{=21}$ 21 VNCs; NB>*wdb*-DN VNC: median 9, average 8.1 Dpn/Ph3+ cells $n^{= 11}$ 11 VNC; NB>*mts*-DN VNC: median 13.5, average 14.7 Dpn/Ph3+ cells $n^{= 10}$ 10 VNCs). *p*=Wilcoxon rank-sum test. *p*>0.05 ns (non-significant), ***p*<0.05, ****p*<0.001. Yellow arrowheads indicate dividing pNBs. All images are single focal planes, anterior up. Scale bar: 10 µm.

# CHAPTER 3

# DISCUSSION

## 3.1 Understanding NSC quiescence and activated states: the significance of the research area and the foundation of this study

NSCs must actively maintain a balance between quiescent and reactivated states; it is crucial for NSC longevity, proper brain homeostasis and functioning (Cheung and Rando, 2013; Chaker *et al.,* 2016; Cavallucci *et al*,. 2016; Tian *et al.,* 2018). As described in chapter 1, the transition between NSC quiescence and NSC reactivation requires a myriad of extrinsic and intrinsic signals, including systemic nutritional and metabolic signals, growth factors, neurotransmitters, epigenetic modifications and transcription factors. How the NSCs orchestrate a barrage of external and internal signals and appropriately decide which fate to choose is a continuing area of research, essential for NSC-based therapies. Studying NSCs has been difficult due to their relatively low number within an intricate environmental niche. However, our understand- ing of NSCs and their complex heterogeneity was enabled with the development of flow cytometry, cell sorting and transcriptomic techniques (Beckervordersandforth *et al.,* 2010; Beckervordersandforth *et al.,* 2017; Codega *et al.,* 2014; Mich *et al.,* 2014; Llorens-Bobadilla *et al.,* 2015; Dulken *et al.,* 2017).

Transcriptomic profiling of mammalian quiescent NSCs versus activated NSCs is starting to decipher the functional properties and regulatory mechanisms governing these different states (Martynoga *et al.,* 2013; Llorens-Bobadilla *et al.,* 2015). As described in the Introduction, research exposed various individual molecules and signalling pathways, for example, BMP and InR/PI3K/Akt signalling to be crucial for NSC maintenance (Mathieu *et al.,* 2008; Ziegler *et al.,* 2015). Contrary to the previous idea that NSC quiescence is a passive process, current research indicates that both quiescence and proliferation states, as well as the transition, requires active and specific genomic and proteomic programs (**Figure 3.1**). Understanding how NSCs integrate, interpret and appropriately respond to the variety of information received is critical to the development of safe, and effective NSC-based regenerative therapy for brain disorders (Llorens-Bobadilla *et al.,* 2015; Chaker *et al.,* 2016; Lee *et al*., 2018; Xiao *et al*., 2018; Fouad, 2019; Chou *et al*., 2015; Tang, Y *et al*., 2017;

Portnow *et al*., 2017; Baker *et al*., 2019; Willis *et al*., 2020).

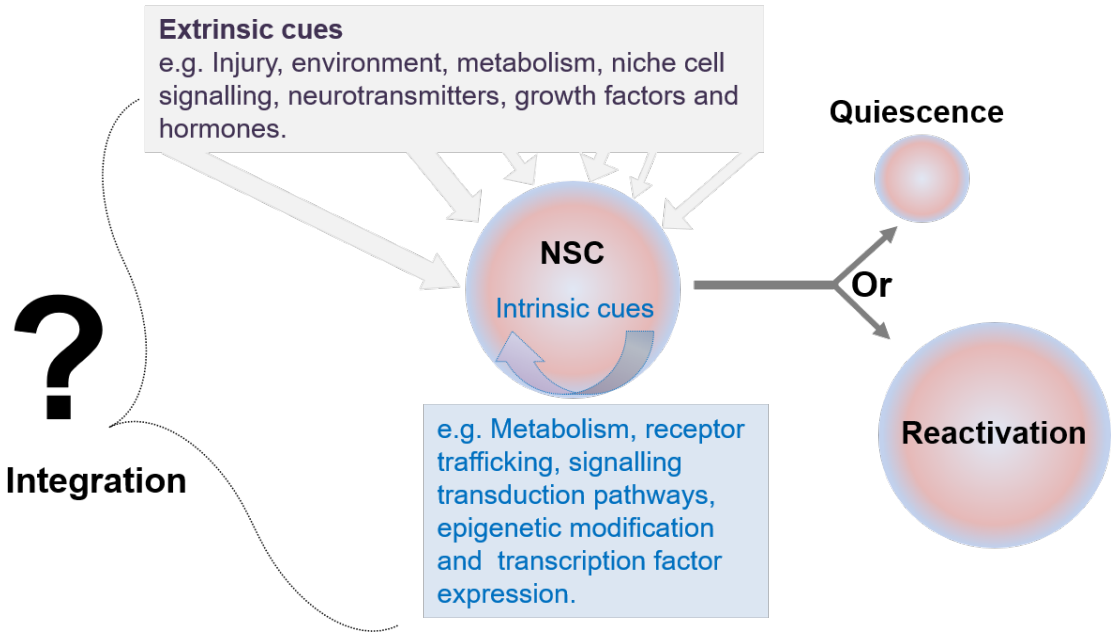


**Figure 3.1. Integration of intrinsic and extrinsic signals influence NSC transit between quiescence and proliferation stages.** A simplified overview of influential factors governing NSC behaviour (see Introduction for more details). NSCs orchestrate a barrage of signals to transition between quiescent and proliferative states. Quiescent and activated behaviours require individual intrinsic genomic and proteomic programs and are regulated by a variety of extrinsic factors including systemic and local niche-derived signals (Cheung and Rando, 2013; Chaker *et al.,* 2016; Cavallucci *et al*,. 2016; Tian *et al.,* 2018).

To contribute to this area of research, our laboratory performed a small-scale transcriptome analysis comparing individual quiescent pNBs and reactivating pNBs harvested from live *Drosophila* larval brains (Gil-Ranedo *et al.,* 2019). Analysis of the data revealed 145 genes upregulated and 51 genes downregulated in reactivating versus quiescent pNBs, and the differential expression of a large set was validated. Most identified targets are enriched in the larval CNS (Chintapalli *et al.,* 2007), 63% and 66% have highly conserved mouse and human orthologs, respectively, and some of these had been found in previous NSC quiescence and activated microarray or RNA sequencing data profiles (Martynoga *et al.,* 2013; Llorens-Bobadilla *et al.,* 2015). Thus, the transcriptome data promised the identification of novel and conserved molecular signals potentially involved in NSC quiescence and/or reactivation.

Most relevant to my studies was the identification of transcripts encoding for members of the highly conserved STRIPAK complex - *mob4*, *cka* and the catalytic subunit of PP2A, *mts*. *mts* transcript was found downregulated, and *mob4* and *cka* transcripts were found upregulated in reactivating pNBs versus quiescent pNBs; together forming the foundation of my studies. Using the *in-vivo* model *Drosophila,* I characterised Mob4 expression in pNBs, performed *mob4* functional analysis during pNB reactivation, and identified a potential mechanism of *mob4* function on pNB reactivation. I also began and made a significant contribution to studies in our group with *cka* and *mts*, also found in the screen, as well as with the regulatory subunit of PP2A, *wdb*. My results, together with additional data acquired in the laboratory (discussed below) led to a proposed model whereby Mob4, Cka and PP2A/Mts orchestrate the InR/PI3K/Akt and Hippo pathways promoting pNB reactivation. In summary, PP2A/Mts with its regulatory subunit Wdb inhibits the InR/PI3K/Akt signalling pathway via Akt inactivation during NSC quiescence, yet rising levels of Mob4 and Cka recruit PP2A/Mts into a STRIPAK complex to inhibit Hippo, inactivating the Hippo pathway and promoting NSC reactivation (Gil-Ranedo *et al.,* 2019).

### 3.2. Mob4 acts primarily cell-autonomously in pNBs to promote reactivation

*mob4* transcript was found upregulated in reactivating versus quiescent pNBs, the result validated by quantitative real-time PCR (Gil-Ranedo *et al.,* 2019). I confirmed these results at the protein level. Mob4 protein expression is present throughout the CNS, including the glia, which are known regulators of pNB reactivation. Mob4 protein in the glia appeared weaker in comparison to surrounding pNBs, although expression in glia was not quantified (see **Figure 2.1**). Upon analysis of the *mob4* mutants, I observed that the pNBs in the BLs and the VNC are of equivalent size compared to the WT controls at 0-1h ALH (**Figure 2.2**). However, by 4h ALH, I observed that the WT pNBs are beginning to enlarge, whereas the *mob4* mutant pNBs remain small and quiescent. By 24h ALH many of the WT pNBs in the BLs and the VNC are reactivated; fully enlarged and mitotically active. Interestingly, at 24h ALH, I observed that the *mob4* mutant pNBs in the BLs and the VNC increase slightly in size by 1um, however overall they remain small and mitotically quiescent. It is possible that *mob4* mutant pNBs can still initiate some response to start pNB cell growth, but the loss of Mob4 prevents progression of this process. In conclusion, pNB reactivation was abolished in *mob4* mutants, indicating a requirement of Mob4 for the transition from

quiescence to reactivated states. Upon pNB-specific knockdown of *mob4* using RNAi (Schulte *et al.,* 2010) at 18h ALH, I observed a small but significant delay in pNB cell size growth and a striking reduction in mitosis; however, the overall effect was weaker compared to the *mob4* mutants. The weaker effect is likely due to the efficacy of the RNAi, which causes only partial inhibition, whereas *mob4* mutants are devoid of all *mob4* (Schulte *et al.,* 2010). My results indicated that Mob4 might act cell-autonomously on pNB reactivation.

Upon Mob4 reintroduction specifically into *mob4* mutant pNBs, I observed that the pNB size and divisions in the BLs and the VNC were rescued to control levels at 18h ALH, whereas the *mob4* mutant pNBs retained their characteristic quiescent appearance (**Figure 2.8**). This result is supportive of the mentioned above findings, suggest- ing a cell-autonomous role of Mob4 in pNBs.

Due to the prominent role of glia relaying Insulin-like signalling to pNBs towards pNB reactivation, Mob4 was also reintroduced into glia of *mob4* mutants. I observed that the pNB size in the BLs and the VNC showed a minor (0.4um) increase compared to the *mob4* mutant pNBs but far from reaching control values. I also observed a significant increase in pNB divisions in the BLs, but not in VNCs; however, the increase was again minor and far from levels in controls (**Figure 2.9**). Furthermore, upon glia-specific *mob4* overexpression in a WT background, I observed no pNB size differences in the BLs, or differences in the number of dividing pNBs within the BLs or the VNCs, compared to the controls, at 18h ALH. Yet, I observed a very small yet significant increase (0.4um), in VNC pNB diameters compared to the controls (**Figure 2.9**). A relatively low number of *mob4 mt, glia>mob4* and *glia>mob4* VNCs was sampled (n=2 and n=2, respectively) and therefore with increased VNCs scored the minor effects may no longer be significant, albeit many pNBs were scored per sample. It is also possible that the small effects observed may be due to inhibition on the Hippo pathway within niche glia cells, which in turn reflects on pNB reactivation, although not as strong as analogous direct effects in pNBs (Ding *et al.,* 2016; discussed later in section **3.5**). Overall, reintroducing Mob4 into glia of *mob4* mutants cannot rescue pNB reactivation (enlargement or division) to control levels, in contrast to the results upon Mob4 reintroduction in pNBs. Furthermore, glia-specific overexpression of mob4 in a WT background produced no effect except for a minor

VNC pNB size increase, in contrast to overexpression of Mob4 in pNBs that leads to accelerated reactivation (see next section). The findings suggest that *mob4* functions primarily in pNBs promoting reactivation, in agreement with the *mob4* mutant and *mob4*-RNAi data.

### 3.3. Mob4 functions in pNBs during the stage of reactivation

I observed a loss of pNB reactivation in *mob4* mutants. I also observed that overexpression of Mob4 in pNBs leads to premature pNB enlargement in the BLs and VNCs, but no significant differences in the number of dividing pNBs, at 6h ALH (**Figure 2.11**). At 18h ALH, no further pNB enlargement was seen, but an increased number of pNBs dividing in the BL and VNC was observed. These results suggest that Mob4 accelerates pNB reactivation, and I next investigated if its overexpression would cause pNB overproliferation at later ages.

Upon *mob4* overexpression in pNBs at 48h ALH, I observed a small yet significant increase in the number of dividing pNBs in the VNC only (**Figure 2.13**). Despite many pNBs being reactivated by 24h ALH, pNB reactivation occurs up to approximately 48h ALH (Ito and Hotta, 1992; Truman and Bate, 1988; Chell and Brand, 2010; Sousa-Nunes, *et al.,* 2011). The effect observed is likely to be a consequence of accelerated pNB reactivation still at 48h ALH. As mentioned in the Introduction, anterior pNB reactivation begins before the posterior pNBs, and therefore the effect of Mob4 overexpression may still occur in the VNCs at this point. At late larval stages (94h ALH), no differences in dividing pNBs in the BLs or VNCs were observed (**Figure 2.13**).

My Mob4 overexpression data indicates that Mob4 promotes pNB reactivation from early stages throughout the entire reactivation period up to 48h ALH, but seems not involved in controlling the total number divisions pNBs go through during larval stages. Therefore, Mob4 appears to function only within the time-period of pNBs reactivation.

As described in the introduction, during nutrition restriction, the Insulin signalling pathway is inhibited, and pNB reactivation does not occur. However, these defects can be bypassed by reintroducing components or targets of the InR/PI3K/Akt pathway in pNBs and/or in glia (Chell and Brand, 2010; Sousa-Nunes *et al.,* 2011). Owing to

the reliable data showing that Mob4 promotes the pNB reactivation, I assessed if overexpression of Mob4 in pNBs would be strong enough to bypass the lack of external nutritional stimuli and Insulin-signalling. Upon Mob4 overexpression in pNBs in larvae reared on a sucrose only diet, I observed a small but significant increase in pNB enlargement but no re-entry into mitosis in VNCs, and no increase in either size or divisions of pNB divisions in BLs (**Figure 2.14**). I concluded that Mob4 function in pNBs is not sufficient to bypass the lack of extrinsic nutrition signals required for reactivation.

### 3.4. Mob4 function in pNB reactivation may be evolutionary conserved

*Drosophila* Mob4 scores highly in terms of evolutionary orthology conservation to its human match (MOB4, also known as Phocein), using the *Drosophila* RNAi Screening Center Integrative Ortholog Prediction Tool (DIOPT; http://www.flyrnai.org/diopt). The DIOPT score is the number of individual ortholog prediction algorithms used by this resource that predict a specified ortholog pair. A DIOPT score of 3 is considered adequate, and Mob4 scores 13 out of 15. Mob4 and human MOB4/Phocein proteins are 78% identical, demonstrating high conservation (**Table 1.**). Interestingly, in addition to the Mob1/phocein family domain characterising the MOB family of proteins, a Pleckstrin Homology-like (PH-like) domain exists in both *Drosophila* and human proteins with 73% conservation. While the function of the PH-like domain in Mob4/Phocein is unknown, other proteins containing similar domains have been shown to bind phosphatidylinositol lipids and implicated in a variety of processed ranging from cell signalling transduction to cytoskeleton rearrangements (Lemmon *et al.,* 2002; Scheffzek and Welti, 2012; Lemmon *et al.,* 2000).

Excitingly, upon overexpression of human-MOB4/Phocein in *Drosophila* pNBs (**Figure 2.12**), I observed significant increases in pNB enlargement and mitotic activity, similar to the *Drosophila* Mob4 overexpression effect (**Figure 2.11**). In addition to highly conserved amino acid sequences, these results suggest that Mob4/Phocein may also have a conserved function in NSC reactivation, although expression and functional experiments in human cells, tissue and mammalian models would be needed to validate this.

| Species | ID | aa length | aa % similarity | aa % identity | aa % gap | DIOPT score | Known domains (% conserved) |
|---|---|---|---|---|---|---|---|
| *Drosophila Melanogaster* | Mob4 | 227 | | | | | PH-like (73%) Mob1 |
| *Homo sapiens* | MOB4/ Phocein | 225 | 86% | 78% | 3% | 13 | Phocein (84%) |

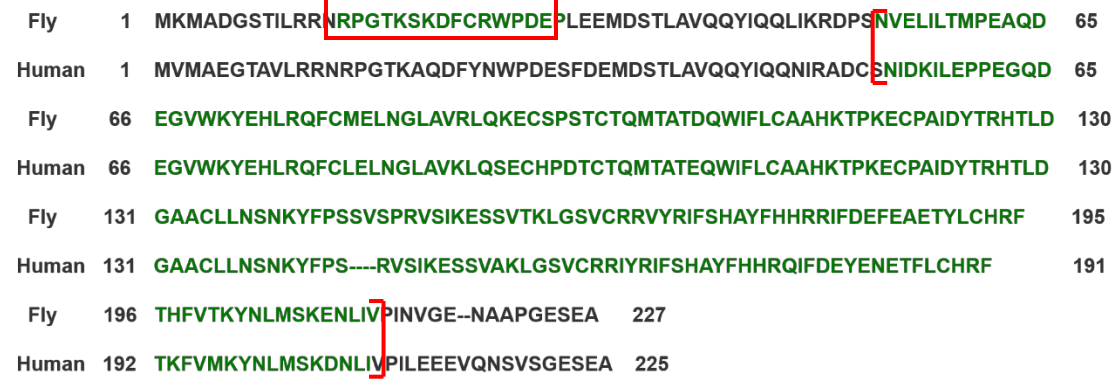


**Table 1. Mob4 and its human orthologue MOB4/Phocein are highly conserved.** A table summarising *Drosophila* Mob4 and human MOB4/Phocein amino acid (a.a) length, % alignment, % similarity, % identity, % gaps, DIOPT score, and known protein domains (http://www.flyrnai.org/diopt). The green highlights represent conserved domain regions extracted from RefSeq protein records (Hu *et al.,* 2011). The red box highlights the PH-like domain. The red brackets encompass the sequence that corresponds to the MOB family of proteins.

## 3.5. Mechanism of Mob4 action in pNBs

### 3.5.1 Mob4 and the Hippo and InR/PI3K/Akt signalling pathways

The data discussed thus far indicates that Mob4 is required primarily cell-autonomously for pNB reactivation; however, the mechanistic action of Mob4 remained elusive and therefore I, and other members of our laboratory, performed a variety of assays to dissect it (see Results and Appendix). Mob4 is part of the highly conserved MOB family of globular scaffold proteins comprising four subgroups (MOB1-4). As mentioned in the Introduction section, MOB1 and 2 have been implicated in the regulation of kinases that contribute to cell cycle control (Gundogdu

and Hergovich, 2019).

MOB4 is the most divergent member of the family (BLAST; Trammell *et al.,* 2008; He *et al.,* 2005) but in *Drosophila* S2 cells, it has been shown to contribute to mitotic spindle fibre focusing, independent of centrosome function (Trammell *et al.,* 2008). My data suggest that Mob4 action in pNB reactivation is independent of that reported in spindle fibre focusing as analysis of the *mob4* mutants shows impairment of pNB cell enlargement before mitotic spindle assembly, and in addition, proliferation of mbNBs, which never enter quiescence, was readily observed (**Figure 2.2-2.5**). The next step was to investigate the relation of Mob4 with InR/PI3K/Akt and Hippo pathways in pNBs, which are critical to activate them or maintain quiescence in pNBs, respectively (Sousa-Nunes *et al.,* 2011; Chell and Brand, 2010; Ding *et al.,* 2016; Poon *et al.,* 2016).

As detailed in the Introduction, Insulin signalling is also known to regulate NSC activation in mammals (Chaker *et al.,* 2016; Bracko *et al.,* 2012; Arsenijevic, *et al.,* 2001; Renault *et al.,* 2009; Kippin *et al.,* 2005; Brandhorst *et al.,* 2015). In *Drosophila*, Insulin signalling is relayed to the pNBs via niche glia. Glia secrete Insulin-like peptides (dILPs) that bind the Insulin-like receptor (InR) in pNBs activating the InR/PI3K/Akt cascade leading to pNB cell size growth and re-entry into division. Secretion of dILPs by glia depends on co-ordinated $Ca^{2+}$ oscillations. Glia also enwrap the developing pNBs and their lineages to ensure their survival (see Introduction; Spéder and Brand, 2014; Spéder and Brand, 2018). It is not known if a similar mechanism occurs between mammalian glia and NSCs. However, astrocytes are known to support neurogenesis and display a protective role to NSCs (Gengatharan *et al.,* 2016; Sloan and Barres, 2014). It is possible that mammalian Insulin signalling is also relayed to adult NSCs via niche glia as in *Drosophila*, yet further studies are required to demonstrate it.

On the other hand, although Hippo signalling has not yet been shown to act in mammalian NSC quiescence, it has been associated with maintaining quiescence in liver progenitors (Wang *et al.,* 2017; Zhou *et al.,* 2009). Inactivating Hippo signalling in the mouse liver quiescent progenitor cells by knocking down the mammalian Hippo

kinase (Mst1/2), caused loss of Yap (mammalian Yki) phosphorylation leading to cell cycle activation and hepatocellular carcinoma. This overgrowth could be rescinded by activating Mst1/2 (Zhou *et al.,* 2009). In mammalian epidermal stem cells, the Hippo signalling effector Yap1 was shown to regulate proliferation and tissue expansion and negatively regulated by upstream α-Catenin (Schlegelmilch *et al.,* 2011). α-Catenin modulates Yap1 activity and interaction with 14-3-3 and PP2A (Schlegelmilch *et al.,* 2011). Furthermore, YAP was shown to maintain basal epidermal progenitors and morphogenesis (Zhang *et al.,* 2011). Finally, in the intestine, YAP is required for homeostasis, and YAP inhibition or activation can cause a myriad of phenotypes (Zhou *et al.,* 2011; Barry *et al.,* 2013). For example, transgenic Yap expression causes loss of intestinal crypts and inhibits regeneration by repressing Wnt signals, whereas Yap inhibition caused microadenomas (Barry *et al.,* 2013).

I have shown that the pNB reactivation defects in *mob4* mutants could be rescued by activating InR/PI3K/Akt signalling in pNBs via overexpressing Rheb (**Figure 2.15**), or by inhibiting the Hippo pathway via targeted RNAi expression against the core kinases Hippo and Warts (**Figure 2.16**). The data suggest that InR/PI3K/Akt signalling is inhibited and Hippo signalling is active in *mob4* mutant pNBs, consistent with my data showing that *mob4* mutant pNBs fail to exit quiescence (**Figure 2.2-2.6**). Although deactivating the Hippo pathway (**Figure 2.16**) or activating InR/PI3K/Akt signalling (**Figure 2.15**) improved the enlargement and mitotic activity of the *mob4* mutant pNBs, the rescues were only partial, as the levels did not reach the control levels. Note that the same manipulations in a WT background produce premature pNB reactivation (Chell and Brand, 2010; Sousa-Nunes *et al.,* 2011; Ding *et al.,* 2016). My results could reflect inadequate activation or inactivation of InR/PI3K/Akt signalling or the Hippo pathway signals, and that regulation of both pathways is necessary for effective pNB reactivation.

The idea that the InR/PI3K/Akt signalling is inhibited in *mob4* mutants was supported by a western blot assay I performed on *mob4* mutant CNS lysates, which showed lower p-Akt expression levels in the *mob4* mutant brains compared to the WT controls, yet total Akt levels remain unchanged (**Figure 2.15**). These results were repeated and confirmed in our laboratory (Dr C. Barros) with additional brain lysate samples I prepared (Gil-Ranedo *et al.,* 2019). The downstream target of InR/PI3K/Akt

signalling, Akt, is recruited by PIP3 through its pleckstrin homology (PH) PH-domain, and AKT becomes activated by phosphorylation. Akt phosphorylation/activation can be examined using a (PH) domain-GFP fusion protein (PH-GFP) which binds to PIP3; shown as strong membrane-bound PH-GFP in reactivated pNBs (Britton, *et al.,* 2002; Chell and Brand, 2010). Using this tool, Drs Barros and Gil-Ranedo in our team showed that *mob4* mutant pNBs show weak and diffused PH-GFP signal (Gil-Ranedo *et al.,* 2019), confirming InR/PI3K/Akt signalling inhibition upon Mob4 loss.

*bantam* (*ban*) microRNA expression is known to be regulated by Hippo signalling (Nolo *et al.,* 2006; Thompson and Cohen, 2006). Active *ban* microRNA promotes pNB enlargement and divisions (Ding *et al.,* 2016). During pNB quiescence, activated Hippo pathway signalling inhibits *ban* transcription (Ding *et al.,* 2016). *ban* activity/Hippo pathway signalling can be monitored using a GFP-sensor system, wherein loss of GFP signal equals *ban* activity (Brennecke *et al.,* 2003). No GFP is detected in control re- activated pNBs indicating *ban* activity (Ding *et al.,* 2016). However, using this tool in a *mob4* mutant background, Drs Barros and Gil-Ranedo observed that pNBs express GFP signal, which indicates a lack of *ban* activity and confirms activated Hippo signalling (Gil-Ranedo *et al.,* 2019).

In conclusion, together with the results obtained by other team members, the data I generated suggested that Mob4 affects both Hippo and InR/PI3K/Akt pathways, with the former remaining active and the latter inhibited in pNBs upon *mob4* loss. How can Mob4 directly or indirectly regulate these pathways is what was next investigated. One clue available was that Mob4 genetically and physically interacts with Hippo and is a known member of the STRIPAK complex, known to inhibit Hippo signalling (Shi *et al.,* 2016; Zheng *et al.,* 2017; Couzens *et al.,* 2013; Ribeiro *et al.,* 2010), which I discuss below.

### 3.5.2. Mob4 and another STRIPAK/PP2A complex member, Cka, combine actions to promote pNBs reactivation

Mob4 is a core member of the STRIPAK protein complex. A large amount of data arose from a seminal combined proteomic and genomic study investigating *Drosophila* STRIPAK/PP2A and its inhibitory action on the Hippo pathway (Ribeiro *et al.,* 2010).

STRIPAK is made up of multiple components, including various kinases and the pleiotropic PP2A phosphatase. It is striking that STRIPAK members can form mutually exclusive complexes, and are therefore able to direct the kinases or PP2A to different targets (Virshup and Shenolikar, 2009; Ribeiro *et al.,* 2010; Shi *et al.,* 2016). STRIPAK complexes are highly conserved from fungi, to fly, to mammals, including humans (Castets *et al.,* 2000) and their pleiotropic potential allows them to regulate a variety of pathways and processes.

The main components of the STRIPAK complexes identified in *Drosophila* and humans can be found in **Table 2.** The main components of human STRIPAK are the striatin (STRN) proteins, comprising STRN1, STRN3 (also known as S/G2 nuclear autoantigen; SG2NA) or STRN4 (also known as Zinedin); the pleiotropic PP2A enzyme with α/β variants; a member of Ste20-related germinal center kinases (GCK) family (Stk24/25, Mst4), and adaptor molecules including cerebral cavernous malformations 3 (CCM3), Sarcolemmal membrane-associated protein (SLMAP), STRN-interacting protein 1/2 (Strip1/2, also named FAM40A/B), suppressor of IKBKE 1 (SIKE1) also known as fibroblast growth factor oncogene partner 2 (FGFR1OP2), and MOB4 (Virshup and Shenolikar, 2009; Ribeiro *et al.,* 2010; Glatter *et al.,* 2009; Goudreault *et al.,* 2009; Castets *et al.,* 2000; Chen *et al.,* 2002; Couzens *et al.,* 2013; Hauri *et al.,* 2013; Sakuma and Chihara, 2017; Shi *et al.,* 2016). The STRIPAK complex is implicated in human diseases such as cancer (Shi *et al.,* 2016; Hwang and Pallas, 2014) and is known to associate with mammalian Hippo (Mst1/2) in the Hippo pathway, which is also implicated in human diseases (Polesello *et al.,* 2006; Ribeiro *et al.,* 2010; Zheng *et al.,* 2017; Huang *et al.,* 2013).

| STRIPAK subunit | *Drosophila* | Human |
|---|---|---|
| Striatin | Cka | STRN1/3/4 |
| PP2AA | PP2A-29B | PP2AAα/β |
| PP2AC | Mts | PP2Acα/β |
| Mob | Mob4 | MOB4/Phocein |
| SLMAP | CG17494 | SLMAP |
| GCK | GckIII, Hpo, Msn | Mst1/2, Stk24/25, Mst4 |
| SIKE/FGFR1OP2 | FGOP2 | SIKE/FGFR1OP2 |
| CCM3 | CG5073 | CCM3 or PDCD10 |
| STRIP | CG11526/Strip | STRIP1/2 |

**Table 2. The core subunits of STRIPAK complex in *Drosophila* and Humans.** Table modified from (Ribeiro *et al.,* 2010; Pracheil *et al.,* 2012; Goudreault *et al.,* 2009; Frost *et al.,* 2012; Bloemendal *et al.,* 2012, and Hwang and Pallas, 2014).

In *Drosophila* STRIPAK (**Table 2**), the components comprise PP2A (PP2A-29B structural subunit and Microtubule star, Mts, the *Drosophila* ortholog of the catalytic subunit of PP2A); Cka (the sole *Drosophila* STRN); Mob4 (*Drosophila* ortholog of MOB4/Phocein); CG10158 (the *Drosophila* ortholog of FGFR1OP2); CG11526 (*Drosophila* ortholog of FAM40A); CG5073/Strip (*Drosophila* ortholog of CCM3); CG17494 (*Drosophila* ortholog of SLMAP); and Hpo, Misshapen (Msn) and Germinal centre kinases (GCKIII in *Drosophila*, MST4 and STK24/25 in mammals). Using the previously described DIOPT tool, evolutionary conservation between *Drosophila* and human STRIPAK subunits is evident (**Figure 3.2. B, and E**). The conserved PP2A phosphatase is a trimeric enzyme composed of a catalytic, a structural and regulatory subunit, the latter responsible for directing it to specific targets (**Figure 3.2A, C**). STRIPAK members act as regulatory subunits of PP2A. Yet, PP2A has also a variety of other functions independent of STRIPAK, relying on multiple different proteins functioning as regulatory subunits to directing it to specific targets (Janssens and Goris, 2001; Wang *et al.,* 2009; Zheng *et al.,* 2015).

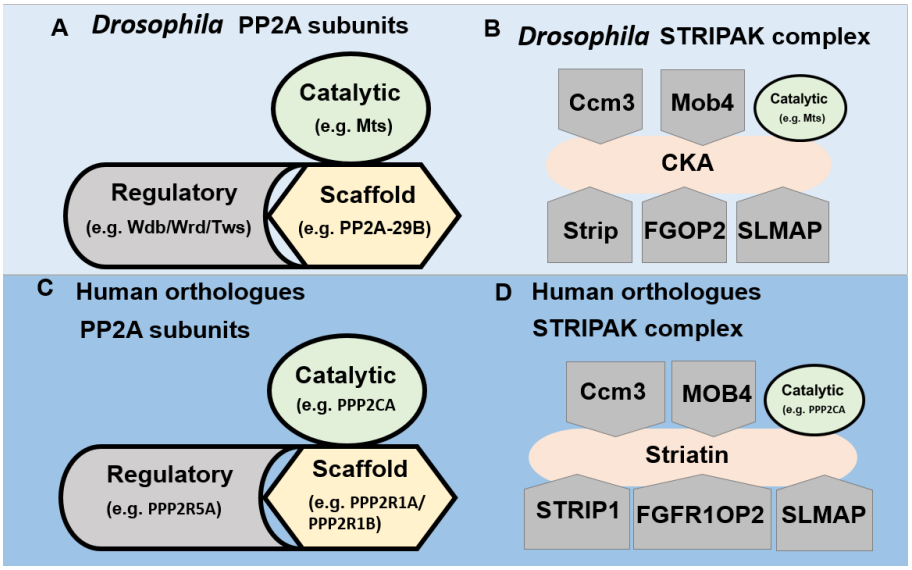


E

| Drosophila STRIPAK | DIOPT Score |
|---|---|
| Mob4 | 13/15 |
| Mts | 14/15 |
| Cka | 15/15 |
| Wdb | 13/15 |
| Wrd | 13/15 |
| Tws | 15/15 |
| Ccm3 | 14/15 |
| Strip | 14/15 |
| FGOP2 | 13/15 |
| SLMAP | 8/15 |

**Figure 3.2. *Drosophila* and Human core STRIPAK/PP2A complex components inhibit Hippo signalling**. The *Drosophila* PP2A subunits (A) have human counterparts (C). *Drosophila* STRIPAK subunits (B) also have human counterparts (D). The DIOPT tool was used to obtain conservation scores to human orthologues (E) (http://www.flyrnai.org/diopt; Hu *et al.,* 2011).

In *Drosophila* and in mammals, including in human cells, a STRIPAK complex has been shown to deactivate the Hippo pathway, via recruitment of PP2A, which dephosphorylates Hpo kinase (human MST1/2) (Zheng *et al.,* 2017; Huang *et al.,* 2013; Polesello *et al.,* 2006; Ribeiro *et al.,* 2010; Bae *et al.,* 2017). In *Drosophila* cells, Cka binds to Hpo and Cka overexpression could block Hpo activity, and Cka overexpression was also shown to increase Yki activity (Ribeiro *et al*,. 2010). The Cka-Hpo interaction is reduced when Mts is knocked down by RNAi; therefore, Cka-Hpo interactions depend upon a stable PP2A complex (Ribeiro *et al.,* 2010).

Ribeiro *et al* demonstrated a genetic relationship between Hpo and Cka (Ribeiro *et al.,* 2010). Hpo overexpression in the eye leads to a reduction in size and a rough-like phenotype (Wu *et al.,* 2003; Pantalacci *et al.,* 2003; Harvey *et al.,* 2003; Udan *et al.,* 2003); and this phenotype is enhanced after removing one copy of Cka (Ribeiro, *et al.,* 2010). Hpo knockdown by RNAi causes an overgrowth phenotype in the developing wing, however simultaneously knocking down Cka or FGOP2 by RNAi suppresses the overgrowth phenotype (Ribeiro *et al*,. 2010). Co-depletion of Hpo and Mob4 by RNAi could also suppress this phenotype (Ribeiro *et al*,. 2010). Interestingly, Toll receptor signalling activates Hippo signalling by causing Cka degradation (Liu *et al.,* 2016).

*Drosophila* PP2A/Mts encodes the catalytic subunit for PP2A and functions as a tumour suppressor by inhibiting self-renewal capacity in pNBs (Wang *et al.,* 2009). In cells, Mts negatively regulates Hpo; Mts inhibition caused increased Hpo and Yki phosphorylation (Ribeiro *et al.,* 2010). Our lab also recently showed that Mts inhibits the Hippo pathway in pNBs (Gil-Ranedo *et al.,* 2019). An upstream component of the Hippo pathway, Salvador (sav) was shown to bind to PP2A and inhibit its activity, which leads to increased Hippo signalling (Bae *et al.,* 2017). In cells, PP2A/STRIPAK inhibits Hippo signalling (Tang *et al.,* 2019). PP2A and STRNS (mammalian Cka) form a complex which recruits other STRIPAK members to secure MST1/2 (mammalian Hpo) with the STRIPAK complex, destabilising the complex diminished the ability of STRIPAK to regulate Hippo signalling (Tang *et al*,. 2019). This complex is mediated by SLMAP (Tang *et al*,. 2019) which has previously been reported to link STRIPAK to MST1/2 in cells and to Hpo in flies (Couzens *et al.,* 2013; Hauri *et al.,* 2013; Bae *et al.,* 2017; Zheng *et al.,* 2017; Goudreault *et al.,* 2009). Moreover, SIKE1 (mammalian FGOP2) and Strip are required to recruit SLMAP to STRN (Tang *et al*,. 2019). Strip can bind to PP2A, and Strip and SLMAP also directly bind to MST1/2 which collectively aids Hippo pathway regulations (Tang *et al.,* 2019).

Within STRIPAK, CCM3 can direct GCK localisation and also function as bridges, connecting STRNS to GCKs (Shi *et al.,* 2016). Human GCK kinases, together with STRIPAK, can phosphorylate MOB1/Lats (*Drosophila* Wts), together with Salvador (*Drosophila* Sav; Yu and Guan, 2013; Pantalacci *et al.,* 2003; Wu *et al.,* 2003; Tapon *et al.,* 2002; Udan *et al.,* 2003). This effect is in contrast to a recent study showing Sav1 inhibiting the STRIPAK/PP2A complex to promote Hippo signalling (Bae *et al.,* 2017). Therefore, a great deal of crosstalk exists between STRIPAK components and Hippo pathway activity to control growth.

Despite a large amount of data on the Hippo pathway and its inhibition by STRIPAK/PP2A complex, STRIPAK had not yet been implicated in NSC quiescence or reactivation. However, three of the core members were identified on the pNB quiescent vs reactivating transcriptome analysis performed in our laboratory: Cka, Mob4 and Mts, the catalytic subunit of PP2A (Gil-Ranedo *et al.,* 2019). Both *mob4*

and *cka* were found upregulated in reactivating versus quiescent pNBs (**Figure 3.2**). I confirmed the Mob4 differential protein expression (**Figure 2.1**) and Cka expression was also confirmed by our group. I found that overexpressing Mob4 and Cka together in pNBs leads to increased pNB reactivation (**Figure 2.17**), generating a stronger increase in pNB cell enlargement as well as the number of pNB divisions than the Mob4 overexpression (**Figure 2.12**), or Cka overexpression, alone. The latter, performed by Dr Gil-Ranedo, resulted in similar results as Mob4 single overexpression. Also, Dr Gil- Ranedo found that depletion of *cka* by RNAi impairs pNB reactivation similarly to Mob4 inhibition (Gil-Ranedo *et al.,* 2019). Interestingly, in mammalian cells, STRN4 knockdown suppressed cancer cell division, migration and invasion (Wong *et al.,* 2014). Together, the data indicated that Mob4 and Cka might work together in pNB reactivation, possibly as part of STRIPAK and suggesting a new function for the complex.

Dr Gil-Ranedo continued investigating the STRIPAK members using *Drosophila* S2 cells in culture to perform co-immunoprecipitation assays and found that depletion of Mob4 and/or of Cka by RNAi impairs the binding of Mts, the catalytic subunit of PP2A, to Hippo, and a consequent increase in Hippo kinase phosphorylation as previously reported (Ribeiro *et al.,* 2010; Couzens *et al.,* 2013). Mts/Hippo binding was almost abolished by simultaneous *mob4* and *cka* RNAi knockdown, suggestive of cooperative action between Mob4 and Cka in bringing Mts and Hippo together to inactivate Hippo (Gil-Ranedo *et al.,* 2019). Finally, to demonstrate an inhibitory function of PP2A/Mts on the Hippo pathway in pNBs, Drs Barros and Gil-Ranedo combined *mts*-DN and *ban*-GFP sensor *Drosophila* lines to visualise *ban* activity as a read-out of Hippo signalling in pNBs. Early pNBs (6h ALH) expressing *mts*-DN were observed to have significantly less *ban*-activity as seen by more GFP signal than controls, indicating that PP2A/Mts can inhibit Hippo pathway signalling in pNBs.

Together, the findings indicate that Mob4 functions together with Cka, forming with PP2A a STRIPAK complex to target Hippo, leading to Hippo pathway inhibition. These results are also consistent with the observations that the Hippo pathway remains active in *mob4* mutant pNBs (Gil-Ranedo *et al.,* 2019), rendering them quiescent.

### 3.5.3 PP2A with its regulatory subunit Wdb promotes pNB quiescence

If PP2A would only work in pNBs within STRIPAK to inhibit Hippo signalling, prolonged pNB quiescence could be assumed by knocking it down. Interestingly, the expression of the PP2A catalytic subunit, Mts, was found down-regulated at the mRNA level in reactivating versus quiescent pNBs in the transcriptome analysis performed in our team, the opposite to Cka and Mob4 (Gil-Ranedo *et al.,* 2019). I obtained various mutants strains for *mts*; however, it was not possible to examine pNB reactivation in $mts^{XE-2258}$ null mutants, due to embryonic lethality (Snaith *et al.,* 1996). Yet, by combining $mts^{XE-2258}$ null mutants with $mts^{299}$ hypomorphic mutants, I was able to examine $mts^{299}/mts^{XE-2258}$ transheterozygotes which survive to pupal stages (Wang *et al.,* 2009). In contrast to prolonged pNB quiescence as anticipated, I observed increased pNB enlargement in $mts^{299}/mts^{XE-2258}$ transheterozygotes compared to controls, at 18h ALH (**Figure 2.18**). Next, I used a dominant-negative *mts* mutant (*mts*-DN, **Figure 2.19**) which lacks the N-terminal region of the phosphatase domain (Hannus *et al.,* 2002) to analyse the effect of Mts inhibition specifically in pNBs. I observed increased pNB enlargement and mitosis compared to controls at 18h ALH (**Figure 2.19**). In our group, similar assays were performed to analyse pNBs at 6h ALH, and premature pNB reactivation observed (Gil-Ranedo *et al.,* 2019). These results support the $mts^{299}/mts^{XE-2258}$ transheterozygotes mutant data, and interestingly produced a more substantial effect, demonstrating a significant role of PP2A/Mts in pNBs to maintain quiescence.

The *mts* mutant results were initially quite surprising. However, PP2A is notoriously pleiotropic and, in addition to its function within STRIPAK, it is known to use mutually exclusive regulatory B subunits (**Figure 3.2**) to target a variety of different signalling pathways (Ribeiro *et al.,* 2010; Shi *et al.,* 2016; Janssens and Goris, 2001; Wang *et al.,* 2009; Zheng, Y. *et al.,* 2015). In *Drosophila*, known regulatory B subunits of PP2A (**Figure 3.2**) are Widerborst (wdb), B56/Well rounded (Wrd) and Twins (Tws). In dividing *Drosophila* NBs, PP2A/Tws regulates proper aPKC localisation and NB homeostasis (Chabu and Doe, 2009; Ogawa et al., 2009). Also, PP2A was shown to bind and phosphorylate/deactivate Bazooka (Baz) to regulate Apical-Basal polarity (Krahn *et al.,* 2009). Here, immunoprecipitates containing Baz, PP2A, and the catalytic subunit of PP2A/Mts were identified (Krahn *et al.,* 2009). The study found that

the Mts/PP2A/Baz complexes contained the regulatory B subunits of PP2A, Tws and B56, whereas no interaction with Wdb was found (Krahn *et al.,* 2009). Also, Tws was the sole regulatory B subunit shown to assist the PP2A/Mts dephosphorylation of Baz (Krahn *et al.,* 2009). Wdb is known to inhibit Notch signalling (Bose *et al.,* 2014) and can physically and genetically interact with the cell-cycle regulator, Cyclin G (CycG), in-*vitro* and in-*vivo* (Johnson and Walker, 1999; McCright *et al.,* 1996; Stanyon *et al.,* 2004; Fischer *et al.,* 2015; Nagel *et al.,* 2016)*;* even rescuing the growth defects observed in *cycG* mutants (Nagel *et al.,* 2016). Very interesting and in relation to my findings, is the fact that both Wdb and its *C.elegans* orthologue, PPTR-1, were shown to inhibit InR/Pi3K/AKT signalling pathway by directing PP2A to Akt (Padmanabhan *et al.,* 2009; Vereshchagina *et al.,* 2008). Furthermore, *wdb* overexpression caused decreased organ size (eye and wing), reduced AKT phosphorylation/activation and increased longevity (Funakoshi *et al.,* 2011). In vertebrates including in human cells, inhibition of Akt by PP2A using Wdb orthologues has also been observed (Rodgers, *et al.,* 2011; Funakoshi *et al.,* 2011; Nagel *et al.,* 2016). I therefore performed a functional analysis of Wdb in pNBs to analyse its possible role on quiescence/reactivation. Using a truncated *wdb* mutant (Hannus *et al.,* 2002) that acts as a dominant-negative (*wdb*-DN) and expressing it in pNBs, I observed increased pNB enlargement in the BLs and VNCs compared to controls, at 18h ALH (**Figure 2.19**), consistent with the effects of *mts*-DN expression (**Figure 2.19**). Further work completed by other members of the laboratory showed that *wdb*-DN expressing pNBs enlarged prematurely at 6h ALH, again similar to the results upon *mts*-DN expression (Gil-Ranedo *et al.,* 2019). Moreover, using a p-AKT specific antibody, *mts*-DN pNBs displayed early p-AKT signal compared to the controls at 6h ALH, demonstrating premature InR/PI3K/Akt signalling activity upon PP2A/Mts depletion (Gil-Ranedo *et al.,* 2019). Finally, Dr Gil-Ranedo also demonstrated that depletion of Cka and/or Mob4 in S2 cells did not affect Mts-Akt association nor the levels of phosphorylated/activated AKT (Gil-Ranedo *et al.,* 2019).

Overall my data and the work completed by other laboratory members suggest that PP2A/Mts functions with Wdb to inhibit the InR/PI3K/Akt signalling in pNBs, and this role seems independent of that of PP2A/Mts within STRIPAK and its components Cka and Mob4.

### 3.5.4. Proposed mechanistic action of Mob4, Cka and PP2A in pNB quiescence to reactivation transition

As discussed above, my results (**Figure 2.19**) together with data obtained from other team members in our laboratory show that PP2A using the Wdb regulatory subunit maintains pNB quiescence by inhibiting the InR/PI3K/Akt signalling cascade via inactivation/ dephosphorylation of Akt **(Figure 3.3)**. These findings are consistent with previous reports of PP2A/Wdb inhibiting Akt by in other cells and tissues (Johnson and Walker, 1999; McCright *et al.,* 1996; Stanyon *et al.,* 2004; Fischer *et al.,* 2015; Nagel *et al.,* 2016; Padmanabhan *et al.,* 2009; Vereshchagina *et al.,* 2008; Brownlee, *et al.,* 2011; Funakoshi *et al.,* 2011). Interestingly, PP2A has also been implicated in cellular quiescence in different contexts (Naetar *et al.,* 2014; Kolupaeva *et al.,* 2008; Kolupaeva *et al.,* 2013; Sun and Buttitta, 2015; Kurimchak *et al.,* 2013; Kurimchak and Grana, 2013).

The *Drosophila* eye becomes quiescent ~24h after pupal formation (Buttitta *et al.,* 2007). By testing different PP2A B subunits, Sun and Buttitta demonstrated that PP2A/*wdb* restricts CyclinE/Cdk2 to promote quiescence (Sun and Buttitta, 2015). Knocking down PP2A/*mts* or of PP2A/*wdb* by RNAi in the eye caused an increased S-phase (EdU) positive cells and cell cycle gene expression (Sun and Buttitta, 2015). They determined that loss of PP2A/*wdb* in the *Drosophila* eye and wing, allowed cells to bypass entry into quiescence, which leads to extra divisions (Sun and Buttitta, 2015). In human glioblastoma immortalised cells in culture, PP2A and its regulatory B56γ subunit is required for inducing stable quiescence via Ras signalling (Naetar *et al.,* 2015). Inhibition of PP2A using okadaic acid during G2 interferes with quiescence and establishing the next G1 (Naetar *et al.,* 2014). The decision to enter quiescence was thought to occur in G1; however in this study, they showed that Ras inhibition by PP2A/ B56γ occurred during G2 only, and this pathway helps determine the cell-cycle length and quality of the next cell-cycle (Naetar *et al.,* 2014).

The results from my expression and functional analysis of the evolutionarily conserved STRIPAK core component Mob4, demonstrate that it promotes pNB reactivation, primarily in a cell-autonomous fashion. The data also suggest that Mob4 cooperates with Cka, another core STRIPAK complex member. It is known that the Hippo

pathway maintains pNB quiescence (Ding *et al.,* 2016; Poon *et al.,* 2016), whereas InR/PI3K/Akt signalling activation is necessary for pNB reactivation (Chell and Brand, 2010; Sousa-Nunes *et al.,* 2011). Upon loss of Mob4, pNBs are unable to reactivate, with Hippo pathway remaining activated and InR/PI3K/Akt signalling inhibited (Gil-Ranedo *et al.,* 2019). I have further shown that overexpressing the InR/PI3K/Akt signalling activator Rheb, or inhibiting the Hippo pathway core kinases Hpo or Wts specifically in *mob4* mutant pNBs, can rescue reactivation, suggesting that Mob4 is required to regulate Hippo and InR/PI3K/Akt signalling pathways in pNBs. Cka and Mob4 were known to assist PP2A-inhibition of Hippo (Ribeiro *et al.,* 2010), and our team demonstrated that inhibition of Cka and/or Mob4 indeed prevents PP2A/Mts physical association to Hippo kinase, leading to Hippo signalling activation. In accordance, PP2A/Mts inhibition in pNBs also leads to increased Hippo signalling, but the effect is not sufficient to overcome the premature activation of InR/Pi3K/AKT signalling that also occurs, resulting in early reactivation despite Hippo activity (Gil-Ranedo *et al.,* 2019).

Collectively, the data supports the idea that as Mob4 and Cka levels increase in pNBs, a STRIPAK/PP2A complex assembles and acts as a 'molecular switch' to redirect PP2A/Mts to inhibit Hippo signalling and allow activation of InR/PI3K/Akt signalling in pNBs, promoting reactivation (**Figure 3.3)**.

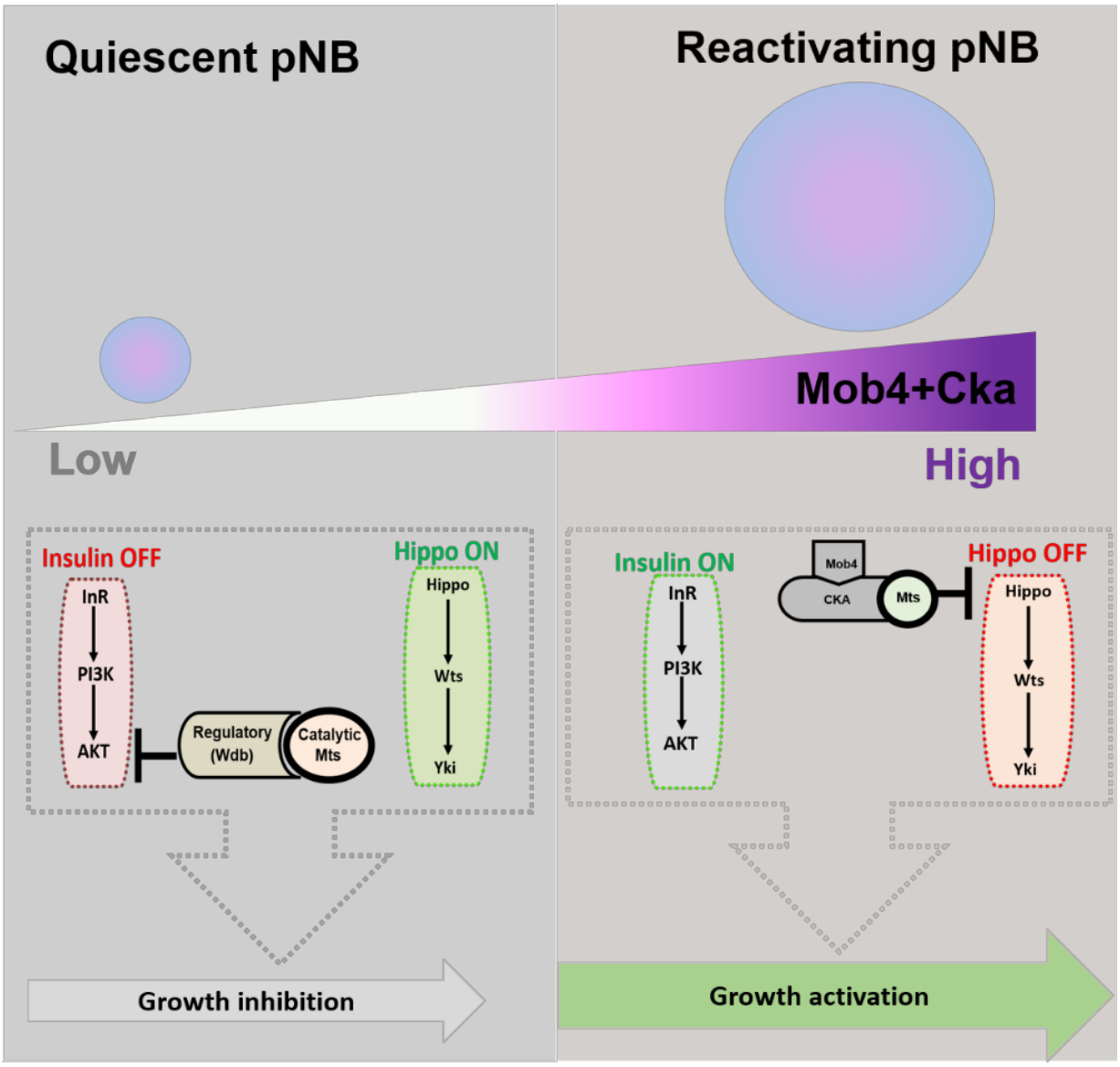


**Figure 3.3. The STRIPAK members Mob4, Cka and PP2A contribute to pNB transition from quiescence to reactivation.** In quiescent pNBs, the levels of Mob4 and Cka are low, and PP2A/Mts phosphatase is directed to Akt by the regulatory subunit, Wdb. PP2A/Mts-Wdb dephosphorylates (deactivates) Akt, inhibiting InR/Pi3K/Akt signalling, which is required for pNB reactivation (Chell and Brand, 2010; Sousa-Nunes *et al.,* 2011). The Hippo pathway, which maintains quiescence (Ding *et al.,* 2016; Poon *et al.,* 2016) remains active. During pNB reactivation, the levels of Mob4 and Cka surge, assembling a Mob4/Cka/PP2A STRIPAK complex that redirects Mts to dephosphorylate Hpo, inactivating the Hippo pathway. InR/PI3K/Akt signalling activates, promoting pNB reactivation.

Interestingly, a similar STRIPAK/PP2A-dependent mechanism regulates the *Drosophila* circadian oscillator (Andreazza *et al.,* 2015). The CLOCK (CLK) and CYCLE (CYC) bHL transcription factors temporally activate circadian rhythm genes such as *period*, *timeless* and *pdp1,* which in-turn repress or activate CLK and CYC

(Hardin, 2011; Ozkaya and Rosato, 2012; Sathyanarayanan *et al.,* 2004). CLK is highly phosphorylated and inactive in the morning, but hypophosphorylated and active in the evening. These temporally controlled oscillating loops of repression and activation, creating *hyper*-or-*hypo*-phosphorylated CLK, are vital for *Drosophila* circadian regulation. Andreazza *et al.,* show that PP2A comprising the regulatory (Wdb) and catalytic (Mts) subunits (PP2A-Mts/Wdb) act to stabilise CLK, without affecting its phosphorylation. However, a complex made of PP2A/Mts and the STRIPAK components Cka and Strip (Strip/Cka/PP2A-Mts) cause CLK dephosphorylation during daytime (Andreazza *et al.,* 2015).

### 3.6. Conclusion

We are slowly demystifying the brain, NSCs, and how adult NSCs maintain adult brain homeostasis (Morales, 2019; Obernier, 2019; Tian *et al*., 2018; Chaker *et al.,* 2016; Cheung and Rando, 2013). Improved techniques, such as brain cell sorting, identification, and transcriptome and proteome characterisation, have significantly advanced research efforts (Codega *et al.,* 2014; Beckervordersandforth *et al.,* 2010; Daynac *et al.,* 2015; Mich *et al.,* 2014; Llorens-Bobadilla *et al.,* 2015; Shin *et al.,* 2015; Dulken *et al.,* 2017; Morizur *et al.,* 2018; Berg *et al.,* 2019).

My studies towards a PhD degree aimed to examine candidate genes that arose from a small-scale single-cell transcriptome analysis comparing quiescent and reactivating *Drosophila* NSCs (Gil-Ranedo *et al.,* 2019). Mob4 was a gene identified together with other STRIPAKS members Cka and PP2A. I have investigated Mob4 expression in NSCs, performed functional analysis of Mob4, as well as of Cka and PP2A, and contributed to the identification of a mechanism of Mob4 action together with Cka and PP2A in NSC quiescence to reactivation transition; accomplishing all proposed objectives of this work.

My work described in this dissertation, together with work from other members of our team, indicated in the above Discussion sections, led us to the propose a model of action: In pNBs, PP2A/Wdb functions to inhibit InR/PI3K/Akt signalling promoting quiescence. As Mob4 and Cka levels increase, a STRIPAK/PP2A complex forms and acts as a ‘molecular switch’ to redirect PP2A to inhibit Hippo signalling, allowing InR/PI3K/Akt signalling activation and promoting pNB reactivation. Thus, Mob4, Cka

and PP2A orchestrate in pNBs Hippo and InR/PI3K/Akt signals, two major pathways controlling quiescence and reactivation, respectively. The studies were recently included in a paper published in Cell Reports in which I am a shared first author (see appendix for full publication).

It is fascinating how PP2A subunits and the STRIPAK complex members collaborate so efficiently to achieve a plethora of functions, across vast cell types, regulating many signalling systems and cellular processes. It is remarkable that PP2A is known to target over 300 substrates and modulate most major signalling cascades such as the Hippo pathway, InR/PI3K/Akt, mTOR, c-Jun N-terminal kinases (JNK), mitogen-activated protein kinase (MAPK), extracellular signal-regulated kinases (ERK), Notch, Wnt and implicated in a variety of human diseases (Remmerie and Janssens, 2019; Eichhorn *et al.,* 2009; Wlodarchak and Xing, 2016; Grech *et al.,* 2016; Ruvolo *et al.,* 2016; Kiely *et al.,* 2015; Westermarck *et al.,* 2008; Sangodkar *et al.,* 2016; Schuhmacher *et al.,* 2019; Clark and Ohlmeyer, 2019).

I have contributed to identifying one mechanism whereby STRIPAK members and PP2A integrate different signalling pathways that are highly conserved from fly to human. This mechanism adds to current knowledge of NSC behaviour and regulation, and may also contribute to the development of future NSC-based therapies against brain-related diseases such as neurodegeneration, autism and even brain tumours. My findings likely have relevance in other stem cells, which also rely on smooth transitions between quiescent and activation states. It will be interesting to examine the expression and function of the highly conserved Mob4, and other STRIPAK members, in mammalian NSCs.

# CHAPTER 4.
# MATERIALS AND METHODS

## 4.1. MATERIALS

### 4.1.1. Antibodies and cell proliferation assay kit

The following tables **3** and **4** list the primary and secondary antibodies used for immunostainings and western blotting of *Drosophila* larval brains described in the Results chapter. Antibody name and species made in, source and dilutions used are indicated. Table 5 describes the commercial kit used for EdU incorporation assays shown in section **2.2.** of Results.

| Primary Antibodies | Source | Dilution |
|---|---|---|
| Rabbit anti-GFP | Gift from U. Mayor (U. Mayor and A.H. Brand, unpublished) | 1:1000 |
| Chicken anti-GFP | Millipore AB_310288 | 1:500 |
| Guinea pig anti-Dpn | Gift from J. Knoblich (Levy and Larsen, 2013) AB_2314299 | 1:2000 |
| Rat anti-Dpn | Abcam AB_195173 | 1:100 |
| Guinea pig anti-Mob4 | Gift from T. Littleton (Schulte, *et al.,* 2010) | 1:1000 |
| Mouse anti-Dlg | DSHB AB_528203 | 1:50 |
| Rabbit anti-pH3 | Abcam AB_304763 | 1:1000 |
| Rabbit anti-pAKT$^{S505}$ | CST AB_331414 | 1:400 |
| Rabbit anti-Akt | CST AB_329827 | 1:400 |
| Rabbit anti-b-Actin | CST AB_330288 | 1:50 |
| Rat anti-Grainyhead | Gift from Prof. Steven Thor laboratory (Sweden) | 1:1000 |
| Mouse anti-Prospero | DSHB AB_528440 | 1:50 |
| Mouse anti-Repo | DSHB AB_528448 | 1:50 |

**Table 3. Primary antibodies used for Immunohistochemistry or western blotting.**

| Secondary Antibodies | Source | Dilution |
|---|---|---|
| Goat Anti-Rat 633 | Thermo Fisher A-21094 | 1:200 |
| Goat Anti-Chicken 488 | Thermo Fisher A-11039 | 1:200 |
| Goat Anti-Guinea pig 568 | Thermo Fisher A-11075 | 1:200 |
| Goat Anti-Rabbit 633 | Thermo Fisher A-35562 | 1:200 |
| Goat Anti-Mouse 488 | Thermo Fisher A-10667 | 1:200 |
| Goat Anti-Rat 568 | Thermo Fisher A-11077 | 1:200 |
| Goat Anti Rabbit IgG–Horse radish peroxidase (HRP) | Cell signalling Technologies #7074 | 1:1000 |

**Table 4. Secondary antibodies used for Immunohistochemistry or western blotting.**

| Resource | Source | Identifier |
|---|---|---|
| Click-iT EdU Alexa Fluor 594 Imaging Kit | Invitrogen | Cat# C10339 |

**Table 5. Cell proliferation kit.**

### 4.1.2. *Drosophila* strains

The table below lists the *Drosophila* strains used in this study, including those enabling the generation of lines via genetic recombination or combination mentioned in the Results chapter. For each line, the genotype, source and identification number (identifier) are indicated.

| Strains | Source | Identifier |
|---|---|---|
| D. *melanogaster*: mob4 mutant: y[1] w[*]; Mob4[EYDeltaL3]/CyO | Bloomington *Drosophila* Stock Center (Schulte, *et al.,* 2010) | BDSC: 36331; FlyBase: FBst0036331 |
| D. *melanogaster*: UAS line expressing mob4 RNAi: P{UAS-Mob4.RNAi.JS1}attP2 | Bloomington *Drosophila* Stock Centre (Schulte, *et al.,* 2010) | BDSC:36488; FlyBase: FBst0036488 |
| D. *melanogaster*: UAS line expressing mob4: y[1] v[1]; P{y[+t7.7] v[+t1.8]=UAS-Mob4.S}attP2 | Bloomington *Drosophila* Stock Center (Schulte, *et al.,* 2010) | BDSC: 36329; FlyBase: FBst0036329 |
| D. *melanogaster*: UAS line expressing hMOB4: y[1] v[1]; P{y[+t7.7] v[+t1.8]=UAS-phocein.1}attP2 | Bloomington *Drosophila* Stock Center (Schulte, *et al.,* 2010) | BDSC: 36330; FlyBase: FBst0036330 |
| D. *melanogaster*: UAS line expressing wdb-DN: w[*]; P{w[+mC]=UAS-wdb.95-524.HA}6 | Bloomington *Drosophila* Stock Centre (Hannus, *et al.,* 2002) | BDSC: 55053; FlyBase: FBst0055053 |
| D. *melanogaster*: UAS line expressing wts RNAi: y[1] sc[*] v[1]; P{y[+t7.7] v[+t1.8]=TRiP.GL01331}attP 2 | Bloomington *Drosophila* Stock Center (Ding, *et al.,* 2016) | BDSC: 41899; FlyBase: FBst0041899 |
| D. *melanogaster*: UAS line expressing hpo RNAi: y[1] v[1]; P{y[+t7.7] v[+t1.8]=TRiP.HMS00006}attP2 | Bloomington *Drosophila* Stock Center (Ding, *et al.,* 2016) | BDSC: 33614; FlyBase: FBst0033614 |

| | | |
|---|---|---|
| D. *melanogaster*: Wild type: Oregon-R | Gift from M. Akam (Bossing and Technau, 1994) | FlyBase: FBsn0000276 |
| D. *melanogaster*: UAS line expressing rheb: w[*]; P{w[+mC]=UAS-Rheb.Pa}3 | Gift from R. Sousa-Nunes (Sousa-Nunes, *et al.,* 2011) | BDSC: 9689; FlyBase: FBst0009689 |
| D. *melanogaster*: Gal4 line under the control of grh: Grh-Gal4 | Gift from A.H. Brand (Chell and Brand, 2010) | N/A |
| D. *melanogaster*: UAS line expressing mts-DN-HA: UAS-mts.dn181-HA | Gift from S. Eaton (Hannus, *et al.,* 2002) | N/A |
| D. *melanogaster*: $mts^{XE225839}$ mutant: $mts^{XE2258}$/CyO, P{sevRas1.V12}F1 and $mts^{299}$ mutant. | Gifts from H. Wang (Wang, *et al.,* 2009) | BDSC: 5684; FlyBase: FBst0005684 N/A for $mts^{299}$ |
| D. *melanogaster*: Gal4 line under the control of insc: w[*]; P{w[+mW.hs]=GawB}insc[Mz1407] | Bloomington *Drosophila* Stock Center | BDSC: 8751; FlyBase: FBst0008751 |
| D. *melanogaster*: Gal4 line under the control of repo: w[1118]; P{w[+m*]=GAL4}repo/TM6, tb | Gift from A. Hidalgo | N/A |
| D. *melanogaster*: UAS line expressing CD8-GFP: y[1] w[*]; P{w[+mC]=UAS-mCD8::GFP.L}LL5, P{UAS-mCD8::GFP.L}2 | (Lee and Luo, 1999) | BDSC: 5137; FlyBase: FBst0005137 |
| D. *melanogaster*: UAS line expressing dicer2: UAS-dicer2 | (Ding, *et al.,* 2016) | N/A |

| | | |
|---|---|---|
| D. *melanogaster*: UAS line expressing cka-eGFP: w[*];P{w[+mC]=UASp-Cka.EGFP.C}2 | Bloomington *Drosophila* Stock Center | BDSC: 53756; FlyBase: FBst0053756 |
| D. *melanogaster*: Double Balancer line w[*]; l(2)*[*]/CyO; D[1]/TM6B, Tb[+] | Bloomington *Drosophila* Stock Center | BDSC: 7197; FlyBase: FBst0007197 |
| D. *melanogaster*: Double Balancer line y[1] w[*]; Eps-15[e75]/CyO, P{w[+mC]=GAL4-twi.G}2.2, P{w[+mC]=UAS-2xE-GFP}AH2.2 | Bloomington *Drosophila* Stock Center | BDSC: 24900; FBst0024900 |

**Table 6. *Drosophila* strains.**

## 4.2.METHODS

### 4.2.1. *Drosophila* husbandry

Fly stocks were maintained in vials for long-term storage at 18°C and at 25°C for ongoing experiments, with the exception of RNAi assays that were performed at 29°C. The fly stocks were kept in standard *Drosophila* fly food. Egg collections and larvae rearing were performed on agar juice plates supplemented with yeast paste. Egg lays were collected in either 30 minutes or 1h time-windows.

**Protocol to prepare *Drosophila* food:** 750 ml boiling water, 100 g sugar, 50 g yeast, 80 g organic flour, 2 g Ammonium sulphate, (NH4)S04, 5 g tartaric acid, 1.5 g Potassium phosphate monobasic, KH2P04, 22 g agar soaked into 300 ml grape juice (in two batches of 150 ml), 10 ml propionic acid, 1 g Nipagin, Vials, Cotton plugs.
Dissolve the sugar completely in the boiling water. Add the 50 g of yeast and dissolve completely. Mix the 80 g of organic flour into 200-300 ml of water until a smooth paste is formed and then add it to the boiling water to dissolve. Add 2 g of ammonium sulphate, 5 g tartaric acid and 1.5 g potassium phosphate monobasic to the water and boil for 10 minutes. Slowly add one of the agar/grape juice batches (11 g:150 ml) to

the boiling water. Take the other agar/grape juice batch and microwave it until boiling and slowly add it to the mixture and boil for a further 10 minutes. Let the mixture cool down until it reaches ~70°C. Add 1 g of Nipagin using a scalpel to the mixture. On top of the Nipagin pour 10 ml of propionic acid and allow to mix well. Add approximately 1 inch high of food per vial or bottle.

### Protocol to prepare *Drosophila* egg-lay collection plates:

1 l water, 21 g agar, 200 ml grape juice, plates, 2 l beaker.

Pour 1l of water into a 2 l beaker and microwave until boiling (14 minutes). Set the heater to 270°C and the stirrer to 420 rpm. Place the 2 l beaker onto the heater and wait until the water is boiling. Mix half the 21 g of agar and 100 ml of grape juice in a flask and stir. Add the agar solution to the boiling water. Add the rest of the agar in another 100 ml of grape juice and pour into the mixture. Stir and boil the juice mixture in the 2 l beaker for no longer than 2 minutes. Pour juice mixture into small petri dish plates used for egg-lay collections.

For nutritional deprivation experiments, freshly hatched larvae were transferred to agar plates prepared with amino-acid free media (5% sucrose, 1% agar in phosphate buffered saline, PBS).

Prepare 10x PBS (phosphate buffered saline): dissolve 80 g of NaCl, 2 g of KCl, 26.8 g pf $Na_2HPO_4$-7H2O, 2.4 g $KH_2PO_4$ in 800 ml of ddH2O, adjust the pH to 7.4 with HCl and bring the total volume to 1 litre.

Prepare 1 x PBS: 1:10 dilution of 10xPBS in ddH2O

### 4.2.2. *Drosophila* strains and genetic crosses

Fly stocks were maintained in vials long-term at 18°C and at 25°C for ongoing experiments, with the exception of RNAi assays performed at 29°C. The fly stocks were kept in standard *Drosophila* fly food in vials or bottles. Fly strains needed for experiments were grown in multiple bottles at 25°C to yield maximum female virgin collections. Female virgins were collected every 3 hours (maximum) and stored with the appropriate males at 18°C. The resulting fly cross would be transferred to an egg-lay chamber at 25°C. Egg collections and larvae rearing were performed on agar juice plates supplemented with yeast paste. Embryos were transferred to fresh plates and stored at the appropriate temperature. Embryos with GFP balancers were

selected for, or against, the next day using a fluorescent microscope; the desired embryos transferred to a fresh plate supplemented with yeast.

*Drosophila* strains used in this study are listed in **Table 6.** *Drosophila* stocks obtained from the Bloomington *Drosophila* Stock Center were: *mob4*$^{EY\Delta L3}$ (36331) (Schulte, *et al.,* 2010) rebalanced over *CyO*, P(GAL4-*twi.G*)2.2; *UAS-mob4*$^{RNAi}$ (36488) (Schulte, *et al.,* 2010); *UAS-mob4* (36329) (Schulte, *et al.,* 2010); *UAS-hMOB4* (*Phocein*) (36330) (Schulte, *et al.,* 2010); *UAS-cka-eGFP* (53756); *UAS-wdb-DN* (*UAS-wdb.95-524.HA*; 55053) (Hannus, *et al.,* 2002); *UAS-wts*$^{RNAi}$ (41899) (Ding, *et al.,* 2016) and *UAS-hpo*$^{RNAi}$ (33614) (Ding, *et al.,* 2016). Other stocks used were: Wild-type *Oregon-R* (kind gift from M. Akain); *UAS-rheb* (Blomington 9689) (Sousa-Nunes, *et al.,* 2011) (kind gift from R. Sousa-Nunes); *grh-Gal4* (Chell and Brand, 2010) (kind gift from A.H. Brand); *UAS-mts-DN* (*UAS-mts.dn181-HA*) (Hannus, *et al.,* 2002) (kind gift from S. Eaton); *mts*$^{299}$ and *mts*$^{XE2258}$ (Wang, *et al.,* 2009) (kind gifts from H. Wang). NSC-specific RNAi and overexpression assays were performed using *insc-Gal4* (w$^{1118}$; p{GAWB}*insc*MZ1407). Glial-specific expression assays used *repo-Gal4* (w$^{1118}$; p{GAWB}*repo/TM6*b, iab-lacZ). The *grh-Gal4* driver had been recombined with *UAS-CD8-GFP* (chromosome II) in the laboratory (Gil-Renado *et al.,* 2019). For rescue experiments, *insc-Gal4* and *repo-Gal4* drivers were recombined or combined with the *mob4*$^{EY\Delta L3}$ mutant strain. For other assays, the *insc-Gal4* driver was recombined with *UAS-CD8-GFP* or a strain already combining it with *UAS-dicer2* and *UAS-CD8-GFP* was used (Ding, *et al.,* 2016). Genetic combinations or recombinations, balancing and/or re-balancing of *Drosophila* stocks on the II and or III chromosome, followed standard genetic cross procedures (Greenspan, 2004).

### 4.2.3. Immunohistochemistry and EdU incorporation

Prepare 1xPBST: 1x PBS with 1% Triton X

Prepare fixative solution: 4% formaldehyde in PBS with added EGTA (0.5 M) and MgCL2 (1 M). For 1 ml: 894 µl PBS 1 x + 100 µl formaldehyde + 1 µl EGTA (0.5 M) + 5 µl MGCl2 (1 M). Vortex.

Prepare blocking solution: 10% goat serum in PBS-1% Triton. For 1 ml: 900 µl of 1x PBS-1% Triton + 100 µl 100% Goat serum. Vortex and store at 4C. All chemicals were purchased from SIGMA.

Prior to dissections, larvae were transferred to a silicon dissecting dish in 1xPBS and (if necessary) larvae were checked under the fluorescent microscope. Using a light microscope, larval CNSs were extracted using fine forceps and scissors and fixed for 20 minutes in fixative solution, followed by washes in PBS (2 x 10 min, 3 rinses between washes) and 1 hour block in 1 x PBST (PBS, 1% Triton X-100) with 10% fetal bovine serum, at room temperature on a shaker. Primary antibodies (**Table 3)** were incubated in 1 x PBST overnight or for 2 nights at 4ºC. CNSs were washed in 1xPBST (2 x 5 min, 3 rinses between washes) before incubating with secondary antibodies (**Table 4**) for 2 hours at room temperature. Secondary antibodies were washed off with 1 x PBST (2 x 10 min, 3 rinses between washes) and successively embedded in 50% (>30 mins) and 70% glycerol (>3 hours) before carefully mounting on slides in a 1:1 mix of 70% glycerol and Vectashield (Vector Laboratories) and covered by a coverslip.

EdU incorporation assays were performed as previously described (Sousa-Nunes, *et al.,* 2011). Briefly, CNSs were dissected in PBS and incubated in 10 µm EdU/PBS for 1h at room temperature. CNSs were fixed for 15 minutes in 4% formaldehyde/PBS and incorporated EdU detected using Click-iT EdU Imaging kit following manufacturer instructions (Invitrogen).

### 4.2.4. Image acquisition and processing

Images were obtained on a Leica SP8 confocal laser-scanning microscope using LAS X software. Quantifications were made using z-stacks of 1.5 µm step size, comprising whole-brain lobes, VNCs or CNSs. Representative images shown are single optical sections, with the exception of EdU incorporations **(Fig 2.4),** which are z-projection stacks encompassing whole CNSs. Images were processed in Fiji v2.0 or Adobe Photoshop CS6 and assembled in Adobe Illustrator CS6. NSC sizes (maximum diameters) (Chell and Brand, 2010), pH3 scorings, and Mob4 signal intensities (pixel intensity/ NSC maximum area) and EdU voxel quantification were performed using Fiji v2.0.

### 4.2.5. Western blotting

Whole larval brain were harvested and lysed in lysis buffer (1% Triton) supplemented with protease inhibitor (Complete, EDTA-free; Sigma) and phosphatase inhibitors (cocktails B+C; Santa Cruz Biotechnology). CNS extracts were spun at 14000 rpm for

30 minutes at 4ºC and proteins quantified (BCA protein assay, Pierce). Detection of proteins was performed using standard sodium dodecyl sulfate (SDS) polyacrylamide gel electrophoresis (SDS-PAGE) and western blotting using ECL or ECL Plus chemiluminescent substrate (Pierce) with the following specifications. CNS lysates were run on a 10% polyacrylamide gel at 120 V and transferred onto a nitrocellulose membrane, before blocking with 5% BSA (p-AKT), 3% BSA (β-Actin and AKT), in 0.1% TBS- Tween and incubated with the primary antibody overnight at 4°C under rotation.

### 4.2.6. Data quantification and statistical analysis

Statistics were performed using SigmaPlot Version 12.5 (Systat software): Shapiro-Wilk and equal variance tests used to evaluate normality; Student´s *t*-test applied when data fitted a normal distribution; Wilcoxon rank-sum test used for non-parametric data; $p<0.05$ considered significant. Data from *Drosophila in vivo* assays were obtained from a minimum of two biological replica sets; sample numbers are indicated in figure legends. Histograms show mean ± standard error of the mean. Box plots represent $25^{th}$ and $75^{th}$ percentiles, and black line indicates median, dashed line specifies mean, whiskers indicate $10^{th}$ and $90^{th}$ percentiles.

## BIBLIOGRAPHY


Abdissa, D. (2020) 'Review Article on adult neurogenesis in humans', *Translational Research in Anatomy*. Elsevier GmbH., p. 100074. doi: 10.1016/j.tria.2020.100074.

Ables, J. L. *et al.* (2011) 'Not(ch) just development: Notch signalling in the adult brain.', *Nature reviews. Neuroscience*, 12(5), pp. 269–83. doi: 10.1038/nrn3024.

Akam, M. (1987) 'The molecular basis for metameric pattern in the *Drosophila* embryo', *Development*.

Ali, F. R. *et al.* (2014) 'The phosphorylation status of Ascl1 is a key determinant of neuronal differentiation and maturation in vivo and in vitro'. doi: 10.1242/dev.106377.

Altman, J. (1962) 'Are new neurons formed in the brains of adult mammals?', *Science*, 135(3509), pp. 1127–1128. doi: 10.1126/science.135.3509.1127.

Altman, J. (1963) 'Autoradiographic investigation of cell proliferation in the brains of rats and cats', *The Anatomical Record*, 145(4), pp. 573–591. doi: 10.1002/ar.1091450409.

Altman, J. (1969) 'Autoradiographic and histological studies of postnatal neurogenesis.', *Journal of Comparative Neurology*, 137(4), pp. 433–457.

Alvarez-Buylla, A., García-Verdugo, J. M. and Tramontin, A. D. (2001) 'A unified hypothesis on the lineage of neural stem cells.', *Nature reviews. Neuroscience*, 2(4), pp. 287–93. doi: 10.1038/35067582.

Alvarez, E. O. *et al.* (2009) 'Cognitive dysfunction and hippocampal changes in experimental type 1 diabetes', *Behavioural Brain Research*. doi: 10.1016/j.bbr.2008.11.001.

Álvarez, J. A. and Díaz-Benjumea, F. J. (2018) 'Origin and specification of type II neuroblasts in the *Drosophila* embryo', *Development (Cambridge)*. Company of Biologists Ltd, 145(7). doi: 10.1242/dev.158394.

An, H. *et al.* (2017) 'Inscuteable maintains type I neuroblast lineage identity via Numb/Notch signaling in the *Drosophila* larval brain', *Journal of Genetics and Genomics*. doi: 10.1016/j.jgg.2017.02.005.

Anacker, C. (2014) 'Adult hippocampal neurogenesis in depression: behavioral

implications and regulation by the stress system.', *Current topics in behavioral neurosciences*, 18, pp. 25–43. doi: 10.1007/7854_2014_275.

Anacker, C. and Hen, R. (2017) 'Adult hippocampal neurogenesis and cognitive flexibility-linking memory and mood', *Nature Reviews Neuroscience*. Nature Publishing Group, pp. 335–346. doi: 10.1038/nrn.2017.45.

Andreazza, S. *et al.* (2015) 'Daytime CLOCK Dephosphorylation Is Controlled by STRIPAK Complexes in *Drosophila*', *Cell Reports*, 11(8), pp. 1266–1279. doi: 10.1016/j.celrep.2015.04.033.

Andreu, Z. *et al.* (2015) 'The cyclin-dependent kinase inhibitor p27 kip1 regulates radial stem cell quiescence and neurogenesis in the adult hippocampus.', *Stem Cells*. Wiley-Blackwell, 33(1), pp. 219–29. doi: 10.1002/stem.1832.

Anthony, T. E. *et al.* (2004) 'Radial glia serve as neuronal progenitors in all regions of the central nervous system', *Neuron*, 41(6), pp. 881–890. doi: 10.1016/S0896-6273(04)00140-0.

Apple, D. M., Fonseca, R. S. and Kokovay, E. (2017) 'The role of adult neurogenesis in psychiatric and cognitive disorders', *Brain Research*. Elsevier B.V., pp. 270–276. doi: 10.1016/j.brainres.2016.01.023.

Arsenijevic, Y. *et al.* (2001) 'Isolation of multipotent neural precursors residing in the cortex of the adult human brain', *Experimental Neurology*. doi: 10.1006/exnr.2001.7691.

Arvidsson, A. *et al.* (2002) 'Neuronal replacement from endogenous precursors in the adult brain after stroke', *Nature Medicine*, 8(9), pp. 963–970. doi: 10.1038/nm747.

Arya, R. *et al.* (2015) 'Neural stem cell progeny regulate stem cell death in a Notch and Hox dependent manner', *Cell Death and Differentiation*. doi: 10.1038/cdd.2014.235.

Ashraf, S. I. and Ip, Y. T. (2001) 'The Snail protein family regulates neuroblast expression of inscuteable and string, genes involved in asymmetry and cell division in *Drosophila*', *Development*.

Bae, S. J. *et al.* (2017) 'SAV1 promotes Hippo kinase activation through antagonizing the PP2A phosphatase STRIPAK', *eLife*, 6, pp. 1–28. doi: 10.7554/eLife.30278.

Bahrampour, S., Jonsson, C. and Thor, S. (2019) ‘Brain expansion promoted by polycomb-mediated anterior enhancement of a neural stem cell proliferation program’, *PLoS Biology*, 17(2), pp. 1–22. doi: 10.1371/journal.pbio.3000163.

Baker, E. W., Kinder, H. A. and West, F. D. (2019) ‘Neural stem cell therapy for stroke: A multimechanistic approach to restoring neurological function’, *Brain and Behavior*. John Wiley and Sons Ltd. doi: 10.1002/brb3.1214.

Ballas, N. *et al.* (2005) ‘REST and Its Corepressors Mediate Plasticity of Neuronal Gene Chromatin throughout Neurogenesis The State University of New York at Stony Brook’, *Cell*, 121(4), pp. 645–657. doi: 10.1016/j.cell.2005.03.013.

Barrett, A. L., Krueger, S. and Datta, S. (2008) ‘Branchless and Hedgehog operate in a positive feedback loop to regulate the initiation of neuroblast division in the *Drosophila* larval brain’, *Developmental Biology*. doi: 10.1016/j.ydbio.2008.02.025.

Barry, E. R. *et al.* (2013) ‘Restriction of intestinal stem cell expansion and the regenerative response by YAP’, *Nature*. doi: 10.1038/nature11693.

Basak, O. *et al.* (2012) ‘Neurogenic subventricular zone stem/progenitor cells are Notch1-dependent in their active but not quiescent state’, *Journal of Neuroscience*, 32(16), pp. 5654–5666. doi: 10.1523/JNEUROSCI.0455-12.2012.

Basak, O. *et al.* (2018) ‘Troy+ brain stem cells cycle through quiescence and regulate their number by sensing niche occupancy’, *Proceedings of the National Academy of Sciences of the United States of America*. National Academy of Sciences, 115(4), pp. E610–E619. doi: 10.1073/pnas.1715911114.

Baumgardt, M. *et al.* (2009) ‘Neuronal Subtype Specification within a Lineage by Opposing Temporal Feed-Forward Loops’, *Cell*. doi: 10.1016/j.cell.2009.10.032.

Baumgardt, M. *et al.* (2014) ‘Global Programmed Switch in Neural Daughter Cell Proliferation Mode Triggered by a Temporal Gene Cascade’, *Developmental Cell*. doi: 10.1016/j.devcel.2014.06.021.

Bayraktar, O. A. *et al.* (2010) ‘*Drosophila* type II neuroblast lineages keep Prospero levels low to generate large clones that contribute to the adult brain central complex’, *Neural Development*. doi: 10.1186/1749-8104-5-26.

Beckervordersandforth, R. *et al.* (2010) ‘In vivo fate mapping and expression analysis

reveals molecular hallmarks of prospectively isolated adult neural stem cells', *Cell Stem Cell*. doi: 10.1016/j.stem.2010.11.017.

Beckervordersandforth, R. *et al.* (2017) 'Role of Mitochondrial Metabolism in the Control of Early Lineage Progression and Aging Phenotypes in Adult Hippocampal Neurogenesis', *Neuron*. doi: 10.1016/j.neuron.2016.12.017.

Bello, B. C. *et al.* (2008) 'Amplification of neural stem cell proliferation by intermediate progenitor cells in *Drosophila* brain development', *Neural Development*. doi: 10.1186/1749-8104-3-5.

Bello, B. C., Hirth, F. and Gould, A. P. (2003) 'A pulse of the *Drosophila* Hox protein Abdominal-A schedules the end of neural proliferation via neuroblast apoptosis', *Neuron*. doi: 10.1016/S0896-6273(02)01181-9.

Bello, B., Reichert, H. and Hirth, F. (2006) 'The brain tumor gene negatively regulates neural progenitor cell proliferation in the larval central brain of *Drosophila*', *Development*. doi: 10.1242/dev.02429.

Berg, D. A. *et al.* (2019) 'A Common Embryonic Origin of Stem Cells Drives Developmental and Adult Neurogenesis', *Cell*. doi: 10.1016/j.cell.2019.02.010.

Bergmann, O. *et al.* (2012) 'The age of olfactory bulb neurons in humans.', *Neuron*, 74(4), pp. 634–9. doi: 10.1016/j.neuron.2012.03.030.

Bertet, C. *et al.* (2014) 'Temporal patterning of neuroblasts controls notch-mediated cell survival through regulation of hid or reaper', *Cell*. doi: 10.1016/j.cell.2014.07.045.

Bertrand, N., Castro, D. S. and Guillemot, F. (2002) 'Proneural genes and the specification of neural cell types', *Nature reviews. Neuroscience*, 3(7), pp. 517–30. doi: 10.1038/nrn874.

Betschinger, J., Mechtler, K. and Knoblich, J. A. (2006) 'Asymmetric Segregation of the Tumor Suppressor Brat Regulates Self-Renewal in *Drosophila* Neural Stem Cells', *Cell*. doi: 10.1016/j.cell.2006.01.038.

Birkholz, O. *et al.* (2015) 'Bridging the gap between postembryonic cell lineages and identified embryonic neuroblasts in the ventral nerve cord of *Drosophila melanogaster*', *Biology Open*, 4(4), pp. 420–434. doi: 10.1242/bio.201411072.

Blau, H. M., Brazelton, T. R. and Weimann, J. M. (2001) 'The evolving concept of a

stem cell: Entity or function?', *Cell*. Cell Press, pp. 829–841. doi: 10.1016/S0092-8674(01)00409-3.

Bloemendal, S. *et al.* (2012) 'A homologue of the human STRIPAK complex controls sexual development in fungi', *Molecular Microbiology*. doi: 10.1111/j.1365-2958.2012.08024.x.

Bolborea, M. and Dale, N. (2013) 'Hypothalamic tanycytes: potential roles in the control of feeding and energy balance.', *Trends in neurosciences*, 36(2), pp. 91–100. doi: 10.1016/j.tins.2012.12.008.

Bonaguidi, M. A. *et al.* (2008) 'Noggin expands neural stem cells in the adult hippocampus', *Journal of Neuroscience*, 28(37), pp. 9194–9204. doi: 10.1523/JNEUROSCI.3314-07.2008.

Bonaguidi, M. A. *et al.* (2011) 'In vivo clonal analysis reveals self-renewing and multipotent adult neural stem cell characteristics.', *Cell*, 145(7), pp. 1142–55. doi: 10.1016/j.cell.2011.05.024.

Bond, A. M., Bhalala, O. G. and Kessler, J. A. (2012) 'The dynamic role of bone morphogenetic proteins in neural stem cell fate and maturation', *Developmental Neurobiology*, 72(7), pp. 1068–1084. doi: 10.1002/dneu.22022.

Bond, A. M., Ming, G. L. and Song, H. (2015) 'Adult Mammalian Neural Stem Cells and Neurogenesis: Five Decades Later', *Cell Stem Cell*. Cell Press, pp. 385–395. doi: 10.1016/j.stem.2015.09.003.

Boone, J. Q. and Doe, C. Q. (2008) 'Identification of *Drosophila* type II neuroblast lineages containing transit amplifying ganglion mother cells', *Developmental Neurobiology*. doi: 10.1002/dneu.20648.

Bose, A., Majot, A. T. and Bidwai, A. P. (2014) 'The Ser/Thr phosphatase PP2A regulatory subunit widerborst inhibits notch signaling', *PLoS ONE*. doi: 10.1371/journal.pone.0101884.

Bossing, T. *et al.* (2012) 'Disruption of Microtubule Integrity Initiates Mitosis during CNS Repair', *Developmental Cell*. doi: 10.1016/j.devcel.2012.06.002.

Bowman, S. K. *et al.* (2008) 'The Tumor Suppressors Brat and Numb Regulate Transit-Amplifying Neuroblast Lineages in *Drosophila*', *Developmental Cell*. doi:

10.1016/j.devcel.2008.03.004.

Bracko, O. *et al.* (2012) ‘Gene expression profiling of neural stem cells and their neuronal progeny reveals IGF2 as a regulator of adult hippocampal neurogenesis’, *Journal of Neuroscience*. doi: 10.1523/JNEUROSCI.4248-11.2012.

Bragado Alonso, S. *et al.* (2019) ‘An increase in neural stem cells and olfactory bulb adult neurogenesis improves discrimination of highly similar odorants’, *The EMBO Journal*. EMBO, 38(6), p. e98791. doi: 10.15252/embj.201798791.

Brand, A. H. and Perrimon, N. (1993) ‘Targeted gene expression as a means of altering cell fates and generating dominant phenotypes’, *Development*.

Brandhorst, S. *et al.* (2015) ‘A Periodic Diet that Mimics Fasting Promotes Multi-System Regeneration, Enhanced Cognitive Performance, and Healthspan’, *Cell Metabolism*. doi: 10.1016/j.cmet.2015.05.012.

Brennecke, J. *et al.* (2003) ‘bantam encodes a developmentally regulated microRNA that controls cell proliferation and regulates the proapoptotic gene hid in *Drosophila*’, *Cell*. doi: 10.1016/S0092-8674(03)00231-9.

Britton, J. S. and Edgar, B. a (1998) ‘Environmental control of the cell cycle in *Drosophila*: nutrition activates mitotic and endoreplicative cells by distinct mechanisms.’, *Development (Cambridge, England)*, 125(11), pp. 2149–2158. Available at: http://dev.biologists.org/content/develop/125/11/2149.full.pdf.

Callan, M. A. *et al.* (2010) ‘Fragile X protein controls neural stem cell proliferation in the *Drosophila* brain’, *Human Molecular Genetics*, 19(15), pp. 3068–3079. doi: 10.1093/hmg/ddq213.

Callan, M. A. *et al.* (2012) ‘Fragile X Protein is required for inhibition of insulin signaling and regulates glial-dependent neuroblast reactivation in the developing brain’, *Brain Research*. Elsevier B.V., 1462, pp. 151–161. doi: 10.1016/j.brainres.2012.03.042.

Callan, M. A. and Zarnescu, D. C. (2011) ‘Heads-up: New roles for the fragile X mental retardation protein in neural stem and progenitor cells’, *Genesis*, 49(6), pp. 424–440. doi: 10.1002/dvg.20745.

Cameron, H. A. and Mckay, R. D. G. (2001) ‘Adult neurogenesis produces a large

pool of new granule cells in the dentate gyrus', *Journal of Comparative Neurology*, 435(4), pp. 406–417. doi: 10.1002/cne.1040.

Castets, F. *et al.* (2000) 'Zinedin, SG2NA, and striatin are calmodulin-binding, WD repeat proteins principally expressed in the brain', *Journal of Biological Chemistry*. doi: 10.1074/jbc.M909782199.

Castro, D. S. *et al.* (2011) 'A novel function of the proneural factor Ascl1 in progenitor proliferation identified by genome-wide characterization of its targets', *Genes and Development*, 25(9), pp. 930–945. doi: 10.1101/gad.627811.

Cavallucci, V., Fidaleo, M. and Pani, G. (2016) 'Neural Stem Cells and Nutrients: Poised Between Quiescence and Exhaustion', *Trends in Endocrinology and Metabolism*. Elsevier Ltd, 27(11), pp. 756–769. doi: 10.1016/j.tem.2016.06.007.

Caygill, E. E. and Brand, A. H. (2016) 'The GAL4 system: A versatile system for the manipulation and analysis of gene expression', in *Methods in Molecular Biology*. doi: 10.1007/978-1-4939-6371-3_2.

Cenci, C. and Gould, A. P. (2005) '*Drosophila* Grainyhead specifies late programmes of neural proliferation by regulating the mitotic activity and Hox-dependent apoptosis of neuroblasts', *Development*. doi: 10.1242/dev.01932.

Chabu, C. and Doe, C. Q. (2009) 'Twins/PP2A regulates aPKC to control neuroblast cell polarity and self-renewal', *Developmental Biology*. Elsevier Inc., 330(2), pp. 399–405. doi: 10.1016/j.ydbio.2009.04.014.

Chaker, Z., Codega, P. and Doetsch, F. (2016) 'A mosaic world: puzzles revealed by adult neural stem cell heterogeneity.', *Wiley interdisciplinary reviews. Developmental biology*, 5(6), pp. 640–658. doi: 10.1002/wdev.248.

Chang, E. H. *et al.* (2016) 'Traumatic brain injury activation of the adult subventricular zone neurogenic niche', *Frontiers in Neuroscience*. Frontiers Media S.A. doi: 10.3389/fnins.2016.00332.

Chell, J. M. and Brand, A. H. (2010) 'Nutrition-responsive glia control exit of neural stem cells from quiescence', *Cell*. Elsevier Inc., 143(7), pp. 1161–1173. doi: 10.1016/j.cell.2010.12.007.

Chen, D. *et al.* (2008) 'Tissue-specific regulation of SIRT1 by calorie restriction',

*Genes and Development*. doi: 10.1101/gad.1650608.

Chen, H.-W. *et al.* (2002) 'CKA, a Novel Multidomain Protein, Regulates the JUN N-Terminal Kinase Signal Transduction Pathway in *Drosophila*', *Molecular and Cellular Biology*. doi: 10.1128/mcb.22.6.1792-1803.2002.

Cheung, T. H. and Rando, T. A. (2013) 'Molecular regulation of stem cell quiescence', *Nature Reviews Molecular Cell Biology*, pp. 329–340. doi: 10.1038/nrm3591.

Chintapalli, V. R., Wang, J. and Dow, J. A. T. (2007) 'Using FlyAtlas to identify better *Drosophila melanogaster* models of human disease', *Nature Genetics*. doi: 10.1038/ng2049.

Cho, I. J. *et al.* (2019) 'Mechanisms, Hallmarks, and Implications of Stem Cell Quiescence', *Stem Cell Reports*. ElsevierCompany., 12(6), pp. 1190–1200. doi: 10.1016/j.stemcr.2019.05.012.

Choksi, S. P. *et al.* (2006) 'Prospero Acts as a Binary Switch between Self-Renewal and Differentiation in *Drosophila* Neural Stem Cells', *Developmental Cell*. doi: 10.1016/j.devcel.2006.09.015.

Chou, C.-H., Fan, H.-C. and Hueng, D.-Y. (2015) 'Potential of Neural Stem Cell-Based Therapy for Parkinson's Disease'. doi: 10.1155/2015/571475.

Christian, K. M., Song, H. and Ming, G. (2014) 'Functions and Dysfunctions of Adult Hippocampal Neurogenesis', *Annual Review of Neuroscience*. Annual Reviews, 37(1), pp. 243–262. doi: 10.1146/annurev-neuro-071013-014134.

Clark, A. R. and Ohlmeyer, M. (2019) 'Protein phosphatase 2A as a therapeutic target in inflammation and neurodegeneration', *Pharmacology and Therapeutics*. doi: 10.1016/j.pharmthera.2019.05.016.

Clelland, C. D. *et al.* (2009) 'A functional role for adult hippocampal neurogenesis in spatial pattern separation', *Science*, 325(5937), pp. 210–213. doi: 10.1126/science.1173215.

Codega, P. *et al.* (2014) 'Prospective Identification and Purification of Quiescent Adult Neural Stem Cells from Their In Vivo Niche', *Neuron*. Cell Press, 82(3), pp. 545–559. doi: 10.1016/j.neuron.2014.02.039.

Cohen, D. E. et al. (2009) ‘Neuronal SIRT1 regulates endocrine and behavioral responses to calorie restriction’, Genes and Development. doi: 10.1101/gad.1839209.

Cohen, H. Y. *et al.* (2004) ‘Calorie restriction promotes mammalian cell survival by inducing the SIRT1 deacetylase’, *Science*. doi: 10.1126/science.1099196.

Colombani, J. *et al.* (2003) ‘A nutrient sensor mechanism controls *Drosophila* growth’, *Cell*, 114(6), pp. 739–749. doi: 10.1016/S0092-8674(03)00713-X.

Costa, M. R. *et al.* (2011) ‘Continuous live imaging of adult neural stem cell division and lineage progression in vitro’, *Development*, 138(6), pp. 1057–1068. doi: 10.1242/dev.061663.

Couzens, A. L. *et al.* (2013) ‘Protein interaction network of the mammalian hippo pathway reveals mechanisms of kinase-phosphatase interactions’, *Science Signaling*. doi: 10.1126/scisignal.2004712.

Curt, J. R., Yaghmaeian Salmani, B. and Thor, S. (2019) ‘Anterior CNS expansion driven by brain transcription factors’, *eLife*, 8, pp. 1–26. doi: 10.7554/elife.45274.

Curtis, M. A. *et al.* (2007a) ‘Human neuroblasts migrate to the olfactory bulb via a lateral ventricular extension.’, *Science (New York, N.Y.)*, 315(5816), pp. 1243–9. doi: 10.1126/science.1136281.

Curtis, M. A., Faull, R. L. M. and Eriksson, P. S. (2007b) ‘The effect of neurodegenerative diseases on the subventricular zone’, *Nature Reviews Neuroscience*, pp. 712–723. doi: 10.1038/nrn2216.

Datta, Sumana (1995) ‘Control of proliferation activation in quiescent neuroblasts of the *Drosophila* central nervous system.’, *Development (Cambridge, England)*, 121(4), pp. 1173–1182.

Datta, S. (1999) ‘Activation of neuroblast proliferation in explant culture of the *Drosophila* larval CNS’, *Brain Research*. doi: 10.1016/S0006-8993(98)01292-X.

Daynac, M. *et al.* (2015) ‘Cell sorting of neural stem and progenitor cells from the adult mouse subventricular zone and live-imaging of their cell cycle dynamics’, *Journal of Visualized Experiments*. doi: 10.3791/53247.

Delgado, A. C. *et al.* (2014) ‘Endothelial NT-3 delivered by vasculature and CSF

promotes quiescence of subependymal neural stem cells through nitric oxide induction.', *Neuron*, 83(3), pp. 572–85. doi: 10.1016/j.neuron.2014.06.015.

Deng, W. *et al.* (2009) 'Adult-born hippocampal dentate granule cells undergoing maturation modulate learning and memory in the brain', *Journal of Neuroscience*. doi: 10.1523/JNEUROSCI.3362-09.2009.

Ding, R. *et al.* (2016) 'The Hippo signalling pathway maintains quiescence in *Drosophila* neural stem cells', *Nature Communications*. Nature Publishing Group, 7, pp. 1–12. doi: 10.1038/ncomms10510.

Ding, W. Y., Huang, J. and Wang, H. (2020) 'Waking up quiescent neural stem cells: Molecular mechanisms and implications in neurodevelopmental disorders', *PLoS Genetics*. Public Library of Science, p. e1008653. doi: 10.1371/journal.pgen.1008653.

Doe, C. Q. *et al.* (1991) 'The prospero gene specifies cell fates in the *Drosophila* central nervous system', *Cell*. doi: 10.1016/0092-8674(91)90463-9.

Doe, C. Q. (1992) 'Molecular markers for identified neuroblasts and ganglion mother cells in the *Drosophila* central nervous system', *Development*.

Doe, C. Q. (2008) 'Neural stem cells: Balancing self-renewal with differentiation', *Development*. doi: 10.1242/dev.014977.

Doe, C. Q. (2017) 'Temporal Patterning in the *Drosophila* CNS', *Annual Review of Cell and Developmental Biology Annu. Rev. Cell Dev. Biol*, 33, pp. 219–40. doi: 10.1146/annurev-cellbio-111315.

Doetsch, F. *et al.* (1999) 'Subventricular zone astrocytes are neural stem cells in the adult mammalian brain', *Cell*. Cell Press, 97(6), pp. 703–716. doi: 10.1016/S0092-8674(00)80783-7.

Doetsch, F. (2019) 'Release of stem cells from quiescence reveals multiple gliogenic domains in the adult brain', pp. 1–19.

Dubrovsky, J. G. and Ivanov, V. B. (2003) 'Celebrating 50 years of the cell cycle [1]', *Nature*. Macmillan Magazines Ltd, p. 759. doi: 10.1038/426759a.

Duffy, J. B. (2002) 'GAL4 system in *Drosophila*: A fly geneticist's Swiss army knife', *Genesis*. doi: 10.1002/gene.10150.

Dulken, B. W. *et al.* (2017) 'Single-Cell Transcriptomic Analysis Defines Heterogeneity and Transcriptional Dynamics in the Adult Neural Stem Cell Lineage', *Cell Reports*. Elsevier B.V., 18(3), pp. 777–790. doi: 10.1016/j.celrep.2016.12.060.

Dyer, M. A. (2003) 'Regulation of proliferation, cell fate specification and differentiation by the homeodomain proteins Prox1, Six3, and Chx10 in the developing retina.', *Cell cycle (Georgetown, Tex.)*. doi: 10.4161/cc.2.4.429.

Ebens, A. J. *et al.* (1993) 'The *Drosophila* anachronism locus: A glycoprotein secreted by glia inhibits neuroblast proliferation', *Cell*. doi: 10.1016/0092-8674(93)90291-W.

Egger, B. *et al.* (2007) 'Regulation of spindle orientation and neural stem cell fate in the *Drosophila* optic lobe', *Neural Development*. doi: 10.1186/1749-8104-2-1.

Ehm, O. *et al.* (2010) 'RBPJκ-dependent signaling is essential for long-term maintenance of neural stem cells in the adult hippocampus', *Journal of Neuroscience*, 30(41), pp. 13794–13807. doi: 10.1523/JNEUROSCI.1567-10.2010.

Eichenbaum, H. (2004) 'Hippocampus: Cognitive processes and neural representations that underlie declarative memory', *Neuron*, pp. 109–120. doi: 10.1016/j.neuron.2004.08.028.

Eichhorn, P. J. A., Creyghton, M. P. and Bernards, R. (2009) 'Protein phosphatase 2A regulatory subunits and cancer', *Biochimica et Biophysica Acta - Reviews on Cancer*. doi: 10.1016/j.bbcan.2008.05.005.

Elliott, D. A. and Brand, A. H. (2008) 'The GAL4 system : a versatile system for the expression of genes.', *Methods in molecular biology (Clifton, N.J.)*. doi: 10.1007/978-1-59745-583-1_5.

Elmi, M. *et al.* (2010) 'TLX activates MASH1 for induction of neuronal lineage commitment of adult hippocampal neuroprogenitors', *Molecular and Cellular Neuroscience*, 45(2), pp. 121–131. doi: 10.1016/j.mcn.2010.06.003.

Encinas, J. M. *et al.* (2011) 'Division-coupled astrocytic differentiation and age-related depletion of neural stem cells in the adult hippocampus', *Cell Stem Cell*, 8(5), pp. 566–579. doi: 10.1016/j.stem.2011.03.010.

Engler, A. *et al.* (2018) 'Notch2 Signaling Maintains NSC Quiescence in the Murine

Ventricular-Subventricular Zone', *Cell Reports*. doi: 10.1016/j.celrep.2017.12.094.

Eriksson, P. S. *et al.* (1998) 'Neurogenesis in the adult human hippocampus', *Nature Medicine*, 4(11), pp. 1313–1317. doi: 10.1038/3305.

Ernst, A. *et al.* (2014) 'Neurogenesis in the striatum of the adult human brain', *Cell*, 156(5), pp. 1072–1083. doi: 10.1016/j.cell.2014.01.044.

Fabian, M. R., Sonenberg, N. and Filipowicz, W. (2010) 'Regulation of mRNA Translation and Stability by microRNAs', *Annual Review of Biochemistry*. doi: 10.1146/annurev-biochem-060308-103103.

Faigle, R. and Song, H. (2013) 'Signaling mechanisms regulating adult neural stem cells and neurogenesis', *Biochimica et Biophysica Acta (BBA)-General Subjects*, 1830(2), pp. 2435–2448. doi: 10.1016/j.bbagen.2012.09.002.Signaling.

Faiz, M. *et al.* (2015) 'Adult Neural Stem Cells from the Subventricular Zone Give Rise to Reactive Astrocytes in the Cortex after Stroke', *Cell stem cell*. Cell Press, 17(5), pp. 624–634. doi: 10.1016/j.stem.2015.08.002.

Fernando, R. N. *et al.* (2011) 'Cell cycle restriction by histone H2AX limits proliferation of adult neural stem cells', *Proceedings of the National Academy of Sciences of the United States of America*. National Academy of Sciences, 108(14), pp. 5837–5842. doi: 10.1073/pnas.1014993108.

Fischer, P. *et al.* (2015) 'Cyclin G Functions as a Positive Regulator of Growth and Metabolism in *Drosophila*', *PLoS Genetics*, 11(8), pp. 1–23. doi: 10.1371/journal.pgen.1005440.

Fischer, P., Preiss, A. and Nagel, A. C. (2016) 'A triangular connection between Cyclin G, PP2A and Akt1 in the regulation of growth and metabolism in *Drosophila*', *Fly*, 10(1), pp. 11–18. doi: 10.1080/19336934.2016.1162362.

Foskolou, I. P. *et al.* (2013) 'Prox1 suppresses the proliferation of neuroblastoma cells via a dual action in p27-Kip1 and Cdc25A', *Oncogene*. doi: 10.1038/onc.2012.129.

Fouad, G. I. (2019) 'Stem cells as a promising therapeutic approach for Alzheimer's disease: a review', *Bulletin of the National Research Centre*. Springer Science and Business Media LLC, 43(1), pp. 1–20. doi: 10.1186/s42269-019-0078-x.

Frost, A. *et al.* (2012) ‘Functional repurposing revealed by comparing S. pombe and S. cerevisiae genetic interactions’, *Cell*. doi: 10.1016/j.cell.2012.04.028.

Fuentealba, L. C. *et al.* (2015) ‘Embryonic Origin of Postnatal Neural Stem Cells’, *Cell*. doi: 10.1016/j.cell.2015.05.041.

Fuentealba, L. C., Obernier, K. and Alvarez-Buylla, A. (2012) ‘Adult neural stem cells bridge their niche’, *Cell Stem Cell*, pp. 698–708. doi: 10.1016/j.stem.2012.05.012.

Funakoshi, M. *et al.* (2011) ‘A gain-of-function screen identifies wdb and lkb1 as lifespan-extending genes in *Drosophila*’, *Biochemical and Biophysical Research Communications*. Elsevier Inc., 405(4), pp. 667–672. doi: 10.1016/j.bbrc.2011.01.090.

Furutachi, S. *et al.* (2013) ‘p57 controls adult neural stem cell quiescence and modulates the pace of lifelong neurogenesis.’, *The EMBO journal*, 32(7), pp. 970–81. doi: 10.1038/emboj.2013.50.

Furutachi, S. *et al.* (2015) ‘Slowly dividing neural progenitors are an embryonic origin of adult neural stem cells’, *Nature Neuroscience*. doi: 10.1038/nn.3989.

Gao, Z. *et al.* (2011) ‘The master negative regulator REST/NRSF controls adult neurogenesis by restraining the neurogenic program in quiescent stem cells’, *Journal of Neuroscience*, 31(26), pp. 9772–9786. doi: 10.1523/JNEUROSCI.1604-11.2011.

Gao, Z., Ding, P. and Hsieh, J. (2012) ‘Profiling of REST-dependent microrna reveals dynamic modes of expression’, *Frontiers in Neuroscience*, (MAY). doi: 10.3389/fnins.2012.00067.

Garcia-Estrada, J., Garcia-Segura, L. M. and Torres-Aleman, I. (1992) ‘Expression of insulin-like growth factor I by astrocytes in response to injury’, *Brain Research*. doi: 10.1016/0006-8993(92)91695-B.

Géminard, C., Rulifson, E. J. and Léopold, P. (2009) ‘Remote Control of Insulin Secretion by Fat Cells in *Drosophila*’, *Cell Metabolism*. doi: 10.1016/j.cmet.2009.08.002.

Gengatharan, A., Bammann, R. R. and Saghatelyan, A. (2016) ‘The role of astrocytes in the generation, migration, and integration of new neurons in the adult olfactory bulb’, *Frontiers in Neuroscience*. doi: 10.3389/fnins.2016.00149.

Giachino, C. *et al.* (2014) ‘Molecular diversity subdivides the adult forebrain neural stem cell population.’, *Stem cells (Dayton, Ohio)*, 32(1), pp. 70–84. doi: 10.1002/stem.1520.

Gil-Ranedo, J. *et al.* (2019) ‘STRIPAK Members Orchestrate Hippo and Insulin Receptor Signaling to Promote Neural Stem Cell Reactivation’, *Cell Reports*. ElsevierCompany., 27(10), pp. 2921-2933.e5. doi: 10.1016/j.celrep.2019.05.023.

Glatter, T. *et al.* (2009) ‘An integrated workflow for charting the human interaction proteome: Insights into the PP2A system’, *Molecular Systems Biology*. doi: 10.1038/msb.2008.75.

Gobeske, K. T. *et al.* (2009) ‘BMP signaling mediates effects of exercise on hippocampal neurogenesis and cognition in mice.’, *PloS one*, 4(10), p. e7506. doi: 10.1371/journal.pone.0007506.

Goldman, S. A. and Chen, Z. (2011) ‘Perivascular instruction of cell genesis and fate in the adult brain’, *Nature Neuroscience*. doi: 10.1038/nn.2963.

Göritz, C. and Frisén, J. (2012) ‘Neural stem cells and neurogenesis in the adult’, *Cell stem cell*, 10(6), pp. 657–659. doi: 10.1016/j.stem.2012.04.005.

Goudreault, M. *et al.* (2009) ‘A PP2A phosphatase high density interaction network identifies a novel striatin-interacting phosphatase and kinase complex linked to the cerebral cavernous malformation 3 (CCM3) protein’, *Molecular and Cellular Proteomics*. doi: 10.1074/mcp.M800266-MCP200.

Gould, E., Reeves, A. J., *et al.* (1999a) ‘Hippocampal neurogenesis in adult Old World primates’, *Proceedings of the National Academy of Sciences of the United States of America*, 96(9), pp. 5263–5267. doi: 10.1073/pnas.96.9.5263.

Gould, E., Beylin, A., *et al.* (1999b) ‘Learning enhances adult neurogenesis in the hippocampal formation’, *Nature Neuroscience*, 2(3), pp. 260–265. doi: 10.1038/6365.

Gould, E. and Tanapat, P. (1999) ‘Stress and hippocampal neurogenesis’, in *Biological Psychiatry*, pp. 1472–1479. doi: 10.1016/S0006-3223(99)00247-4.

Grech, G. *et al.* (2016) ‘Deregulation of the protein phosphatase 2A, PP2A in cancer: complexity and therapeutic options’, *Tumor Biology*. doi: 10.1007/s13277-016-5145-4.

Guillemot, F. (2007) ‘Spatial and temporal specification of neural fates by transcription factor codes’, *Development*, pp. 3771–3780. doi: 10.1242/dev.006379.

Guillemot, F. and Hassan, B. A. (2017) ‘Beyond proneural: emerging functions and regulations of proneural proteins’, *Current Opinion in Neurobiology*. Elsevier Ltd, pp. 93–101. doi: 10.1016/j.conb.2016.11.011.

Gundogdu and Hergovich (2019) ‘MOB (Mps one Binder) Proteins in the Hippo Pathway and Cancer’, *Cells*, 8(6), p. 569. doi: 10.3390/cells8060569.

Haan, N. *et al.* (2013) ‘Fgf10-expressing tanycytes add new neurons to the appetite/energy-balance regulating centers of the postnatal and adult hypothalamus.’, *The Journal of neuroscience : the official journal of the Society for Neuroscience*, 33(14), pp. 6170–80. doi: 10.1523/JNEUROSCI.2437-12.2013.

Hakes, A. E. and Brand, A. H. (2019) ‘Neural stem cell dynamics: the development of brain tumours’, *Current Opinion in Cell Biology*. Elsevier Ltd, 60, pp. 131–138. doi: 10.1016/j.ceb.2019.06.001.

Halder, G. and Johnson, R. L. (2011) ‘Hippo signaling: Growth control and beyond’, *Development*. doi: 10.1242/dev.045500.

Han, J. *et al.* (2015) ‘Vascular Endothelial Growth Factor Receptor 3 Controls Neural Stem Cell Activation in Mice and Humans’, *Cell Reports*. doi: 10.1016/j.celrep.2015.01.049.

Hannus, M. *et al.* (2002) ‘Planar cell polarization requires widerborst, a B’ regulatory subunit of protein phosphatase 2A’, *Development*.

Hansen, D. V. *et al.* (2010) ‘Neurogenic radial glia in the outer subventricular zone of human neocortex’, *Nature*, 464(7288), pp. 554–561. doi: 10.1038/nature08845.

Hardin, P. E. (2011) ‘Molecular genetic analysis of circadian timekeeping in *Drosophila*’, in *Advances in Genetics*. doi: 10.1016/B978-0-12-387690-4.00005-2.

Harding, K. and White, K. (2018) ‘*Drosophila* as a Model for Developmental Biology: Stem Cell-Fate Decisions in the Developing Nervous System’, *Journal of Developmental Biology*, 6(4), p. 25. doi: 10.3390/jdb6040025.

Harding, K. and White, K. (2019) ‘Decoupling developmental apoptosis and neuroblast proliferation in *Drosophila*’, *Developmental Biology*. Elsevier Ltd, (April).

doi: 10.1016/j.ydbio.2019.08.004.

Harvey, K. F., Pfleger, C. M. and Hariharan, I. K. (2003) 'The *Drosophila* Mst ortholog, hippo, restricts growth and cell proliferation and promotes apoptosis', *Cell*. doi: 10.1016/S0092-8674(03)00557-9.

Harvey, K. and Tapon, N. (2007) 'The Salvador-Warts-Hippo pathway - An emerging tumour-suppressor network', *Nature Reviews Cancer*. doi: 10.1038/nrc2070.

Hauri, S. *et al.* (2013) 'Interaction proteome of human Hippo signaling: Modular control of the co-activator YAP1', *Molecular Systems Biology*. doi: 10.1002/msb.201304750.

Hergovich, A. (2016) 'The roles of NDR protein kinases in hippo signalling', *Genes*, 7(5), pp. 1–16. doi: 10.3390/genes7050021.

Hill, A. S., Sahay, A. and Hen, R. (2015) 'Increasing Adult Hippocampal Neurogenesis is Sufficient to Reduce Anxiety and Depression-Like Behaviors', *Neuropsychopharmacology*. Nature Publishing Group, 40(10), pp. 2368–2378. doi: 10.1038/npp.2015.85.

Hirata, J. *et al.* (1995) 'Asymmetric segregation of the homeodomain protein Prospero during *Drosophila* development', *Nature*. doi: 10.1038/377627a0.

Hitoshi, S. *et al.* (2002) 'Notch pathway molecules are essential for the maintenance, but not the generation, of mammalian neural stem cells.', *Genes & development*, 16(7), pp. 846–58. doi: 10.1101/gad.975202.

Homem, C. C. F. *et al.* (2014) 'Ecdysone and mediator change energy metabolism to terminate proliferation in *Drosophila* neural stem cells', *Cell*. Elsevier Inc., 158(4), pp. 874–888. doi: 10.1016/j.cell.2014.06.024.

Homem, C. C. F. and Knoblich, J. A. (2012) '*Drosophila* neuroblasts: a model for stem cell biology', *Development*, 139(23), pp. 4297–4310. doi: 10.1242/dev.080515.

Howard, A. and Pelc, S. R. (1986) 'Synthesis of desoxyribonucleic acid in normal and irradiated cells and its relation to chromosome breakage', *International Journal of Radiation Biology*. Informa Healthcare, 49(2), pp. 207–218. doi: 10.1080/09553008514552501.

Hu, Y. *et al.* (2011) 'An integrative approach to ortholog prediction for disease-

focused and other functional studies', *BMC Bioinformatics*. doi: 10.1186/1471-2105-12-357.

Huang, H. L. *et al.* (2013) 'Par-1 Regulates Tissue Growth by Influencing Hippo Phosphorylation Status and Hippo-Salvador Association', *PLoS Biology*. doi: 10.1371/journal.pbio.1001620.

Huang, J. and Wang, H. (2018) 'Hsp83/Hsp90 Physically Associates with Insulin Receptor to Promote Neural Stem Cell Reactivation', *Stem Cell Reports*. ElsevierCompany., 11(4), pp. 883–896. doi: 10.1016/j.stemcr.2018.08.014.

Hwang, J. and Pallas, D. C. (2014) 'STRIPAK complexes: Structure, biological function, and involvement in human diseases', *International Journal of Biochemistry and Cell Biology*. doi: 10.1016/j.biocel.2013.11.021.

Ikeshima-Kataoka, H. *et al.* (1997) 'Miranda directs Prospero to a daughter cell during *Drosophila* asymmetric divisions', *Nature*. doi: 10.1038/37641.

Imayoshi, I. *et al.* (2010) 'Essential roles of Notch signaling in maintenance of neural stem cells in developing and adult brains.', *The Journal of neuroscience : the official journal of the Society for Neuroscience*, 30(9), pp. 3489–98. doi: 10.1523/JNEUROSCI.4987-09.2010.

Imayoshi, I. *et al.* (2013) 'Oscillatory control of factors determining multipotency and fate in mouse neural progenitors', *Science*. American Association for the Advancement of Science, 342(6163), pp. 1203–1208. doi: 10.1126/science.1242366.

Ito, K. and Hotta, Y. (1992) 'Proliferation pattern of postembryonic neuroblasts in the brain of *Drosophila melanogaster*', *Developmental Biology*, 149(1), pp. 134–148. doi: 10.1016/0012-1606(92)90270-Q.

Jan, Y. N. and Jan, L. Y. (1998) 'Asymmetric cell division.', *Nature*, 392(6678), pp. 775–8. doi: 10.1038/33854.

Janssens, V. and Goris, J. (2001) 'Protein phosphatase 2A: A highly regulated family of serine/threonine phosphatases implicated in cell growth and signalling', *Biochemical Journal*. doi: 10.1042/0264-6021:3530417.

Jeibmann, A. and Paulus, W. (2009) '*Drosophila melanogaster* as a model organism of brain diseases', *International Journal of Molecular Sciences*. doi:

10.3390/ijms10020407.

Jessberger, S. and Kempermann, G. (2003) ‘Adult-born hippocampal neurons mature into activity-dependent responsiveness.’, *The European journal of neuroscience*, 18(10), pp. 2707–12. doi: 10.1111/j.1460-9568.2003.02986.x.

Johnson, D. G. and Walker, C. L. (1999) ‘CYCLINS AND CELL CYCLE CHECKPOINTS’, *Annual Review of Pharmacology and Toxicology*. doi: 10.1146/annurev.pharmtox.39.1.295.

Joppé, S. E. *et al.* (2015) ‘Bone morphogenetic protein dominantly suppresses epidermal growth factor-induced proliferative expansion of adult forebrain neural precursors’, *Frontiers in Neuroscience*. Frontiers Media S.A., 9(OCT). doi: 10.3389/fnins.2015.00407.

Karcavich, R. and Doe, C. Q. (2005) ‘*Drosophila* neuroblast 7-3 cell lineage: A model system for studying programmed cell death, notch/numb signaling, and sequential specification of ganglion mother cell identity’, *Journal of Comparative Neurology*. doi: 10.1002/cne.20371.

Karlsson, D., Baumgardt, M. and Thor, S. (2010) ‘Segment-specific neuronal subtype specification by the integration of anteroposterior and temporal cues’, *PLoS Biology*. doi: 10.1371/journal.pbio.1000368.

Kawaguchi, D. *et al.* (2013) ‘Dll1 maintains quiescence of adult neural stem cells and segregates asymmetrically during mitosis’, *Nature Communications*, 4. doi: 10.1038/ncomms2895.

Kemperman, H. *et al.* (2004) ‘B-type natriuretic peptide (BNP) and N-terminal proBNP in patients with end-stage heart failure supported by a left ventricular assist device.’, *Clinical chemistry*, 50(9), pp. 1670–2. doi: 10.1373/clinchem.2003.030510.

Kempermann, G. *et al.* (2003) ‘Early determination and long-term persistence of adult-generated new neurons in the hippocampus of mice.’, *Development (Cambridge, England)*, 130(2), pp. 391–9. doi: 10.1242/dev.00203.

Kempermann, G. *et al.* (2004) ‘Milestones of neuronal development in the adult hippocampus.’, *Trends in neurosciences*, 27(8), pp. 447–52. doi: 10.1016/j.tins.2004.05.013.

Kempermann, G. (2011) ‘Seven principles in the regulation of adult neurogenesis.’, *The European journal of neuroscience*, 33(6), pp. 1018–24. doi: 10.1111/j.1460-9568.2011.07599.x.

Kempermann, G., Song, H. and Gage, F. H. (2015) ‘Neurogenesis in the Adult Hippocampus’, *Cold Spring Harbor Perspectives in Biology*. Cold Spring Harbor Laboratory Press, 7(9), p. a018812. doi: 10.1101/cshperspect.a018812.

Khandelwal, R. *et al.* (2017) ‘Combinatorial action of Grainyhead, Extradenticle and Notch in regulating Hox mediated apoptosis in *Drosophila* larval CNS’, *PLoS Genetics*. doi: 10.1371/journal.pgen.1007043.

Kiely, M. and Kiely, P. A. (2015) ‘PP2A: The wolf in sheep’s clothing?’, *Cancers*, 7(2), pp. 648–669. doi: 10.3390/cancers7020648.

Kippin, T. E., Kapur, S. and Van Der Kooy, D. (2005) ‘Dopamine specifically inhibits forebrain neural stem cell proliferation, suggesting a novel effect of antipsychotic drugs’, *Journal of Neuroscience*. doi: 10.1523/JNEUROSCI.1120-05.2005.

Knoblich, J. A., Jan, L. Y. and Jan, Y. N. (1995) ‘Asymmetric segregation of numb and prospero during cell division’, *Nature*. doi: 10.1038/377624a0.

Kodl, C. T. and Seaquist, E. R. (2008) ‘Cognitive dysfunction and diabetes mellitus’, *Endocrine Reviews*. doi: 10.1210/er.2007-0034.

Kokovay, E. *et al.* (2012) ‘VCAM1 is essential to maintain the structure of the SVZ niche and acts as an environmental sensor to regulate SVZ lineage progression’, *Cell Stem Cell*, 11(2), pp. 220–230. doi: 10.1016/j.stem.2012.06.016.

Kolupaeva, V., Laplantine, E. and Basilico, C. (2008) ‘PP2A-mediated dephosphorylation of p107 plays a critical role in chondrocyte cell cycle arrest by FGF’, *PLoS ONE*. doi: 10.1371/journal.pone.0003447.

Komarnitsky, S. I. *et al.* (1998) ‘DBF2 Protein Kinase Binds to and Acts through the Cell Cycle-Regulated MOB1 Protein’, *Molecular and Cellular Biology*. doi: 10.1128/mcb.18.4.2100.

Kotlo, K. *et al.* (2014) ‘PR65A phosphorylation regulates PP2A complex signaling’, *PLoS ONE*. doi: 10.1371/journal.pone.0085000.

Krahn, M. P., Egger-Adam, D. and Wodarz, A. (2009) ‘PP2A Antagonizes

Phosphorylation of Bazooka by PAR-1 to Control Apical-Basal Polarity in Dividing Embryonic Neuroblasts', *Developmental Cell*. doi: 10.1016/j.devcel.2009.04.011.

Kraut, R. *et al.* (1996) 'Role of inscuteable in orienting asymmetric cell divisions in *Drosophila*', *Nature*. doi: 10.1038/383050a0.

Kriegstein, A. and Alvarez-Buylla, A. (2009) 'The Glial Nature of Embryonic and Adult Neural Stem Cells', *Annual Review of Neuroscience*. Annual Reviews, 32(1), pp. 149–184. doi: 10.1146/annurev.neuro.051508.135600.

Kurimchak, A. and Graña, X. (2012) 'PP2A counterbalances Phosphorylation of pRB and mitotic proteins by multiple CDKs: Potential implications for PP2A disruption in cancer', *Genes and Cancer*. doi: 10.1177/1947601912473479.

Lai, S. L. and Doe, C. Q. (2014) 'Transient nuclear Prospero induces neural progenitor quiescence', *eLife*, 3(October2014), pp. 1–12. doi: 10.7554/eLife.03363.

Lai, Z. C. *et al.* (2005) 'Control of cell proliferation and apoptosis by mob as tumor suppressor, mats', *Cell*. doi: 10.1016/j.cell.2004.12.036.

Lee, C. Y. *et al.* (2006) 'Brat is a Miranda cargo protein that promotes neuronal differentiation and inhibits neuroblast self-renewal', *Developmental Cell*. doi: 10.1016/j.devcel.2006.01.017.

Lee, D. A. *et al.* (2012) 'Tanycytes of the hypothalamic median eminence form a diet-responsive neurogenic niche.', *Nature neuroscience*, 15(5), pp. 700–2. doi: 10.1038/nn.3079.

Lee, D. A. *et al.* (2014) 'Dietary and sex-specific factors regulate hypothalamic neurogenesis in young adult mice', *Frontiers in Neuroscience*. Frontiers Research Foundation, (8 JUN). doi: 10.3389/fnins.2014.00157.

Lee, D. A. and Blackshaw, S. (2012) 'Functional implications of hypothalamic neurogenesis in the adult mammalian brain', *International Journal of Developmental Neuroscience*, pp. 615–621. doi: 10.1016/j.ijdevneu.2012.07.003.

Lee, D. A. and Blackshaw, S. (2014) 'Feed Your Head: Neurodevelopmental Control of Feeding and Metabolism', *Annual Review of Physiology*. doi: 10.1146/annurev-physiol-021113-170347.

Lee, J.-T., Tsai, C.-K. and Chou, C.-H. (2018) 'Development of Neural Stem Cell-

Based Therapies for Parkinson's Disease', in *Parkinson's Disease - Understanding Pathophysiology and Developing Therapeutic Strategies*. InTech. doi: 10.5772/intechopen.73870.

Lee, J. *et al.* (2000) 'Dietary restriction increases the number of newly generated neural cells, and BDNF expression, in the dentate gyrus of rats', *Journal of Molecular Neuroscience*. doi: 10.1385/JMN:15:2:99.

Lee, M. *et al.* (2018) 'Hippo-yap signaling in ocular development and disease', *Developmental Dynamics*. doi: 10.1002/dvdy.24628.

Lee, M. M., Reif, A. and Schmitt, A. G. (2013) 'Major depression: a role for hippocampal neurogenesis?', *Current topics in behavioral neurosciences*, 14, pp. 153–79. doi: 10.1007/7854_2012_226.

Lee, S. E. *et al.* (2001) 'Order of function of the budding-yeast mitotic exit-network proteins Tem1, Cdc15, Mob1, Dbf2, and Cdc5', *Current Biology*. doi: 10.1016/S0960-9822(01)00228-7.

Lemmon, M. A. and Ferguson, K. M. (2000) 'Signal-dependent membrane targeting by pleckstrin homology (PH) domains', *Biochemical Journal*. doi: 10.1042/0264-6021:3500001.

Lemmon, M. A., Ferguson, K. M. and Abrams, C. S. (2002) 'Pleckstrin homology domains and the cytoskeleton', *FEBS Letters*. doi: 10.1016/S0014-5793(01)03243-4.

Li, L. *et al.* (2010) 'Focal cerebral ischemia induces a multilineage cytogenic response from adult subventricular zone that is predominantly gliogenic.', *Glia*, 58(13), pp. 1610–9. doi: 10.1002/glia.21033.

Li, N. and Clevers, H. (2010) 'Coexistence of quiescent and active adult stem cells in mammals', *Science*, pp. 542–545. doi: 10.1126/science.1180794.

Li, S. *et al.* (2012) 'Characterization of TLX Expression in Neural Stem Cells and Progenitor Cells in Adult Brains', *PLoS ONE*. doi: 10.1371/journal.pone.0043324.

Li, S., Koe, C. T., *et al.* (2017) 'An intrinsic mechanism controls reactivation of neural stem cells by spindle matrix proteins', *Nature Communications*. Springer US, 8(1). doi: 10.1038/s41467-017-00172-9.

Lillie, S. H. and Pringle, J. R. (1980) 'Reserve carbohydrate metabolism in

Saccharomyces cerevisiae: responses to nutrient limitation', *Journal of Bacteriology*, 143(3), pp. 1384–1394.

Lim, D. A. *et al.* (2000) 'Noggin antagonizes BMP signaling to create a niche for adult neurogenesis', *Neuron*. Cell Press, 28(3), pp. 713–726. doi: 10.1016/S0896-6273(00)00148-3.

Lim, D. A. and Alvarez-Buylla, A. (1999) 'Interaction between astrocytes and adult subventricular zone precursors stimulates neurogenesis', *Proceedings of the National Academy of Sciences of the United States of America*, 96(13), pp. 7526–7531. doi: 10.1073/pnas.96.13.7526.

Lim, D. A. and Alvarez-Buylla, A. (2014) 'Adult neural stem cells stake their ground', *Trends in Neurosciences*. Elsevier Ltd, 37(10), pp. 563–571. doi: 10.1016/j.tins.2014.08.006.

Lim, D. A. and Alvarez-Buylla, A. (2016) 'The adult ventricular–subventricular zone (V-SVZ) and olfactory bulb (OB) neurogenesis', *Cold Spring Harbor Perspectives in Biology*. Cold Spring Harbor Laboratory Press, 8(5). doi: 10.1101/cshperspect.a018820.

Liu, B. *et al.* (2016) 'Toll Receptor-Mediated Hippo Signaling Controls Innate Immunity in *Drosophila*', *Cell*. doi: 10.1016/j.cell.2015.12.029.

Liu, B. and Bossing, T. (2016) 'Single neuron transcriptomics identify SRSF/SR protein B52 as a regulator of axon growth and Choline acetyltransferase splicing', *Scientific Reports*. doi: 10.1038/srep34952.

Liu, H.-K. K. *et al.* (2008) 'The nuclear receptor tailless is required for neurogenesis in the adult subventricular zone', *Genes and Development*. doi: 10.1101/gad.479308.

Liu, H. C., Enikolopov, G. and Chen, Y. (2012) 'Cul4B regulates neural progenitor cell growth', *BMC Neuroscience*. doi: 10.1186/1471-2202-13-112.

Liu, H. K. *et al.* (2010) 'The nuclear receptor tailless induces long-term neural stem cell expansion and brain tumor initiation', *Genes and Development*, 24(7), pp. 683–695. doi: 10.1101/gad.560310.

Liu, X. *et al.* (2005) 'Nonsynaptic GABA signaling in postnatal subventricular zone controls proliferation of GFAP-expressing progenitors', *Nature Neuroscience*, 8(9),

pp. 1179–1187. doi: 10.1038/nn1522.

Liu, X. *et al.* (2006) ‘GFAP-expressing cells in the postnatal subventricular zone display a unique glial phenotype intermediate between radial glia and astrocytes’, *GLIA*. doi: 10.1002/glia.20392.

Lledo, P.-M., Alonso, M. and Grubb, M. S. (2006) ‘Adult neurogenesis and functional plasticity in neuronal circuits.’, *Nature reviews. Neuroscience*, 7(3), pp. 179–93. doi: 10.1038/nrn1867.

Llorens-Bobadilla, E. *et al.* (2015) ‘Single-Cell Transcriptomics Reveals a Population of Dormant Neural Stem Cells that Become Activated upon Brain Injury.’, *Cell stem cell*, 17(3), pp. 329–40. doi: 10.1016/j.stem.2015.07.002.

Lois, C. and Alvarez-Buylla, A. (1994) ‘Long-distance neuronal migration in the adult mammalian brain’, *Science*. doi: 10.1126/science.8178174.

Loyer, N. and Januschke, J. (2020) ‘Where does asymmetry come from? Illustrating principles of polarity and asymmetry establishment in *Drosophila* neuroblasts’, *Current Opinion in Cell Biology*. Elsevier Ltd, pp. 70–77. doi: 10.1016/j.ceb.2019.07.018.

Luca, F. C. and Winey, M. (1998) ‘Mob1, an essential yeast gene required for completion of mitosis and maintenance of ploidy’, *Molecular Biology of the Cell*. doi: 10.1091/mbc.9.1.29.

Luque-Molina, I. *et al.* (2019) ‘The Orphan Nuclear Receptor TLX Represses Hes1 Expression, Thereby Affecting NOTCH Signaling and Lineage Progression in the Adult SEZ’, *Stem Cell Reports*. doi: 10.1016/j.stemcr.2019.05.004.

Ly, P. T. *et al.* (2019) ‘CRL4Mahj E3 ubiquitin ligase promotes neural stem cell reactivation’, *PLoS biology*, 17(6), p. e3000276. doi: 10.1371/journal.pbio.3000276.

Ma, L. *et al.* (2019) ‘WNT/NOTCH Pathway Is Essential for the Maintenance and Expansion of Human MGE Progenitors’, *Stem Cell Reports*. Cell Press, 12(5), pp. 934–949. doi: 10.1016/j.stemcr.2019.04.007.

MacDonald, P. E. and Rorsman, P. (2006) ‘Oscillations, intercellular coupling, and insulin secretion in pancreatic β cells’, *PLoS Biology*. doi: 10.1371/journal.pbio.0040049.

Magnusson, J. P. et al. (2014) ‘A latent neurogenic program in astrocytes regulated by Notch signaling in the mouse’, Science. doi: 10.1126/science.346.6206.237.

Mah, A. S., Jang, J. and Deshaies, R. J. (2001) ‘Protein kinase Cdc15 activates the Dbf2-Mob1 kinase complex’, *Proceedings of the National Academy of Sciences of the United States of America*. doi: 10.1073/pnas.141098998.

Malam, Z. and Cohn, R. D. (2014) ‘Stem cells on alert: Priming quiescent stem cells after remote injury’, *Cell Stem Cell*. Cell Press, pp. 7–8. doi: 10.1016/j.stem.2014.06.012.

Manansala, M. C., Min, S. and Cleary, M. D. (2013) ‘The *Drosophila* SERTAD protein Taranis determines lineage-specific neural progenitor proliferation patterns’, *Developmental Biology*, 376(2), pp. 150–162. doi: 10.1016/j.ydbio.2013.01.025.

Marcy, G. and Raineteau, O. (2019) ‘Concise Review: Contributions of Single-Cell Approaches for Probing Heterogeneity and Dynamics of Neural Progenitors Throughout Life’, *Stem Cells*. doi: 10.1002/stem.3071.

Martynoga, B. *et al.* (2013) ‘Epigenomic enhancer annotation reveals a key role for NFIX in neural stem cell quiescence.’, *Genes & development*, 27(16), pp. 1769–86. doi: 10.1101/gad.216804.113.

Maurange, C., Cheng, L. and Gould, A. P. (2008) ‘Temporal Transcription Factors and Their Targets Schedule the End of Neural Proliferation in *Drosophila*’, *Cell*. doi: 10.1016/j.cell.2008.03.034.

Maurange, C. and Gould, A. P. (2005) ‘Brainy but not too brainy: Starting and stopping neuroblast divisions in *Drosophila*’, *Trends in Neurosciences*, 28(1), pp. 30–36. doi: 10.1016/j.tins.2004.10.009.

McCright, B. *et al.* (1996) ‘The B56 family of protein phosphatase 2A (PP2A) regulatory subunits encodes differentiation-induced phosphoproteins that target PP2A to both nucleus and cytoplasm’, *Journal of Biological Chemistry*. doi: 10.1074/jbc.271.36.22081.

McNay, D. E. G. *et al.* (2012) ‘Remodeling of the arcuate nucleus energy-balance circuit is inhibited in obese mice.’, *The Journal of clinical investigation*, 122(1), pp. 142–52. doi: 10.1172/JCI43134.

Metzis, V. *et al.* (2018) ‘Nervous System Regionalization Entails Axial Allocation before Neural Differentiation’, *Cell*. doi: 10.1016/j.cell.2018.09.040.

Mich, J. K. *et al.* (2014) ‘Prospective identification of functionally distinct stem cells and neurosphere-initiating cells in adult mouse forebrain’, *eLife*. doi: 10.7554/eLife.02669.

Ming, G.-L. li and Song, H. (2011) ‘Adult Neurogenesis in the Mammalian Brain: Significant Answers and Significant Questions’, *Neuron*, 70(4), pp. 687–702. doi: 10.1016/j.neuron.2011.05.001.

Mira, H. *et al.* (2010) ‘Signaling through BMPR-IA regulates quiescence and long-term activity of neural stem cells in the adult hippocampus.’, *Cell stem cell*, 7(1), pp. 78–89. doi: 10.1016/j.stem.2010.04.016.

Mira, H. *et al.* (2020) ‘Neurogenesis From Embryo to Adult – Lessons From Flies and Mice’, 8(June), pp. 1–20. doi: 10.3389/fcell.2020.00533.

Mirzadeh, Z. *et al.* (2008) ‘Neural Stem Cells Confer Unique Pinwheel Architecture to the Ventricular Surface in Neurogenic Regions of the Adult Brain’, *Cell Stem Cell*. doi: 10.1016/j.stem.2008.07.004.

Miyares, R. L. and Lee, T. (2019) ‘Temporal control of *Drosophila* central nervous system development’, *Current Opinion in Neurobiology*. doi: 10.1016/j.conb.2018.10.016.

Mohammad, K. *et al.* (2019) ‘Quiescence entry, maintenance, and exit in adult stem cells’, *International Journal of Molecular Sciences*, 20(9), pp. 1–43. doi: 10.3390/ijms20092158.

Monaghan, A. P. *et al.* (1995) ‘The mouse homolog of the orphan nuclear receptor tailless is expressed in the developing forebrain’, *Development*, 121(3), pp. 839–853.

Monedero Cobeta, I., Salmani, B. Y. and Thor, S. (2017) ‘Anterior-Posterior Gradient in Neural Stem and Daughter Cell Proliferation Governed by Spatial and Temporal Hox Control’, *Current Biology*. doi: 10.1016/j.cub.2017.03.023.

Monyak, R. E. *et al.* (2017) ‘Insulin signaling misregulation underlies circadian and cognitive deficits in a *Drosophila* fragile X model’, *Molecular Psychiatry*. Nature Publishing Group, 22(8), pp. 1140–1148. doi: 10.1038/mp.2016.51.

Mora, N. *et al.* (2018) ‘A Temporal Transcriptional Switch Governs Stem Cell Division, Neuronal Numbers, and Maintenance of Differentiation’, *Developmental Cell*. doi: 10.1016/j.devcel.2018.02.023.

Morales, A. V. and Mira, H. (2019) ‘Adult Neural Stem Cells: Born to Last’, *Frontiers in Cell and Developmental Biology*. Frontiers Media SA, 7(June), pp. 1–10. doi: 10.3389/fcell.2019.00096.

Morell, M., Tsan, Y. and O’Shea, K. S. (2015) ‘Inducible expression of noggin selectively expands neural progenitors in the adult SVZ’, *Stem Cell Research*, 14(1), pp. 79–94. doi: 10.1016/j.scr.2014.11.001.

Mori, T., Buffo, A. and Götz, M. (2005) ‘The novel roles of glial cells revisited: the contribution of radial glia and astrocytes to neurogenesis.’, *Current topics in developmental biology*, 69, pp. 67–99. doi: 10.1016/S0070-2153(05)69004-7.

Morizur, L. *et al.* (2018) ‘Distinct Molecular Signatures of Quiescent and Activated Adult Neural Stem Cells Reveal Specific Interactions with Their Microenvironment’, *Stem Cell Reports*. doi: 10.1016/j.stemcr.2018.06.005.

Mouret, A. *et al.* (2008) ‘Learning and survival of newly generated neurons: When time matters’, *Journal of Neuroscience*, 28(45), pp. 11511–11516. doi: 10.1523/JNEUROSCI.2954-08.2008.

Mrkobrada, S. *et al.* (2006) ‘Structural and Functional Analysis of Saccharomyces cerevisiae Mob1’, *Journal of Molecular Biology*. doi: 10.1016/j.jmb.2006.07.007.

Mukherjee, S. *et al.* (2016) ‘REST regulation of gene networks in adult neural stem cells’, *Nature Communications*. Nature Publishing Group, 7. doi: 10.1038/ncomms13360.

Murai, K. *et al.* (2014) ‘Nuclear receptor TLX stimulates hippocampal neurogenesis and enhances learning and memory in a transgenic mouse model’, *Proceedings of the National Academy of Sciences of the United States of America*. doi: 10.1073/pnas.1406779111.

Naetar, N. *et al.* (2014) ‘PP2A-mediated regulation of ras signaling in G2 is essential for stable quiescence and normal G1 length’, *Molecular Cell*. Elsevier Inc., 54(6), pp. 932–945. doi: 10.1016/j.molcel.2014.04.023.

Nagel, A. C. *et al.* (2016) '*Drosophila* cyclin G is a regulator of the Notch signalling pathway during wing development', *PLoS ONE*, 11(3), pp. 1–17. doi: 10.1371/journal.pone.0151477.

Nakatomi, H. *et al.* (2002) 'Regeneration of hippocampal pyramidal neurons after ischemic brain injury by recruitment of endogenous neural progenitors', *Cell*. Cell Press, 110(4), pp. 429–441. doi: 10.1016/S0092-8674(02)00862-0.

Nemirovich-Danchenko, N. M. and Khodanovich, M. Y. (2019) 'New neurons in the post-ischemic and injured brain: Migrating or resident?', *Frontiers in Neuroscience*. Frontiers Media S.A. doi: 10.3389/fnins.2019.00588.

Niu, W. *et al.* (2011) 'Activation of Postnatal Neural Stem Cells Requires Nuclear Receptor TLX', *Journal of Neuroscience*, 31(39), pp. 13816–13828. doi: 10.1523/JNEUROSCI.1038-11.2011.

Niwa, A. *et al.* (2016) 'Voluntary exercise induces neurogenesis in the hypothalamus and ependymal lining of the third ventricle.', *Brain structure & function*, 221(3), pp. 1653–66. doi: 10.1007/s00429-015-0995-x.

Noctor, S. C. *et al.* (2004) 'Cortical neurons arise in symmetric and asymmetric division zones and migrate through specific phases.', *Nature neuroscience*, 7(2), pp. 136–44. doi: 10.1038/nn1172.

Nolo, R. *et al.* (2006) 'The bantam MicroRNA Is a Target of the Hippo Tumor-Suppressor Pathway', *Current Biology*. doi: 10.1016/j.cub.2006.08.057.

Obernier, K. *et al.* (2011) 'Expression of Tlx in both stem cells and transit amplifying progenitors regulates stem cell activation and differentiation in the neonatal lateral subependymal zone', *Stem Cells*. doi: 10.1002/stem.682.

Obernier, K. and Alvarez-Buylla, A. (2019) 'Neural stem cells: Origin, heterogeneity and regulation in the adult mammalian brain', *Development (Cambridge)*, 146(4). doi: 10.1242/dev.156059.

Ogawa, H. *et al.* (2009) 'Protein phosphatase 2A negatively regulates aPKC signaling by modulating phosphorylation of Par-6 in *Drosophila* neuroblast asymmetric divisions', *Journal of Cell Science*, 122(18), pp. 3242–3249. doi: 10.1242/jcs.050955.

Oh, H. and Irvine, K. D. (2008) ‘In vivo regulation of Yorkie phosphorylation and localization’, *Development*. doi: 10.1242/dev.015255.

Oishi, K. *et al.* (2009) ‘Selective induction of neocortical GABAergic neurons by the PDK1-Akt pathway through activation of Mash1.’, *Proceedings of the National Academy of Sciences of the United States of America*, 106(31), pp. 13064–9. doi: 10.1073/pnas.0808400106.

Oppenheim, R. W. (2019) ‘Adult Hippocampal Neurogenesis in Mammals (and Humans): The Death of a Central Dogma in Neuroscience and its Replacement by a New Dogma’, *Developmental Neurobiology*, 79(3), pp. 268–280. doi: 10.1002/dneu.22674.

Otsuki, L. and Brand, A. H. (2017) ‘The vasculature as a neural stem cell niche’, *Neurobiology of Disease*. Elsevier Inc., 107, pp. 4–14. doi: 10.1016/j.nbd.2017.01.010.

Otsuki, L. and Brand, A. H. (2018) ‘Cell cycle heterogeneity directs the timing of neural stem cell activation from quiescence.’, *Science*, 360(6384), pp. 99–102. doi: 10.1126/science.aan8795.

Otsuki, L. and Brand, A. H. (2019) ‘Dorsal-Ventral Differences in Neural Stem Cell Quiescence Are Induced by p57KIP2/Dacapo’, *Developmental Cell*. Cell Press, 49(2), pp. 293-300.e3. doi: 10.1016/j.devcel.2019.02.015.

Ottone, C. *et al.* (2014) ‘Direct cell-cell contact with the vascular niche maintains quiescent neural stem cells’, *Nature Cell Biology*. doi: 10.1038/ncb3045.

Padmanabhan, S. *et al.* (2009) ‘A PP2A Regulatory Subunit Regulates C. elegans Insulin/IGF-1 Signaling by Modulating AKT-1 Phosphorylation’, *Cell*. doi: 10.1016/j.cell.2009.01.025.

Paik, J. *et al.* (2009) ‘FoxOs cooperatively regulate diverse pathways governing neural stem cell homeostasis.’, *Cell stem cell*, 5(5), pp. 540–53. doi: 10.1016/j.stem.2009.09.013.

Pandey, U. B. and Nichols, C. D. (2011) ‘Human disease models in *Drosophila melanogaster* and the role of the fly in therapeutic drug discovery’, *Pharmacological Reviews*. doi: 10.1124/pr.110.003293.

Pantalacci, S., Tapon, N. and Léopold, P. (2003) ‘The salvador partner Hippo promotes apoptosis and cell-cycle exit in *Drosophila*’, *Nature Cell Biology*. doi: 10.1038/ncb1051.

Pardee, A. B. (1974) ‘A restriction point for control of normal animal cell proliferation’, *Proceedings of the National Academy of Sciences of the United States of America*, 71(4), pp. 1286–1290. doi: 10.1073/pnas.71.4.1286.

Parent, J. M. *et al.* (1997) ‘Dentate granule cell neurogenesis is increased by seizures and contributes to aberrant network reorganization in the adult rat hippocampus’, *Journal of Neuroscience*, 17(10), pp. 3727–3738. doi: 10.1523/jneurosci.17-10-03727.1997.

Park, Y. *et al.* (2001) ‘Even skipped is required to produce a trans-acting signal for larval neuroblast proliferation that can be mimicked by ecdysone’, *Development*.

Park, Y. *et al.* (2003) ‘*Drosophila* Perlecan modulates FGF and Hedgehog signals to activate neural stem cell division’, *Developmental Biology*, 253(2), pp. 247–257. doi: 10.1016/S0012-1606(02)00019-2.

Petrik, D. and Encinas, J. M. (2019) ‘Perspective: Of Mice and Men – How Widespread Is Adult Neurogenesis?’, *Frontiers in Neuroscience*, 13(August), pp. 1–6. doi: 10.3389/fnins.2019.00923.

Philippidou, P. and Dasen, J. S. (2013) ‘Hox Genes: Choreographers in Neural Development, Architects of Circuit Organization’, *Neuron*. Elsevier Inc., 80(1), pp. 12–34. doi: 10.1016/j.neuron.2013.09.020.

Pierce, A. A. and Xu, A. W. (2010) ‘De novo neurogenesis in adult hypothalamus as a compensatory mechanism to regulate energy balance’, *Journal of Neuroscience*, 30(2), pp. 723–730. doi: 10.1523/JNEUROSCI.2479-09.2010.

Pineda, J. R. *et al.* (2013) ‘Vascular-derived TGF-β increases in the stem cell niche and perturbs neurogenesis during aging and following irradiation in the adult mouse brain.’, *EMBO molecular medicine*, 5(4), pp. 548–62. doi: 10.1002/emmm.201202197.

Poon, C. L. C. C. *et al.* (2016) ‘The Hippo Pathway Regulates Neuroblasts and Brain Size in *Drosophila melanogaster*.’, *Current biology : CB*. Elsevier Ltd, 26(8), pp. 1034–42. doi: 10.1016/j.cub.2016.02.009.

Portnow, J. *et al.* (2017) 'Neural stem cell-based anticancer gene therapy: A first-in-human study in recurrent high-grade glioma patients', *Clinical Cancer Research*. American Association for Cancer Research Inc., 23(12), pp. 2951–2960. doi: 10.1158/1078-0432.CCR-16-1518.

Poulose, S. M. *et al.* (2017) 'Nutritional Factors Affecting Adult Neurogenesis and Cognitive Function', *Advances in Nutrition: An International Review Journal*. doi: 10.3945/an.117.016261.

Pracheil, T., Thornton, J. and Liu, Z. (2012) 'TORC2 Signaling Is Antagonized by Protein in Saccharomyces cerevisiae', 190(April), pp. 1325–1339. doi: 10.1534/genetics.111.138305.

Prokop, A. *et al.* (1998) 'Homeotic regulation of segment-specific differences in neuroblast numbers and proliferation in the *Drosophila* central nervous system', *Mechanisms of Development*. doi: 10.1016/S0925-4773(98)00068-9.

Prokop, A. and Technau, G. M. (1991) 'The origin of postembryonic neuroblasts in the ventral nerve cord of *Drosophila melanogaster*', *Development*.

Qu, Q., Sun, G., Li, W., Yang, S., Ye, P., Zhao, C., Yu, Ruth T., *et al.* (2010) 'Orphan nuclear receptor TLX activates Wnt/B-catenin signalling to stimulate neural stem cell proliferation and self-renewal', *Nature Cell Biology*. doi: 10.1038/ncb2001.

Ramon-Cañellas, P., Peterson, H. P. and Morante, J. (2019) 'From Early to Late Neurogenesis: Neural Progenitors and the Glial Niche from a Fly's Point of View', *Neuroscience*. doi: 10.1016/j.neuroscience.2018.12.014.

Ramón y Cajal, S. (1909) *Histologie du système nerveux de l'homme & des vertébrés.* Paris : Maloine,. doi: 10.5962/bhl.title.48637.

Reiter, L. T. *et al.* (2001) 'A systematic analysis of human disease-associated gene sequences in *Drosophila melanogaster*', *Genome Research*. doi: 10.1101/gr.169101.

Remmerie, M. and Janssens, V. (2019) 'PP2A: A promising biomarker and therapeutic target in endometrial cancer', *Frontiers in Oncology*. doi: 10.3389/fonc.2019.00462.

Renault, V. M. *et al.* (2009) 'FoxO3 regulates neural stem cell homeostasis.', *Cell stem cell*, 5(5), pp. 527–39. doi: 10.1016/j.stem.2009.09.014.

Reynolds, B. A. and Weiss, S. (1992) 'Generation of neurons and astrocytes from isolated cells of the adult mammalian central nervous system', *Science*, 255(5052), pp. 1707–1710. doi: 10.1126/science.1553558.

Rhee, D. Y. *et al.* (2014) 'Transcription factor networks in *Drosophila melanogaster*', *Cell Reports*. doi: 10.1016/j.celrep.2014.08.038.

Ribeiro, P. S. *et al.* (2010) 'Combined Functional Genomic and Proteomic Approaches Identify a PP2A Complex as a Negative Regulator of Hippo Signaling', *Molecular Cell*, 39(4), pp. 521–534. doi: 10.1016/j.molcel.2010.08.002.

Richards, L. J., Kilpatrick, T. J. and Bartlett, P. F. (1992) 'De novo generation of neuronal cells from the adult mouse brain', *Proceedings of the National Academy of Sciences of the United States of America*. doi: 10.1073/pnas.89.18.8591.

Robins, S. C. *et al.* (2013) 'α-Tanycytes of the adult hypothalamic third ventricle include distinct populations of FGF-responsive neural progenitors', *Nature Communications*, 4. doi: 10.1038/ncomms3049.

Rodgers, J. T. *et al.* (2014) 'MTORC1 controls the adaptive transition of quiescent stem cells from G 0 to GAlert', *Nature*. Nature Publishing Group, 510(7505), pp. 393–396. doi: 10.1038/nature13255.

Rodgers, J. T., Vogel, R. O. and Puigserver, P. (2011) 'Clk2 and B56β Mediate Insulin-Regulated Assembly of the PP2A Phosphatase Holoenzyme Complex on Akt', *Molecular Cell*. doi: 10.1016/j.molcel.2011.02.007.

Rodríguez, E. M. *et al.* (2005) 'Hypothalamic tanycytes: A key component of brain-endocrine interaction', *International review of cytology*, 247, pp. 89–164. doi: 10.1016/S0074-7696(05)47003-5.

Rodríguez, J. J. and Verkhratsky, A. (2011) 'Neurogenesis in Alzheimer's disease', *Journal of Anatomy*, pp. 78–89. doi: 10.1111/j.1469-7580.2011.01343.x.

Rosenberg, M. I., Lynch, J. A. and Desplan, C. (2009) 'Heads and tails: Evolution of antero-posterior patterning in insects', *Biochimica et Biophysica Acta - Gene Regulatory Mechanisms*. NIH Public Access, pp. 333–342. doi: 10.1016/j.bbagrm.2008.09.007.

Ruvolo, P. P. (2016) 'The broken "Off" switch in cancer signaling: PP2A as a

regulator of tumorigenesis, drug resistance, and immune surveillance', *BBA Clinical*. doi: 10.1016/j.bbacli.2016.08.002.

Sahay, A. *et al.* (2011) 'Increasing adult hippocampal neurogenesis is sufficient to improve pattern separation.', *Nature*, 472(7344), pp. 466–70. doi: 10.1038/nature09817.

Sailor, K. A., Schinder, A. F. and Lledo, P. M. (2017) 'Adult neurogenesis beyond the niche: its potential for driving brain plasticity', *Current Opinion in Neurobiology*. Elsevier Ltd, 42, pp. 111–117. doi: 10.1016/j.conb.2016.12.001.

Sakaue-Sawano, A. *et al.* (2008) 'Visualizing Spatiotemporal Dynamics of Multicellular Cell-Cycle Progression', *Cell*. doi: 10.1016/j.cell.2007.12.033.

Sakuma, C. and Chihara, T. (2017) 'Role of the STRIPAK complex and the hippo pathway in synaptic terminal formation', *Neural Regeneration Research*, 12(4), pp. 578–579. doi: 10.4103/1673-5374.205089.

Sangodkar, J. *et al.* (2016) 'All roads lead to PP2A: Exploiting the therapeutic potential of this phosphatase', *FEBS Journal*. doi: 10.1111/febs.13573.

Santo, E. E. and Paik, J. (2018) 'FOXO in Neural Cells and Diseases of the Nervous System', in *Current Topics in Developmental Biology*. Academic Press Inc., pp. 105–118. doi: 10.1016/bs.ctdb.2017.10.002.

Sathyanarayanan, S. *et al.* (2004) 'Posttranslational Regulation of *Drosophila* PERIOD Protein by Protein Phosphatase 2A', *Cell*. doi: 10.1016/S0092-8674(04)00128-X.

Saucedo, L. J. and Edgar, B. A. (2007) 'Filling out the Hippo pathway', *Nature Reviews Molecular Cell Biology*. doi: 10.1038/nrm2221.

Scheffzek, K. and Welti, S. (2012) 'Pleckstrin homology (PH) like domains - Versatile modules in protein-protein interaction platforms', *FEBS Letters*. doi: 10.1016/j.febslet.2012.06.006.

Schlegelmilch, K. *et al.* (2011) 'Yap1 acts downstream of α-catenin to control epidermal proliferation', *Cell*. doi: 10.1016/j.cell.2011.02.031.

Schmidt, H. *et al.* (1997) 'The embryonic central nervous system lineages of *Drosophila melanogaster*: II. Neuroblast lineages derived from the dorsal part of the

nueroectoderm', *Developmental Biology*. doi: 10.1006/dbio.1997.8660.

Schnorrenberg, S. *et al.* (2016) 'In vivo super-resolution RESOLFT microscopy of *Drosophila melanogaster*', *eLife*. doi: 10.7554/eLife.15567.

Schuhmacher, D., Sontag, J. M. and Sontag, E. (2019) 'Protein phosphatase 2A: More than a passenger in the regulation of epithelial cell-cell junctions', *Frontiers in Cell and Developmental Biology*. doi: 10.3389/fcell.2019.00030.

Schulte, J. *et al.* (2010) 'DMob4 / Phocein Regulates Synapse Formation , Axonal Transport , and Microtubule Organization', *Wild*, 30(15), pp. 5189–5203. doi: 10.1523/JNEUROSCI.5823-09.2010.

Scopa, C. *et al.* (2020) 'Impaired adult neurogenesis is an early event in Alzheimer's disease neurodegeneration, mediated by intracellular Aβ oligomers', *Cell Death & Differentiation*. Springer Science and Business Media LLC. doi: 10.1038/s41418-019-0409-3.

Shen, C. P., Jan, L. Y. and Jan, Y. N. (1997) 'Miranda is required for the asymmetric localization of prospero during mitosis in *Drosophila*', *Cell*. doi: 10.1016/S0092-8674(00)80505-X.

Shen, Q. *et al.* (2008) 'Adult SVZ Stem Cells Lie in a Vascular Niche: A Quantitative Analysis of Niche Cell-Cell Interactions', *Cell Stem Cell*, 3(3), pp. 289–300. doi: 10.1016/j.stem.2008.07.026.

Shetty, A. K., Hattiangady, B. and Shetty, G. A. (2005) 'Stem/progenitor cell proliferation factors FGF-2, IGF-1, and VEGF exhibit early decline during the course of aging in the hippocampus: Role of astrocytes', *GLIA*. doi: 10.1002/glia.20187.

Shi, Y. *et al.* (2004) 'Expression and function of orphan nuclear receptor TLX in adult neural stem cells.', *Nature*, 427(6969), pp. 78–83. doi: 10.1038/nature02211.

Shi, Y. (2009) 'Serine/Threonine Phosphatases: Mechanism through Structure', *Cell*, 139(3), pp. 468–484. doi: 10.1016/j.cell.2009.10.006.

Shi, Z., Jiao, S. and Zhou, Z. (2016) 'STRIPAK complexes in cell signaling and cancer', *Oncogene*. Nature Publishing Group, 35(35), pp. 4549–4557. doi: 10.1038/onc.2016.9.

Shimojo, H., Ohtsuka, T. and Kageyama, R. (2008) 'Oscillations in Notch Signaling

Regulate Maintenance of Neural Progenitors', *Neuron*, 58(1), pp. 52–64. doi: 10.1016/j.neuron.2008.02.014.

Shin, J. Y. J. J. Y. *et al.* (2015) 'Single-Cell RNA-Seq with Waterfall Reveals Molecular Cascades underlying Adult Neurogenesis', *Cell stem cell*. Cell Press, 17(3), pp. 360–72. doi: 10.1016/j.stem.2015.07.013.

Shohayeb, B. *et al.* (2018) 'Factors that influence adult neurogenesis as potential therapy', *Translational Neurodegeneration*. doi: 10.1186/s40035-018-0109-9.

Simpson, E. H., Kellendonk, C. and Kandel, E. (2010) 'A Possible Role for the Striatum in the Pathogenesis of the Cognitive Symptoms of Schizophrenia', *Neuron*, pp. 585–596. doi: 10.1016/j.neuron.2010.02.014.

Skeath, J. B. *et al.* (1992) 'Gene regulation in two dimensions: The proneural achaete and scute genes are controlled by combinations of axis-patterning genes through a common intergenic control region', Genes and Development. doi: 10.1101/gad.6.12b.2606.

Skeath, J. B. and Carroll, S. B. (1991) 'Regulation of achaete-scute gene expression and sensory organ pattern formation in the *Drosophila* wing', *Genes and Development*. Cold Spring Harbor Laboratory Press, 5(6), pp. 984–995. doi: 10.1101/gad.5.6.984.

Skeath, J. B. and JB, S. (1999) 'At the Nexus Between Pattern Formation and Cell-Type Specification: The Generation of Individual Neuroblast Fates in the *Drosophila* Embryonic Central Nervous System', 21(11), pp. 922–931. doi: 10.1002/(SICI)1521-1878(199911)21:11<922::AID-BIES4>3.0.CO;2-T.

Sloan, S. A. and Barres, B. A. (2014) 'Mechanisms of astrocyte development and their contributions to neurodevelopmental disorders', *Current Opinion in Neurobiology*. doi: 10.1016/j.conb.2014.03.005.

Snaith, H. A. *et al.* (1996) 'Deficiency of protein phosphatase 2A uncouples the nuclear and centrosome cycles and prevents attachment of microtubules to the kinetochore in *Drosophila* microtubule star (mts) embryos', *Journal of Cell Science*.

Snyder, J. S. *et al.* (2005) 'A role for adult neurogenesis in spatial long-term memory', *Neuroscience*, 130(4), pp. 843–852. doi: 10.1016/j.neuroscience.2004.10.009.

Snyder, J. S. *et al.* (2009) 'Adult-born hippocampal neurons are more numerous, faster maturing, and more involved in behavior in rats than in mice', *Journal of Neuroscience*. doi: 10.1523/JNEUROSCI.1768-09.2009.

Sobhan, P. K. and Funa, K. (2017) 'TLX—Its Emerging Role for Neurogenesis in Health and Disease', *Molecular Neurobiology*. doi: 10.1007/s12035-015-9608-1.

Song, J., M. Christian, K., *et al.* (2012a) 'Modification of hippocampal circuitry by adult neurogenesis', *Developmental Neurobiology*, 72(7), pp. 1032–1043. doi: 10.1002/dneu.22014.

Song, J., Zhong, C., *et al.* (2012b) 'Neuronal circuitry mechanism regulating adult quiescent neural stem-cell fate decision.', *Nature*, 489(7414), pp. 150–4. doi: 10.1038/nature11306.

Sousa-Nunes, R. and Somers, W. G. (2013) 'Mechanisms of Asymmetric Progenitor Divisions in the *Drosophila* Central Nervous System', in *Advances in experimental medicine and biology*. Adv Exp Med Biol, pp. 79–102. doi: 10.1007/978-94-007-6621-1_6.

Sousa-Nunes, R., Yee, L. L. and Gould, A. P. (2011) 'Fat cells reactivate quiescent neuroblasts via TOR and glial insulin relays in *Drosophila*', *Nature*. Nature Publishing Group, 471(7339), pp. 508–513. doi: 10.1038/nature09867.

Spalding, K. L. *et al.* (2013) 'XDynamics of hippocampal neurogenesis in adult humans', *Cell*. Cell Press, 153(6), p. 1219. doi: 10.1016/j.cell.2013.05.002.

Spéder, P. and Brand, A. H. (2014) 'Gap junction proteins in the blood-brain barrier control nutrient-dependent reactivation of *Drosophila* neural stem cells', *Developmental Cell*, 30(3), pp. 309–321. doi: 10.1016/j.devcel.2014.05.021.

Spéder, P. and Brand, A. H. (2018) 'Systemic and local cues drive neural stem cell niche remodelling during neurogenesis in *Drosophila*.', *eLife*, 7, pp. 1–16. doi: 10.7554/eLife.30413.

Spéder, P., Liu, J. and Brand, A. H. (2011) 'Nutrient control of neural stem cells', *Current Opinion in Cell Biology*, 23(6), pp. 724–729. doi: 10.1016/j.ceb.2011.08.004.

Spinelli, M., Fusco, S. and Grassi, C. (2019) 'Brain Insulin Resistance and Hippocampal Plasticity: Mechanisms and Biomarkers of Cognitive Decline', *Frontiers*

*in Neuroscience*, 13(July), pp. 1–13. doi: 10.3389/fnins.2019.00788.

Staley, B. K. and Irvine, K. D. (2010) 'Warts and yorkie mediate intestinal regeneration by influencing stem cell proliferation', *Current Biology*. doi: 10.1016/j.cub.2010.07.041.

Stanyon, C. A. *et al.* (2004) 'A *Drosophila* protein-interaction map centered on cell-cycle regulators.', *Genome biology*. doi: 10.1186/gb-2004-5-12-r96.

Stranahan, A. M. *et al.* (2008) 'Diet-induced insulin resistance impairs hippocampal synaptic plasticity and cognition in middle-aged rats', *Hippocampus*. doi: 10.1002/hipo.20470.

Stranahan, A. M. (2008) *Opposing effects of diabetes and physical activity on hippocampal structure and function*, *Dissertation Abstracts International: Section B: The Sciences and Engineering*.

Straßburger, K. *et al.* (2012) 'Insulin/IGF signaling drives cell proliferation in part via Yorkie/YAP', *Developmental Biology*. Elsevier, 367(2), pp. 187–196. doi: 10.1016/j.ydbio.2012.05.008.

Sueda, R. *et al.* (2019) 'High Hes1 expression and resultant Ascl1 suppression regulate quiescent vs. active neural stem cells in the adult mouse brain', *Genes & development*. NLM (Medline), 33(9–10), pp. 511–523. doi: 10.1101/gad.323196.118.

Suh, H. *et al.* (2007) 'In vivo fate analysis reveals the multipotent and self-renewal capacities of Sox2+ neural stem cells in the adult hippocampus.', *Cell stem cell*, 1(5), pp. 515–28. doi: 10.1016/j.stem.2007.09.002.

Sullivan, L. F., Warren, T. L. and Doe, C. Q. (2019) 'Temporal identity establishes columnar neuron morphology, connectivity, and function in a *Drosophila* navigation circuit', *eLife*. doi: 10.7554/eLife.43482.

Sun, D. and Buttitta, L. (2015) 'Protein phosphatase 2A promotes the transition to G0 during terminal differentiation in *Drosophila*', *Development*, 142(17), pp. 3033–3045. doi: 10.1242/dev.120824.

Sun, G. Q. *et al.* (2007) 'Orphan nuclear receptor TLX recruits histone deacetylases to repress transcription and regulate neural stem cell proliferation', *Proceedings of the National Academy of Sciences of the United States of America*. doi:

10.1073/pnas.0704089104.

Sun, Jiaqi *et al.* (2011) 'Epigenetic regulation of neurogenesis in the adult mammalian brain', *European Journal of Neuroscience*. doi: 10.1111/j.1460-9568.2011.07607.x.

Sun, Y.-M. *et al.* (2005) 'Distinct Profiles of REST Interactions with Its Target Genes at Different Stages of Neuronal Development', *Molecular Biology of the Cell*, 16(12), pp. 5630–5638. doi: 10.1091/mbc.e05-07-0687.

Sung, P. S. *et al*. (2020) 'Neuroinflammation and neurogenesis in alzheimer's disease and potential therapeutic approaches', International Journal of Molecular Sciences, 21(3). doi: 10.3390/ijms21030701.

Tang, Y. *et al.* (2019) 'Architecture, substructures, and dynamic assembly of STRIPAK complexes in Hippo signaling', *Cell Discovery*, 5(1). doi: 10.1038/s41421-018-0077-3.

Tang, Y., Yu, P. and Cheng, L. (2017) 'Current progress in the derivation & therapeutic application of neural stem cells', *Cell Death and Disease*. Nature Publishing Group, p. 3108. doi: 10.1038/cddis.2017.504.

Tarpey, P. S. *et al.* (2007) 'Mutations in CUL4B, which encodes a ubiquitin E3 ligase subunit, cause an X-linked mental retardation syndrome associated with aggressive outbursts, seizures, relative macrocephaly, central obesity, hypogonadism, pes cavus, and tremor', *American Journal of Human Genetics*. doi: 10.1086/511134.

Tavazoie, S. F. *et al.* (2008) 'Endogenous human microRNAs that suppress breast cancer metastasis', *Nature*. doi: 10.1038/nature06487.

Temple, S. (2001) 'The development of neural stem cells', *Nature*, 414(6859), pp. 112–117. doi: 10.1038/35102174.

Tian, Z. *et al.* (2018) 'Methods of reactivation and reprogramming of neural stem cells for neural repair', *Methods*. Elsevier Inc., 133, pp. 3–20. doi: 10.1016/j.ymeth.2017.08.014.

Trammell, M. A. *et al.* (2008) 'Mob4 plays a role in spindle focusing in *Drosophila* S2 cells', *Journal of Cell Science*, 121(8), pp. 1284–1292. doi: 10.1242/jcs.017210.

Tremblay, A. M. and Camargo, F. D. (2012) 'Hippo signaling in mammalian stem

cells', *Seminars in Cell and Developmental Biology*. doi: 10.1016/j.semcdb.2012.08.001.

Truman, J. W. and Bate, M. (1988) 'Spatial and temporal patterns of neurogenesis in the central nervous system of *Drosophila melanogaster*', *Developmental Biology*. doi: 10.1016/0012-1606(88)90067-X.

Tsuji, T., Hasegawa, E. and Isshiki, T. (2008) 'Neuroblast entry into quiescence is regulated intrinsically by the combined action of spatial Hox proteins and temporal identity factors', *Development*, 135(23), pp. 3859–3869. doi: 10.1242/dev.025189.

Tumaneng, K., Russell, R. C. and Guan, K. L. (2012) 'Organ size control by Hippo and TOR pathways', *Current Biology*. doi: 10.1016/j.cub.2012.03.003.

Tzivion, G., Dobson, M. and Ramakrishnan, G. (2011) 'FoxO transcription factors; Regulation by AKT and 14-3-3 proteins', *Biochimica et Biophysica Acta - Molecular Cell Research*. Elsevier B.V., 1813(11), pp. 1938–1945. doi: 10.1016/j.bbamcr.2011.06.002.

Udan, R. S. *et al.* (2003) 'Hippo promotes proliferation arrest and apoptosis in the Salvador/Warts pathway', *Nature Cell Biology*, 5(10), pp. 914–920. doi: 10.1038/ncb1050.

Ulvklo, C. *et al.* (2012) 'Control of neuronal cell fate and number by integration of distinct daughter cell proliferation modes with temporal progression', *Development*. doi: 10.1242/dev.074500.

Urbach, R., Schnabel, R. and Technau, G. M. (2003) 'The pattern of neuroblast formation, mitotic domains and proneural gene expression during early brain development in *Drosophila*', *Development*. doi: 10.1242/dev.00528.

Urbán, N. *et al.* (2016) 'Return to Quiescence of mouse neural stem cells by degradation of a proactivation protein', *Science*, 353(6296), pp. 292–295. doi: 10.1126/science.aaf4802.

Urbán, N. and Guillemot, F. (2014) 'Neurogenesis in the embryonic and adult brain: same regulators, different roles.', *Frontiers in cellular neuroscience*, 8, p. 396. doi: 10.3389/fncel.2014.00396.

Valley, M. T. *et al.* (2009) 'Ablation of mouse adult neurogenesis alters olfactory bulb

structure and olfactory fear conditioning', *Frontiers in Neuroscience*, 3(NOV). doi: 10.3389/neuro.22.003.2009.

van Velthoven, C. T. J. and Rando, T. A. (2019) 'Stem Cell Quiescence: Dynamism, Restraint, and Cellular Idling', *Cell Stem Cell*. Elsevier Inc., 24(2), pp. 213–225. doi: 10.1016/j.stem.2019.01.001.

Vereshchagina, N. *et al.* (2008) 'The protein phosphatase PP2A-B′ subunit Widerborst is a negative regulator of cytoplasmic activated Akt and lipid metabolism in *Drosophila*', *Journal of Cell Science*. doi: 10.1242/jcs.035220.

Virshup, D. M. and Shenolikar, S. (2009) 'From Promiscuity to Precision: Protein Phosphatases Get a Makeover', *Molecular Cell*. Elsevier Inc., 33(5), pp. 537–545. doi: 10.1016/j.molcel.2009.02.015.

Voigt, A. *et al.* (2002) 'Perlecan participates in proliferation activation of quiescent *Drosophila* neuroblasts', *Developmental Dynamics*, 224(4), pp. 403–412. doi: 10.1002/dvdy.10120.

Walsh, K. T. and Doe, C. Q. (2017) '*Drosophila* embryonic type II neuroblasts: origin, temporal patterning, and contribution to the adult central complex', *Development*, p. dev.157826. doi: 10.1242/dev.157826.

Wang, C. *et al.* (2009) 'Protein phosphatase 2A regulates self-renewal of *Drosophila* neural stem cells', *Development*, 136(17), pp. 3031–3031. doi: 10.1242/dev.042432.

Wang, C. *et al.* (2011) 'Identification and characterization of neuroblasts in the subventricular zone and rostral migratory stream of the adult human brain.', *Cell research*, 21(11), pp. 1534–1550. doi: 10.1038/cr.2011.83.

Wang, C. *et al.* (2014) 'Human and monkey striatal interneurons are derived from the medial ganglionic eminence but not from the adult subventricular zone', *Journal of Neuroscience*. Society for Neuroscience, 34(33), pp. 10906–10923. doi: 10.1523/JNEUROSCI.1758-14.2014.

Wang, R. N. *et al.* (2014) 'Bone Morphogenetic Protein (BMP) signaling in development and human diseases', *Genes and Diseases*. Chongqing Medical University, pp. 87–105. doi: 10.1016/j.gendis.2014.07.005.

Wang, T. and Xiong, J. Q. (2016) 'The Orphan Nuclear Receptor TLX/NR2E1 in

Neural Stem Cells and Diseases', *Neuroscience Bulletin*. Science Press, pp. 108–114. doi: 10.1007/s12264-015-0004-7.

Wang, X. *et al.* (2016) 'Traumatic brain injury stimulates neural stem cell proliferation via mammalian target of rapamycin signaling pathway activation', *eNeuro*. Society for Neuroscience, 3(5). doi: 10.1523/ENEURO.0162-16.2016.

Wang, Y., Liu, H. K. and Schütz, G. (2013) 'Role of the nuclear receptor tailless in adult neural stem cells', *Mechanisms of Development*. Elsevier Ireland Ltd, pp. 388–390. doi: 10.1016/j.mod.2013.02.001.

Wei, X., Shimizu, T. and Lai, Z. C. (2007) 'Mob as tumor suppressor is activated by Hippo kinase for growth inhibition in *Drosophila*', *EMBO Journal*. doi: 10.1038/sj.emboj.7601630.

Weiss, S. *et al.* (1996) 'Multipotent CNS stem cells are present in the adult mammalian spinal cord and ventricular neuroaxis', *Journal of Neuroscience*, 16(23), pp. 7599–7609. doi: 10.1523/jneurosci.16-23-07599.1996.

Weng, M., Golden, K. L. and Lee, C. Y. (2010) 'dFezf/Earmuff Maintains the Restricted Developmental Potential of Intermediate Neural Progenitors in *Drosophila*', *Developmental Cell*. doi: 10.1016/j.devcel.2009.12.007.

Weng, R. and Cohen, S. M. (2012) '*Drosophila* miR-124 regulates neuroblast proliferation through its target anachronism', *Development*. doi: 10.1242/dev.075143.

Werner-Washburne, M. *et al.* (1993) 'Stationary phase in the yeast Saccharomyces cerevisiae', *Microbiological Reviews*, 57(2), pp. 383–401.

Westermarck, J. and Hahn, W. C. (2008) 'Multiple pathways regulated by the tumor suppressor PP2A in transformation', *Trends in Molecular Medicine*. doi: 10.1016/j.molmed.2008.02.001.

Whalley, K. (2012) 'Neurogenesis: Hypothalamic neurogenesis regulates weight gain', *Nature Reviews Neuroscience*, 13(5), p. 289. doi: 10.1038/nrn3245.

Wheeler, S. R., Stagg, S. B. and Crews, S. T. (2009) 'MidExDB: A database of *Drosophila* CNS midline cell gene expression', *BMC Developmental Biology*. doi: 10.1186/1471-213X-9-56.

White, K. and Kankel, D. R. (1978) 'Patterns of cell division and cell movement in the

formation of the imaginal nervous system in *Drosophila melanogaster*', *Developmental Biology*. doi: 10.1016/0012-1606(78)90029-5.

Willis, C. M. *et al.* (2020) 'The neural stem cell secretome and its role in brain repair', *Brain Research*. Elsevier B.V., p. 146615. doi: 10.1016/j.brainres.2019.146615.

Winner, B. and Winkler, J. (2015) 'Adult neurogenesis in neurodegenerative diseases', Cold Spring Harbor Perspectives in Biology. doi: 10.1101/cshperspect.a021287.

Wlodarchak, N. and Xing, Y. (2016) 'PP2A as a master regulator of the cell cycle', *Critical Reviews in Biochemistry and Molecular Biology*. doi: 10.3109/10409238.2016.1143913.

Wodarz, A. *et al.* (1999) 'Bazooka provides an apical cue for inscuteable localization in *Drosophila* neuroblasts', *Nature*. doi: 10.1038/990128.

Wodarz, A. *et al.* (2000) '*Drosophila* atypical protein kinase C associates with Bazooka and controls polarity of epithelia and neuroblasts', *Journal of Cell Biology*. doi: 10.1083/jcb.150.6.1361.

Wodarz, A. (2005) 'Molecular control of cell polarity and asymmetric cell division in *Drosophila* neuroblasts', *Current Opinion in Cell Biology*. Elsevier Ltd, pp. 475–481. doi: 10.1016/j.ceb.2005.08.005.

Wong, M. *et al.* (2014) 'Silencing of STRN4 suppresses the malignant characteristics of cancer cells', *Cancer Science*. doi: 10.1111/cas.12541.

Wu, S. *et al.* (2003) 'hippo encodes a Ste-20 family protein kinase that restricts cell proliferation and promotes apoptosis in conjunction with salvador and warts', *Cell*. doi: 10.1016/S0092-8674(03)00549-X.

Xiao, J. *et al.* (2018) 'Neural Stem Cell-Based Regenerative Approaches for the Treatment of Multiple Sclerosis', *Molecular Neurobiology*. Humana Press Inc., pp. 3152–3171. doi: 10.1007/s12035-017-0566-7.

Xu, Y., Tamamaki, N., Noda, T., Kimura, K., Itokazu, Y., Matsumoto, N., *et al*. (2005). Neurogenesis in the ependymal layer of the adult rat 3rd ventricle. Exp. Neurol. 192, 251–264. doi: 10.1016/j.expneurol.2004.12.021

Yaghmaeian Salmani, B. *et al.* (2018) 'Evolutionarily conserved anterior expansion of

the central nervous system promoted by a common PcG-Hox program', *Development (Cambridge, England)*, 145(7). doi: 10.1242/dev.160747.

Yokoyama, A. *et al.* (2008) 'Transrepressive Function of TLX Requires the Histone Demethylase LSD1', *Molecular and Cellular Biology*. doi: 10.1128/mcb.02030-07.

Yu, F., Kuo, C. T. and Jan, Y. N. (2006) '*Drosophila* Neuroblast Asymmetric Cell Division: Recent Advances and Implications for Stem Cell Biology', Neuron. doi: 10.1016/j.neuron.2006.06.016.

Yu, F. X. and Guan, K. L. (2013) 'The Hippo pathway: Regulators and regulations', *Genes and Development*, 27(4), pp. 355–371. doi: 10.1101/gad.210773.112.

Yu, R. T. et al. (1994) 'Relationship between *Drosophila* gap gene tailless and a vertebrate nuclear receptor Tlx', *Nature*. doi: 10.1038/370375a0.

Zelentsova, K. et al. (2017) 'Protein S Regulates Neural Stem Cell Quiescence and Neurogenesis', Stem Cells. doi: 10.1002/stem.2522.

Zhang, C. L. *et al.* (2006) 'Nuclear receptor TLX prevents retinal dystrophy and recruits the corepressor atrophin1', *Genes and Development*. doi: 10.1101/gad.1413606.

Zhang, C. L. *et al.* (2008a) 'A role for adult TLX-positive neural stem cells in learning and behaviour', *Nature*. doi: 10.1038/nature06562.

Zhang, H., Pasolli, H. A. and Fuchs, E. (2011) 'Yes-associated protein (YAP) transcriptional coactivator functions in balancing growth and differentiation in skin', *Proceedings of the National Academy of Sciences of the United States of America*. doi: 10.1073/pnas.1019603108.

Zhang, J. and Jiao, J. (2015) 'Molecular Biomarkers for Embryonic and Adult Neural Stem Cell and Neurogenesis', *BioMed Research International*. doi: 10.1155/2015/727542.

Zhang, R. *et al.* (2004) 'Activated neural stem cells contribute to stroke-induced neurogenesis and neuroblast migration toward the infarct boundary in adult rats.', *Journal of Cerebral Blood Flow and Metabolism*, 24(4), pp. 441–8. doi: 10.1097/00004647-200404000-00009.

Zhang, R. *et al.* (2019) 'Id4 Downstream of Notch2 Maintains Neural Stem Cell

Quiescence in the Adult Hippocampus', *Cell Reports*. ElsevierCompany., 28(6), pp. 1485-1498.e6. doi: 10.1016/j.celrep.2019.07.014.

Zhang, R. L., Zhang, Z. G. and Chopp, M. (2008b) 'Ischemic stroke and neurogenesis in the subventricular zone', *Neuropharmacology*. NIH Public Access, 55(3), pp. 345–352. doi: 10.1016/j.neuropharm.2008.05.027.

Zhao, C. *et al.* (2009) 'A feedback regulatory loop involving microRNA-9 and nuclear receptor TLX in neural stem cell fate determination', *Nature Structural and Molecular Biology*. doi: 10.1038/nsmb.1576.

Zheng, Y. *et al.* (2015) 'Identification of Happyhour/MAP4K as Alternative Hpo/Mst-like Kinases in the Hippo Kinase Cascade', *Developmental Cell*. doi: 10.1016/j.devcel.2015.08.014.

Zheng, Y. *et al.* (2017) 'Homeostatic Control of Hpo/MST Kinase Activity through Autophosphorylation-Dependent Recruitment of the STRIPAK PP2A Phosphatase Complex', *Cell Reports*. Elsevier B.V., 21(12), pp. 3612–3623. doi: 10.1016/j.celrep.2017.11.076.

Zhou, D. *et al.* (2009) 'Mst1 and Mst2 Maintain Hepatocyte Quiescence and Suppress Hepatocellular Carcinoma Development through Inactivation of the Yap1 Oncogene', *Cancer Cell*. doi: 10.1016/j.ccr.2009.09.026.

Zhou, D. *et al.* (2011) 'Mst1 and Mst2 protein kinases restrain intestinal stem cell proliferation and colonic tumorigenesis by inhibition of Yes-associated protein (Yap) overabundance', *Proceedings of the National Academy of Sciences of the United States of America*. doi: 10.1073/pnas.1110428108.

Zhou, Y. *et al.* (2018) 'Autocrine Mfge8 Signaling Prevents Developmental Exhaustion of the Adult Neural Stem Cell Pool', *Cell Stem Cell*, 23, pp. 444-452.e4. doi: 10.1016/j.stem.2018.08.005.

Zhu, Y. *et al.* (2018) 'Hemopexin is required for adult neurogenesis in the subventricular zone/olfactory bulb pathway article', *Cell Death and Disease*. Nature Publishing Group, 9(3). doi: 10.1038/s41419-018-0328-0.

Ziebell, F. *et al.* (2018) 'Revealing age-related changes of adult hippocampal neurogenesis using mathematical models', *Development (Cambridge)*. Company of Biologists Ltd, 145(1). doi: 10.1242/dev.153544.

Ziegler, A. N., Levison, S. W. and Wood, T. L. (2015) ‘Insulin and IGF receptor signalling in neural-stem-cell homeostasis’, *Nature Reviews Endocrinology*. Nature Publishing Group, 11(3), pp. 161–170. doi: 10.1038/nrendo.2014.208.

Zismanov, V. *et al.* (2016) ‘Phosphorylation of eIF2α is a Translational Control Mechanism Regulating Muscle Stem Cell Quiescence and Self-Renewal’, *Cell Stem Cell*. doi: 10.1016/j.stem.2015.09.020.

Zou, Y. *et al.* (2007) ‘Mutation in CUL4B, which encodes a member of cullin-RING ubiquitin ligase complex, causes X-linked mental retardation’, *American Journal of Human Genetics*. doi: 10.1086/512489.

# APPENDIX.

Article

Cell Reports

# STRIPAK Members Orchestrate Hippo and Insulin Receptor Signaling to Promote Neural Stem Cell Reactivation

## Graphical Abstract

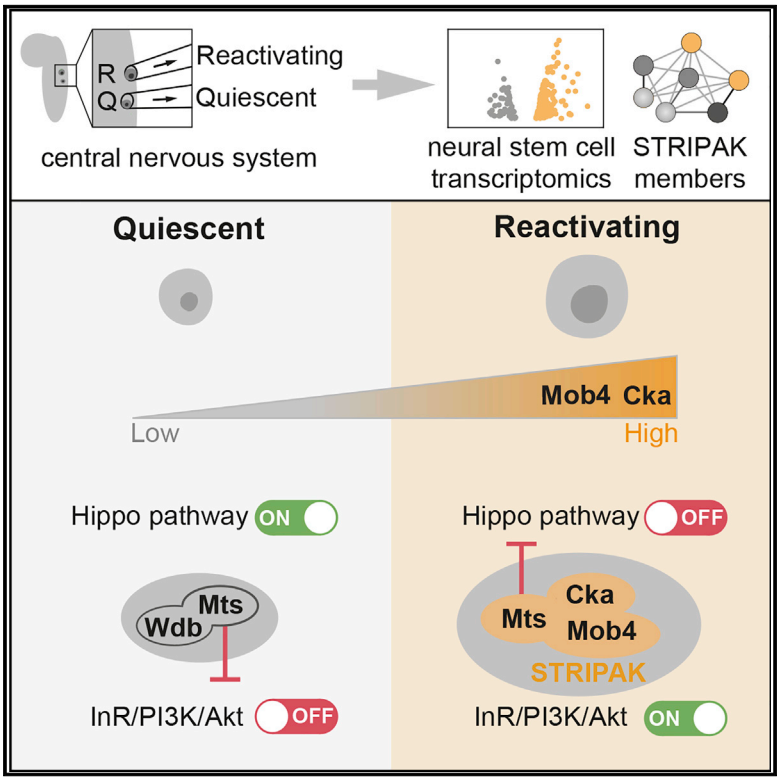


## Highlights

- Transcriptional profiling of reactivating versus quiescent NSCs identifies STRIPAK members
- PP2A/Mts phosphatase inhibits Akt activation, maintaining NSC quiescence
- Mob4 and Cka target Mts to Hippo to inhibit its activity and promote NSC reactivation
- Mob4/Cka/Mts coordinate Hippo and InR/PI3K/Akt signaling in NSCs

## Authors

Jon Gil-Ranedo, Eleanor Gonzaga, Karolina J. Jaworek, Christian Berger, Torsten Bossing, Claudia S. Barros

## Correspondence

claudia.barros@plymouth.ac.uk

## In Brief

The integration of signals allowing stem cell reactivation from quiescence is unclear. Gil-Ranedo et al. identify STRIPAK members Mob4, Cka, and PP2A/Mts through reactivating versus quiescent neural stem cell (NSC) transcriptional profiling. Their findings suggest that Mob4/Cka/Mts functions as an intrinsic molecular switch coordinating Hippo and InR/PI3K/Akt pathways, enabling NSC reactivation.

Gil-Ranedo et al., 2019, Cell Reports 27, 2921–2933
June 4, 2019 
https://doi.org/10.1016/j.celrep.2019.05.023

CellPress

Cell Reports
Article



# STRIPAK Members Orchestrate Hippo and Insulin Receptor Signaling to Promote Neural Stem Cell Reactivation

Jon Gil-Ranedo,[1,3] Eleanor Gonzaga,[1,3] Karolina J. Jaworek,[1,4] Christian Berger,[2,5] Torsten Bossing,[1] and Claudia S. Barros[1,6,*]
[1]Faculty of Medicine and Dentistry, University of Plymouth, PL6 8BU Plymouth, UK
[2]Institute of Genetics, Johannes Gutenberg University, 55099 Mainz, Germany
[3]These authors contributed equally
[4]Present address: Living Systems Institute, University of Exeter, EX4 4QD Exeter, UK
[5]Sanofi Aventis Deutschland GmbH, 55126 Mainz, Germany
[6]Lead Contact
*Correspondence: claudia.barros@plymouth.ac.uk
https://doi.org/10.1016/j.celrep.2019.05.023

## SUMMARY

**Adult stem cells reactivate from quiescence to maintain tissue homeostasis and in response to injury. How the underlying regulatory signals are integrated is largely unknown. *Drosophila* neural stem cells (NSCs) also leave quiescence to generate adult neurons and glia, a process that is dependent on Hippo signaling inhibition and activation of the insulin-like receptor (InR)/PI3K/Akt cascade. We performed a transcriptome analysis of individual quiescent and reactivating NSCs harvested directly from *Drosophila* brains and identified the conserved STRIPAK complex members *mob4*, *cka*, and *PP2A* (*microtubule star*, *mts*). We show that PP2A/Mts phosphatase, with its regulatory subunit Widerborst, maintains NSC quiescence, preventing premature activation of InR/PI3K/Akt signaling. Conversely, an increase in Mob4 and Cka levels promotes NSC reactivation. Mob4 and Cka are essential to recruit PP2A/Mts into a complex with Hippo kinase, resulting in Hippo pathway inhibition. We propose that Mob4/Cka/Mts functions as an intrinsic molecular switch coordinating Hippo and InR/PI3K/Akt pathways and enabling NSC reactivation.**

## INTRODUCTION

Brain homeostasis and damage repair depend on the generation of new neurons and glia by neural stem cells (NSCs). In adult brains, most NSCs are found to be quiescent but can enter proliferation if prompted by extrinsic and intrinsic stimuli. The balance between quiescence and reactivation is critical for the maintenance of an NSC reservoir (Cavallucci et al., 2016; Chaker et al., 2016). Mechanistic insight underlying NSC quiescence and reactivation remains limited—in particular, how regulatory signals are integrated.

In the model organism *Drosophila*, embryonic NSCs give rise to the larval functional CNS. Similar to mammals, NSCs become quiescent at the end of embryogenesis and reactivate postembryonically to generate neurons and glia of the adult brain (Truman and Bate, 1988). Quiescence entry is regulated by Hox proteins, temporal transcription factors, and levels of the homeodomain transcription factor Prospero (Otsuki and Brand, 2019; Lai and Doe, 2014; Tsuji et al., 2008). NSCs are kept quiescent by the canonical Hippo pathway, whereby its core kinases Hippo and Warts prevent the transcriptional co-activator Yorkie from entering the nucleus and triggering growth (Ding et al., 2016; Poon et al., 2016). This signaling can be modulated by niche glia cells via the upstream regulators Crumbs and Echinoid, expressed in both glia and NSCs (Ding et al., 2016). NSC reactivation involves cell size increase, from 4 to 5 μm during quiescence, followed by entry into division (Ding et al., 2016; Chell and Brand, 2010; Prokop and Technau, 1991; Truman and Bate, 1988). NSCs continue to enlarge, reaching up to 10–15 μm when proliferating (Prokop and Technau, 1991; Truman and Bate, 1988). Nutrition stimulates reactivation (Britton and Edgar, 1998): dietary amino acids in the young larvae induce a systemic signal that triggers blood-brain barrier glia to secrete *Drosophila* insulin-like peptides (dILPs), a process that depends on gap junction proteins and synchronized calcium pulses (Spéder and Brand, 2014). dILPs activate the insulin-like receptor (InR)/phosphoinositide 3-kinase (PI3K)/Akt cascade in neighboring NSCs, promoting quiescence exit (Sousa-Nunes et al., 2011; Chell and Brand, 2010). The conserved heat shock protein 38/90 chaperone associates with InR to promote reactivation, and Spindle matrix proteins, including Chromator, function downstream of InR/PI3K/Akt signaling in this process (Huang and Wang, 2018; Li et al., 2017).

We performed a small-scale transcriptome analysis using single quiescent and reactivating NSC samples obtained directly from live *Drosophila* brains. Members of the evolutionary conserved striating-interacting phosphatase and kinase (STRIPAK) complex (Shi et al., 2016; Ribeiro et al., 2010) were identified and validated: monopolar spindle-one-binder family member 4 (Mob4); connector of kinase to AP-1 (Cka), which is

the sole *Drosophila* Striatin protein; and the catalytic subunit of protein phosphatase 2A (PP2A; *Drosophila* Microtubule Star [Mts]). STRIPAK contains multiple components, some of which are mutually exclusive, and STRIPAK members are part of a variety of regulatory proteins that can direct the pleiotropic PP2A to specific targets (Shi et al., 2016; Ribeiro et al., 2010; Virshup, 2000). In *Drosophila* and mammals, a STRIPAK-PP2A complex containing Mob4 and Cka was reported to inhibit Hippo signaling (Zheng et al., 2017; Couzens et al., 2013; Ribeiro et al., 2010). We show that PP2A/Mts, with its regulatory subunit Widerborst (Wdb), contributes to NSC quiescence via the inactivation of Akt, an essential component of the InR/PI3K/Akt signaling cascade. Conversely, NSC reactivation requires Mob4 and Cka, which are necessary within STRIPAK for Mts association to Hippo and subsequent Hippo pathway inhibition. These findings suggest a mechanism coordinating Hippo and InR/PI3K/Akt signaling in NSCs, enabling the transition from quiescence to proliferation.

## RESULTS

### Transcriptome Analysis of Reactivating NSCs: Identification of Mob4, Cka, and PP2A/Mts

To identify the mechanisms regulating NSC reactivation, we performed a small-scale analysis comparing single-cell transcriptomes of quiescent and reactivating NSCs from *Drosophila* larval brains. By combining *grh-Gal4* with *UAS-CD8-GFP* transgenic lines, cell membranes of approximately one-third of all NSCs (Chell and Brand, 2010) were specifically labeled *in vivo*. NSCs were individually harvested from 17 h after larval hatching (ALH) brains, when both quiescent (small; diameter 4–5 μm) (Ding et al., 2016; Chell and Brand, 2010) and reactivating (enlarged) cells can be easily distinguished. Of the enlarged NSCs, only non-dividing cells without any progeny were harvested. Cells were removed from the second and third thoracic segments of the ventral nerve cords (VNCs), minimizing potential differences from spatial positioning and avoiding retrieving a mix of type I and II NSCs, as the latter are absent from VNCs. Using our single-cell transcriptome protocol (Liu and Bossing, 2016; Bossing et al., 2012), cDNA from each NSC was readily obtained. Quantitative real-time PCRs confirmed that quiescent and reactivating cells expressed the NSC markers *deadpan* (*dpn*) and *asense* (*ase*), with higher levels in the latter. Single NSC transcriptomes were compared in pairs (three reactivating versus quiescent NSC pairs) on whole-genome *Drosophila* microarrays (Figure 1A). We used a limma moderated paired t test (Ritchie et al., 2015) to shortlist potential candidates, since the limited sample size did not support false discovery rate (FDR) correction. We identified 196 genes with consistent fold expression changes across all 3 replicates ($p < 0.05$), of which 145 are upregulated and 51 are downregulated (Figure 1B; Table S1; see Method Details). For quality control, we performed quantitative real-time PCR using independent single NSC samples on a subset of candidates classed mainly into *nervous system development* and *neurogenesis* Gene Ontology categories. Up- or downregulated expression for all 18 candidates tested in reactivating versus quiescent NSCs was confirmed, including *echinoid* (*ed*) and *ras homolog enriched in brain* (*rheb*), which are known to maintain NSC quiescence and promote reactivation, respectively (Ding et al., 2016; Sousa-Nunes et al., 2011) (Figures 1B and 1C).

Using FlyAtlas data (Chintapalli et al., 2007), we noted that our dataset ($p < 0.05$) is mostly enriched in genes expressed in the larval CNS, whereas among adult tissues, the highest enrichment is seen for genes expressed in ovaries, supporting reported gene sets associated with both NSC and germline stem cell maintenance and growth (Yan et al., 2014) (Figure S1A; Table S2). Most genes have highly conserved mouse (63%) and human orthologs (66%), and only 10% have no mammalian counterpart (Figure S1B; Table S1). When comparing the 175 mouse orthologs identified (single best matches) with transcripts found by previous studies as differentially expressed in quiescent versus activated mouse embryonic (Martynoga et al., 2013) or adult NSCs (Llorens-Bobadilla et al., 2015; Codega et al., 2014) and other stem cell types (Fukada et al., 2007; Venezia et al., 2004), we observed that the overlap is always highest (17–21 targets, 10%–12%) with any of the studies examining NSC transcriptomes (Figure S1C; Table S3). These results suggest that our small-scale single-cell transcriptome analysis generated high-quality data exposing conserved genes that are potentially involved in NSC reactivation. The analysis reveals transcripts encoding for some of the core STRIPAK complex members: *mob4* and *cka* upregulated in reactivating versus quiescent NSCs, whereas *mts*, encoding the catalytic subunit of PP2A, downregulated (Figures 1C and 1D; Table S1). STRIPAK is involved in a variety of cellular functions (Shi et al., 2016), but it has no known role in NSC reactivation. To functionally test the components identified, we focused initially on Mob4.

### Loss of Mob4 Prevents NSC Reactivation

Mob4 is highly expressed in the mammalian and *Drosophila* CNS (Schulte et al., 2010; Baillat et al., 2001). After validating the differential expression of *mob4* detected in NSCs (Figure 1C), we examined its protein levels. Immunostaining of NSCs highlighted with membrane-tagged GFP and Deadpan (Dpn) together with Mob4 antibodies in 17 h ALH brains, revealed higher Mob4 levels in reactivating (enlarged) versus quiescent (small) NSCs (Figures 2A–2C). To investigate the potential function of Mob4 in NSC reactivation, we first examined *mob4* null mutants ($mob4^{EY\Delta L3}$, hereafter $mob4^{\Delta L3}$), of which 10% survive to third-instar stages (Schulte et al., 2010). NSC ($Dpn^{+}$) membranes labeled with anti-Discs large (Dlg) and mitosis with anti-phospho-histone H3 (pH3) antibodies enabled the scoring of size (maximum diameters) and proliferation. In newly hatched larvae (1 h ALH), no differences are detected between NSCs of *mob4* mutants and controls in either brain lobes or VNCs (Figures 2D, 2G, 2J, S2A, S2D, and S2G). All NSCs are quiescent, with the exception of four mushroom body NSCs (MbNSCs) per brain lobe that continuously proliferate from embryonic stages (Ito and Hotta, 1992). However, as early as 4 h ALH, while NSCs in controls start to enlarge, those in *mob4* mutants remain small. No NSC mitosis re-entry is detected in either group (Figures 2E, 2H, 2J, S2B, S2E, and S2G). At the end of the first-instar larval stage (24 h ALH), when many NSCs in controls are enlarged and dividing, the reduction in both NSC size and proliferation in mutants is striking, with the only mitotic NSCs corresponding to MbNSCs

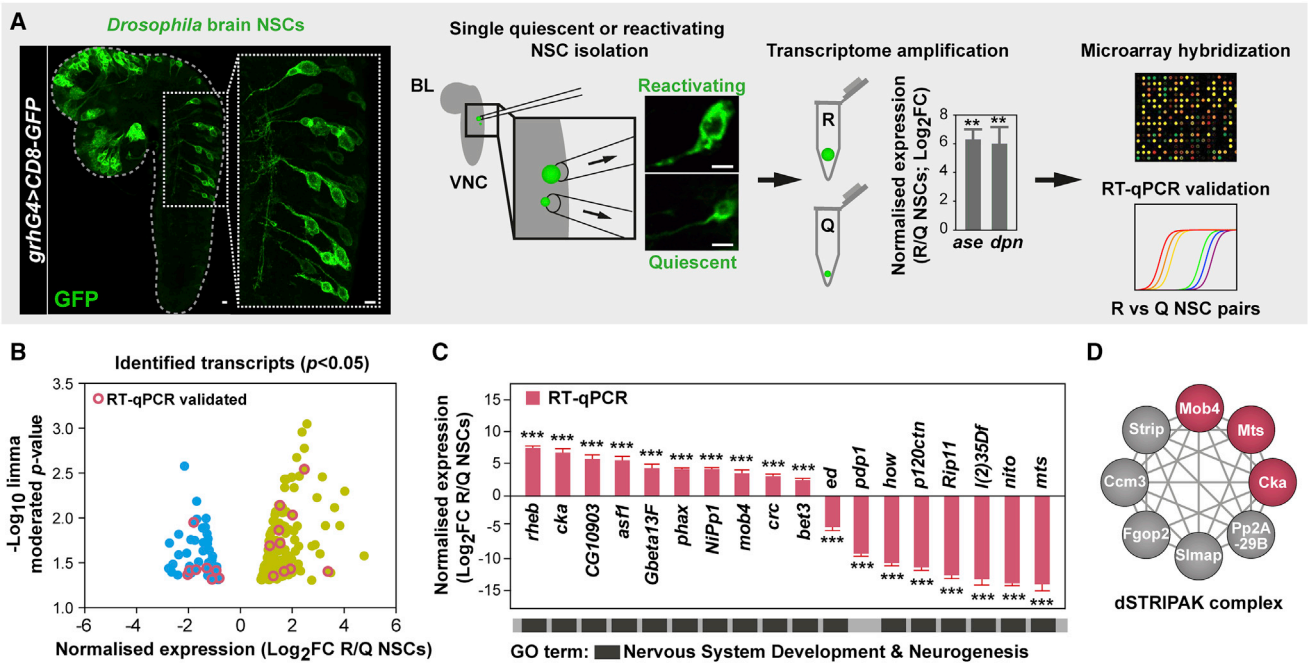


**Figure 1. Single-Cell Transcriptome Analysis of Reactivating NSCs**

(A) Workflow: individual quiescent (Q) and reactivating (R) NSCs expressing *CD8-GFP* driven by *grh-Gal4* were harvested from 17 h ALH CNSs, their mRNA reverse transcribed, and resulting cDNA amplified. Quantitative real-time PCRs confirmed higher *ase* and *dpn* expression in reactivating versus quiescent NSCs (normalized fold change [$\log_2$FC]; n = 3 NSC reactivating/quiescent pairs; error bars: SEMs; Student's t test, **p < 0.01). NSC transcriptomes were compared on whole-genome microarrays (reactivating versus quiescent; three pairs) and a subset of identified targets validated by quantitative real-time PCRs. ALH, after larval hatching; BL, brain lobe; VNC, ventral nerve cord. Scale bars: 10 μm.

(B) Distribution of identified transcripts according to average fold change expression (x axis; $\log_2$FC) and p value (y axis; limma moderated t test; $-\log_{10}$ p value; p < 0.05). See also Table S1 and Figure S1.

(C) Normalized expression levels in reactivating versus quiescent NSCs obtained by quantitative real-time PCR for a subset of targets ($\log_2$FC; n = 3 NSC reactivating/quiescent pairs; error bars: SEMs; Student's t test; ***p < 0.001). The results validate the data from the microarray analysis. Most of the targets selected are classified under "nervous system development" and "neurogenesis" GO terms.

(D) STRING-based interaction network of a *Drosophila* PP2A-STRIPAK complex reported to inhibit Hippo signaling (Zheng et al., 2017; Liu et al., 2016; Ribeiro et al., 2010), highlighting (pink) the components identified in our transcriptome analysis and functionally characterized in this study.

(Figures 2F, 2I, 2J, S2C, S2F, and S2G). 5-Ethynyl-2′-deoxyuridine (EdU) incorporation assays monitoring entry into S phase confirmed that NSCs in *mob4* CNSs are not able to re-enter the cell cycle (Figures S2H–S2J). NSC reactivation defects in *mob4* mutants were similarly observed in brain lobes and VNCs. We focused subsequent studies on brain lobes.

Since niche glial cells are involved in NSC reactivation (Sousa-Nunes et al., 2011; Chell and Brand, 2010) and Mob4 is ubiquitous in the larval CNS (Schulte et al., 2010), we next tested whether Mob4 action is cell autonomous. We ectopically expressed *mob4* specifically in NSCs or in glia of *mob4* mutants using *insc-Gal4* and *repo-Gal4* drivers, respectively. NSCs were analyzed at 18 h ALH, when mitotic reactivation is ongoing. Re-introduction of Mob4 in NSCs of *mob4* mutants rescued both NSC size growth and division to the levels observed in controls (Figures 2K–2M and 2P). We observed a small increase in NSC size and division when Mob4 was expressed from glia, but levels are markedly lower than in controls (Figures 2M–2P). Finally, we inhibited Mob4 specifically in NSCs by expressing *mob4-RNAi* (Schulte et al., 2010) using *insc-Gal4*, resulting in a significant, albeit small, reduction in NSC size and a decrease in NSC division at 18 h ALH (Figures S2K–S2M). We conclude that Mob4 functions primarily cell autonomously to promote NSC reactivation.

## Overexpression of Mob4 or Its Human Ortholog Accelerates NSC Reactivation

Mob4 is highly conserved (78% identical at the amino acid level) to its human ortholog MOB4 (hMOB4, also known as Phocein), and ubiquitous expression of *hMOB4* fully rescues the lethality of *mob4* null larvae (Schulte et al., 2010). To determine whether increasing Mob4 or hMOB4 levels can promote NSC reactivation, we overexpressed these specifically in NSCs using *insc-Gal4*. Simultaneous expression of membrane-tagged GFP allowed for NSC size examination, and divisions were labeled with pH3 antibodies. At 6 h ALH, NSCs in controls have yet to re-enter mitosis. At this stage, Mob4 or hMOB4 overexpression results in a premature NSC size increase. No re-entry into division was seen upon Mob4 overexpression, but hMOB4 induced a minor but significant increase (Figures 3A–3C and 3G). At 18 h ALH, no difference in NSC size was detected upon Mob4 overexpression, but more NSCs were found in mitosis compared to

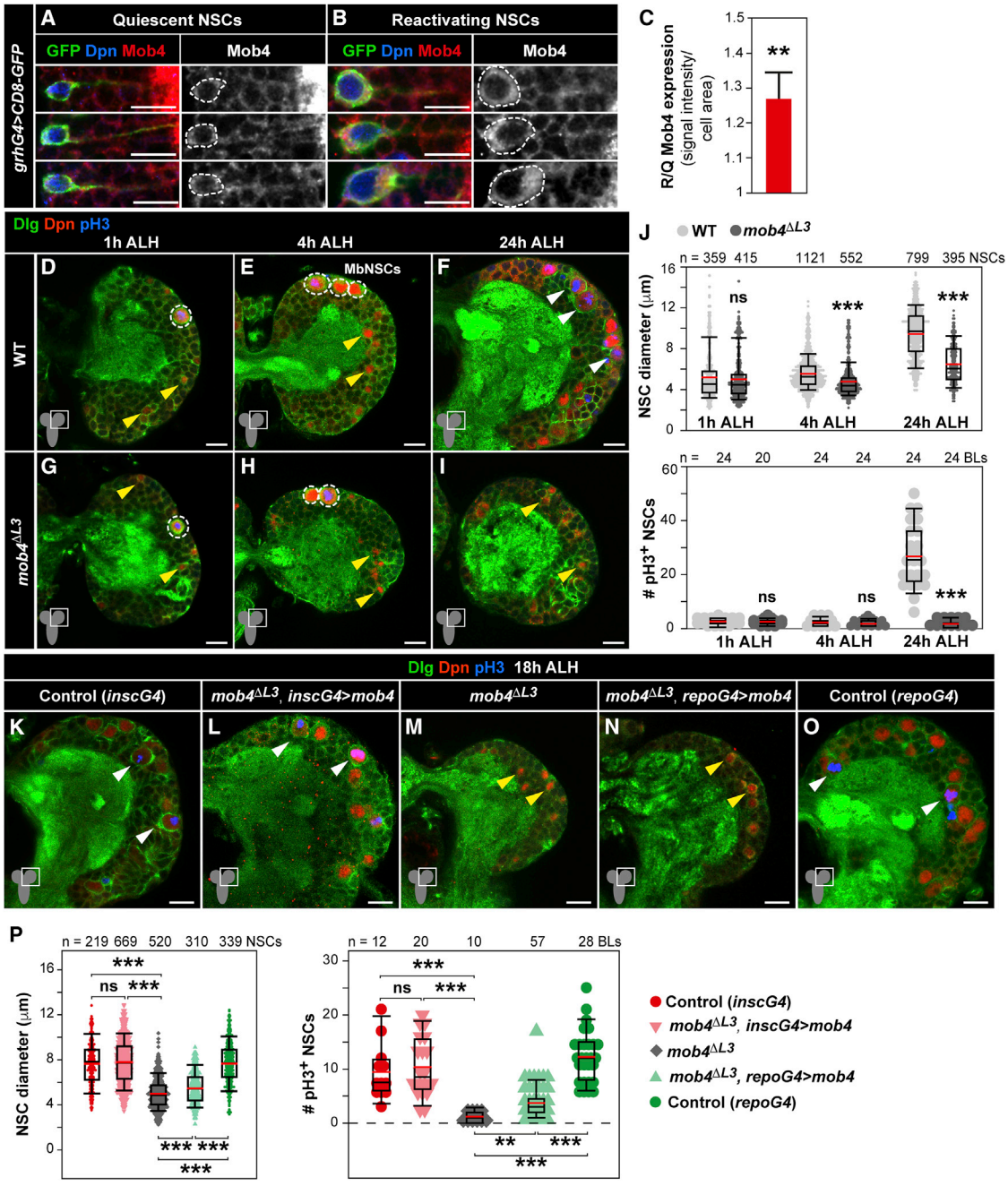


**Figure 2. Loss of Mob4 Prevents NSC Mitotic Reactivation**

(A–C) Mob4 is upregulated in reactivating versus quiescent NSCs. Examples of quiescent (small, A) and reactivating (enlarged, B) NSCs in 17 h ALH CNSs (VNC thoracic region) labeled with *grh-Gal4* driving *CD8-GFP* (GFP, green), Mob4 (red), and Dpn (blue). Mob4 channel also shown in monochrome. Dashed lines: cell bodies. (C) Mob4 protein quantification in reactivating normalized to quiescent NSCs (reactivating NSCs: n = 50, 8 BLs, 8 brains; quiescent NSCs: n = 50, 8 BLs, 8 brains; error bars: SEMs).

(D–J) NSC enlargement and division are impaired in *mob4*$^{\Delta L3}$ mutants. Wild-type (WT; D, 1 h ALH; E, 4 h ALH; F, 24 h ALH) and *mob4*$^{\Delta L3}$ brain lobes (G, 1 h ALH; H, 4 h ALH; I, 24 h ALH). NSCs (Dpn, red), cell membranes (Dlg, green), and divisions (pH3, blue). Yellow arrowheads: quiescent NSCs; white arrowheads: reactivated NSCs. Mushroom body NSCs (MbNSCs; dashed circles) are large and do not enter quiescence. At 1 and 4 h ALH, there are no NSC divisions, except in MbNSCs.

(J) Quantification of NSC diameters (1 h ALH: WT n = 359 NSCs, 10 BLs, 5 brains; *mob4*$^{\Delta L3}$ n = 415 NSCs, 10 BLs, 7 brains; 4 h ALH: WT n = 1,121 NSCs, 14 BLs, 7 brains; *mob4*$^{\Delta L3}$ n = 552 NSCs, 10 BLs, 5 brains; 24 h ALH: WT n = 799 NSCs, 10 BLs, 7 brains; *mob4*$^{\Delta L3}$ n = 395 NSCs, 18 BLs, 9 brains) and proliferation (1 h ALH: WT n = 24 BLs, 12 brains; *mob4*$^{\Delta L3}$ n = 20 BLs, 12 brains; 4 h ALH: WT n = 24 BLs, 12 brains; *mob4*$^{\Delta L3}$ n = 24 BLs, 12 brains; 24 h ALH: WT n = 24 BLs, 12 brains; *mob4*$^{\Delta L3}$ n = 24 BLs, 12 brains).

*(legend continued on next page)*

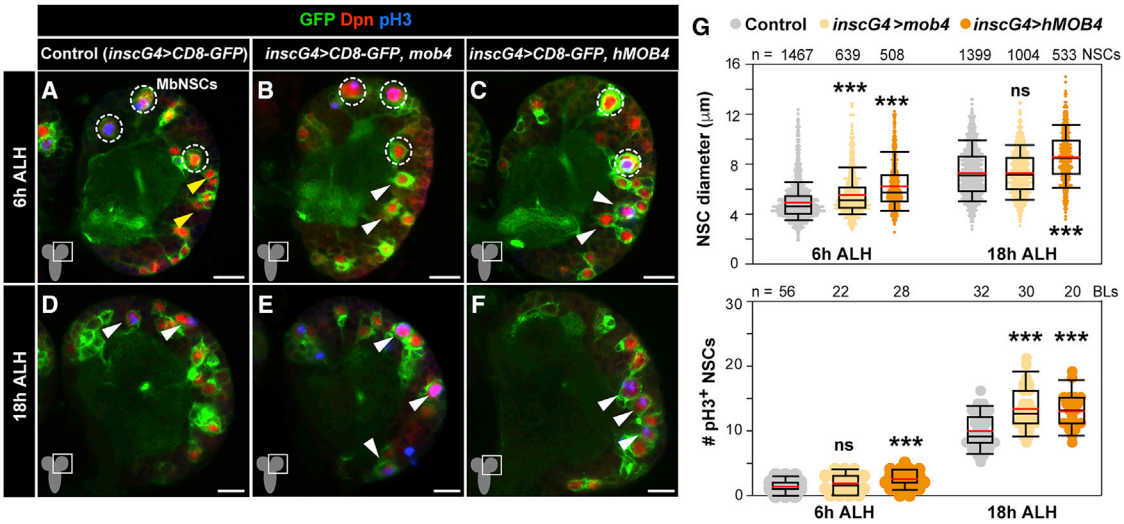


**Figure 3. Overexpression of Mob4 or hMOB4 Increases NSC Growth and Division**

(A–G) NSC-specific *mob4* or human *MOB4* (*hMOB4*) overexpression leads to premature NSC enlargement and mitosis entry. Brain lobes of control (A and D, *insc-gal4 > CD8-GFP*) and *mob4* (B and E, *insc-gal4 > CD8-GFP, mob4*) or *hMOB4* (C and F, *insc-gal4 > CD8-GFP, hMOB4*) overexpressing brains at 6 and 18 h ALH. NSCs in green (GFP) and red (Dpn), and divisions in blue (pH3). Dashed circles: MbNSCs; yellow arrowheads: quiescent NSC examples; white arrowheads: prematurely enlarging (B and C) and dividing NSC examples (D–F). Anterior up. Scale bars: 10 μm.

(G) Quantification of NSC diameters (6 h ALH: *insc-gal4 > CD8-GFP* n = 1,467 NSCs, 20 BLs, 15 brains; *insc-gal4 > CD8-GFP, mob4* n = 639 NSCs, 10 BLs, 5 brains; *insc-gal4 > CD8-GFP, hMOB4* n = 508 NSCs, 7 BLs, 5 brains; 18 h ALH: *insc-gal4 > CD8-GFP* n = 1,399 NSCs, 18 BLs, 15 brains; *insc-gal4 > CD8-GFP, mob4* n = 1,004 NSCs, 13 BLs, 9 brains; *insc-gal4 > CD8-GFP, hMOB4* n = 533 NSCs, 7 BLs, 5 brains) and proliferation (6 h ALH: *insc-gal4 > CD8-GFP* n = 56 BLs, 28 brains; *insc-gal4 > CD8-GFP, mob4* n = 22 BLs, 11 brains; *insc-gal4 > CD8-GFP, hMOB4* n = 28 BLs, 14 brains; 18 h ALH: *insc-gal4 > CD8-GFP* n = 32 BLs, 16 brains; *insc-gal4 > CD8-GFP, mob4* n = 30 BLs, 15 brains; *insc-gal4 > CD8-GFP, hMOB4* n = 20 BLs, 10 brains).

Wilcoxon rank-sum tests; ***p < 0.001; p > 0.05: ns.

See also Figure S3.

controls. hMOB4 ectopic expression increased NSC size and induced a similar increase in the number of dividing NSCs as seen upon Mob4 overexpression (Figures 3D–3G). We next tested whether Mob4 overexpression leads to NSC overproliferation. Scoring of NSC divisions in late larval brain lobes (94 h ALH) revealed no differences from controls, indicating that Mob4 overexpression effects are restricted to the NSC reactivation process (Figures S3A–S3C). Finally, since NSC reactivation depends on nutritional stimulus (Britton and Edgar, 1998), we inquired as to whether Mob4 overexpression in NSCs could induce reactivation under diet-restriction conditions. In larvae reared in the absence of dietary amino acids, NSCs overexpressing Mob4 remained quiescent (Figures S3D–S3F). We conclude that increased Mob4 levels accelerate NSC reactivation, and this function may be evolutionary conserved. Yet, Mob4 is not sufficient to bypass the extrinsic nutrition stimulus required for NSC reactivation.

## Mob4 Regulates InR/PI3K/Akt and Hippo Signaling Activity in NSCs

The Hippo pathway maintains NSCs in quiescence (Ding et al., 2016; Poon et al., 2016), whereas activation of InR/PI3K/Akt signaling cascade triggers reactivation (Sousa-Nunes et al., 2011; Chell and Brand, 2010). To assess how Mob4 function relates to both pathways, we first examined their activity in the absence of Mob4. Upon activation, insulin receptors recruit PI3K to the cell membrane to convert phosphoinositol(4,5)P2 (PIP2) into phosphoinositol(3,4,5)P3 (PIP3), which in turn recruits the Akt protein kinase through its pleckstrin homology (PH) domain, becoming activated by phosphorylation. This process can be monitored using a PH domain-GFP fusion protein (PH-GFP) binding PIP3 (Britton et al., 2002). We confirmed strong membrane-bound accumulation of PH-GFP in reactivated NSCs (Figures 4A and 4A') (Chell and Brand, 2010). In contrast, NSCs in *mob4* mutants show weak and diffused PH-GFP signals

(K–P) Mob4 expression in NSCs, but not in glia, rescues NSC reactivation in $mob4^{\Delta L3}$ mutants to control levels. Brain lobes of control (K, *insc-gal4*), $mob4^{\Delta L3}$ expressing Mob4 in NSCs (L, $mob4^{\Delta L3}$, *insc-gal4 > mob4*), $mob4^{\Delta L3}$ (M), $mob4^{\Delta L3}$ expressing Mob4 in glia (N, $mob4^{\Delta L3}$, *repo-gal4 > mob4*), and control (O, *repo-gal4*) at 18 h ALH.

(P) Quantification of NSC diameters (*insc-gal4* n = 219 NSCs, 3 BLs, 3 brains; $mob4^{\Delta L3}$, *insc-gal4* > mob4 n = 669, 10 BLs, 5 brains; $mob4^{\Delta L3}$ n = 520 NSCs, 7 BLs, 7 brains; $mob4^{\Delta L3}$, *repo-gal4 > mob4* n = 310 NSCs, 6 BLs, 6 brains; *repo-gal4* n = 339, 5 BLs, 5 brains) and proliferation (*insc-gal4* n = 12 BLs, 12 brains; $mob4^{\Delta L3}$, *insc-gal4* > mob4 n = 20 BLs, 10 brains; $mob4^{\Delta L3}$ n = 10 BLs, 10 brains; $mob4^{\Delta L3}$, *repo-gal4 > mob4* n = 57 BLs, 29 brains; *repo-gal4* n = 28 BLs, 14 brains) at 18 h ALH.

Wilcoxon rank-sum tests; **p < 0.01, ***p < 0.001; p > 0.05: non-significant (ns). BLs, brain lobes. Anterior up. Scale bars: 10 μm.

See also Figure S2.

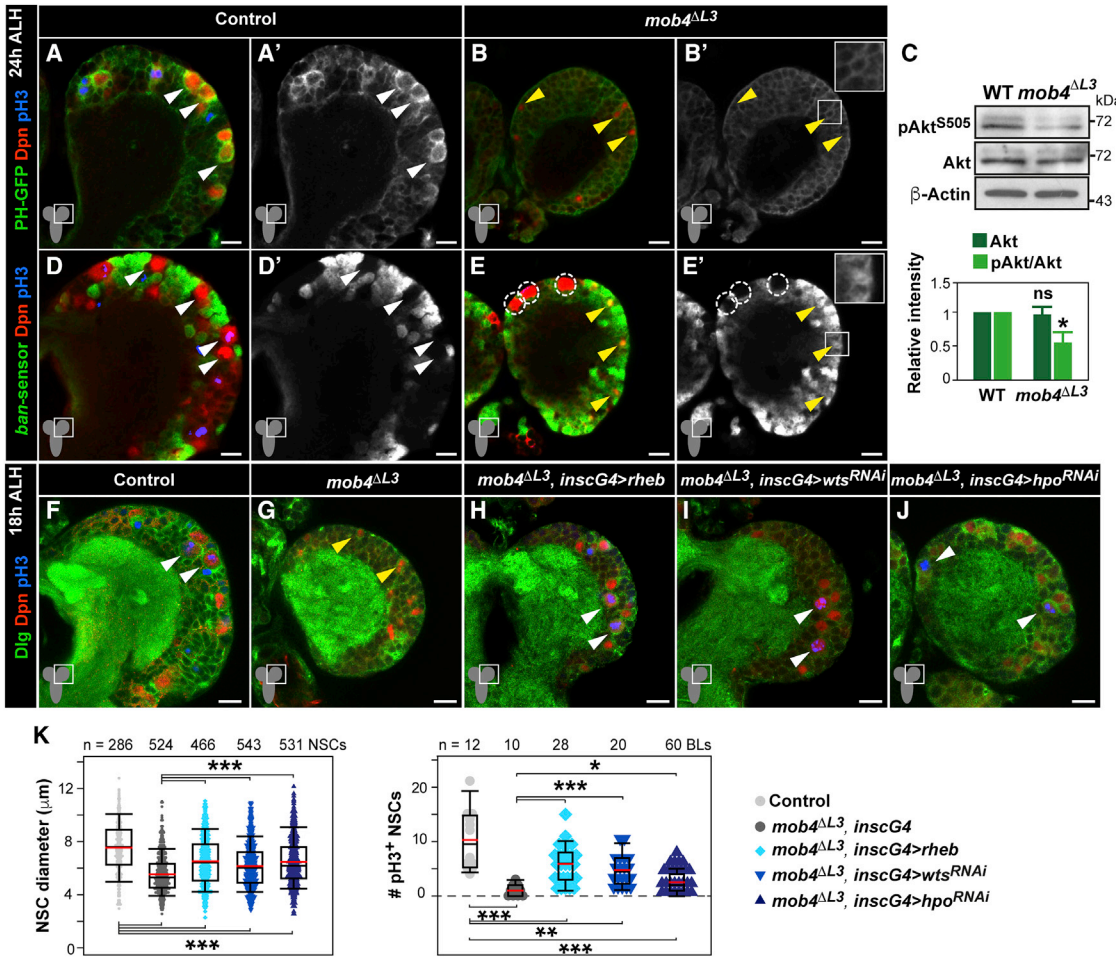


**Figure 4. InR/PI3K/Akt Pathway Activation or Hippo Signaling Inhibition Rescues NSC Reactivation in *mob4* Mutants**

(A–C) InR/PI3K/Akt signaling is strongly reduced in *mob4* NSCs. Expression of pleckstrin homology (PH) domain-GFP fusion (GFP, green) does not accumulate at NSC membranes of *mob4* mutants as in controls. Brain lobes of control (A) and *mob4*$^{\Delta L3}$ mutants (B) at 24 h ALH. NSCs in red (Dpn) and divisions in blue (pH3). GFP channel also shown in monochrome (A' and B'). Inset displays higher magnification (B'). Yellow arrowheads: quiescent NSC examples; white arrowheads: reactivated NSC examples.

(C) Phospho-Akt (pAkt$^{S505}$) is reduced in *mob4* mutant brains, while total Akt levels are comparable to those in controls (24 h ALH brain extracts; β-actin: loading control). Quantification of protein signals (bottom; error bars: SEMs; n = 3 independent assays; Student's t tests; *p < 0.05; p > 0.05: ns.

(D–E') Hippo signaling remains active in *mob4* NSCs. In contrast to controls, NSCs in *mob4* mutants show no *ban* activity, except in MbNSCs (dashed circles). *ban*-activity sensor, in which decreased GFP signal (green) reflects increased *ban* activity, in brain lobes of control (D and D') and *mob4*$^{\Delta L3}$ mutants (E and E') at 24 h ALH. NSCs in red (Dpn) and divisions in blue (pH3). GFP channel also shown in monochrome (D' and E'). Inset showing higher magnification (E').

(F–K) NSC-specific expression of *rheb* activating InR/PI3K/Akt signaling and of *warts (wts)*-RNAi or *hippo (hpo)*-RNAi inactivating Hippo signaling can rescue NSC reactivation in *mob4* mutants. Brain lobes of control (F, *insc-gal4*), *mob4*$^{\Delta L3}$ (G), *mob4*$^{\Delta L3}$ expressing Rheb in NSCs (H, *mob4*$^{\Delta L3}$, *insc-gal4* > *rheb*), *mob4*$^{\Delta L3}$ expressing *wts*-RNAi in NSCs (I, *mob4*$^{\Delta L3}$, *insc-gal4* > *wts*$^{RNAi}$), and *mob4*$^{\Delta L3}$ expressing *hpo*-RNAi in NSCs (J, *mob4*$^{\Delta L3}$, *insc-gal4* > *hpo*$^{RNAi}$) at 18 h ALH. NSCs in red (Dpn), cell membranes in green (Dlg), and divisions in blue (pH3). Anterior up. Scale bars: 10 μm and 17 μm in insets.

(K) Quantification of NSC diameters (*insc-gal4* n = 286 NSCs, 4 BLs, 3 brains; *mob4*$^{\Delta L3}$ n = 524 NSCs, 7 BLs, 7 brains; *mob4*$^{\Delta L3}$, *insc-gal4* > *rheb* n = 466 NSCs, 6 BLs, 5 brains; *mob4*$^{\Delta L3}$, *insc-gal4* > *wts*$^{RNAi}$ n = 543 NSCs, 8 BLs, 5 brains; *mob4*$^{\Delta L3}$, *insc-gal4* > *hpo*$^{RNAi}$ n = 531 NSCs, 8 BLs, 5 brains) and divisions (*insc-gal4* n = 12 BLs, 12 brains; *mob4*$^{\Delta L3}$ n = 10 BLs, 10 brains; *mob4*$^{\Delta L3}$, *insc-gal4* > *rheb* n = 28 BLs, 14 brains; *mob4*$^{\Delta L3}$; *insc-gal4* > *wts*$^{RNAi}$ n = 20 BLs, 10 brains; *mob4*$^{\Delta L3}$, *insc-gal4* > *hpo*$^{RNAi}$ n = 60 BLs, 30 brains).

Wilcoxon rank-sum tests; *p < 0.05, **p < 0.01, ***p < 0.001.

(Figures 4B and 4B'). We also observed reduced phosphorylated Akt levels in *mob4* whole CNS lysates compared to controls, whereas total Akt levels were equivalent (Figure 4C). To examine Hippo signaling, we tested the activity of *bantam* (*ban*) microRNA that promotes NSC size growth and division (Ding et al., 2016). In quiescent NSCs, active Hippo signaling prevents *ban* transcription (Ding et al., 2016). We used a *ban* GFP-sensor system, in which GFP signal reduction reflects an increase in *ban* activity (Brennecke et al., 2003). No GFP is observed in control reactivated NSCs demonstrating *ban* activity (Ding et al., 2016) (Figures 4D and 4D'). However, the GFP signal is detected in the NSCs of *mob4* mutants, indicating the absence of *ban* activity

and Hippo pathway activation (Figures 4E and 4E'). We next tested whether activating InR/PI3K/Akt cascade or inhibiting Hippo pathways in the NSCs of *mob4* mutants could rescue reactivation defects. Stimulation of target of rapamycin (TOR) signaling by Rheb overexpression activates the InR/PI3K/Akt cascade, promoting premature NSC exit from quiescence (Li et al., 2017; Sousa-Nunes et al., 2011). Overexpressing Rheb in the NSCs of *mob4* mutants led to NSC size increase and division re-entry (Figures 4F–4H, and 4K). To inhibit Hippo signaling, we used RNAi against *warts* (*wts*) or *hippo*, which induce earlier NSC reactivation (Ding et al., 2016). In *mob4* brains, expression of *wts*-RNAi or *hippo*-RNAi in NSCs induced cell size growth and mitosis re-entry (Figures 4F, 4G, and 4I–4K). We conclude that the InR/PI3K/Akt signaling cascade is inhibited, while the Hippo pathway stays active in NSCs upon the loss of Mob4, consistent with NSCs in *mob4* mutants being unable to exit quiescence. Activation of InR/PI3K/Akt or inhibition of Hippo pathways can restore reactivation. However, the rescues are partial, with the NSC size and proliferation increase observed in *mob4* mutant brains not reaching control levels (Figures 4F–4K). The results contrast with the effect of expressing *rheb*, *hippo-RNAi*, or *wts-RNAi* in a control background, where NSC growth and division surpass control levels (Li et al., 2017; Ding et al., 2016; Sousa-Nunes et al., 2011) and may also reflect insufficient activation or inactivation of the respective signals and/or regulation of both pathways that are essential for effective NSC reactivation.

## Mob4 and Cka Cooperate to Reactivate NSCs and Assemble a PP2A-Hippo Complex

Our analysis of single NSC transcriptomes also identified the STRIPAK scaffold protein Cka, which is expressed throughout the CNS (Shi et al., 2016; Chen et al., 2002). Similar to Mob4, we found *cka* transcript and protein upregulated in reactivating versus quiescent NSCs (Figures 1C and S4A–S4C). To examine its function, we overexpressed Cka specifically in NSCs and observed premature NSC enlargement at 6 h ALH (Figures 5A, 5B, and 5G), as well as increased NSC size and divisions at 18 h ALH (Figures 5D, 5E, and 5G). Conversely, the expression of *cka*-RNAi resulted in a small but significant reduction in NSC size and decreased NSC mitosis at 18 h ALH (Figures S4D–S4F). Next, we simultaneously overexpressed Mob4 and Cka in NSCs and observed stronger effects compared to those upon single Mob4 or Cka overexpression (Figures 5A–5G; see also Figures 3B, 3E, and 3G).

STRIPAK negatively regulates Hippo signaling via the dephosphorylation of Hippo kinase by PP2A phosphatase (Couzens et al., 2013; Ribeiro et al., 2010). We examined whether the STRIPAK components Mob4 and Cka are essential for mediating the association of PP2A to Hippo. Co-immunoprecipitations (coIPs) were conducted on S2R$^{+}$ cell lysates expressing FLAG-tagged Hippo or control FLAG-NTAN, plus Myc-tagged Mts. In addition, we performed RNAi targeting *mob4* and/or *cka,* which effectively depletes the respective proteins (Figure S5A), using RNAi as a control against *DsRed* targeting red fluorescent protein. FLAG-Hippo co-immunoprecipitates Myc-Mts, as reported (Ribeiro et al., 2010), and no association is found with FLAG-NTAN. However, depletion of Mob4, Cka, or both impairs Hippo/Mts binding, with the latter nearly abolishing association (Figures 5H and 5I). We verified that the inhibition of Mob4 and Cka results in increased Hippo activation, as reported (Zheng et al., 2017; Ribeiro et al., 2010), and that chemical inhibition of PP2A with okadaic acid targeting PP2A, and to a lesser extent PP1 (Takai et al., 1992), leads to Hippo hyperphosphorylation as a positive control (Figure S5B). We conclude that Mob4 and Cka cooperate to promote NSC reactivation and are both required for the association of PP2A to Hippo, leading to its inactivation, which is consistent with the Hippo pathway remaining active in NSCs upon *mob4* loss (Figures 4D–4E').

## PP2A Inactivates Akt Independently of STRIPAK Cka and Mob4 Members and Maintains Quiescent NSCs

If PP2A/Mts would only function in NSCs to inactivate Hippo signaling via STRIPAK, then a prolonged NSC quiescence could be anticipated upon Mts inhibition. However, PP2A is also a well-established negative regulator of the insulin receptor signaling cascade, including by the dephosphorylation of Akt (Padmanabhan et al., 2009; Vereshchagina et al., 2008; Janssens and Goris, 2001). Using S2R$^{+}$ cells, we observed that Mts inhibition with okadaic acid increases Akt phosphorylation, regardless of RNAi-mediated depletion of *cka* and *mob4* (Figure S6A). In addition, in S2R$^{+}$ cells expressing hemagglutinin (HA)-tagged Mts and Myc-tagged Akt, Mts co-immunoprecipitates with Akt. However, unlike for Mts/Hippo interaction, the depletion of *cka* and *mob4* does not disturb Mts/Akt association, nor does it disturb the levels of phosphorylated Akt with or without insulin stimulation (Figures S6A–S6C). Next, we examined whether impaired Mts function affects NSC reactivation. Since *mts* null mutants ($mts^{XE\text{-}2258}$) are embryonic lethal (Snaith et al., 1996), we analyzed transheterozygotes harboring an *mts* hypomorphic allele surviving to pupal stages ($mts^{299}$) (Wang et al., 2009) and $mts^{XE\text{-}2258}$. Reactivating NSCs in $mts^{299}/mts^{XE\text{-}2258}$ mutants shows a mild increased cell size as compared to controls (Figures 6A–6C). To knock down *mts* specifically in NSCs, we expressed a dominant-negative *mts* mutant (*mts*-DN) lacking the N-terminal region of the phosphatase domain (Hannus et al., 2002). Premature NSC size increase and entry into division were observed (Figures 6D, 6E, 6G, 6H, and 6J), strengthening the results using *mts* transheterozygotes. We then examined whether the regulatory PP2A subunit Wdb, shown to modulate Akt downstream of InR/PI3K/Akt signaling in both vertebrates and invertebrates (Rodgers et al., 2011; Padmanabhan et al., 2009; Vereshchagina et al., 2008), may also function in NSCs. Similar to *mts-DN*, expression of a truncated *wdb* mutant form acting as a dominant negative (*wdb*-DN) (Hannus et al., 2002) leads to increased NSC size growth at 6 h ALH and a higher number of mitotic NSCs at 18 h ALH (Figures 6D, 6F, 6G, 6I, and 6J). Next, we ascertained whether PP2A/Mts inhibition affects pAkt levels. A premature increase in pAkt is seen in NSCs expressing *mts*-DN, which indicates abnormal InR/PI3K/Akt activation (Figures 6K–6L'). In this condition, a moderate but significant reduction of *ban* activity (indicated by *ban*-GFP sensor signal increase) is also observed (Figures 6M–6O). The results suggest that the inhibition of Mts can promote Hippo signaling activity in NSCs, but the effect is insufficient, possibly due to the availability of endogenous Mob4/Cka levels at this stage, or otherwise

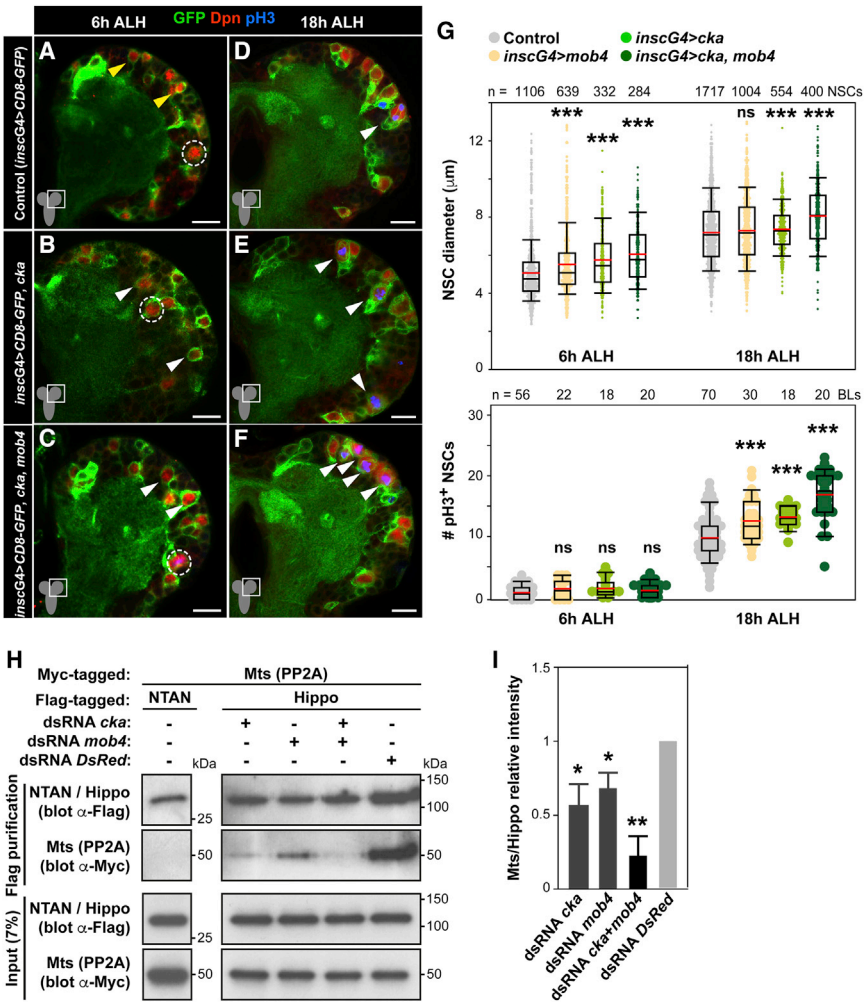


**Figure 5. Cka and Mob4 Cooperate to Promote NSC Reactivation and Are Required for PP2A/Hippo Interaction**

(A–G) NSC-specific *cka* or *cka* and *mob4* double overexpression leads to premature enlargement and increased mitotic NSCs. Double overexpression results in stronger effects (see also Figure 3). Brain lobes of control (A and D, *insc-gal4 > CD8-GFP*), *cka* (B and E, *insc-gal4 > CD8-GFP, cka*), and double *cka* and *mob4* (C and F, *insc-gal4 > CD8-GFP, cka, mob4*) overexpressing brains at 6 and 18 h ALH. NSCs in green (GFP) and red (Dpn), and divisions in blue (pH3). Dashed circles: MbNSCs; yellow arrowheads: quiescent NSCs; white arrowheads: prematurely enlarging (B and C) and dividing NSCs (D–F). Anterior up. Scale bars: 10 µm.

(G) Quantification of NSC diameters (6 h ALH: *insc-gal4 > CD8-GFP* n = 1,106 NSCs, 15 BLs, 10 brains; *insc-gal4 > CD8-GFP, mob4* n = 639 NSCs, 10 BLs, 5 brains; *insc-gal4 > CD8-GFP, cka* n = 332 NSCs, 5 BLs, 5 brains; *insc-gal4 > CD8-GFP, cka, mob4* n = 284 NSCs, 8 BLs, 8 brains; 18 h ALH: *insc-gal4 > CD8-GFP* n = 1,717 NSCs, 19 BLs, 14 brains; *insc-gal4 > CD8-GFP, mob4* n = 1,004 NSCs, 13 BLs, 9 brains; *insc-gal4 > CD8-GFP, cka* n = 554 NSCs, 8 BLs, 4 brains; *insc-gal4 > CD8-GFP, cka, mob4* n = 400 NSCs, 6 BLs, 4 brains) and divisions (6 h ALH: *insc-gal4 > CD8-GFP* n = 56 BLs, 28 brains; *insc-gal4 > CD8-GFP, mob4* n = 22 BLs, 11 brains; *insc-gal4 > CD8-GFP, cka* n = 18 BLs, 9 brains; *insc-gal4 > CD8-GFP, cka, mob4* n = 20 BLs, 10 brains; 18 h ALH: *insc-gal4>CD8-GFP* n = 70 BLs, 38 brains; *insc-gal4 > CD8-GFP, mob4* n = 30 BLs, 15 brains; *insc-gal4 > CD8-GFP, cka* n = 18 BLs, 9 brains; *insc-gal4 > CD8-GFP, cka, mob4* n = 20 BLs, 10 brains). Wilcoxon rank-sum tests, ***p < 0.001; p > 0.05: ns. See also Figure S4.

(H and I) Depletion of Mob4 and/or Cka inhibits PP2A/Mts association to Hippo.

(H) CoIP assays using S2R$^+$ cells expressing Myc-Mts and FLAG-Hippo or control FLAG-NTAN, in addition to RNAi against *mob4* and/or *cka* or control *DsRed* (see also Figure S5). Lysates and FLAG-purified immunoprecipitates analyzed by western blot with indicated antibodies.

(I) Quantification of relative binding of Myc-Mts to FLAG-Hippo shown as a mean of the ratio between Myc-Mts and FLAG-Hippo signal intensities relative to control (*DsRed* RNAi) levels (n = 3 independent assays; error bars: SEMs; Student's t tests; *p < 0.05 and **p < 0.01).

dominated by InR/PI3K/AKT activation, with the final outcome being premature NSC reactivation. Our data indicate that PP2A/Mts may play a dual role in early postembryonic NSCs: first with Wdb to target Akt contributing to quiescence maintenance and second with STRIPAK components Mob4 and Cka targeting Hippo signaling to promote reactivation (Figure 6P).

## DISCUSSION

Neural replenishment depends on the ability of NSCs to tightly control the balance between quiescence and proliferation (Tian et al., 2018; Chaker et al., 2016; Cheung and Rando, 2013). Recent advances in profiling quiescent and activated NSCs are increasing our understanding of these cell states. Most approaches have relied on brain tissue dissociation, cell sorting, and culturing procedures (Llorens-Bobadilla et al., 2015; Codega et al., 2014; Martynoga et al., 2013). Here, we reveal a transcript profile of single quiescent versus reactivating NSC samples obtained directly from live brains. The analysis of identified individual cells taken directly from living tissues at desired time points allows us to precisely examine the transcriptional control at the crossroads of crucial cell fates. Due likely to the reduced sample number and single-cell cDNA amplification variability (Tung et al., 2017; Macaulay and Voet, 2014) (Pearson's r correlations obtained: quiescent NSCs 0.75 < r < 0.81, mean: 0.77; reactivating NSCs 0.58 < r < 0.67, mean: 0.61), our analysis did not support FDR correction. However, the identified genes meeting significance (limma moderated t test, p < 0.05) show consistent expression changes across replicates, and the regulation of all of the targets tested was independently validated. The high conservation with mammalian genes and partial overlap with orthologs reported to be differentially expressed in mouse quiescent versus activated NSCs suggest that our dataset is also a valuable resource for mammalian NSC research.

Adult NSCs must orchestrate extrinsic signals according to the organism's status with intrinsic factors to transit between

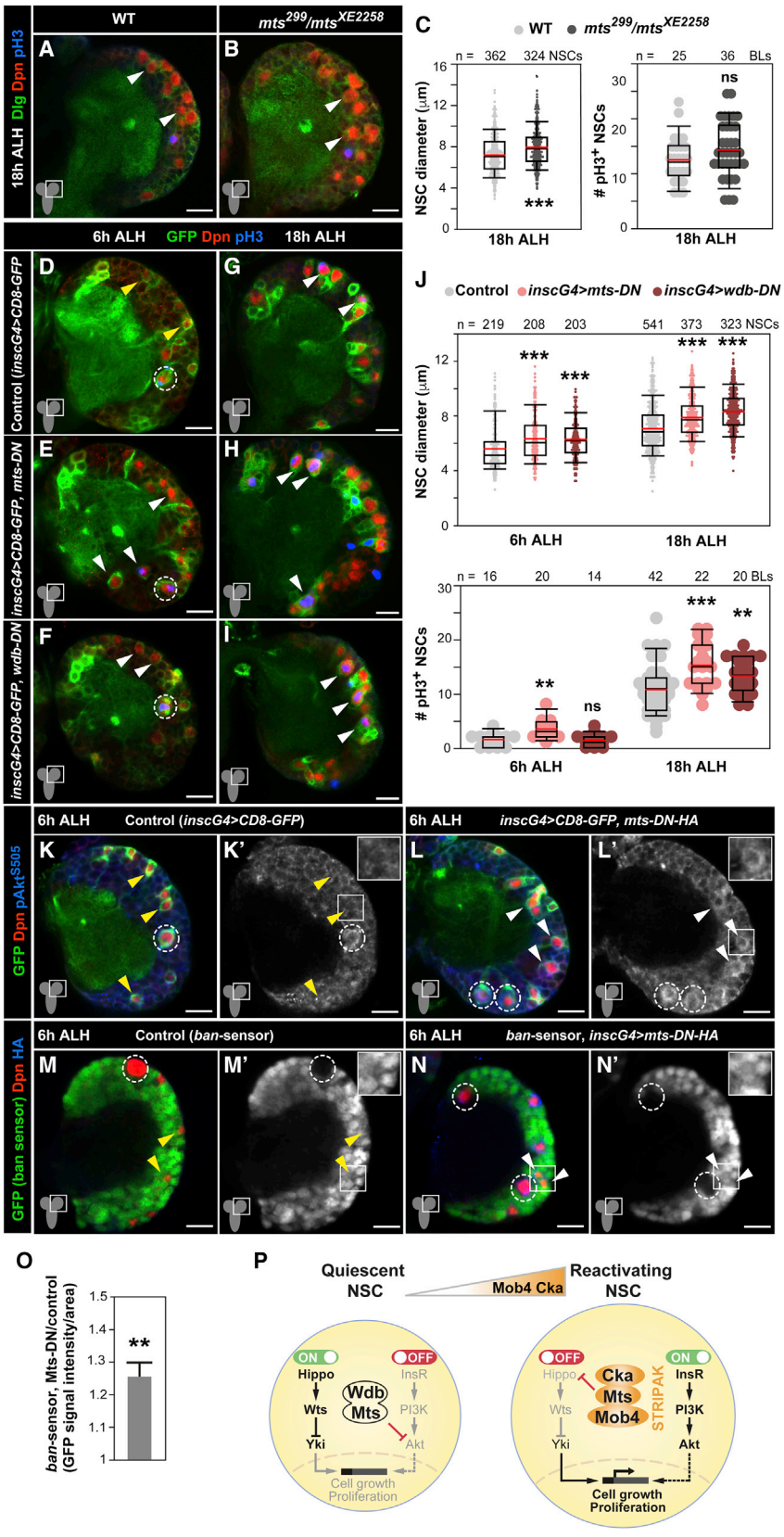


**Figure 6. Inactivation of PP2A Phosphatase Results in Premature NSC Reactivation**

(A–C) *PP2A/mts* hypomorphic mutants show premature NSC size growth. Brain lobes of WT (A) and $mts^{299}/mts^{XE2258}$ mutants (B) at 18 h ALH. NSCs in red (Dpn), cell membranes in green (Dlg), and divisions in blue (pH3). Arrowheads: NSC examples.

(C) Quantification of NSC diameters (WT n = 362 NSCs, 5 BLs, 3 brains; $mts^{299}/mts^{XE2258}$ n = 324 NSCs, 6 BLs, 5 brains) and divisions (WT n = 25 BLs, 13 brains; $mts^{299}/mts^{XE2258}$ n = 36 BLs, 27 brains). Wilcoxon rank-sum tests; ***p < 0.001; p > 0.05: ns.

(D–J) NSC-specific expression of dominant-negative (DN) forms of PP2A catalytic subunit Mts or regulatory subunit Wdb results in premature NSC size growth and an increased number of mitotically reactivated NSCs. Brain lobes of control (D and G, *insc-gal4 > CD8-GFP*), *mts-DN* (E and H, *insc-gal4 > CD8-GFP, mts-DN*), and *wdb-DN* (F and I, *insc-gal4 > CD8-GFP, wdb-DN*) expressing brains at 6 and 18 h ALH. NSC in green (GFP) and red (Dpn), and divisions in blue (pH3). Dashed circles: MbNSCs; yellow arrowheads: quiescent NSC examples; white arrowheads: prematurely enlarging (E and F) and mitotically reactivated NSCs (G–I).

(J) Quantification of NSC diameters (6 h ALH: *insc-gal4 > CD8-GFP* n = 219 NSCs, 5 BLs, 5 brains; *insc-gal4 > wdb-DN* n = 208 NSCs, 5 BLs, 5 brains; *insc-gal4 > mts-DN* n = 203 NSCs, 5 BLs, 5 brains; 18 h ALH: *insc-gal4 > CD8-GFP* n = 541 NSCs, 8 BLs, 5 brains; *insc-gal4 > CD8-GFP, wdb-DN* n = 373 NSCs, 5 BLs, 5 brains; *insc-gal4 > CD8-GFP, mts-DN* n = 323 NSCs, 5 BLs, 5 brains) and divisions (6 h ALH: *insc-gal4 > CD8-GFP* n = 16 BLs, 8 brains; *insc-gal4 > CD8-GFP, wdb-DN* n = 20 BLs, 10 brains; *insc-gal4 > CD8-GFP, mts-DN* n = 14 BLs, 7 brains; 18 h ALH: *insc-gal4 > CD8-GFP* n = 42 BLs, 21 brains; *insc-gal4 > CD8-GFP, wdb-DN* n = 22 BLs, 12 brains; *insc-gal4 > CD8-GFP, mts-DN* n = 20 BLs, 10 brains). Wilcoxon rank-sum tests; **p < 0.01, ***p < 0.001; p > 0.05: ns.

(K–O) NSC-specific expression of *mts-DN* results in the increased expression of phosphorylated Akt, as well as a decrease in *ban* activity. (K–L') Brain lobes of control (K and K', *insc-gal4 > CD8-GFP*) and *mts-DN* (L and L', *insc-gal4 > CD8-GFP, mts-DN*) expressing brains at 6 h ALH. NSCs in green (GFP) and red (Dpn), and $pAkt^{S505}$ (blue). $pAkt^{S505}$ also shown in monochrome; insets showing higher magnifications (K' and L').

(M–O) *ban*-activity sensor, in which a decrease in GFP signal (green) reflects an increase in *ban* activity, in brain lobes of control (M and M') and *mts-DN* expressing brains (N and N') at 6 h ALH. NSCs in red (Dpn) and Mts-DN (HA-tag, blue). GFP channel also shown in monochrome; insets showing higher magnification (M' and N').

(O) GFP signal (*ban*-activity sensor) quantification in NSCs expressing *mts-DN* normalized to control NSCs (n = 84 *mts-DN* NSCs, 19 BLs, 14 brains; n = 46 control NSCs, 8 BLs, 5 brains; error bars: SEMs; Wilcoxon rank-sum test; **p < 0.01). Anterior up. Scale bars: 10 µm and 17 µm in insets.

*(legend continued on next page)*

quiescence and proliferation. As in mammals, *Drosophila* NSCs are dependent on niche signals relaying external stimuli for both quiescence and reactivation (Tian et al., 2018; Chaker et al., 2016). In response to a nutritional cue, niche glia cells activate InR/PI3K/Akt signaling in NSCs to promote reactivation (Sousa-Nunes et al., 2011; Chell and Brand, 2010). Niche glia cells also contribute to quiescence by maintaining Hippo signaling activation in NSCs (Ding et al., 2016). In mammals, the insulin and insulin-like growth factor pathway also plays a major role in adult NSC reactivation (Renault et al., 2009; Kippin et al., 2005; Arsenijevic et al., 2001), and while regulation of the Hippo pathway has not yet been implicated in this process, Hippo signaling maintains liver progenitors in quiescence and is indispensable for skin and intestinal regeneration (Wang et al., 2017; Zhou et al., 2009). Here, we show that Mob4, Cka, and PP2A phosphatase, identified in our transcriptome analysis, regulate NSC quiescence to reactivation states, and we propose that they function as an intrinsic integration mechanism of InR/PI3K/Akt and Hippo signals.

We detected the catalytic subunit of PP2A, Mts, downregulated at the transcript level in reactivating versus quiescent NSCs. Mts maintains NSCs in quiescence, preventing premature phosphorylation of Akt, a key component of the InR/PI3K/Akt signaling cascade. PP2A substrate specificity depends on the choice from a variety of regulatory subunits (Shi et al., 2016). In *Drosophila*, the regulatory subunit Wdb was shown to physically interact and negatively regulate Akt in ovaries (Vereshchagina et al., 2008), and has also been implicated in the inhibition of insulin signaling, controlling organism growth and metabolic regulation (Fischer et al., 2015). Wdb orthologs in *Caenorhabditis elegans* (PPTR1) and mammals (B56β) also dephosphorylate Akt to modulate InR/PI3K/Akt, indicating a conserved role (Rodgers et al., 2011; Padmanabhan et al., 2009). We demonstrate that the inhibition of Mts or of Wdb leads to similar premature NSC reactivation effects, suggesting that Wdb/Mts function together to maintain quiescence. PP2A has been linked to cellular quiescence in different contexts. In the developing *Drosophila* eye and wing, PP2A/Wdb contributes to a quiescent state upon terminal cell differentiation (Sun and Buttitta, 2015); in cycling human cells, PP2A is also required for stable quiescence, a function that is dependent on the B56γ subunit (Naetar et al., 2014). Thus, PP2A may also have an evolutionary conserved function in maintaining quiescence in NSCs, modulating the InR/PI3K/Akt signaling cascade. PP2A is a pleiotropic phosphatase. In proliferating *Drosophila* NSCs, it contributes to apical-basal polarity and prevents excess self-renewal at later larval stages. Here, Wdb was shown to play no role and instead Twins, a B55 subunit ortholog, regulated PP2A/Mts action (Chabu and Doe, 2009; Krahn et al., 2009; Ogawa et al., 2009; Wang et al., 2009).

In contrast to Mts, we found that Mob4 and Cka upregulated in reactivating versus quiescent NSCs. Both are scaffold proteins of STRIPAK, a large molecular complex that is highly conserved from fungi to humans containing PP2A (Shi et al., 2016). We demonstrate that the loss of Mob4 or Cka impairs NSC reactivation, while their overexpression can accelerate it. Furthermore, ectopic expression of human Mob4 also induced premature NSC size growth and mitosis entry, suggesting a conserved function. In cultured S2 cells, Mob4 was shown to focus spindle fibers during mitosis (Trammell et al., 2008). Our Mob4 analysis in NSCs exposed a function in cell size growth before mitosis and additionally showed that MbNSCs, which do not enter quiescence, continue dividing in the absence of Mob4, indicating that the role of Mob4 in NSC reactivation is independent of that reported in spindle fibers.

STRIPAK/PP2A associates with Hippo in *Drosophila* and mammalian cells, and restricts *Drosophila* Hippo kinase activity via dephosphorylation (Liu et al., 2016; Couzens et al., 2013; Ribeiro et al., 2010). Previous reports revealed cross-talk inhibition between Hippo and InR/PI3K/Akt pathways in both mammalian and *Drosophila* tissues (Straßburger et al., 2012; Tumaneng et al., 2012). We demonstrate that Mob4 and Cka are both required for the physical association of Mts to Hippo and its subsequent inhibition, as reported (Ribeiro et al., 2010). We also show that upon loss of Mob4, the Hippo pathway consistently remains switched on in NSCs, and InR/PI3K/Akt signaling is inhibited. Finally, we determined that the inhibition of Mts can enhance Hippo signaling in NSCs but that the effect is overcome by premature activation of InR/PI3K/Akt, resulting in earlier NSC reactivation, despite Hippo activity. Our data suggest that as the levels of STRIPAK members Mob4 and Cka increase in NSCs, a complex with Hippo kinase assembles recruiting PP2A/Mts protein to inactivate Hippo signaling. This may function as an intrinsic molecular switch to turn off Hippo signaling and allow the InR/PI3K/Akt cascade to turn on (Figure 6P). Given their large and versatile composition, it is not surprising that STRIPAK complexes are assigned to an increasing number of functions and linked to clinical conditions, including autism and cancer (Shi et al., 2016). It will be important to determine whether and how STRIPAK proteins contribute to regulating the reactivation of other stem cells.

## STAR★METHODS

Detailed methods are provided in the online version of this paper and include the following:

- KEY RESOURCES TABLE
- CONTACT FOR REAGENT AND RESOURCES SHARING
- EXPERIMENTAL MODEL AND SUBJECT DETAILS
  - *Drosophila* strains and husbandry
  - S2R+ cell culture, transfection and drug treatment
- METHOD DETAILS
  - NSC transcriptome analysis
  - Immunohistochemistry and EdU incorporation

(P) A model of action of STRIPAK Mob4/Cka/PP2A members: in quiescent NSCs, Mob4 and Cka levels are low, while PP2A (Mts/Wdb) phosphatase targets Akt, ensuring that InR/PI3K/Akt signaling is maintained switched off. Hippo signaling is active (Ding et al., 2016; Poon et al., 2016). Mob4 and Cka levels increase, promoting NSC size growth and entry into division; both are required to direct Mts to switch off Hippo signaling, while the InR/PI3K/Akt cascade becomes active (Sousa-Nunes et al., 2011; Chell and Brand, 2010).

## SUPPLEMENTAL INFORMATION

Supplemental Information can be found online at https://doi.org/10.1016/j.celrep.2019.05.023.

## ACKNOWLEDGMENTS

We thank FlyChip (Cambridge Systems Biology Centre, University of Cambridge, UK) and the Bloomington *Drosophila* Stock Center for their services. We are very grateful to those that kindly provided antibodies, fly lines, and plasmids (indicated in Method Details). We also thank Bettina Fisher, Steve Russell, and Matthias Futschik for helpful discussions. This work was supported by the Leverhulme Trust (ECF2010/0526), the BBSRC (BB/M004392/1), the DFG (BE4278/1-1), the Johannes Gutenberg University, Germany, and the Faculty of Medicine and Dentistry, University of Plymouth, UK.

## AUTHOR CONTRIBUTIONS

All of the authors designed and performed the experiments. J.G.-R. and C.S.B. wrote the manuscript.

## DECLARATION OF INTERESTS

The authors declare no competing interests.

Received: October 13, 2018
Revised: April 14, 2019
Accepted: May 3, 2019
Published: June 4, 2019

## SUPPORTING CITATIONS

The following references appear in the Supplemental Information: Berger et al., 2012; Kohyama-Koganeya et al., 2008; Zitserman et al., 2012.

## REFERENCES

Arsenijevic, Y., Weiss, S., Schneider, B., and Aebischer, P. (2001). Insulin-like growth factor-I is necessary for neural stem cell proliferation and demonstrates distinct actions of epidermal growth factor and fibroblast growth factor-2. J. Neurosci. *21*, 7194–7202.

Baillat, G., Moqrich, A., Castets, F., Baude, A., Bailly, Y., Benmerah, A., and Monneron, A. (2001). Molecular cloning and characterization of phocein, a protein found from the Golgi complex to dendritic spines. Mol. Biol. Cell *12*, 663–673.

Berger, C., Harzer, H., Burkard, T.R., Steinmann, J., van der Horst, S., Laurenson, A.S., Novatchkova, M., Reichert, H., and Knoblich, J.A. (2012). FACS purification and transcriptome analysis of drosophila neural stem cells reveals a role for Klumpfuss in self-renewal. Cell Rep. *2*, 407–418.

Bolstad, B.M., Irizarry, R.A., Astrand, M., and Speed, T.P. (2003). A comparison of normalization methods for high density oligonucleotide array data based on variance and bias. Bioinformatics *19*, 185–193.

Bossing, T., and Technau, G.M. (1994). The fate of the CNS midline progenitors in *Drosophila* as revealed by a new method for single cell labelling. Development *120*, 1895–1906.

Bossing, T., Barros, C.S., Fischer, B., Russell, S., and Shepherd, D. (2012). Disruption of microtubule integrity initiates mitosis during CNS repair. Dev. Cell *23*, 433–440.

Brennecke, J., Hipfner, D.R., Stark, A., Russell, R.B., and Cohen, S.M. (2003). bantam encodes a developmentally regulated microRNA that controls cell proliferation and regulates the proapoptotic gene hid in Drosophila. Cell *113*, 25–36.

Britton, J.S., and Edgar, B.A. (1998). Environmental control of the cell cycle in Drosophila: nutrition activates mitotic and endoreplicative cells by distinct mechanisms. Development *125*, 2149–2158.

Britton, J.S., Lockwood, W.K., Li, L., Cohen, S.M., and Edgar, B.A. (2002). Drosophila's insulin/PI3-kinase pathway coordinates cellular metabolism with nutritional conditions. Dev. Cell *2*, 239–249.

Cavallucci, V., Fidaleo, M., and Pani, G. (2016). Neural Stem Cells and Nutrients: Poised Between Quiescence and Exhaustion. Trends Endocrinol. Metab. *27*, 756–769.

Chabu, C., and Doe, C.Q. (2009). Twins/PP2A regulates aPKC to control neuroblast cell polarity and self-renewal. Dev. Biol. *330*, 399–405.

Chaker, Z., Codega, P., and Doetsch, F. (2016). A mosaic world: puzzles revealed by adult neural stem cell heterogeneity. Wiley Interdiscip. Rev. Dev. Biol. *5*, 640–658.

Chell, J.M., and Brand, A.H. (2010). Nutrition-responsive glia control exit of neural stem cells from quiescence. Cell *143*, 1161–1173.

Chen, H.W., Marinissen, M.J., Oh, S.W., Chen, X., Melnick, M., Perrimon, N., Gutkind, J.S., and Hou, S.X. (2002). CKA, a novel multidomain protein, regulates the JUN N-terminal kinase signal transduction pathway in Drosophila. Mol. Cell. Biol. *22*, 1792–1803.

Cheung, T.H., and Rando, T.A. (2013). Molecular regulation of stem cell quiescence. Nat. Rev. Mol. Cell Biol. *14*, 329–340.

Chintapalli, V.R., Wang, J., and Dow, J.A. (2007). Using FlyAtlas to identify better Drosophila melanogaster models of human disease. Nat. Genet. *39*, 715–720.

Codega, P., Silva-Vargas, V., Paul, A., Maldonado-Soto, A.R., Deleo, A.M., Pastrana, E., and Doetsch, F. (2014). Prospective identification and purification of quiescent adult neural stem cells from their in vivo niche. Neuron *82*, 545–559.

Couzens, A.L., Knight, J.D., Kean, M.J., Teo, G., Weiss, A., Dunham, W.H., Lin, Z.Y., Bagshaw, R.D., Sicheri, F., Pawson, T., et al. (2013). Protein interaction network of the mammalian Hippo pathway reveals mechanisms of kinase-phosphatase interactions. Sci. Signal. *6*, rs15.

Ding, R., Weynans, K., Bossing, T., Barros, C.S., and Berger, C. (2016). The Hippo signalling pathway maintains quiescence in Drosophila neural stem cells. Nat. Commun. *7*, 10510.

Fischer, P., La Rosa, M.K., Schulz, A., Preiss, A., and Nagel, A.C. (2015). Cyclin G Functions as a Positive Regulator of Growth and Metabolism in Drosophila. PLoS Genet. *11*, e1005440.

Fukada, S., Uezumi, A., Ikemoto, M., Masuda, S., Segawa, M., Tanimura, N., Yamamoto, H., Miyagoe-Suzuki, Y., and Takeda, S. (2007). Molecular signature of quiescent satellite cells in adult skeletal muscle. Stem Cells *25*, 2448–2459.

Hamaratoglu, F., Willecke, M., Kango-Singh, M., Nolo, R., Hyun, E., Tao, C., Jafar-Nejad, H., and Halder, G. (2006). The tumour-suppressor genes NF2/Merlin and Expanded act through Hippo signalling to regulate cell proliferation and apoptosis. Nat. Cell Biol. *8*, 27–36.

Hannus, M., Feiguin, F., Heisenberg, C.P., and Eaton, S. (2002). Planar cell polarization requires Widerborst, a B′ regulatory subunit of protein phosphatase 2A. Development *129*, 3493–3503.

Hansson, E.M., Teixeira, A.I., Gustafsson, M.V., Dohda, T., Chapman, G., Meletis, K., Muhr, J., and Lendahl, U. (2006). Recording Notch signaling in real time. Dev. Neurosci. *28*, 118–127.

Hu, Y., Flockhart, I., Vinayagam, A., Bergwitz, C., Berger, B., Perrimon, N., and Mohr, S.E. (2011). An integrative approach to ortholog prediction for disease-focused and other functional studies. BMC Bioinformatics *12*, 357.

Huang, J., and Wang, H. (2018). Hsp83/Hsp90 Physically Associates with Insulin Receptor to Promote Neural Stem Cell Reactivation. Stem Cell Reports *11*, 883–896.

Ito, K., and Hotta, Y. (1992). Proliferation pattern of postembryonic neuroblasts in the brain of *Drosophila melanogaster*. Dev. Biol. *149*, 134–148.

Janssens, V., and Goris, J. (2001). Protein phosphatase 2A: a highly regulated family of serine/threonine phosphatases implicated in cell growth and signalling. Biochem. J. *353*, 417–439.

Kippin, T.E., Martens, D.J., and van der Kooy, D. (2005). p21 loss compromises the relative quiescence of forebrain stem cell proliferation leading to exhaustion of their proliferation capacity. Genes Dev. *19*, 756–767.

Kohyama-Koganeya, A., Kim, Y.J., Miura, M., and Hirabayashi, Y. (2008). A Drosophila orphan G protein-coupled receptor BOSS functions as a glucose-responding receptor: loss of boss causes abnormal energy metabolism. Proc. Natl. Acad. Sci. USA *105*, 15328–15333.

Krahn, M.P., Egger-Adam, D., and Wodarz, A. (2009). PP2A antagonizes phosphorylation of Bazooka by PAR-1 to control apical-basal polarity in dividing embryonic neuroblasts. Dev. Cell *16*, 901–908.

Lai, S.L., and Doe, C.Q. (2014). Transient nuclear Prospero induces neural progenitor quiescence. eLife. https://doi.org/10.7554/eLife.03363.

Lee, T., and Luo, L. (1999). Mosaic analysis with a repressible cell marker for studies of gene function in neuronal morphogenesis. Neuron *22*, 451–461.

Levy, P., and Larsen, C. (2013). Odd-skipped labels a group of distinct neurons associated with the mushroom body and optic lobe in the adult Drosophila brain. J. Comp. Neurol. *521*, 3716–3740.

Li, S., Wang, C., Sandanaraj, E., Aw, S.S., Koe, C.T., Wong, J.J., Yu, F., Ang, B.T., Tang, C., and Wang, H. (2014). The SCFSlimb E3 ligase complex regulates asymmetric division to inhibit neuroblast overgrowth. EMBO Rep. *15*, 165–174.

Li, S., Koe, C.T., Tay, S.T., Tan, A.L.K., Zhang, S., Zhang, Y., Tan, P., Sung, W.K., and Wang, H. (2017). An intrinsic mechanism controls reactivation of neural stem cells by spindle matrix proteins. Nat. Commun. *8*, 122.

Liu, B., and Bossing, T. (2016). Single neuron transcriptomics identify SRSF/SR protein B52 as a regulator of axon growth and Choline acetyltransferase splicing. Sci. Rep. *6*, 34952.

Liu, B., Zheng, Y., Yin, F., Yu, J., Silverman, N., and Pan, D. (2016). Toll Receptor-Mediated Hippo Signaling Controls Innate Immunity in Drosophila. Cell *164*, 406–419.

Livak, K.J., and Schmittgen, T.D. (2001). Analysis of relative gene expression data using real-time quantitative PCR and the 2(-Delta Delta C(T)) Method. Methods *25*, 402–408.

Llorens-Bobadilla, E., Zhao, S., Baser, A., Saiz-Castro, G., Zwadlo, K., and Martin-Villalba, A. (2015). Single-Cell Transcriptomics Reveals a Population of Dormant Neural Stem Cells that Become Activated upon Brain Injury. Cell Stem Cell *17*, 329–340.

Macaulay, I.C., and Voet, T. (2014). Single cell genomics: advances and future perspectives. PLoS Genet. *10*, e1004126.

Martynoga, B., Mateo, J.L., Zhou, B., Andersen, J., Achimastou, A., Urbán, N., van den Berg, D., Georgopoulou, D., Hadjur, S., Wittbrodt, J., et al. (2013). Epigenomic enhancer annotation reveals a key role for NFIX in neural stem cell quiescence. Genes Dev. *27*, 1769–1786.

Naetar, N., Soundarapandian, V., Litovchick, L., Goguen, K.L., Sablina, A.A., Bowman-Colin, C., Sicinski, P., Hahn, W.C., DeCaprio, J.A., and Livingston, D.M. (2014). PP2A-mediated regulation of Ras signaling in G2 is essential for stable quiescence and normal G1 length. Mol. Cell *54*, 932–945.

Ogawa, H., Ohta, N., Moon, W., and Matsuzaki, F. (2009). Protein phosphatase 2A negatively regulates aPKC signaling by modulating phosphorylation of Par-6 in Drosophila neuroblast asymmetric divisions. J. Cell Sci. *122*, 3242–3249.

Otsuki, L., and Brand, A.H. (2019). Dorsal-Ventral Differences in Neural Stem Cell Quiescence Are Induced by p57(KIP2)/Dacapo. Dev. Cell *49*, 293–300.e3.

Padmanabhan, S., Mukhopadhyay, A., Narasimhan, S.D., Tesz, G., Czech, M.P., and Tissenbaum, H.A. (2009). A PP2A regulatory subunit regulates C. elegans insulin/IGF-1 signaling by modulating AKT-1 phosphorylation. Cell *136*, 939–951.

Poon, C.L., Mitchell, K.A., Kondo, S., Cheng, L.Y., and Harvey, K.F. (2016). The Hippo Pathway Regulates Neuroblasts and Brain Size in Drosophila melanogaster. Curr. Biol. *26*, 1034–1042.

Prokop, A., and Technau, G.M. (1991). The origin of postembryonic neuroblasts in the ventral nerve cord of *Drosophila melanogaster*. Development *111*, 79–88.

Renault, V.M., Rafalski, V.A., Morgan, A.A., Salih, D.A., Brett, J.O., Webb, A.E., Villeda, S.A., Thekkat, P.U., Guillerey, C., Denko, N.C., et al. (2009). FoxO3 regulates neural stem cell homeostasis. Cell Stem Cell *5*, 527–539.

Ribeiro, P.S., Josué, F., Wepf, A., Wehr, M.C., Rinner, O., Kelly, G., Tapon, N., and Gstaiger, M. (2010). Combined functional genomic and proteomic approaches identify a PP2A complex as a negative regulator of Hippo signaling. Mol. Cell *39*, 521–534.

Ritchie, M.E., Phipson, B., Wu, D., Hu, Y., Law, C.W., Shi, W., and Smyth, G.K. (2015). limma powers differential expression analyses for RNA-sequencing and microarray studies. Nucleic Acids Res. *43*, e47.

Rodgers, J.T., Vogel, R.O., and Puigserver, P. (2011). Clk2 and B56β mediate insulin-regulated assembly of the PP2A phosphatase holoenzyme complex on Akt. Mol. Cell *41*, 471–479.

Schulte, J., Sepp, K.J., Jorquera, R.A., Wu, C., Song, Y., Hong, P., and Littleton, J.T. (2010). DMob4/Phocein regulates synapse formation, axonal transport, and microtubule organization. J. Neurosci. *30*, 5189–5203.

Shi, Z., Jiao, S., and Zhou, Z. (2016). STRIPAK complexes in cell signaling and cancer. Oncogene *35*, 4549–4557.

Snaith, H.A., Armstrong, C.G., Guo, Y., Kaiser, K., and Cohen, P.T. (1996). Deficiency of protein phosphatase 2A uncouples the nuclear and centrosome cycles and prevents attachment of microtubules to the kinetochore in Drosophila microtubule star (mts) embryos. J. Cell Sci. *109*, 3001–3012.

Sousa-Nunes, R., Yee, L.L., and Gould, A.P. (2011). Fat cells reactivate quiescent neuroblasts via TOR and glial insulin relays in Drosophila. Nature *471*, 508–512.

Spéder, P., and Brand, A.H. (2014). Gap junction proteins in the blood-brain barrier control nutrient-dependent reactivation of Drosophila neural stem cells. Dev. Cell *30*, 309–321.

Straßburger, K., Tiebe, M., Pinna, F., Breuhahn, K., and Teleman, A.A. (2012). Insulin/IGF signaling drives cell proliferation in part via Yorkie/YAP. Dev. Biol. *367*, 187–196.

Sun, D., and Buttitta, L. (2015). Protein phosphatase 2A promotes the transition to G0 during terminal differentiation in Drosophila. Development *142*, 3033–3045.

Szklarczyk, D., Franceschini, A., Wyder, S., Forslund, K., Heller, D., Huerta-Cepas, J., Simonovic, M., Roth, A., Santos, A., Tsafou, K.P., et al. (2015). STRING v10: protein-protein interaction networks, integrated over the tree of life. Nucleic Acids Res. *43*, D447–D452.

Takai, A., Murata, M., Torigoe, K., Isobe, M., Mieskes, G., and Yasumoto, T. (1992). Inhibitory effect of okadaic acid derivatives on protein phosphatases. A study on structure-affinity relationship. Biochem. J. *284*, 539–544.

Tian, Z., Zhao, Q., Biswas, S., and Deng, W. (2018). Methods of reactivation and reprogramming of neural stem cells for neural repair. Methods *133*, 3–20.

Trammell, M.A., Mahoney, N.M., Agard, D.A., and Vale, R.D. (2008). Mob4 plays a role in spindle focusing in Drosophila S2 cells. J. Cell Sci. *121*, 1284–1292.

Truman, J.W., and Bate, M. (1988). Spatial and temporal patterns of neurogenesis in the central nervous system of *Drosophila melanogaster*. Dev. Biol. *125*, 145–157.

Tsuji, T., Hasegawa, E., and Isshiki, T. (2008). Neuroblast entry into quiescence is regulated intrinsically by the combined action of spatial Hox proteins and temporal identity factors. Development *135*, 3859–3869.

Tumaneng, K., Russell, R.C., and Guan, K.L. (2012). Organ size control by Hippo and TOR pathways. Curr. Biol. *22*, R368–R379.

Tung, P.Y., Blischak, J.D., Hsiao, C.J., Knowles, D.A., Burnett, J.E., Pritchard, J.K., and Gilad, Y. (2017). Batch effects and the effective design of single-cell gene expression studies. Sci. Rep. *7*, 39921.

Venezia, T.A., Merchant, A.A., Ramos, C.A., Whitehouse, N.L., Young, A.S., Shaw, C.A., and Goodell, M.A. (2004). Molecular signatures of proliferation and quiescence in hematopoietic stem cells. PLoS Biol. *2*, e301.

Vereshchagina, N., Ramel, M.C., Bitoun, E., and Wilson, C. (2008). The protein phosphatase PP2A-B' subunit Widerborst is a negative regulator of cytoplasmic activated Akt and lipid metabolism in Drosophila. J. Cell Sci. *121*, 3383–3392.

Virshup, D.M. (2000). Protein phosphatase 2A: a panoply of enzymes. Curr. Opin. Cell Biol. *12*, 180–185.

Wang, C., Chang, K.C., Somers, G., Virshup, D., Ang, B.T., Tang, C., Yu, F., and Wang, H. (2009). Protein phosphatase 2A regulates self-renewal of Drosophila neural stem cells. Development *136*, 2287–2296.

Wang, Y., Yu, A., and Yu, F.X. (2017). The Hippo pathway in tissue homeostasis and regeneration. Protein Cell *8*, 349–359.

Weng, L., and Wei, D. (2002). Role of Cka in imaginal disc growth and differentiation. Drosoph. Inf. Serv. *85*, 8–12.

Yan, D., Neumüller, R.A., Buckner, M., Ayers, K., Li, H., Hu, Y., Yang-Zhou, D., Pan, L., Wang, X., Kelley, C., et al. (2014). A regulatory network of Drosophila germline stem cell self-renewal. Dev. Cell *28*, 459–473.

Zheng, Y., Liu, B., Wang, L., Lei, H., Pulgar Prieto, K.D., and Pan, D. (2017). Homeostatic Control of Hpo/MST Kinase Activity through Autophosphorylation-Dependent Recruitment of the STRIPAK PP2A Phosphatase Complex. Cell Rep. *21*, 3612–3623.

Zhou, D., Conrad, C., Xia, F., Park, J.S., Payer, B., Yin, Y., Lauwers, G.Y., Thasler, W., Lee, J.T., Avruch, J., and Bardeesy, N. (2009). Mst1 and Mst2 maintain hepatocyte quiescence and suppress hepatocellular carcinoma development through inactivation of the Yap1 oncogene. Cancer Cell *16*, 425–438.

Zitserman, D., Gupta, S., Kruger, W.D., Karbowniczek, M., and Roegiers, F. (2012). The TSC1/2 complex controls Drosophila pigmentation through TORC1-dependent regulation of catecholamine biosynthesis. PLoS ONE *7*, e48720.

## STAR★METHODS

### KEY RESOURCES TABLE

| REAGENT or RESOURCE | SOURCE | IDENTIFIER |
|---|---|---|
| Antibodies | | |
| Rabbit anti-GFP | Gift from U. Mayor (U. Mayor, personal communication) | N/A |
| Chicken anti-GFP | Millipore | Cat# 06-896, RRID: AB_310288 |
| Guinea pig anti-Dpn | Gift from J. Knoblich (Levy and Larsen, 2013) | RRID: AB_2314299 |
| Guinea pig anti-Mob4 | Gift from T. Littleton (Schulte et al., 2010) | N/A |
| Mouse anti-Dlg | DSHB | Cat# 4F3 anti-discs large, RRID: AB_528203 |
| Rabbit anti-pH3 | Abcam | Cat# ab5176, RRID: AB_304763 |
| Rabbit anti-Cka | Gift from W. Du (Weng and Wei, 2002) | N/A |
| Rabbit anti-pAKT$^{S505}$ | CST | Cat# 4054, RRID: AB_331414 |
| Mouse anti-Flag clone M2 | Sigma | Cat# F3165, RRID: AB_259529 |
| Rat anti-HA clone 3F10 | Roche | Cat# 11867431001, RRID: AB_390919 |
| Rat IgG | Sigma | Cat# I4131, RRID: AB_1163627 |
| Rabbit anti-Akt | CST | Cat# 9272, RRID: AB_329827 |
| Rabbit anti-b-Actin | CST | Cat# 4967, RRID: AB_330288 |
| Mouse anti-Myc clone 9E10 | Santa Cruz Biotechnology | Cat# sc-40, RRID: AB_627268 |
| Rabbit anti-pMST1$^{T183}$/pMST2$^{T180}$ | CST | Cat# 3681S, RRID: AB_330269 |
| Guinea pig anti-Hippo | Gift from G. Halder (Hamaratoglu et al., 2006) | N/A |
| Chemicals, Peptides, and Recombinant Proteins | | |
| Okadaic Acid | CST | Cat# 5934 |
| Critical Commercial Assays | | |
| Click-iT EdU Alexa Fluor 594 Imaging Kit | Invitrogen | Cat# C10339 |
| Co-Immunoprecipitation Kit | Pierce | Cat# 26149 |
| Deposited Data | | |
| Transcriptome data | This paper | GEO: GSE128646 |
| Experimental Models: Cell Lines | | |
| *D. melanogaster*: Cell line S2R+ | Gift from B. Houdsen | FlyBase: FBtc0000150 |
| Experimental Models: Organisms/Strains | | |
| *D. melanogaster*: *mob4* mutant: y[1] w[*]; Mob4[EYDeltaL3]/CyO | Bloomington Drosophila Stock Center (Schulte et al., 2010) | BDSC: 36331; FlyBase: FBst0036331 |
| *D. melanogaster*: UAS line expressing *mob4* RNAi: P{UAS-Mob4.RNAi.JS1}attP2 | Bloomington Drosophila Stock Center (Schulte et al., 2010) | BDSC:36488; FlyBase: FBst0036488 |
| *D. melanogaster*: UAS line expressing *mob4*: y[1] v[1]; P{y[+t7.7] v[+t1.8] = UAS-Mob4.S}attP2 | Bloomington Drosophila Stock Center (Schulte et al., 2010) | BDSC: 36329; FlyBase: FBst0036329 |
| *D. melanogaster*: UAS line expressing *hMOB4*: y[1] v[1]; P{y[+t7.7] v[+t1.8] = UAS-phocein.1}attP2 | Bloomington Drosophila Stock Center (Schulte et al., 2010) | BDSC: 36330; FlyBase: FBst0036330 |
| *D. melanogaster*: UAS line expressing *cka-eGFP*: w[*]; P{w[+mC] = UASp-Cka.EGFP.C}2 | Bloomington Drosophila Stock Center | BDSC: 53756; FlyBase: FBst0053756 |
| *D. melanogaster*: UAS line expressing *wdb-DN*: w[*]; P{w[+mC] = UAS-wdb.95-524.HA}6 | Bloomington Drosophila Stock Center (Hannus et al., 2002) | BDSC: 55053; FlyBase: FBst0055053 |
| *D. melanogaster*: UAS line expressing *wts* RNAi: y[1] sc[*] v[1]; P{y[+t7.7] v[+t1.8] = TRiP.GL01331}attP2 | Bloomington Drosophila Stock Center (Ding et al., 2016) | BDSC: 41899; FlyBase: FBst0041899 |

(*Continued on next page*)

**Continued**

| REAGENT or RESOURCE | SOURCE | IDENTIFIER |
|---|---|---|
| *D. melanogaster*: UAS line expressing *hpo* RNAi: y[1] v[1]; P{y[+t7.7] v[+t1.8] = TRiP.HMS00006}attP2 | Bloomington Drosophila Stock Center (Ding et al., 2016) | BDSC: 33614; FlyBase: FBst0033614 |
| *D. melanogaster*: UAS line expressing *cka* RNAi: y[1] v[1]; P{y[+t7.7] v[+t1.8] = TRiP.HM05138}attP2 | Bloomington Drosophila Stock Center | BDSC: 28927; FlyBase: FBst0028927 |
| *D. melanogaster*: Wild type: Oregon-R | Gift from M. Akam (Bossing and Technau, 1994) | FlyBase: FBsn0000276 |
| *D. melanogaster*: UAS line expressing *rheb*: w[*]; P{w[+mC] = UAS-Rheb.Pa}3 | Gift from R. Sousa-Nunes (Sousa-Nunes et al., 2011) | BDSC: 9689; FlyBase: FBst0009689 |
| *D. melanogaster*: Gal4 line under the control of *grh*: *Grh-Gal4* | Gift from A.H. Brand (Chell and Brand, 2010) | N/A |
| *D. melanogaster*: UAS line expressing *mts-DN-HA*: *UAS-mts.dn181-HA* | Gift from S. Eaton (Hannus et al., 2002) | N/A |
| *D. melanogaster*: line expressing pleckstrin homology domain-GFP fusion protein: *PH-GFP* (tGPH) | Gift from B. Edgar (Britton and Edgar, 1998) | N/A |
| *D. melanogaster*: *bantam* GFP-sensor line, *ban*-sensor (*db20*) | Gift from S.M. Cohen (Brennecke et al., 2003) | N/A |
| *D. melanogaster*: $mts^{XE225839}$ mutant: $mts^{XE2258}$/CyO, P{sevRas1.V12}F1 and $mts^{299}$ mutant | Gifts from H. Wang (Wang et al., 2009) | BDSC: 5684; FlyBase:FBst0005684 N/A for $mts^{299}$ |
| *D. melanogaster*: Gal4 line under the control of *insc*: w[*]; P{w[+mW.hs] = GawB}insc[Mz1407] | Bloomington Drosophila Stock Center | BDSC: 8751; FlyBase:FBst0008751 |
| *D. melanogaster*: Gal4 line under the control of *repo*: w[1118]; P{w[+m*] = GAL4}repo/TM6, tb | Gift from A. Hidalgo | N/A |
| *D. melanogaster*: UAS line expressing *CD8-GFP*: y[1] w[*]; P{w[+mC] = UAS-mCD8::GFP.L}LL5, P{UAS-mCD8::GFP.L}2 | Lee and Luo, 1999 | BDSC: 5137; FlyBase:FBst0005137 |
| *D. melanogaster*: UAS line expressing *dicer2*: *UAS-dicer2* | Ding et al., 2016 | N/A |
| Oligonucleotides | | |
| Primer: Anchored polyT AAGCAGTGGTATCAAC GCAGAGTACT$_{(26)}$VN | Bossing et al., 2012 | N/A |
| Primer: SM AAGCAGTGGTATCAACGCAGAG TACGCrGrGrG | Bossing et al., 2012 | N/A |
| Primer: Nested AAGCAGTGGTATCAACGCAGAGT | Bossing et al., 2012 | N/A |
| Primers used for RT-qPCR | See Table S4 | N/A |
| dsRNA targeting sequence *mob4*: Forward: TAATAC GACTCACTATAGGGagatgtggaagtacgagcacctg | Schulte et al., 2010 | N/A |
| dsRNA targeting sequence *mob4*: Reverse: TAATACG ACTCACTATAGGGagatgcgagaagatgcgatacac | Schulte et al., 2010 | N/A |
| dsRNA targeting sequence *cka*: Forward: TAATACG ACTCACTATAGGGatacgggtccagttctgtgc | This paper | N/A |
| dsRNA targeting sequence *cka*: Reverse: TAATACG ACTCACTATAGGGtgttgtaggccaccacgata | This paper | N/A |
| dsRNA targeting sequence *DsRed*: Forward: TAATAC GACTCACTATAGGGgccgatgaacttcaccttgt | This paper | N/A |
| dsRNA targeting sequence *DsRed*: Reverse: TAATAC GACTCACTATAGGGcgaggacgtcatcaaggagt | This paper | N/A |
| Recombinant DNA | | |
| Plasmid: 12XCSL DsRedExpressDL | Hansson et al., 2006 | Addgene plasmid #47683 |
| Plasmid: Flag-NTAN | Gift from P. Ribeiro (Ribeiro et al., 2010) | N/A |

(*Continued on next page*)

*Continued*

| REAGENT or RESOURCE | SOURCE | IDENTIFIER |
|---|---|---|
| Plasmid: Flag-Hippo | Gift from P. Ribeiro (Ribeiro et al., 2010) | N/A |
| Plasmid: Myc-Mts | Gift from P. Ribeiro (Ribeiro et al., 2010) | N/A |
| Plasmid: HA-Mts | Gift from P. Ribeiro (Ribeiro et al., 2010) | N/A |
| Plasmid: Myc-Akt | Gift from W. Hongyan (Li et al., 2014) | N/A |
| Software and Algorithms | | |
| R/Bioconductor Limma | Ritchie et al., 2015 | https://bioconductor.org/packages/release/bioc/html/limma.html |
| STRING v10.5 | Szklarczyk et al., 2015 | https://string-db.org/cgi/input.pl?sessionId=QMsQ2cmXKFYZ&input_page_show_search=on |
| FlyAtlas | Chintapalli et al., 2007 | http://flyatlas.org/atlas.cgi |
| DIOPT – DRSC Integrative Ortholog Prediction Tool | Hu et al., 2011 | https://www.flyrnai.org/cgi-bin/DRSC_orthologs.pl |

## CONTACT FOR REAGENT AND RESOURCES SHARING

Further information and requests for resources and reagents should be directed to and will be fulfilled by the Lead Contact, Claudia Barros (claudia.barros@plymouth.ac.uk).

## EXPERIMENTAL MODEL AND SUBJECT DETAILS

### *Drosophila* strains and husbandry

*Drosophila* stocks obtained from the Bloomington *Drosophila* Stock Center are: *mob4*$^{EY\Delta L3}$ (36331) (Schulte et al., 2010) rebalanced over *CyO*, P(GAL4-*twi.G*)2.2; *UAS-mob4*$^{RNAi}$ (36488) (Schulte et al., 2010); *UAS-mob4* (36329) (Schulte et al., 2010); *UAS-hMOB4* (36330) (Schulte et al., 2010); *UAS-cka-eGFP* (53756); *UAS-wdb-DN* (*UAS-wdb.95-524.HA*; 55053) (Hannus et al., 2002); *UAS-wts*$^{RNAi}$ (41899) (Ding et al., 2016); *UAS-hpo*$^{RNAi}$ (33614) (Ding et al., 2016) and *UAS-cka*$^{RNAi}$ (28927). Other stocks used are: Wild-type *Oregon-R* (kind gift from M. Akain); *UAS-rheb* (Blomington 9689) (Sousa-Nunes et al., 2011) (kind gift from R. Sousa-Nunes); *grh-Gal4* (Chell and Brand, 2010) (kind gift from A.H. Brand); *UAS-mts-DN* (*UAS-mts.dn181-HA*) (Hannus et al., 2002) (kind gift from S. Eaton); *PH-GFP* (tGPH) (Britton and Edgar, 1998) (kind gift from B. Edgar); *ban*-sensor (*db20*) (Brennecke et al., 2003) (kind gift from S.M. Cohen), *mts*$^{299}$ and *mts*$^{XE2258}$ (Wang et al., 2009) (kind gifts from H. Wang). NSC-specific RNAi and overexpression assays were performed using *insc-Gal4* (w$^{1118}$; p{GAWB}*insc*MZ1407) and glial-specific expression assays used *repo-Gal4* (w$^{1118}$; p{GAWB}*repo*/*TM6*b, iab-lacZ). *grh-Gal4* driver was recombined with *UAS-CD8-GFP*. For rescue experiments, *insc-Gal4* and *repo-Gal4* drivers were recombined or combined with the *mob4*$^{EY\Delta L3}$ mutant strain. For other assays, the *insc-Gal4* driver was recombined with *UAS-CD8-GFP* and/or combined with *UAS-dicer2* (Ding et al., 2016). Fly lines were kept in standard *Drosophila* fly food. Egg collections and larvae rearing were performed on agar juice plates (21 g agar, 200ml of grape juice per l of water) supplemented with yeast paste. Egg lays were collected in either 30min or 1h time-windows. For nutritional deprivation experiments, freshly hatched larvae were transferred to agar plates prepared with amino-acid free media (5% sucrose, 1% agar in phosphate buffered saline, PBS).

### S2R+ cell culture, transfection and drug treatment

S2R+ cells (kind gift from B. Houdsen) were maintained in 25- or 75-cm$^2$ T-flasks at 25°C in Schneider's Medium (GIBCO) with 10% heat-inactivated FBS (One Shot, GIBCO) and antibiotics. For transient transfections, 1.6x10$^6$ cells/well were seeded in 6-well plates. Effectene transfection reagent (Quiagen) was used to transfect 1 μg and/or 2 μg of each appropriate plasmid and/or dsRNA, respectively, following manufacturer guidelines. Cells were incubated 72 hours before harvest. Plasmids used are Flag-NTAN, Flag-Hippo, Myc-Mts, HA-Mts (kind gifts from P. S. Ribeiro) and Myc-AKT (kind gift from W. Hongyan). For okadaic acid experiments, cells were transfected as above, incubated 70 hours and treated with 50 nM okadaic acid (CST) or 0.005% DMSO (vehicle; Corning) for 2 hours prior harvest.

## METHOD DETAILS

### NSC transcriptome analysis

Single NSC harvest, mRNA isolation, cDNA generation and microarray hybridization were performed essentially as previously described (Bossing et al., 2012). Single quiescent (small; 4-5μm) and reactivating (enlarged) NSCs were individually removed from freshly dissected 17 ALH CNS expressing membrane-tagged GFP specifically in NSCs (*grh-Gal4, UAS-CD8-GFP*). Samples with any trace of non-fluorescent material were rejected. Each single cell was expelled in its own Eppendorf tube containing annealing mix: 0.3 μL anchored polyT primer (5′-AAGCAGTGGTATCAACGCAGAGTACT$_{(26)}$VN-3′, 10pM), 0.3 μL SM primer (5′-AAGCAGTGG TATCAACGCAGAGTACGCrGrGrG-3′, 10pM), 0.4 μL RNase inhibitor (Superase, Ambion) and 2 μL Lysis Mix (10% Nonidet P-40, 0.1M DTT in DEPC-treated ultrapure water), and processed in less than 20 min. Each sample was spun (14000rpm, 1min, 4°C), primers annealed (3min, 70°C) and snap-frozen in dry ice/ isopropanol. 1.5 μL of mix 1 (1 μL Invitrogen first strand buffer, 0.5 μL 10mM dNTPs) and 0.5 μL of mix 2 (3 μL Invitrogen Superscript II reverse transcriptase, 0.5 μL Ambion Superase RNase inhibitor) were added per sample. Samples were thawed during centrifugation (14000rpm, 1 min, 4°C) and reverse transcribed (37°C, 90min), followed by enzyme thermal inactivation (65°C, 10 min). RNA was digested in 2 μL digestion mix (0.7 μL Roche RNase H buffer, 0.5 μL Roche RNase H, 0.8 μL ultrapure water) for 20min at 37°C, followed by enzyme thermal inactivation (65°C, 15 min). For cDNA PCR amplification, 2 μL of nested primer (5′-AAGCAGTGGTATCAACGCAGAGT-3′), 2 μL dNTPs (10mM), 5 μL Roche buffer, 0.5 μL Roche Long Expand polymerase and 34.5 μL of ultrapure water were added. PCR program: one cycle (95°C 3min, 50°C 5min, 68°C 15min) followed by 25 cycles (95°C 20 s, 60°C 1min, 68°C 7min). 3 pairs of NSC quiescent/ reactivating samples showing clear banding patterns on agarose gels were sent for microarray analysis (FlyChip, University of Cambridge). 1 μg of each sample were Klenow-labeled using BioPrime DNA Labeling System (Invitrogen) in the presence of Cy3- or Cy5-dCTP (GE Healthcare) for 2 hours 37°C. Unincorporated dye and nucleotides were removed using AutoSeq G-50 columns (GE Healthcare), following manufacturer instructions. Cy3- and Cy5-labeled pairs of samples were combined with salmon sperm DNA as blocking agent and co-hybridized (16 hours, 51°C) in a HybStation hybridization station (Digilab Genomic Solutions) on long oligonucleotides FL003 microarrays (International *Drosophila* Array Consortium; Gene Expression Omnibus accession number GPL14121). Post-hybridization washes were performed according to Full Moon Biosystems protocols. Detailed protocols for labeling, hybridization and washing can be requested from the Cambridge Systems Biology Centre UK (https://www.sysbiol.cam/ac.uk/CSBC). Arrays were scanned at 5 μm resolution (GenePix scanner, Axon Instruments) using optimized PMT gain settings for each channel.

RT-qPCR validation of selected genes was done using SYBRGreen on a StepOnePlus thermal cycler (Applied Biosystems) and primers indicated in Table S4. *ribosomal protein 49* (*rp49*) was used as internal calibrator for all reactions. Single NSC cDNA samples used were obtained as described above. Candidates validated were also selected based on their Gene Ontology (GO) *Nervous system development* and *Neurogenesis* classification (STRING v10.5) (Szklarczyk et al., 2015).

Tissue-specific expression of identified targets was performed using FlyAtlas (Chintapalli et al., 2007). Gene orthology analysis used DIOPT (DRSC Integrative Ortholog Prediction Tool) (Hu et al., 2011). Protein-protein interaction network of *Drosophila* PP2A-STRIPAK components was performed using STRING (v10.5) (Szklarczyk et al., 2015) with experimental-based data only as source, and as previously described (Zheng et al., 2017; Liu et al., 2016; Ribeiro et al., 2010).

### Immunohistochemistry and EdU incorporation

Immunohistochemistry assays were performed as previously described (Chell and Brand, 2010), with minor modifications. Briefly, larval CNSs were dissected in PBS and fixed for 20 min in 4% formaldehyde/PBS with 5 μM $MgCl_2$ and 0.5 μM EGTA or 10 μM $MgCl_2$ and 1 μM EGTA (3$^{rd}$ instar larvae), followed by washes in PBS (2 × 10 min, 3 rinses between washes) and block for 1h in PBST (PBS, 1% Triton X-100) with 10% fetal bovine serum (FBS). Primary antibodies were incubated in PBST overnight or for 2 nights at 4°C. CNSs were washed in PBST and secondary antibodies incubated 2h at room temperature, followed by PBST washes and sequentially embedding in 50% and 70% glycerol before mounting in a 1:1 mix of 70% glycerol and Vectashield (Vector Laboratories). Antibodies used are: rabbit anti-GFP (1:1000, kind gift from U. Mayor), chicken anti-GFP (1:500, Millipore), guinea pig anti-Dpn (1:2000, kind gift from J. Knoblich), guinea pig anti-Mob4 (1:1000, kind gift from T. Littleton), mouse anti-Dlg (1:50, DSHB), rabbit anti-pH3 (1:1000, Abcam), rabbit anti-Cka (1:1000, kind gift from W. Du), rabbit anti-pAKT$^{S505}$ (1:50, CST) and rat anti-HA clone 3F10 (1:1000, Roche). EdU incorporation assays were performed as previously described (Sousa-Nunes et al., 2011). Briefly, CNSs were dissected in PBS and incubated in 10 μM EdU/PBS for 1h at room temperature. CNSs were fixed for 15min in 4% formaldehyde/ PBS and incorporated EdU detected using Click-iT EdU Imaging kit following manufacturer instructions (Invitrogen).

### Image acquisition and processing

Images were obtained on a Leica SP8 confocal laser-scanning microscope using LAS X software. Quantifications were made using z stacks of 1.5 μm step size, comprising whole brain lobes, VNCs or CNSs. Representative images shown are single optical sections, with the exception of Figure 1A, which is a z-projection stack (3 steps, 0.5 μm each), and EdU incorporations, which are z-projection stacks encompassing whole CNSs. Images were processed in Fiji v2.0 or Adobe Photoshop CS6 and assembled in Adobe Illustrator CS6. NSC sizes (maximum diameters) (Chell and Brand, 2010), pH3 scorings, Mob4 and Cka signal intensities (pixel intensity/ NSC maximum area), *ban*-GFP signal intensity (pixel intensity/ NSC maximum area outlined by Dpn staining) and EdU voxel quantification were performed using Fiji v2.0 or Adobe Photoshop CS6.

### dsRNA synthesis

For *cka*, *mob4* and *DsRed* dsRNA, DNA templates of target genes were PCR amplified from larval genomic DNA or 12XCSL-DsRedExpressDL plasmid (Addgene) to include the T7 promoter sequence on both ends. Primers used are: dsRNAmob4_Fwd: 5′-TAATACGACTCACTATAGGGagatgtggaagtacgagcacctg-3′(Schulte et al., 2010), dsRNAmob4_Rev: 5′-TAATACGACTCACTATAGGGagatgcgagaagatgcgatacac-3′(Schulte et al., 2010), dsRNAcka_Fwd: 5′-TAATACGACTCACTATAGGGatacgggtccagttctgtgc-3′, dsRNAcka_Rev: 5′-TAATACGACTCACTATAGGGtgttgtaggccaccacgata-3′, dsRNADsRed_Fwd: 5′-TAATACGACTCACTATAGGGgccgatgaacttcaccttgt-3′, dsRNADsRed_Rev:

5′-TAATACGACTCACTATAGGGcgaggacgtcatcaaggagt-3′. The size of DNA bands was confirmed, purified using QIAquick Gel Extraction Kit (QIAGEN) and used as template for dsRNA synthesis. *In vitro* transcriptions were performed using MEGAscript T7 kit (Invitrogen), incubated for 6 hours at 37°C and treated with TURBO DNase (Invitrogen) for 15 min at 37°C. RNA was precipitated using LiCl precipitation solution (Invitrogen) and re-hydrated in ultrapure water. dsRNA was annealed by incubation at 65°C 30 min and cooled down to room temperature.

### Co-immunoprecipitations and western blotting

S2R+ cells were harvested and lysed in lysis buffer (25mM Tris, 0.15M NaCl, 1mM EDTA, 1% NP-40, 5% glycerol; pH 7.4) supplemented with protease inhibitor (Complete, EDTA-free; Sigma) and phosphatase inhibitors (cocktails B+C; Santa Cruz Biotechnology). Cell extracts were spun at 14000 rpm for 30 min at 4°C and proteins quantified (BCA protein assay, Pierce). Using the Pierce Co-immunoprecipitation kit (Pierce), 20 μg of anti-Flag M2 (Sigma), anti-HA (3F10; Roche), or rat IgG (Sigma) were immobilized in 50 μL of AminoLink Plus Coupling resin slurry following manufacturer instructions. Protein lysates were incubated in the resin on a rotator at 4°C overnight, washed 4 times with PBS and eluted following manufacturer instructions. Detection of proteins was performed using standard SDS-PAGE and western blotting using ECL or ECL Plus chemiluminescent substrate (Pierce). Antibodies used are: rabbit anti-Akt (1:500, CST), rabbit anti-pAkt$^{S505}$ (1:500, CST), rabbit anti-β-Actin (1:1000, CST), mouse anti-Flag clone M2 (1:3000, Sigma), mouse anti-Myc clone 9E10 (1:500, Santa Cruz Biotechnology), rabbit anti-Cka (1:5000, kind gift from W. Du), guinea pig anti-Mob4 (1:5000, kind gift from T. Littleton), rabbit anti-pMST1$^{T183}$/pMST2$^{T180}$ (1:500, CST), guinea pig anti-Hippo (1:5000, kind gift from G. Halder) and rat anti-HA clone 3F10 (1:3000, Roche).

## QUANTIFICATION AND STATISTICAL ANALYSIS

Transcriptome data: all genes with raw signal intensity values below 150 were removed from the analysis, generating a matrix containing 2455 genes. Quantile normalization (Bolstad et al., 2003) across all samples was performed using R/Bioconductor limma package (Ritchie et al., 2015). Remaining genes were analyzed with limma, by fitting a linear model. Adjusting *p-value*s with False Discovery Rate (FDR) did not reach statistical significance. Instead, a limma moderated paired t test was employed. Targets with expression fold changes with associated $p < 0.05$ values were used for subsequent analysis, including expression validation. Expression of selected candidate genes assayed by RT-qPCR was quantified using the Livak method (Livak and Schmittgen, 2001).

Other statistics were performed using SigmaPlot Version 12.5 (Systat software): Shapiro-Wilk and equal variance tests used to evaluate normality; Student's t test applied when data fitted a normal distribution; Wilcoxon rank-sum test used for non-parametric data; $p < 0.05$ considered significant. Data from *Drosophila in vivo* assays were obtained from a minimum of two biological replica sets; sample numbers are indicated in figure legends. Cell culture/ biochemistry results derive from a minimum of three independent assays. Histograms show mean ± standard error of the mean. Boxplots represent 25$^{th}$ and 75$^{th}$ percentiles, black line indicates median, red line specifies mean, whiskers indicate 10$^{th}$ and 90$^{th}$ percentiles.

## DATA AND SOFTWARE AVAILABILITY

Processed transcriptome data is shown in Table S1. Raw transcriptome data has been deposited in the Gene Expression Onmibus (GEO) public database under ID code GSE128646.

**Cell Reports, Volume *27***

## Supplemental Information

# STRIPAK Members Orchestrate Hippo and Insulin Receptor Signaling to Promote Neural Stem Cell Reactivation

**Jon Gil-Ranedo, Eleanor Gonzaga, Karolina J. Jaworek, Christian Berger, Torsten Bossing, and Claudia S. Barros**

## Supplemental Figures and Figure Text

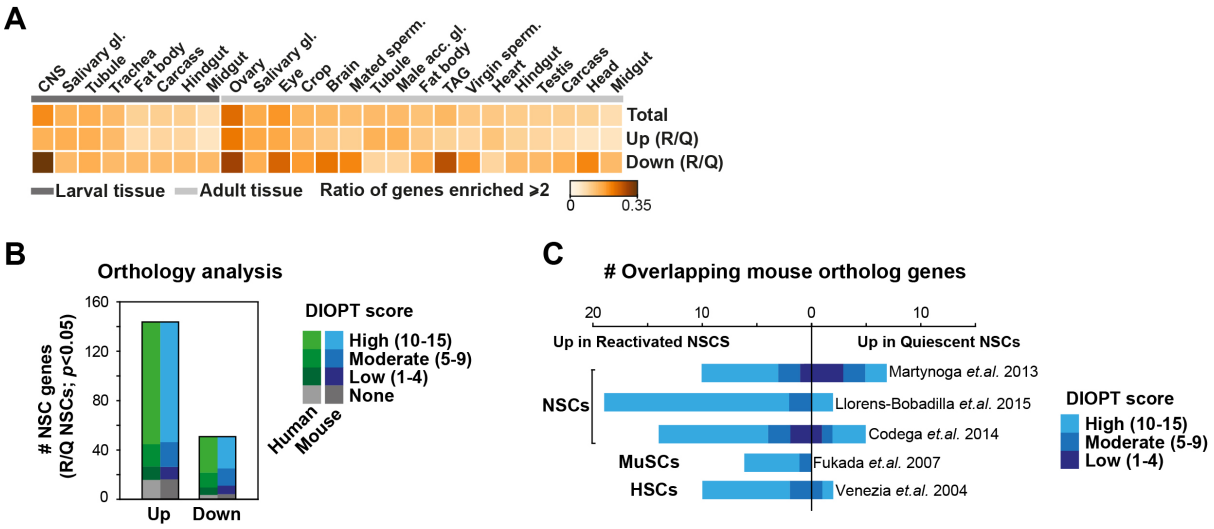


**Figure S1, related to Figure 1. Tissue expression enrichment and orthology conservation of identified targets in transcriptome analysis.** (A) Heatmap depicting identified larval and adult tissue-specific gene sets enriched by a minimum of 2-fold to expression in whole fly. gl: gland. Sperm: spermatheca; acc: accessory; TAG: thoracicoabdominal ganglion. See also Table S2. (B) Number of human and mouse orthologues (single best matches) of identified genes grouped by orthology score (DIOPT) (Hu, et al., 2011). See also Table S1. (C) Number of identified genes with mouse orthologues (single best matches) reported upregulated in quiescent or proliferating mouse embryonic or adult NSCs, skeletal muscle satellite stem cells (MuSCs) and hematopoietic stem cells (HSC). DIOPT score groups indicated. See also Table S3. The data used for the above assays comprise targets identified in our transcriptome analysis as up- or downregulated in reactivating (R) versus quiescent (Q) NSCs (limma moderated *t*-test, $p<0.05$).

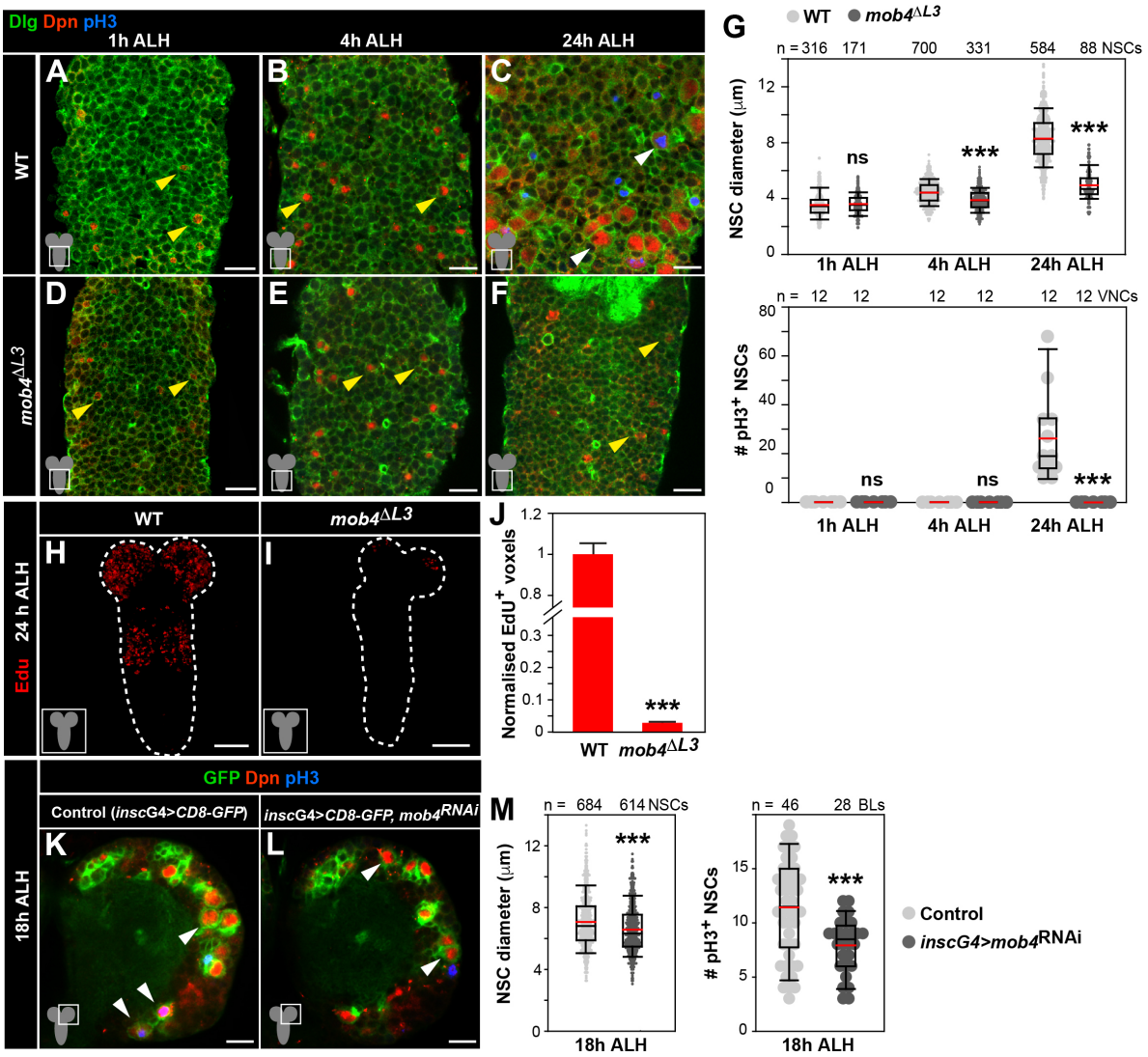


**Figure S2, related to Figure 2. NSC reactivation defects upon Mob4 loss or inhibition.** (A-G) NSC enlargement and division is impaired in *mob4* mutant ventral nerve cords (VNCs). VNCs of WT (A, 1h ALH; B, 4h ALH; C, 24h ALH) and *mob4*$^{\Delta L3}$ (D, 1h ALH; E, 4h ALH; F, 24h ALH). NSCs in red (Dpn), cell membranes in green (Dlg), divisions in blue (pH3). Yellow and white arrowheads indicate quiescent and reactivated NSC examples, respectively. Scale bar: 10µm. Anterior up. (G) Quantification of NSC diameters (1h ALH: WT n=316 NSCs, 7 VNCs; *mob4*$^{\Delta L3}$ n=171 NSCs, 5 VNCs. 4h ALH: WT n=700 NSCs, 6 VNCs; *mob4*$^{\Delta L3}$ n=331 NSCs, 5 VNCs. 24h ALH: WT n=584 NSCs, 5 VNCs; *mob4*$^{\Delta L3}$ n=88 NSCs, 8 VNCs) and proliferation (1h ALH: WT n=12 VNCs; *mob4*$^{\Delta L3}$ n=12 VNCs. 4h ALH: WT n=12 VNCs; *mob4*$^{\Delta L3}$ n=12 VNCs. 24h ALH: WT n=12 VNCs; *mob4*$^{\Delta L3}$ n=12 VNCs). (H-J) NSCs in *mob4* mutant larval brains do not enter S-phase, except the MbNSCs. WT (H) and *mob4*$^{\Delta L3}$ (I) CNSs at 24hph Edu-labelled (red). (J) Quantification of Edu$^{+}$

voxels from CNSs, normalized to controls (WT n=7 CNSs, *mob4*$^{\Delta L3}$ n=8 CNSs; error bars: s.e.m). Scale bar: 50µm. (K-M) NSC-specific expression of *mob4*-RNAi results in a small reduction in cell size and decreased number of NSCs in division. Brain lobes (BLs) of control (K, *insc-gal4>CD8-GFP*) and *mob4*-RNAi expressing brains (L, *insc-gal4> CD8-GFP, mob4*$^{RNAi}$) at 18h ALH. NSCs in green (*CD8-GFP*, GFP) and red (Dpn), divisions in blue (pH3). Arrowheads: NSC examples. Anterior up. Scale bar: 10µm. (M) Quantification of NSC diameters (*insc-gal4>CD8-GFP*, n=684 NSCs, 9 BLs, 9 brains; *insc-gal4> CD8-GFP, mob4*$^{RNAi}$ n=614 NSCs, 8 BLs, 8 brains) and divisions (*insc-gal4>CD8-GFP,* n=46 BLs, 23 brains; *insc-gal4> CD8-GFP, mob4*$^{RNAi}$ n=28 BLs, 14 brains). Wilcoxon rank sum tests, ***$p<0.001$, $p>0.05$: non-significant (ns).

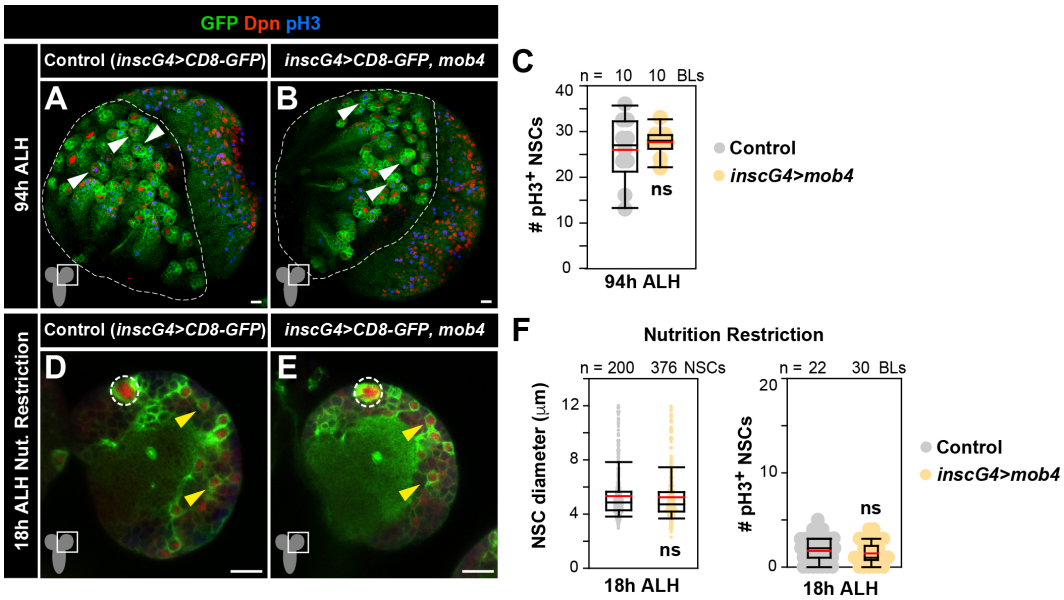


**Figure S3, related to Figure 3. Mob4 overexpression does not lead to NSC overproliferation nor induces NSC reactivation under nutrition restriction.**

NSC-specific *mob4* overexpression does not affect NSC proliferation in late larval brains (A-C) nor promotes reactivation of NSCs in larvae deprived of amino acids (sucrose-only diet; D-F). Brain lobes (BLs) of control (A, D, *insc-gal4>CD8-GFP*) and *mob4* overexpressing brains (B, E, *insc-gal4>CD8-GFP, mob4*) at 94h (A, B) and 18h ALH (D, E). NSCs in green (GFP) and red (Dpn), divisions in blue (pH3). Dashed line: central brain region. White arrowheads: dividing NSC examples. Yellow arrowheads: quiescent NSC examples. Dashed circles: MbNSCs. Scale bar: 10μm. Anterior up. (C) Quantification of NSC divisions (94h ALH: *insc-gal4>CD8-GFP* n=10 BLs, 10 brains; *insc-gal4>CD8-GFP, mob4* n=10 BLs, 10 brains). (F) Quantification of NSC diameters (18h ALH: *insc-gal4>CD8-GFP* n=200 NSCs, 6 BLs, 5 brains; *insc-gal4>CD8-GFP, mob4* n=376 NSCs, 5 BLs, 5 brains) and divisions (18h ALH: *insc-gal4>CD8-GFP* n=22 BLs, 16 brains; *insc-gal4>CD8-GFP, mob4* n=30 BLs, 16 brains). Wilcoxon rank sum tests, $p>0.05$: non-significant (ns).

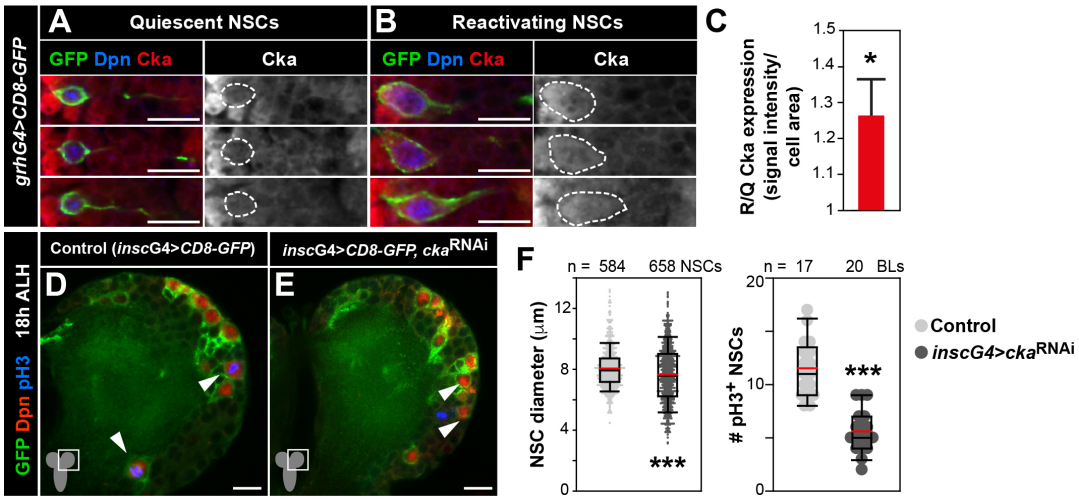


**Figure S4, related to Figure 5. Cka inhibition delays NSC growth and division.** (A-C) Cka is upregulated in reactivating (R) compared with quiescent (Q) NSCs. Examples of quiescent (small; A) and reactivating (enlarged, B) NSCs in 17h ALH brains (VNC thoracic region) labelled with *grh-Gal4* driving *CD8-GFP* (GFP, green), Cka (red) and Dpn (blue). Cka channel also shown in monochrome. Dashed lines: cell bodies. (C) Cka protein quantification in reactivating normalised to quiescent NSCs (n= 20 reactivating NSCs and n=20 quiescent NSCs, 20 BLs, 10 brains; error bars: s.e.m.; Wilcoxon rank sum test, *$p$<0.05). (D-F) NSC-specific expression of *cka*-RNAi results in reduced cell size and decreased number of NSCs in division. Brain lobes (BLs) of control (D, *insc-gal4>CD8-GFP*) and *cka*-RNAi expressing brains (E, *insc-gal4> CD8-GFP, cka*$^{RNAi}$) at 18h ALH. NSCs in green (*CD8-GFP*, GFP) and red (Dpn), divisions in blue (pH3). Arrowheads: NSC examples. Anterior up. Scale bar: 10μm. (F) Quantification of NSC diameters (*insc-gal4>CD8-GFP*, n=584 NSCs, 8 BLs, 4 brains; *insc-gal4> CD8-GFP, cka*$^{RNAi}$ n=658 NSCs, 8 BLs, 4 brains) and divisions (*insc-gal4>CD8-GFP,* n=17 BLs, 9 brains; *insc-gal4> CD8-GFP, cka*$^{RNAi}$ n=20 BLs, 10 brains). Wilcoxon rank sum tests, ***$p$<0.001.

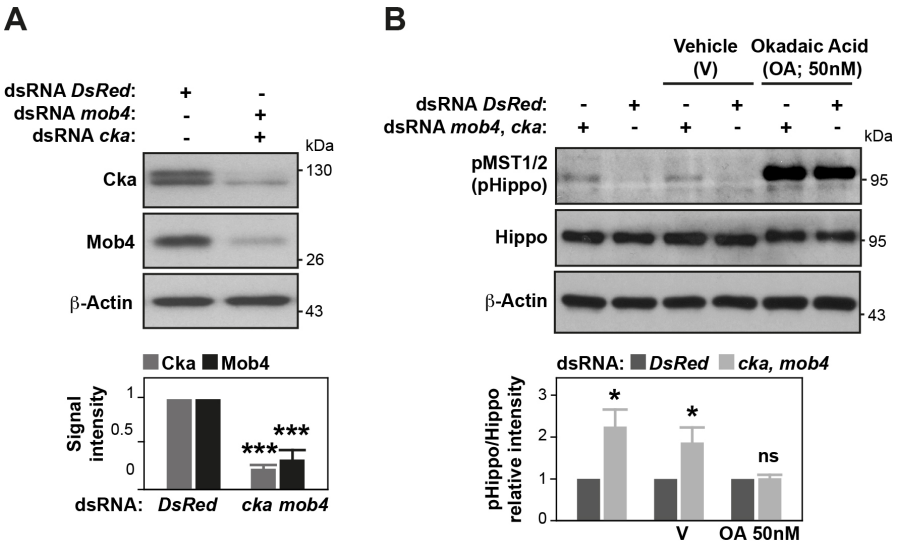


**Figure S5, related to Figure 5. Inhibition of Mob4 and Cka increase Hippo phosphorylation.** (A) Efficiency of *mob4* and *cka* RNAi-mediated depletions used in *Drosophila* S2R+ assays. dsRNAs targeting *mob4* or *cka*, but not *DsRed* control, lead to depletion of Mob4 and Cka proteins. Lysates analysed with indicated antibodies. β-Actin: loading control. Quantification of Mob4 and Cka signal intensities normalised to control (*DsRed* RNAi) levels (lower panel; n=3 independent assays; error bars: s.e.m; Student's *t*-tests, ***$p<0.001$). (B) Mob4/ Cka depletion leads to increased levels of activated (phosphorylated) Hippo (pHippo) in S2R+ cells, consistent with published studies (Zheng, et al., 2017; Liu, et al., 2016; Ribeiro, et al., 2010). *Drosophila* S2R+ cells treated with dsRNAs targeting *mob4* and *cka* or control *DsRed*, as well as in the presence of vehicle (0.0005% DMSO) or Okadaic acid (OA) as a positive control for hippo phosphorylation. Lysates analysed by western-blot with indicated antibodies. β-Actin: loading control. Note the total Hippo band mobility shift due to hyperphosphorylation in OA-treated samples. Quantification of pHippo levels shown as mean of the ratio between pHippo and total Hippo signal intensities relative to control (*DsRed* RNAi) levels (lower panel; n=3 independent assays; error bars: s.e.m; Student's *t*-tests, $p^*<0.05$, $p>0.05$: non-significant, ns).

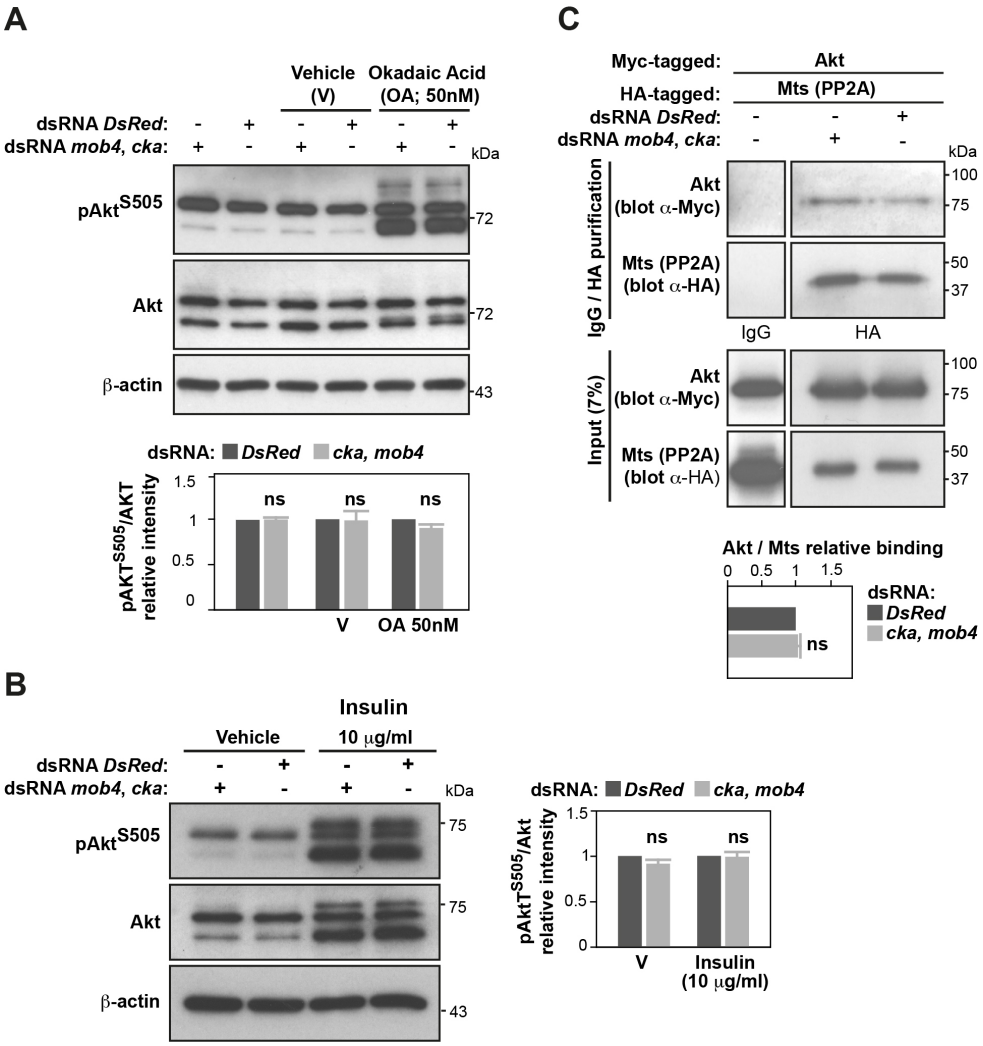


**Figure S6, related to Figure 5. Inhibition of Mob4 and Cka does not affect Akt phosphorylation nor the association of PP2A/Mts to Akt.** (A, B) Depletion of *mob4* and *cka* has no effect in the levels of activated (phosphorylated) Akt (pAkt$^{S505}$) in S2R+ cells (A) with or without stimulation with Insulin (B). (A) *Drosophila* S2R+ cells treated with dsRNAs targeting *mob4* and *cka* or control *DsRed*, as well as in the presence of Okadaic acid (OA) as a positive control for Akt phosphorylation or vehicle (V). Lysates analysed with indicated antibodies. β-Actin: loading control. Quantification of pAkt levels shown as mean of the ratio between pAkt and total Akt signal intensities relative to control (*DsRed* RNAi) levels (lower panel; n=3 independent assays). (B) RNAi-mediated depletion of *mob4* and *cka*, or control *DsRed*, in S2R+ cells treated with Insulin or vehicle. Lysates analysed by western-blot with indicated antibodies. β-Actin: loading control. Quantification of pAkt levels shown as mean of pAkt/ Akt signal intensity ratios relative to control (*DsRed* RNAi) levels (right panel; n=3 independent assays). (C) Co-IP assays using S2R+ cells

expressing Myc-Akt and HA-Mts, in addition to RNAi against *mob4* and *cka* or control *DsRed*. Lysates and HA-purified immunoprecipitates analysed by western-blot with indicated antibodies. Negative control co-IP performed using rat IgG instead of rat anti-HA antibody. Quantification of relative binding of Myc-Akt to HA-Mts shown as mean of the ratio between Myc-Akt and HA-Mts signal intensities relative to control (*DsRed* RNAi) levels (lower panel; n=3 independent assays). Error bars: s.e.m. Wilcoxon rank-sum tests, $p>0.05$: non-significant (ns).

## Supplemental Table

| Gene (Symbol) | Forward Primer (5'→3') | Reverse Primer (5'→3') | Source |
|---|---|---|---|
| *ase* | CACCTACCAACTGCTGACG | GCTGCTGCTGCTAATGTTG | This paper |
| *dpn* | CGCTATGTAAGCCAAATGGATGG | CTATTGGCACACTGGTTAAGATGG | (Berger, et al., 2012) |
| *rheb* | TGAGGTGGTGAAGATCATATACGAA | GCCAGCTTCTTGCCTTCCT | (Zitserman, et al., 2012) |
| *cka* | GGAGACGGAAGGCGTCAT | TCTCGTCGTCGGACATC | This paper |
| *CG10903* | GAGTCTCGGTTGATTTTGGACA | TCTCCCAGAATGACATCCCCA | This paper |
| *asf1* | GGGCGACACATCTTTGTCTTC | GCAGGTAAGCAGAACAATGGTAA | This paper |
| *Gbeta13F* | TGGTGGCTATCTATCGTGCTG | GCCCAAAAACGAGGTTACCTG | This paper |
| *phax* | ATGATGGAACTGCACGCAAAT | CAGGTGGTAAGGGGACTGG | This paper |
| *NiPp1* | ATGGCTAACAGCTACGACATACC | TGTTGCGACCAAATAGATAGCAT | This paper |
| *mob4* | TGGGCACGATCAGATTCTCC | CATCTTCTCGCACGCCTACT | This paper |
| *crc* | GAAAACTGGGAGGATACGTGG | GAGAGGTCTGAATGCCTTTGTC | This paper |
| *bet3* | ATGTCACGACAAGCCTCTCG | GAGTGCTCCGTAGGTGAGT | This paper |
| *ed* | GATGAGCTCCTGTTCTCCGG | GTTGGAATCGCAATGGTCGG | This paper |
| *pdp1* | AATCCCCATTACCAGCGCAA | GGCATTCCCATTCGATCCCT | This paper |
| *how* | AACTTTGTCGGTCGCATTTT | CGTCCTCCTTCTTCTTGTCG | This paper |
| *p120ctn* | AACATGGACCTTTCATTGACGC | ATATCCTGCTGCCGAAAATTGA | This paper |
| *Rip11* | TGGAGTCCGACGCACTGTA | CAATGGTGACGAAGCAGTTGT | This paper |
| *l(2)35Df* | CATCGAAAGAAGCTACATCCTCC | GTGGGTTCGTCATCTGCATTAT | This paper |
| *nito* | ACAAGAAGTTTGGCGATTTTAGC | CTTCAGGCGTTCGGAAGCAA | This paper |
| *mts* | TCCAGTTCCATAAGAGCCGC | CACGATCGCAATGTGGTCAC | This paper |
| *rp49* (calibrator) | GCTAAGCTGTCGCACAAATG | GTTCGATCCGTAACCGATGT | (Kohyama-Koganeya, et al., 2008) |

**Table S4, related to STAR Methods. Primers used for real-time quantitative PCR assays.**